

**SERVICE LIFE OF REINFORCED CONCRETE EXPOSED TO CHLORIDE
ENVIRONMENT HIGHLIGHTING THE EFFECT OF METAKAOLIN IN THE
MIXTURE**

by

© Hossam S. Alalaily, B.Sc., M.Eng.

A thesis submitted to the

School of Graduate Studies

in partial fulfillment of the requirements for the degree of

Doctor of Philosophy (Civil Engineering)

Faculty of Engineering and Applied Science

Memorial University of Newfoundland

October 2017

St. John's, Newfoundland, Canada

ABSTRACT

Experimental and numerical analysis were conducted to investigate the service life of reinforced concrete exposed to chloride attack highlighting the effect of using metakaolin (MK) in concrete mixtures. The research also aims to study and optimize the mixture proportions/composition of MK mixtures in order to maximize their service lifetime. Design tools/charts were also developed in this research to facilitate and simplify the service life prediction of the mixtures. Three main service life periods of reinforced concrete exposed to chloride environment were studied: corrosion initiation, propagation, and damage periods. The research was divided into three stages; the first stage experimentally studied and investigated the three corrosion periods (initiation, propagation, and damage periods) in concrete with MK and concrete with different curing conditions. The second stage developed mechanical and chloride permeability prediction equations for concrete containing MK. Finally, the third stage utilized probabilistic and extended finite element (XFEM) in predicting the corrosion periods for concrete containing MK.

In the first stage, two corrosion testing methods were used to study the three corrosion periods: impressed current corrosion and wet/dry cycles testing methods. Seventy-eight concrete samples were tested under the impressed current corrosion testing. In this investigation, three variables were studied: percentage of MK% (0% to 20%), cover thicknesses (20, 30, and 40 mm), and curing conditions. On the other hand, thirty concrete samples were tested under the wet/dry corrosion testing for two years to study the corrosion period under natural corrosion process and to compare the results with those of the impressed current corrosion testing. The results of the first stage indicated that the

incorporation of MK significantly increased both the initiation and propagation periods with little increase in the damage period. Also, the different curing conditions had a clear effect on the initiation and propagation periods while length of the damage period was not significantly affected. The results from the wet/dry corrosion testing were compared with the impressed current corrosion technique and proved that the impressed current corrosion test can be used effectively to evaluate and compare the corrosion activities in different concrete qualities but cannot be used after the initiation of the first crack.

The second stage tested fifty-three concrete mixtures containing MK to develop prediction equations using statistical analysis. Three factors were considered in this stage: total binder content (350kg/m^3 - 600kg/m^3), the percentage of MK (0%-25%), and the water-to-binder ratio (0.3-0.5). The mixtures were examined based on the rapid chloride permeability test, chloride diffusion test, compressive strength, modulus of elasticity, splitting tensile strength, flexural strength, and cost of mixture per cubic meter. Moreover, bulk diffusion test was adopted for two years to determine the time-dependent coefficient of chloride diffusion for all mixtures based on the error function solution to Fick's law. Finally this stage also included some experimental relationships between the rapid chloride permeability test, chloride diffusion coefficient, and compressive strength results. Moreover, the derived models and design charts based on the experimental results in this stage were useful for optimizing and predicting the concrete mechanical and chloride permeability properties.

Finally, the third stage is divided into two parts: the first part was using probabilistic method to predict the probability of corrosion initiation and the second part was developing

XFEM to enhance predicting the propagation period (corrosion induced cracking). Three variables were investigated in this stage: total binder content (350kg/m^3 - 600kg/m^3), MK% (0%-25%), concrete cover (20 mm- 60 mm) and W/B (0.3-0.5). In the first part, Monte Carlo simulation technique was used to predict probability of corrosion initiation in a concrete structure containing MK with different mixture proportions and concrete covers. Statistical modeling was then utilized to develop prediction models/charts to predict the probability of corrosion initiation for concrete containing MK, and identify the most significant factors affecting this stage. The results showed that the probability of corrosion decreased as the percentage of MK increased. The results also showed that the most significant factor affecting the corrosion probability was found to be MK replacement, W/B ratio, and binder content respectively, in order of significance. On the other hand, the second part utilized XFEM to investigate the crack propagation and expansive behavior of corroded steel bar on the concrete cover for a concrete structure containing MK. statistical analysis was incorporated with XFEM to develop prediction model/charts for the expansive pressure resulted from corrosion products. Finally validation samples were tested under accelerated corrosion to verify the enhanced model. The results indicated that the time required for corrosion-induced cracking obtained from the developed prediction model showed a good agreement with the experimental results of the accelerated corrosion samples. Also, the cracks predicted by the XFEM showed a similar trend of variation with that found in the accelerated corrosion samples.

The developed models and design charts in this research will help designers and engineers to better understand the influence and the importance of various mix design parameters of MK mixtures on the corrosion period estimation.

To my parents, brother, my beloved wife and precious daughter Mariam

ACKNOWLEDGEMENTS

After thanking Almighty "ALLAH" for his numerous blessings and for giving me the strength in life, I want to express my great gratitude to my thesis advisor Dr. Assem Hassan for offering this great chance and being a big brother for me. I also would like to express my gratitude to Dr. Amgad Hussein for his support and endlessly fatherly guidance. Finally I would like to thank my supervisory committee members Dr. Amgad Hussein and Dr. John Molgaard for agreeing to be in my thesis supervisory committee.

Many thanks are due to Mr. Shawn Organ and Mr. Matt Curtis for their constant support and assistance in lab work during my PhD program. The funding provided by Dr. Assem Hassan, School of Graduate Studies, Mitacs- Accelerate Internship Program, and the RDC OISRA grant is greatly acknowledged.

Nothing can express my gratitude to the support and encouragement provided by my parents, brother, and my wife during my studies. Finally, I would embrace this opportunity to thank all my friends for encouraging me to finish this PhD degree, especially Mohamed Abdallah and all other colleagues in Memorial University.

Table of Contents

ABSTRACT.....	ii
ACKNOWLEDGEMENTS	vii
Table of Contents	viii
List of Tables	xii
List of Figures	xiii
List of Symbols, Nomenclature or Abbreviations.....	xv
Co-Authorship Statement.....	xviii
1. Introduction.....	1
1.1 Background and Research Motivation	1
1.2 Research Objectives and Significance	4
1.3 Scope of Research.....	4
1.4 Thesis Outline	6
1.5 Reference	7
2 Influence of Metakaolin and Curing Conditions on Service Life of Reinforced Concrete....	14
2.1 Abstract.....	14
2.2 Introduction.....	14
2.3 Research Significance	18
2.4 Research Program	19
2.5 Experimental Procedure.....	23
2.5.1 Materials.....	23
2.5.2 Samples Details.....	24
2.5.3 Casting, Curing and Test Setup.....	25
2.6 Experimental Results and Discussions.....	29
2.6.1 Effects of Cover Thickness on the Corrosion Initiation/Propagation Periods	31
2.6.2 Effects of Concrete Quality on the Corrosion Initiation and Propagation Periods	32
2.6.3 Effect of MK Replacement on the Corrosion Initiation and Propagation Periods .	36
2.6.4 Damage Period.....	38
2.6.5 Half-Cell Potential Readings.....	40
2.6.6 Theoretical Comparison between Experimental Data and Prediction Models.....	41
2.7 Conclusions.....	46
2.8 Reference	48

3.	A study on the effect of curing temperature and duration on rebar corrosion using wet-dry cycle corrosion test	50
3.1	Abstract	50
3.2	Introduction	50
3.3	Research significance.....	55
3.4	Materials and mixture proportions	55
3.5	Accelerated corrosion sample detail	57
3.6	Testing program	58
3.7	Readings and measurements	61
3.8	Experimental Results and Discussion	65
3.8.1	Effect of curing technique on corrosion activity	66
3.8.2	Effect of curing technique on chloride threshold	69
3.8.3	Effect of curing technique on rebar mass loss.....	71
3.8.4	Comparison between wet-dry cycle and impressed current corrosion tests.....	72
3.9	Conclusion	73
3.10	Reference	75
4.	Refined statistical modeling for chloride permeability and strength of concrete containing metakaolin.....	79
4.1	Abstract	79
4.2	Introduction	80
4.3	Development of Refined Response Surface Method	83
4.4	Research Significance	87
4.5	Experimental Program	88
4.5.1	Materials.....	88
4.5.2	Mixture Proportioning and Casting.....	90
4.5.3	Test Procedures	92
4.6	Results and Discussion.....	93
4.6.1	Compressive Strength (f_c).....	97
4.6.2	Splitting Tensile Strength (STS)	101
4.6.3	Flexural Strength (FS).....	103
4.6.4	Modulus of Elasticity (MOE)	105
4.6.5	Rapid Chloride Permeability Test (RCPT)	107
4.6.6	Diffusion Coefficient (D_a)	109
4.6.7	Cost Analysis	111

4.6.8	Optimization and Validation	113
4.7	Conclusion	114
4.8	Reference	115
5.	Time-Dependence of Chloride Diffusion for Concrete Containing Metakaolin.....	119
5.1	Abstract	119
5.2	Introduction.....	120
5.3	Research significance.....	124
5.4	Development of response surface method	124
5.5	Chloride diffusion reduction coefficient calculation (m).....	126
5.6	Experimental program.....	129
5.6.1	Materials.....	129
5.6.2	Mixture proportioning and casting.....	130
5.6.3	Test methods	132
5.7	Results and discussion	133
5.7.1	Experimental results.....	133
5.7.2	Chloride permeability and chloride diffusion coefficients results	137
5.7.3	Chloride diffusion reduction coefficient m for concrete containing metakaolin .	139
5.7.4	Development of empirical relationships for chloride diffusion coefficient, RCPT, and compressive strength.....	145
5.7.5	Models' performance assessment	147
5.8	Conclusions.....	148
5.9	Reference	150
6.	Probabilistic and statistical modeling of chloride-induced corrosion for concrete containing metakaolin.....	153
6.1	Abstract.....	153
6.2	Introduction.....	154
6.3	Research Significance	158
6.4	Methodology	159
6.4.1	Chloride-Induced Corrosion Prediction	159
6.4.2	Monte Carlo Simulation (MCS).....	161
6.5	Scope of Work	162
6.5.1	Monte Carlo Simulation Modeling (First Part).....	162
6.5.2	Chloride-Induced Corrosion Period Statistical Analysis (Second Part).....	164
6.6	Results and Discussion.....	166

6.6.1	Effect of W/B Ratio on the Probability of Corrosion.....	166
6.6.2	Effect of the Percentage of MK on the Probability of Corrosion.....	167
6.6.3	Effect of Binder Content on the Probability of Corrosion	169
6.6.4	Statistical Analysis Prediction Equations.....	170
6.6.5	Steps of design	171
6.7	Conclusion	174
6.8	Reference	176
7.	Use of eXtended FEM and statistical analysis for modelling the corrosion-induced cracking in reinforced concrete containing metakaolin	181
7.1	Abstract.....	181
7.2	Introduction.....	182
7.3	Research significance.....	185
7.4	Corrosion-induced cracking prediction approach	186
7.5	Scope of work	187
7.5.1	XFEM description.....	188
7.5.2	Statistical analysis and time-to-crack model enhancement.....	190
7.6	Model validation experimental program.....	192
7.7	Materials	193
7.8	Samples details.....	194
7.9	Testing procedure.....	195
7.10	Results and discussion	196
7.10.1	Comparison between XFEM results and thick-wall theory	196
7.10.2	XFEM crack prediction.....	198
7.10.3	Statistical analysis and most significant factor affecting cracks	201
7.10.4	Model validation	206
7.11	Conclusion	206
7.12	Reference	208
8.	Conclusions and Recommendations	212
8.1	Conclusions.....	212
8.2	Recommendations for Future Research	214
	Bibliography	216

List of Tables

Table 2.1 Test Matrix.....	22
Table 2.2 Chemical and Physical Properties of Cement	24
Table 2.3 Mixture Proportions	24
Table 2.4 Description of Different Curing Techniques	27
Table 2.5 Properties of Various Concrete Qualities.....	28
Table 2.6 Service Lifetimes Calculated from the Accelerated Corrosion Tests of all Samples	30
Table 2.7 ANOVA Results for the Effect of Different Factors on the Damage Period.....	40
Table 2.8 Summary of Variables for Calculating Pi (Gjørsv 2009)	43
Table 3.1 Chemical and physical properties of cement	56
Table 3.2 Sieve analysis.....	57
Table 3.3 Mixture proportions for Concrete mixture.....	57
Table 3.4 Mechanical and chloride resistivity test results	65
Table 3.5 Wet-dry cycles corrosion tests results.....	66
Table 3.6 Impressed current accelerated corrosion tests results	73
Table 4.1 Coded and absolute values of investigated parameters.....	86
Table 4.2 Chemical and physical properties	89
Table 4.3 Sieve analysis.....	89
Table 4.4 Mixture proportions	91
Table 4.5 Experimental results.....	93
Table 4.6 Experimental error (fc, STS, FS, and MOE).....	95
Table 4.7 Derived statistical models	97
Table 4.8 Analysis of variance for significant parameters (F-value and P-value).....	99
Table 4.9 Validation of the statistical models.....	114
Table 5.1 Chemical and physical properties	129
Table 5.2 Sieve analysis.....	130
Table 5.3 Mixture proportions and results	131
Table 5.4 Chloride diffusion and chloride diffusion reduction coefficient.....	134
Table 5.5 Derived statistical model.....	136
Table 5.6 Significant factors for statistical models	139
Table 5.7 Validation of the statistical models.....	148
Table 6.1 Chloride diffusion and chloride diffusion reduction models used.....	161
Table 6.2 Input parameter for probabilistic analysis.....	164
Table 6.3 Mixture proportions	165
Table 6.4 Chloride-induced corrosion prediction equations	166
Table 6.5 ANOVA for significant parameters (F-value and P-value)	171
Table 7.1 Mechanical properties equations.....	190
Table 7.2 Parameter values used in analysis.....	191
Table 7.3 Statistical analysis mixture proportions	192
Table 7.4 Chemical and physical properties of cement	193
Table 7.5 Aggregate sieve analysis.....	194
Table 7.6 XFEM results for internal pressure.....	197
Table 7.7 ANOVA results.....	201

List of Figures

Figure 2.1 Typical Electrical Current vs. Time Curve	22
Figure 2.2 Test Specimen Details	25
Figure 2.3 Accelerated Corrosion Schematic	27
Figure 2.4 Half-Cell Potentials Test	29
Figure 2.5 Relationship between Cover Thickness and Initiation/Propagation Periods: a) T_i and b) T_p	32
Figure 2.6 Initiation and Propagation Periods vs. Initial Current.....	34
Figure 2.7 Concrete Quality vs. Chloride Threshold	35
Figure 2.8 Relationship between RCPT/Chloride Diffusion Coefficient (D_a) and: a) T_i and b) T_p .	38
Figure 2.9 Half-Cell Potential Readings.....	41
Figure 2.10 Probabilities of Corrosion Initiation for 40 mm Cover Samples	42
Figure 2.11 Comparison between the Model Predicted Propagation Period and Experiment	45
Figure 3.1 Sample Cross-section detail	58
Figure 3.2 Wet-dry cycles schematic diagram	61
Figure 3.3 Typical current vs. time curve	62
Figure 3.4 Chloride threshold extraction	63
Figure 3.5 pH reading from concrete sample	64
Figure 3.6 Crack width at different	64
Figure 3.7 Rebar mass loss (from top initiation stage, propagation stage and bottom damage stage).....	65
Figure 3.8 Curing technique-cycles relation	68
Figure 3.9 pH vs curing technique and chloride threshold	69
Figure 3.10 Chloride threshold vs. RCPT and diffusion coefficient.....	70
Figure 3.11 Concrete curing technique and mass loss.....	71
Figure 4.1 CCD and FCCD point arrangement.....	81
Figure 4.2 Modified CCD points	84
Figure 4.3 General flow chart on using the design charts	87
Figure 4.4 Compression strength charts with variance W/B content.....	100
Figure 4.5 Splitting tensile strength charts with variance W/B content.....	102
Figure 4.6 Flexural strength charts with various W/B ratios	104
Figure 4.7 Modulus of elasticity charts.....	106
Figure 4.8 RCPT charts with various W/B ratios	108
Figure 4.9 Diffusion coefficient charts with various W/B ratios	110
Figure 4.10 Cost charts with various W/B ratios	112
Figure 5.1 Modified RSM points.....	125
Figure 5.2 Typical chloride diffusion coefficient vs. time (log-log scale)	127
Figure 5.3 Chloride diffusion coefficients at 28, 90, 180, 360, and 720 days	142
Figure 5.4 m_{avr} charts with different W/B ratios	143
Figure 5.5 m_{avr} charts with different W/B ratios	144
Figure 5.6 Chloride diffusion coefficient vs. RCPT	145

Figure 5.7 Chloride diffusion coefficient vs. compressive strength.....	146
Figure 5.8 RCPT vs. compressive strength	147
Figure 6.1 Statistical method point arrangement.....	157
Figure 6.2 Program flowchart	163
Figure 6.3 Sample of program output plot	164
Figure 6.4 Effect of W/B ratio on the probability corrosion (0% MK, 400 kg/m ³ binder, and 40-mm concrete cover)	167
Figure 6.5 Effect of MK replacement on the probability of corrosion (600 kg/m ³ binder, 0.35 W/B ratio, and 40-mm concrete cover)	168
Figure 6.6 Effect of MK replacement at different binder and W/B contents on the probability of corrosion (25% MK and 40-mm concrete cover)	169
Figure 6.7 Effect of binder content on the probability of corrosion (0% MK, 0.4 W/B ratio, and 40-mm concrete cover).....	170
Figure 6.8 Chloride-induced corrosion period (at 10% probability of corrosion initiation) for 30-mm cover	172
Figure 6.9 Chloride-induced corrosion period (at 10% probability of corrosion initiation) for 40 mm cover	173
Figure 6.10 Chloride-induced corrosion period (at 10% probability of corrosion initiation) for 60-mm	174
Figure 7.1 Crack modeling using a thick-wall cylinder approach.....	184
Figure 7.2 XFEM model	189
Figure 7.3 Test specimen details.....	195
Figure 7.4 Accelerated corrosion schematic diagram.....	195
Figure 7.5 Relation between C/D to PcrXFEM	198
Figure 7.6 XFEM cracks propagation reaching concrete surface (principal stresses).....	200
Figure 7.7 Propagation period surface crack	200
Figure 7.8 Samples of crack pattern from experiment and XFEM	201
Figure 7.9 Corrosion cracking pressure for 20-mm cover.....	203
Figure 7.10 Corrosion cracking pressure for 30-mm cover	204
Figure 7.11 Corrosion cracking pressure for 40-mm cover	205
Figure 7.12 Time to corrosion-induced cracking experimental vs. developed model.....	206

List of Symbols, Nomenclature or Abbreviations

ANOVA	Analysis of variance
BC	Boundary condition
C	Concrete cover
CCD	Central composite design
$C(x,t)$	Chloride concentration, measured at depth x and exposure time t
COV	Coefficient of variation
C_s	Surface chloride concentration
C_{th}	Chloride threshold
C_x	Chloride concentration at the level of reinforcement
D	Bar diameter
D_{720}	Chloride diffusion coefficient (720 days)
D_{180}	Chloride diffusion coefficient (180 days)
D_{28}	Chloride diffusion coefficient (28 days)
D_{360}	Chloride diffusion coefficient (360 days)
D_{90}	Chloride diffusion coefficient (90 days)
D_a	Chloride diffusion coefficient (28 days)
df	Different factor
E	Modulus of elasticity
E_{ef}	Effective elastic modulus of concrete
f_c'	Characteristic Compressive Strength of Concrete
FCCD	Faced-Centered composite design
f_t	Tensile Strength of Concrete
G	Fracture energy

$H(x)$	Discontinuity jump function
i	Corrosion rate
m	Diffusion reduction coefficient/diffusion decay index
m_{avr}	Average diffusion reduction coefficient
MCS	Mont Carlo simulation
MK	Metakaolin
MOE	Modulus of elasticity
m_{total}	Total diffusion reduction coefficient
$N_i(x)$	Shape functions
P	Probability
P_{cr}	Radial pressure required to crack the concrete cover
$P_{cr\ thick\ wall}$	Crack pressures calculated by thick-wall theory
$P_{cr\ XFEM}$	Crack pressures calculated by XFEM
P_f	Probability of failure
P_i	Probability of corrosion initiation
RC	Reinforced concrete
RCPT	Rapid chloride permeability test
RF	Reliability function
RSM	Response surface methodology
S	Load effect
SCM	Supplementary cementing materials
STS	Split tensile stress
t	The exposure time
T_{cr}	Time to crack
T_d	Damage period
T_i	Initiation period
$T_{i\ predicted}$	Predicted initiation period

t_{init}	Initiation period
T_p	Propagation period
u_i	Nodal displacement
ν	Poisson's ratio of concrete
W/B	Water-to binder ratio
x	Depth below the exposed surface
XFEM	Extended finite element method
γ_c	Density of the concrete
ϕ_{cr}	Concrete creep coefficient
δ_0	Thickness of the porous zone
\mathbf{a}_I	Nodal enriched degree of freedom vector
$F_\alpha(x)$	Elastic asymptotic crack-tip functions
\mathbf{b}_I^α	Nodal enriched degree of freedom vector

Co-Authorship Statement

I, Hossam Sherif Alalaily, hold a principle author status for all the manuscript chapters (Chapter 2 - 6) in this dissertation. However, each manuscript is co-authored by my supervisor and co-researchers, whose contributions have facilitated the development of this work as described below.

- Paper 1 in Chapter 2: Hossam S. Al-alaily, Ahmed A. Abouhussien, and Assem A. A. Hassan, “Influence of Metakaolin and Curing Conditions on Service Life of Reinforced Concrete” Accepted ASCE's Journal of Materials in Civil Engineering, March 2017.

I was the primary author, with authors 2 - 3 contributing to the idea, its formulation and development, and refinement of the presentation.

- Paper 2 in Chapter 3: Hossam S. Al-alaily and Assem A. A. Hassan, “A study on the effect of curing temperature and duration on rebar corrosion using wet-dry cycles corrosion test” accepted to ASCE's Journal of Materials in Civil Engineering, January 2017.

I was the primary author, with the second author contributing to the idea, its formulation and development, and refinement of the presentation.

- Paper 3 in Chapter 4: Hossam S. Al-alaily and Assem A. A. Hassan, “Refined statistical modeling for chloride permeability and strength of concrete containing metakaolin” Construction and Building Materials, Vol. 114, P. 564–579, July 2016.

I was the primary author, with the second author contributing to the idea, its formulation and development, and refinement of the presentation.

- Paper 4 in Chapter 5: Hossam S. Al-alaily and Assem A. A. Hassan, “Time-Dependence of Chloride Diffusion for Concrete Containing Metakaolin” Journal of Building Engineering, Vol. 7, P. 159–169, September 2016.

I was the primary author, with the second author contributing to the idea, its formulation and development, and refinement of the presentation.

- Paper 5 in Chapter 6: Hossam S. Al-alaily, Assem A. A. Hassan, and Amgad A. Hussein “Probabilistic and statistical modeling of chloride-induced corrosion for concrete containing metakaolin” Accepted Journal of Materials in Civil Engineering, March 2017.

I was the primary author, with the 2-3 authors contributing to the idea, its formulation and development, and refinement of the presentation.

- Paper 6 in Chapter 7: Hossam S. Al-alaily, Assem A. A. Hassan, and Amgad A. Hussein “Modeling the corrosion-induced cracking in reinforced concrete containing metakaolin using eXtended FEM and statistical analysis” submitted to Construction and Building Materials, February 2017.

I was the primary author, with the 2-3 authors contributing to the idea, its formulation and development, and refinement of the presentation.



Hossam S. Alalaily

July 21th, 2017

Date

1. Introduction

1.1 Background and Research Motivation

Concrete is the most widely used construction material around the world due to its easily acquired materials and low cost. Several applications of concrete include the construction of houses and industrial structures which are normally constructed using reinforced concrete (RC). In addition, most infrastructure projects extensively use concrete; such as airports, road and railway bridges, harbors and wharfs, coastal embankments, and dams (Liang et al., 2002). It is well known that chlorides from various sources can result in rebar corrosion in RC leading to serious consequences on the serviceability and functionality of concrete structures (Broomfield, 2007, Vidal et al., 2007, Cabrer, 1996, Poupard et al., 2006). Chloride-induced corrosion is considered to be the most prevalent form of premature concrete deterioration worldwide, due to the expansive nature of rust, which eventually causes cracking and spalling around the rebar. Corrosion results in highly prohibitive costs every year relating to RC structures repair and replacement. Therefore, the development of a corrosion resistant concrete mixture is proposed to counter the rate of corrosion in RC structures. This concrete can be designed by adding supplementary cementing materials (SCMs) to have a dense and less permeable microstructure, thereby improving its durability to protect the embedded rebar from corrosion (Mehta and Monteiro, 1993).

SCMs such as fly ash, silica fume, and/or ground granulated blast furnace slag have been used as cement replacement materials as they can significantly enhance the strength and durability characteristics of concrete in comparison with concrete without SCMs. Utilizing Metakaolin (MK) as a SCM improves the mechanical and durability properties of concrete

and is receiving a great attention nowadays. MK also contributes to the production of environmentally friendly concrete as it does not emit CO₂ and requires lower manufacturing temperatures compared to cement (Malhotra, 2000, Kamarudin et al., 2011). According to previous studies, incorporating MK in the concrete mixture increases its strength and rate of strength gain and improves the overall mixture durability (Akalin et al., 2010, Justice et al., 2005a, Madandoust and Mousavi, 2012). However, the feasibility of using MK in concrete mixtures as an alternative corrosion protection methodology is not investigated in the literature and requires further studies.

Statistical design of experiments is a useful tool to benchmark the optimum mixture components of concrete. The statistical design technique is an effective tool for this purpose as it provides statistical models, which helps in understanding the interactions between parameters that have been optimized (Ghezal and Khayat, 2002). Response surface methodology (RSM) is one of the methods utilized in many fields. RSM is a combination of mathematical and statistical techniques useful for developing, improving and optimizing processes and can be used to evaluate the relative significance of several affecting factors even in the presence of complex interactions (Montgomery 2012). There are numerous models used for optimizing concrete mixtures based on RSM, factorial design, and fractional factorial design (Sonebi, 2004, Soudki et al., 2001, Nehdi and Summer, 2002, Akalin et al., 2010, Rougeron and Aïtcin, 1994, Khayet et al., 2011). Design of experiments method is also widely used in several fields. This method generally relies on the analysis of variance (ANOVA). It selects few points out of the full factorial set that can represent efficient information about the response space. The above mentioned statistical models can

be used effectively in the prediction of the short and long term performance and service lifetime of concrete with MK.

The rebar corrosion mechanism is complex and is greatly affected by the environment and concrete material properties. One of the major challenges in the prediction of service life for RC structures is the scatteredness in mechanical and durability properties of concrete. Even for the same structural member, mechanical and durability properties may vary from one point to another. Therefore, the sources of variation for environmental and material uncertainties should be considered in service life performance assessment. Probability analysis of the structure plays an important role in the performance of its serviceability (Kirkpatrick et al., 2002, Enright and Frangopol, 1998, Marsh and Frangopol, 2008). There are several methods for determining the reliability of structures' performance taking into account the variation of concrete mechanical and durability properties (Quanwang et al., 2015, McNally and Sheils, 2012). Monte Carlo Simulation (MCS) method is a powerful method for reliability analysis that can take different probabilistic parameters into account simultaneously (Ann et al., 2010, Marek, 2001). This method uses a sampling of random variables to construct a set of values that aims to describe the failure and safe spaces. MCS can be described as a repeated statistical sampling process. Yet, the feasibility of utilizing MCS in predicting the probability of corrosion in MK concrete requires further examination.

The extended finite element method (XFEM) was developed recently by Belytschko and Black (Belytschko and Black, 1999). This method has emerged as a powerful numerical procedure for the analysis of crack propagation problems (Zhang and Bui, 2015, Unger et

al., 2007). In comparison to the conventional finite element method, XFEM provides significant benefits in the numerical modeling of crack propagation as it is easier to use. However, so far the application of XFEM for modelling of reinforced concrete corrosion modelling is still very limited.

1.2 Research Objectives and Significance

There are a limited number of studies dealing with the prediction of service life in concrete containing MK. Moreover, limited research has been undertaken that use of statistical analysis, probabilistic methods and XFEM for modeling corrosion periods for concrete containing MK. The main objective of this investigation was to optimize and develop concrete mixtures containing MK to withstand corrosion periods, and develop prediction models/charts by using combination of statistical analysis, XFEM and probabilistic modeling. Moreover, the research looked into identifying the most significant factors affecting the corrosion periods for concrete containing MK. Finally, this research aimed at developing design charts/models to help designers to optimize their concrete mixture and concrete cover thickness to extend the service lifetime of RC structures using concrete with MK.

1.3 Scope of Research

This research was conducted using a comprehensive experimental and analytical program consisted of three successive studies dealing with concrete containing MK. The first stage of this research involved investigating the corrosion periods in RC samples experimentally using both impressed current and wet/dry corrosion testing under different curing

techniques. A total of seventy-eight small-scale RC prism samples with variable concrete cover thicknesses, MK percentage, and concrete quality were tested. Moreover, additional thirty RC prisms were tested under the wet/dry corrosion testing. Three corrosion periods (initiation, propagation and damage periods) were experimentally studied using these samples and were also calculated using some available empirical models in the literature for comparison. The tested samples were evaluated based on the results of wet-dry cycles, accelerated corrosion, rapid chloride permeability test (RCPT), and chloride diffusion tests. The chloride threshold, pH value, current measurement, half-cell, mass loss, and crack width readings were also assessed during wet-dry cycles and impressed current corrosion tests. The second stage involved testing fifty-three concrete mixtures followed by an extensive refined statistical analysis. These mixtures were examined based on the RCPT, chloride diffusion test at different ages (28, 90, 180, 360, and 760 days), time dependent reduction in chloride diffusion coefficient, compressive strength, modulus of elasticity, splitting tensile strength, flexural strength, and cost of mixture per cubic meter. The third and final stage is divided into two analytical methods including probabilistic modeling and XFEM. In the probabilistic modeling part, MCS was utilized to predict the probability of corrosion initiation (1 to 200 years) for concrete containing MK with different mixture proportions and concrete covers. On the other hand, an improved modeling was utilized by combining the XFEM and statistical analysis methods to predict the time for propagation period in concrete containing MK. The XFEM was utilized to predict the radial corrosion pressure required to crack the concrete cover in the propagation period. Statistical analysis was then applied to simplify the process by developing an equation to calculate cracking pressure based on the range of mixture proportions covered in this study.

1.4 Thesis Outline

This thesis consists of eight chapters described as follows:

Chapter 1 demonstrates the background, motivation, objectives, significance, and scope of research conducted in this thesis.

Chapter 2 focuses on studying the effect of using MK and/or different curing conditions on the service life of RC exposed to impressed current corrosion process.

Chapter 3 aims to study the corrosion activity in RC members exposed to different curing temperature/duration using wet-dry cycles corrosion tests.

Chapter 4 contains an experimental investigation to develop design tools using refined statistical analysis to optimize chloride permeability and strength of concrete mixtures containing MK.

Chapter 5 deals with predicting the time dependent reduction in chloride diffusion coefficient for concrete mixtures containing MK.

Chapter 6 includes new models for computing the initiation period for concrete containing MK based on combining MCS and statistical analysis methods.

Chapter 7 presents an improved modeling to predict the time for corrosion-induced cracking in concrete containing MK based on combining XFEM and statistical analysis methods.

Chapter 8 presents the summary and recommendations from the completed research.

1.5 Reference

2012. Design Expert. 9 ed. Minneapolis: Design-Ease® Software
- AKALIN, O., ULAS, A. K. & BAHAR, S. 2010. Self-consolidating high-strength concrete optimization by mixture design method. *ACI Materials Journal*, 107, 357–364.
- ANN, K. Y., PACK, S. W., HWANG, J.-P., SONG, H. W. & KIM, S. H. 2010. Service life prediction of a concrete bridge structure subjected to carbonation. *construction and bulding materials*, 24, 1494-1501.
- BADOGIANNIS, E. & TSIVILIS, S. 2009. Exploitation of poor Greek kaolins: Durability of metakaolin concrete. *Cement and Concrete Composites*, 31, 128-133.
- BAI, J., WILD, S., SABIR, B. B. & KINUTHIA, J. M. 1999. Workability of concrete incorporating pulverized fuel ash and metakaolin. *Magazine of Concrete Research*, 51, 207-216.
- BARNES, P., BENSTED, J. & JONES, T. R. 2003. Metakaolin as pozzolanic addition to concrete. *Structure and performance of cements*. 2 ed. England: CRC press.
- BAYRAMOV, F., TAŞDEMİR, C. & TAŞDEMİR, M. A. 2004. Optimisation of steel fibre reinforced concretes by means of statistical response surface method. *Cement & Concrete Composites*, 26, 665–675.
- BELYTSCHKO, T. & BLACK, T. 1999. Elastic crack growth in finite elements with minimal remeshing. *International journal for numerical methods in engineering*, 601-620.
- BONAKDAR, M., M. BAKHSHI & GHALIBAFIAN, M. 2005. Properties of high-performance concrete containing high reactivity metakaolin. *ACI-SP*, 228, 287-296.
- BROOMFIELD, J. 2007. Corrosion of steel in concrete, understanding, investigating and repair. *Taylor & Francis, London, UK*.
- CABRER, J. G. 1996. Deterioration of concrete due to reinforcement steel corrosion. *Cement and Concrete Composites Journal*, 18, 47–59.

- CASSAGNABÈRE, F., ESCADEILLAS, G. & MOURET, M. 2009. Study of the reactivity of cement/metakaolin binders at early age for specific use in steam cured precast concrete. *Construction and Building Materials*, 23, 775-784.
- CASSAGNABÈRE, F., MOURET, M., ESCADEILLAS, G., BROILLIARD, P. & BERTRAND, A. 2010. Metakaolin, a solution for the precast industry to limit the clinker content in concrete: Mechanical aspects. *Construction and Building Materials*, 24, 1109-1118.
- CHEEWAKET, T., JATURAPITAKKUL, C. & CHALEE, W. 2012. Initial corrosion presented by chloride threshold penetration of concrete up to 10 year-results under marine site, *Constr. . Build. Mater*, 37, 693-698.
- CHEN, J., XU, Q., LI, J. & FAN, S. 2010. Improved response surface method for anti-slide reliability analysis of gravity dam based on weighted regression. *J. Zhejiang Univ.-Sc A.*, 11, 432-439.
- COLEMAN, J. & PAGE, C. L. 1997. Aspects of the pore solution chemistry of hydrated cement pastes containing metakaolin. *Cement and concrete research*, 27, 147-154.
- DHINAKARAN , G., THILGAVATHI, S. & VENKATARAMANA, J. 2012. Compressive strength and chloride resistance of metakaolin concrete. *KSCE Journal of Civil Engineering*, 16, 1209-1217.
- DUBEY, A. & BANTHIA, N. 1998. Influence of high-reactivity metakaolin and silica fume on the flexural toughness of high-performance steel fiber-reinforced concrete. *ACI Materials Journal*, 95, 284-292.
- EHLEN, M. A., THOMAS, M. D. A. & BENTZ, E. C. 2009. Life-365 Service Life Prediction Model™ Version 2.0. *Concrete International*, 31, 41-46.
- ENRIGHT, M. P. & FRANGOPOL, D. M. 1998. Probabilistic analysis of resistance degradation of reinforced concrete bridge beams under corrosion. *Eng. Struct.*, 20, 960-971.
- ERHAN GÜNEYİSİ, GESOĞLU, M., AKOI, A. O. M. & MERMERDAŞ, K. 2014. Combined effect of steel fiber and metakaolin incorporation on mechanical properties of concrete. *Composites Part B: Engineering*, 56, 8-91.

- GHEZAL, A. & KHAYAT, K. H. 2002. Optimizing Self-Consolidating Concrete with Limestone Filler by Using Statistical Factorial Design Methods. *ACI Materials Journal*, 99, 264-272.
- GÜNEYİSİ, E., GESOĞLU, M. & MERMERDAS, K. 2008. Improving strength, drying shrinkage, and pore structure of concrete using metakaolin. . *Materials and Structures*, 41, 937–949.
- GÜNEYİSİ, E. & MERMERDAŞ, K. 2007. Comparative study on strength, sorptivity, and chloride ingress characteristics of air-cured and water-cured concretes modified with metakaolin. *Materials and Structures*, 40, 1161-1171.
- HASSAN, A. A. A., HOSSAIN, K. M. A. & LACHEMI, M. 2009. Corrosion Resistance of Self-Consolidating Concrete in Full-Scale Reinforced Beams. *Cement & Concrete Composites*, 31, 29-38.
- HASSAN, A. A. A., HOSSAIN, K. M. A. & LACHEMI, M. 2012. Effect of Metakaolin and Silica Fume on the Durability of Self-Consolidating Concrete. *Cement & Concrete Composites*, 34, 801-807.
- HOOTON, R. D., GEIKER, M. R. & BENTZ, E. C. 2002. Effects of Curing on Chloride Ingress and Implications on Service Life. *ACI Materials Journal* 99, 201-206.
- JUSTICE, J., KENNISON, L., MOHR, B., BECKWITH, S., MCCORMICK, L., WIGGINS, B., ZHANG, Z. & KURTIS, K. 2005a. Comparison of two metakaolins and a silica fume used as supplementary cementitious materials. *SP-228, ACI, Farmington Hills, Mich*, 213-236.
- JUSTICE, J. M., KENNISON, L. H., MOHR, B. J., BECKWITH, S. L., MCCORMICK, L. E., WIGGINS, B., ZHANG, K. Z. Z. & KURTIS, E. Comparison of two metakaolins and a silica fume used as supplementary cementitious materials. Proc. Seventh International Symposium on Utilization of High-Strength/High Performance Concrete, 2005b Washington D.C.
- KAMARUDIN, H., LIEW, Y., MOHD MUSTAFA AL BAKRI, A., LUQMAN, M., KHAIRUL NIZAR, I. & HEAH, C. 2011. Investigating the possibility of utilization of kaolin and the potential of metakaolin to produce green cement for construction purposes-A review.

- KANG, S. C., KOH, H. M. & CHOO, J. F. 2010. An efficient response surface method using moving least squares approximation for structural reliability analysis. *Probab. Eng. Mech*, 25, 365-371.
- KHATIB, J. M. & CLAY, R. M. 2004. Absorption characteristics of metakaolin concrete. *Cement and Concrete Research*, 34, 19-29.
- KHATIB, J. M. & HIBBERT, J. J. 2005. Selected engineering properties of concrete incorporating slag and metakaolin. *Construction and Building Materials*, 19, 460-472.
- KHAYET, M., COJOCARU, C. & ESSALHI, M. 2011. Artificial neural network modeling and response surface methodology of desalination by reverse osmosis. *Journal of Membrane Science*, 368, 202–14.
- KIRKPATRICK, T. J., WEYERS, R. E., ANDERSON-COOK, C. M. & SPRINKEL, M. M. 2002. Probabilistic model for the chloride-induced corrosion service life of bridge decks. *Cem. Concr. Res.*, 32, 1943–1960.
- LIANG, M., LIN, L. & LIANG, C. 2002. Service life prediction of existing reinforced concrete bridges exposed to chloride environment. *Journal of Infrastructure Systems*, 8, 76-85.
- MADANDOUST, R. & MOUSAVI, S. Y. 2012. Fresh and Hardened Properties of Self-Compacting Concrete Containing Metakaolin. *Construction and Building Materials*, 35, 752-760.
- MALHOTRA, V. M. 2000. Role of supplementary cementing materials in reducing greenhouse gas emissions. In: O.E. GJORN & SAKAI, K. (eds.) *Concrete Technology for a Sustainable Development in the 21st Century*. London, UK: E & FN Spon.
- MAREK, P. 2001. *Probabilistic assessment of structures using Monte Carlo Simulation : background, exercises and software*, Inst. of Theoretical and Applied Mechanics.
- MARSH, P. S. & FRANGOPOL, D. M. 2008. Reinforced concrete bridge deck reliability model incorporating temporal and spatial variations of probabilistic corrosion rate sensor data. *Reliab. Eng. Syst. Saf.*, 93, 394–409.

- MCNALLY, C. & SHEILS, E. 2012. Probability-based assessment of the durability characteristics of concretes manufactured using CEM II and GGBS binders. *construction and Building Materials*, 30, 22-29.
- MEHDIPOUR, I., VAHDANI, M., AMINI, K. & SHEKARCHI, M. 2016. Linking stability characteristics to material performance of self-consolidating concrete-equivalent-mortar incorporating fly ash and metakaolin. 105, 206–217.
- MEHTA, P. K. & MONTEIRO, P. J. M. 1993. *Concrete: Structure, Properties and Materials*, New Jersey, U.S.A., Prentice Hall
- MINDESS, S., YOUNG, F. J. & DARWIN, D. 2003. *Concrete*, Upper Saddle River, Prentice Hall.
- MONTGOMERY, A. D. 2012. *Design and analysis of experiments* New York, Wiley.
- NEHDI, M. L. & SUMMER, J. 2002. Optimization of ternary cementitious mortar blends using factorial experimental plans. *Materials and Structures*, 35, 495–503.
- PAIVA, H., VELOSA, A., CACHIM, P. & FERREIRA, V. M. 2012. Effect of metakaolin dispersion on the fresh and hardened state properties of concrete. *Cement and Concrete Research*, 42, 607-612.
- POON, C. S., KOU, S. C. & LAM, L. 2006. Compressive strength, chloride diffusivity and pore structure of high performance metakaolin and silica fume concrete. *Journal of Construction and Building Materials*, 20, 858–865.
- POUPARD, O., L'HOSTIS, V., CATINAUD, S. & PETRE-LAZAR, I. 2006. Corrosion damage diagnosis of a reinforced concrete beam after 40 years natural exposure in marine environment. *Cement and Concrete Research*, 36, 504–520.
- QIAN, X. Q. & LI, Z. J. 2001. The relationships between stress and strain for high performance concrete with metakaolin,. *Cement and Concrete Research*, 31, 1607-1611.
- QUANWANG, L., KEFEI, L., XINGANG, Z., QINMING, Z. & ZHIHONG, F. 2015. Model-based durability design of concrete structures in Hong Kong–Zhuhai–Macau sea link project. *Structural Safety*, 53, 1-12.

- RAZAK, H. A. & WONG, H. S. 2005. Strength estimation model for high-strength concrete incorporating metakaolin and silica fume. *Cement and Concrete Research*, 35, 688–695.
- RODRIGUEZ, O. G. & HOOTON, R. D. 2003. Influence of cracks on chloride ingress into concrete. *ACI Materials Journal*, 100, 120-126.
- ROUGERON, P. & AİTCIN, P.-C. 1994. Optimization of the composition of a high-performance concrete. *Cement, Concrete and Aggregates*, 16, 115-124.
- ROUGERON, P. & P.C. AİTCIN 1994. Optimization of the Composition of a High-Performance Concrete. *Cement, Concrete and Aggregates*, 16, 115-124.
- SABIR, B. B., WILD, S. & BAI, J. 2001. Metakaolin and calcined clays as pozzolans for concrete: a review. *Cement & Concrete Composites*, 23, 441-454.
- SCHMIDT, S. R. & LAUNSBY, R. G. 1994. *Understanding Industrial Designed Experiments*, Colorado Springs, Colorado, Air Academic Press.
- SONEBI, M. 2004. Medium strength self-compacting concrete containing fly ash: modelling using factorial experimental plans. *Cement and Concrete Research*, 34, 1199–1208.
- SOUDKI, K. A., EL-SALAKAWY, E. F. & ELKUM, N. B. 2001. Full factorial of optimization of concrete mix design for hot climates. *Journal of Materials in Civil Engineering*, 13, 427–433.
- SPEED, T. P. 1987. What is an analysis of variance? (with discussion). *Annals of Statistics*, 15, 885–941.
- UNGER, J. F., ECKARDT, S. & KÖNKE, C. 2007 Modelling of cohesive crack growth in concrete structures with the extended finite element method. *Computer Methods in Applied Mechanics and Engineering*, 196, 4087–4100.
- VIDAL, T., CASTEL, A. & FRANÇOIS, R. 2007. Corrosion process and structural performance of a 17 year old reinforced concrete beam stored in chloride environment. *Cement and Concrete Research*, 37, 1551-61.
- VU, D. D., STROEVEN, P. & BUI, V. B. 2001. Strength and durability aspects of calcined kaolin-blended Portland cement mortar and concrete. *Cement and Concrete Composites*, 23, 471-478.

WONG, S. M., HOBBS, R. E. & ONOF, C. 2005. An adaptive response surface method for reliability analysis of structures with multiple loading sequences. *Structure safety*, 27, 287-308.

ZHANG, X. & BUI, T. Q. 2015. A fictitious crack XFEM with two new solution algorithms for cohesive crack growth modeling in concrete structures. *Engineering Computations*, 32, 473 - 497.

2 Influence of Metakaolin and Curing Conditions on Service Life of Reinforced Concrete

2.1 Abstract

This investigation focuses on studying the effect of using metakaolin (MK) and/or different curing conditions on service life of reinforced concrete exposed to chloride-induced corrosion. Three main stages of service life are studied: corrosion initiation, propagation, and damage periods. The initiation and propagation periods were studied experimentally using small reinforced concrete samples and were also calculated using some available empirical models in the literature for comparison. The experimental variables were the use of MK (0% to 20%), cover thicknesses (20, 30, and 40 mm), and curing conditions (10 different curing temperatures and durations). The experimental results showed that curing conditions had a clear effect on the initiation and propagation periods but showed a non-significant effect (verified by statistical analysis) on the length of the damage period in all tested samples. The incorporation of MK significantly increased both the initiation and propagation periods with little increase in the damage period. The results also indicated that similar trends were found, irrespective of curing condition and cover thickness, from comparing both the initiation and propagation periods using the experimental data and theoretical models.

2.2 Introduction

Reinforced concrete (RC) is widely used in the construction of different types of structures such as: residential buildings, bridge decks, highways, dams, parking garages, and marine structures. Unfortunately, the deterioration of these RC structures could cost hundreds of

millions of dollars in maintenance and repairs. Chlorides from different sources in the surrounding environment can penetrate the concrete cover of these structures leading to rebar corrosion, a process that seriously affects structure serviceability. Due to the expansive nature of corrosion products, rebar corrosion results in a critical deterioration of RC structures in the form of cracking and spalling of concrete around reinforcement. The availability of accurate service life prediction models for RC structures may assist designers and owners to achieve a cost effective strategy for dealing with the exposed structures.

Service life prediction of RC structures subjected to chloride-induced corrosion is generally conducted by estimating two main periods: initiation and propagation (Tuutti, 1982). The first is known as the initiation period (t_{init}), when a certain chloride threshold value reaches the rebar level. This period represents the time taken by the chlorides to penetrate from the external environment through the concrete cover and accumulate at the rebar surface in sufficient amount to breakdown the protective passive layer and initiate corrosion (Mehta and Monteiro, 1993). The length of the initiation period is a function of the depth of concrete cover, concrete quality (curing conditions), exposure conditions, and the chloride threshold required to initiate corrosion (Cady and Weyers, 1983, Maage et al., 1996). The propagation period (t_{prop}) starts when the chloride concentration near the reinforcing bar reaches the chloride threshold. This period is defined as the time required for sufficient corrosion to occur and cause an unacceptable level of damage to the RC structure (ACI 2010). This period is affected by many factors such as concrete cover depth, rate of oxygen diffusion, concrete moisture content and quality, reinforcement bar size, type of structure, and nature of exposure (Browne, 1982).

Alternatively, some service life models of concrete structures subjected to corrosion attack may be divided into three successive stages: diffusion, corrosion, and damage (Bazant, 1979, Cady and Weyers, 1979). These stages include an additional damage stage that follows the onset of cover crack in which severe damage in the concrete cover can eventually lead to cover delamination. The length of the third stage depends on the type of structure and the defined limit states at which the first repair is required. The diffusion phase, in these models, is the time required for chloride ions to ingress into the concrete cover until a certain chloride threshold level at the reinforcement bar is reached. The second phase in these models, the corrosion period, is when corrosion of the reinforcement steel initiates and continues until the first corrosion-induced crack occurs.

Some service life prediction models have been developed to predict the initiation and propagation periods in RC structures based on Fick's law (Maheswaran and Sanjayan, 2004, Wang et al., 2016). For example, LIFE-365 is a computer program that has been designed by the American Concrete Institute to calculate the service life of RC structures. LIFE-365 divides the lifetime into two phases: initiation and propagation. The initiation period in LIFE-365 is calculated using Fick's second law error function solution (Bentz, 2003); however, the propagation period is not accurately predicted and taken as a fixed number of 6 and 20 years when regular and epoxy-coated bars are used, respectively (Bentz, 2003, Life-365, 2015). On the other hand, Liu and Shi (Liu and Shi, 2012) utilized finite element stochastic models to understand the impact of mix design, surface chloride concentrations, cracking level, coarse aggregate, and concrete cover depth on service life of concrete. Recently, Andrade (Andrade, 2015) proposed some improvements of the

available models in the literature to take into account the effect of deterioration rate on the propagation period.

Other models focused on predicting the time from corrosion initiation to corrosion cracking (Bazant, 1979, Morinaga, 1990, Liu and Weyers, 1998, El Maaddawy and Soudki, 2007). Further verification of these models is needed to take into account the influence of concrete quality on the length of this period, especially when using concrete with supplementary cementitious materials (SCMs). The use of SCMs such as fly ash, silica fume, and metakaolin (MK) in the production of durable concrete structures is expected to have a significant impact on the overall service lifetime. For instance, Sangoju et al. (Sangoju et al., 2015) found that the use of fly ash-based portland pozzolana cement can double the predicted service life of RC exposed to chloride-induced corrosion compared with ordinary portland cement. Nevertheless, information about how these materials (especially MK) affect successive stages of service life is still limited. Also, the current available information regarding the severe corrosion stage (especially propagation and damage stages) is insufficient.

Metakaolin is a supplementary cementing material which is produced from carefully calcining kaolin clay between 600 °C and 800 °C to make it reactive. Exceeding this temperature can cause the metakaolin be less reactive or even inert. Metakaolin is composed mainly of alumina and silica phases, which can vary by approximately 10% and 8% respectively depending on the kaolin source. Metakaolin improves concrete performance by reacting with available calcium hydroxide to produce secondary calcium silica hydrate.

The main objective of this investigation was to study the effect of using MK and/or different curing conditions on three corrosion stages throughout the service life of RC structures (initiation, propagation, and damage periods). The characteristics and length of each corrosion period were highlighted in this paper. The ratios between the propagation period and initiation period were found experimentally using small RC samples subjected to an accelerated corrosion process. Meanwhile, the results of both initiation and propagation periods were compared to results calculated using some available empirical prediction models. The effects of curing conditions (variable temperatures and durations), incorporation of MK, and concrete cover thickness on the length of each period were also studied and evaluated in this investigation.

2.3 Research Significance

The current available service life prediction models commonly divide the lifetime of concrete structures into two periods only (initiation and propagation periods) and do not cover the severe corrosion (damage) stage of the structure. In addition, the available models usually assume the propagation period as a fixed period regardless of the concrete type, curing technique, and/or cover thickness. Moreover, there is a lack of information regarding the effect of MK incorporation on the length of initiation, propagation, and damage periods. The influence of different curing techniques, such as cold and hot curing (especially with varied temperatures and durations), on these periods also requires further investigations. This study focused on experimentally identifying three corrosion stages (initiation, propagation, and damage periods) highlighting the effect of concrete curing, cover

thickness, and the use of MK on the lengths of these periods. The study also compares the experimental results of the different corrosion periods with the data obtained from two theoretical models.

2.4 Research Program

The research program described herein studied the corrosion initiation, propagation, and damage periods in 78 concrete specimens subjected to an accelerated corrosion test. Sixty tested specimens were made from one identical normal concrete mixture (without MK) and were divided into three groups of samples characterized by their concrete cover thickness (20, 30, and 40 mm). Each group consisted of 20 specimens with 2 specimens tested under 10 different curing techniques (variable times of heat, cold, air, and water curing). One of these two specimens was designed to study the corrosion initiation and propagation periods, while the second one was made to study the corrosion damage period. **Table 2.1** presents the test matrix including all the variables included in this research program. It is worth noting that, owing to the fact that corrosion is a non-uniform problem, it is recommended to use higher number of replicates to improve the repeatability and reliability of the results. However, the total number of samples tested in this study was limited to 78, due to the relatively long test durations (especially in the samples containing MK). Therefore, further testing on larger number of samples and concrete types is recommended to confirm the outcomes from this preliminary study.

The main reason for having 10 different curing techniques was to develop 10 different concrete qualities in order to study the effect of concrete quality on the corrosion periods. The quality of the concrete, in this investigation, was judged based on the initial electrical

current generated in each specimen right after starting the accelerated corrosion test with applying a constant 12 voltage on all samples. This value of the initial electrical current reflects the resistance of each sample (under the same electrical voltage) with different concrete thicknesses around the embedded bar. In this paper, the quality of concrete is referred as the resistivity of the sample, which is different from both chloride diffusion and permeability of concrete obtained using bulk chloride diffusion and rapid chloride penetration standard tests, respectively(Andrade, 1993).

An additional 18 samples were also prepared using three variable concrete mixtures containing MK (6.5, 12.5, and 20%). The inclusion of MK in these mixtures was expected to develop three additional concrete types with variable chloride diffusion and permeability represented as 6.5% MK, 12.5% MK, and 20% MK. Similar to the 60 samples mentioned above, two specimens were tested for each of the three concrete covers (20, 30, and 40 mm) in each percentage of MK (total of 18 samples). All MK samples were cured using an identical water-curing technique similar to that utilized to develop concrete quality 4 (the highest quality of mixtures without MK) in the normal concrete samples. Owing to using three MK mixtures and one normal concrete with varied curing conditions (10 scenarios), the samples had 13 variable resistances to chlorides (13 concrete qualities). The results of the 13 concrete qualities were given numbers from 1 to 13, as 1 indicates the specimen with the highest concrete resistivity/quality (lowest initial electrical current and lowest chloride diffusion coefficient) and 13 indicates the specimen with the lowest concrete resistivity/quality (highest initial electrical current and highest chloride diffusion coefficient). It should be noted that since mixtures with higher percentages of MK had the

higher concrete quality, mixtures with 20% MK, 12.5% MK, and 6.5% MK were given numbers 1, 2, and 3, respectively.

After casting and curing, all samples were subjected to an accelerated corrosion test; the time versus electrical current history was recorded and plotted for each specimen (**Figure 2.1**). In addition, an average half-cell potential reading was taken for each specimen along its length/perimeter. As shown in **Figure 2.1**, the typical electrical current-time for the tested samples showed a gradual drop of the initial electrical current in the first few hours followed by a gradual increase. The drop of the initial electrical current at the beginning of the test indicates the formation of a passive film around the reinforcing bar, which protects the steel from corrosion. On the other hand, the gradual increase of the electrical current after reaching the lowest point indicates the de-passivation of the protective film (Cornet et al. 1968). The time taken from the start of the test until the electrical current reached the lowest point of the curve was taken in this investigation as the corrosion initiation period (T_i). Moreover, a chloride content test was performed (at the time of detecting corrosion initiation according to the lowest point of the electrical current) to measure the chloride threshold to confirm the initiation of corrosion. Meanwhile, the time taken from the lowest point of the curve until the initiation of the first visual crack was taken as the propagation period (T_p). The damage period (T_d) was measured from the end of the propagation period until the initiation of a 4 mm crack in the specimen (which is often followed by the breaking of the concrete cover). The damage period was also confirmed from the electrical current-time graph, when the electrical current suddenly jumped and reached the highest point because of the crack opening.

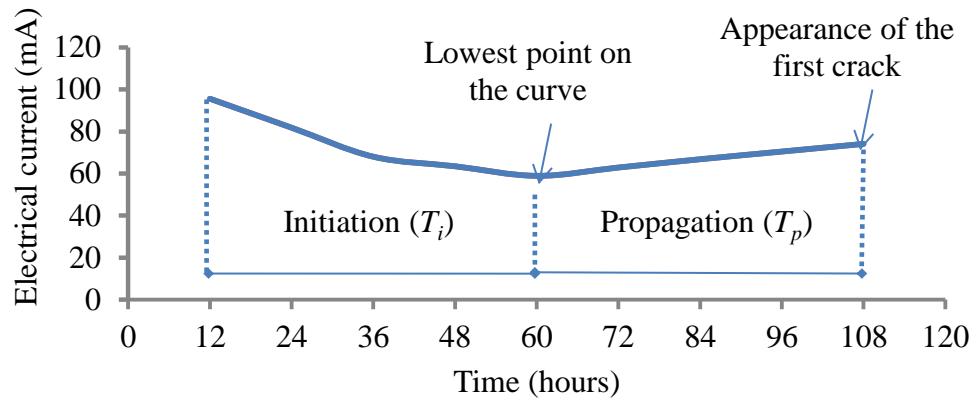


Figure 2.1 Typical Electrical Current vs. Time Curve

Table 2.1 Test Matrix

Total Number of Samples (Replicates)	Test Variables		
	Curing Technique	Mixture Type	Cover Thickness (mm)
60 (2)	Varied (10 different conditions up to 28 days)	Normal Concrete	20, 30 and 40
6 (2)	Cured in water for 28 days at 23° C	6.5% MK	20, 30 and 40
6 (2)	Cured in water for 28 days at 23° C	12.5% MK	20, 30 and 40
6 (2)	Cured in water for 28 days at 23° C	20% MK	20, 30 and 40

The electrical current readings, half-cell potential measurements, and crack widths (once detected) were carefully checked every 12 hours during the accelerated corrosion test. In addition to the experimental investigation, the values of the initiation and propagation periods were also calculated using some available models in the literature (see Section: Theoretical Comparison between Experimental Data and Prediction Model) and compared to those found experimentally. This comparison was performed to investigate/confirm the

impact of concrete quality, use of MK, and cover thickness on the time to corrosion initiation and propagation, which was obtained by accelerated corrosion experiments.

2.5 Experimental Procedure

2.5.1 Materials

In this investigation, 60 tested specimens were made from one concrete mixture. They were identical in terms of mixture proportions and type of materials used. Three additional mixtures, having MK as a partial cement replacement, were used to cast the remaining 18 samples. Type GU Canadian Portland cement similar to ASTM Type I was used in this study. The chemical and physical properties of this cement are shown in **Table 2.2**. The coarse and fine aggregates each have a specific gravity of 2.70 and water absorption of 1%. The MK used was delivered from the Eastern United States by Advanced Cement Technologies; conforming to ASTM Class N. A 20M bar (with nominal diameter of 19.5 mm) was used in all tested specimens. The complete proportions of all mixtures utilized in this paper are shown in **Table 2.3**.

Table 2.2 Chemical and Physical Properties of Cement

Chemical properties %	Cement	MK
SiO ₂	19.64	51-53
Al ₂ O ₃	5.48	42-44
Fe ₂ O ₃	2.38	<2.2
FeO	-	-
TiO ₂	-	<3
C	-	-
P ₂ O ₅	-	<0.2
SO ₄	-	<0.5
CaO	62.44	<0.2
MgO	2.48	<0.1
Na ₂ O	-	<0.05
C ₃ S	52.34	-
C ₂ S	16.83	-
C ₃ A	10.5	-
C ₄ AF	7.24	-
K ₂ O	-	<0.4
Loss on ignition	2.05	<0.5
Physical properties		
Specific density	3.15	2.56
Color	gray	pink
Grain size (μm)	45	60
Surface area(m ² /kg)	320-400	650-1250
Blaine fineness(m ² /kg)	410	19000

Table 2.3 Mixture Proportions

Concrete Type	Total Binder (kg/m ³)	Cement (kg/m ³)	w/c	MK (kg/m ³)	10 mm Stone (kg/m ³)	Sand (kg/m ³)	Water (kg/m ³)	HRWRA (l/m ³)
Normal Concrete	450	450	0.4	0	834	927	180	4.5
6.5% MK	450	421	0.4	29	831	924	180	5.3
12.5% MK	450	394	0.4	56	829	921	180	7.6
20% MK	450	360	0.4	90	826	918	180	8.7

2.5.2 Samples Details

As previously noted, 78 RC specimens were tested under accelerated corrosion tests with the procedure explained in the following section (Casting, Curing and Test Setup). All

specimens were 250 mm in length and contained one 20M steel bar embedded in the center of each specimen. The cross-sectional dimensions and the embedded bar lengths were varied to maintain the required concrete cover for each specimen type (**Figure 2.2**). The specimens were divided into three groups with different concrete covers (20, 30, and 40 mm). Each group contained 26 prisms (two identical samples tested under 13 concrete qualities) and the dimensions are shown in **Figure 2.2**. The reinforcing steel was placed at the center of each sample (by hanging the bars to the sides of the formwork) to ensure equal covers from all directions (**Figure 2.2**). Two wires were attached to the embedded steel bar; the first wire was connected to the power supply while the second one was a spare wire in case the first wire's connection was damaged while the concrete was poured. The second wire was also used to check the connectivity of the main wire with the embedded steel bar (by reading the resistance between the two wires) after pouring the concrete. The surface of the bars was cleaned using a wire brush then the wires were carefully tied to the clean surface and covered/sealed by electrical tape.

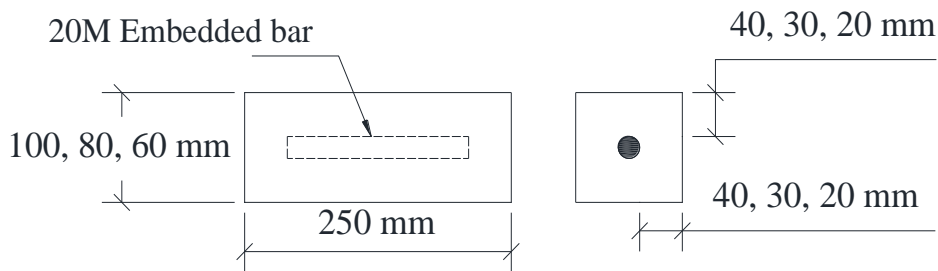


Figure 2.2 Test Specimen Details

2.5.3 Casting, Curing and Test Setup

The mixture ingredients were blended in a rotary mixer. Immediately after mixing the concrete, the specimens were cast in the prepared wooden forms. The molds were removed

the next day and the samples were cured using 10 different curing techniques (for total periods of 28 days) before starting the accelerated corrosion test. The description of these 10 different curing techniques is presented in **Table 2.4**. The specimens were designated according to their concrete cover (20, 30, or 40 mm) and concrete quality (sorted from 1 to 13 based on the specimen 28-day D_a result shown in **Table 2.5**). For example, a specimen with a concrete cover of 20 mm and a quality of 4 was designated as 20S4. In the meantime, additional (102 mm diameter x 203 mm height) cylindrical samples were cast from each concrete mixture to measure both compressive strength and chloride permeability/diffusion. The 28 days chloride permeability was primarily evaluated by means of the RCPT as per ASTM C1202 (1997). Meanwhile, the chloride diffusion coefficient (D_a) for the 13 concrete qualities/mixtures was determined using a bulk diffusion test according to ASTM C1556 (2011).

The accelerated corrosion test setup used in this study consisted of a tank, electrolytic solution (5% NaCl by the weight of water), and a stainless steel mesh placed at the bottom of the tank (similar to (Hassan et al., 2009b, Sangoku et al., 2015, Shaikh et al., 2015, Hassan et al., 2010)). All tested samples were fully submerged in the electrolyte solution and connected to the power supply (**Figure 2.3**). The accelerated corrosion process was conducted by applying an electrical current to the reinforcing bars. The specimen's steel bars and the bottom steel mesh in the tank were connected to a DC power supply applying constant 12 volts for all samples. The direction of the current was arranged so that the steel mesh served as a cathode while the specimen bars served as anodes and the pore solution in the concrete acted as the electrolyte. After the power supply was turned on, the current flowing through the system was recorded, and the cracks were visually monitored during

the test. The crack widths were measured during the damage period using a microscope with a graduated scale of 0.002 mm increments.

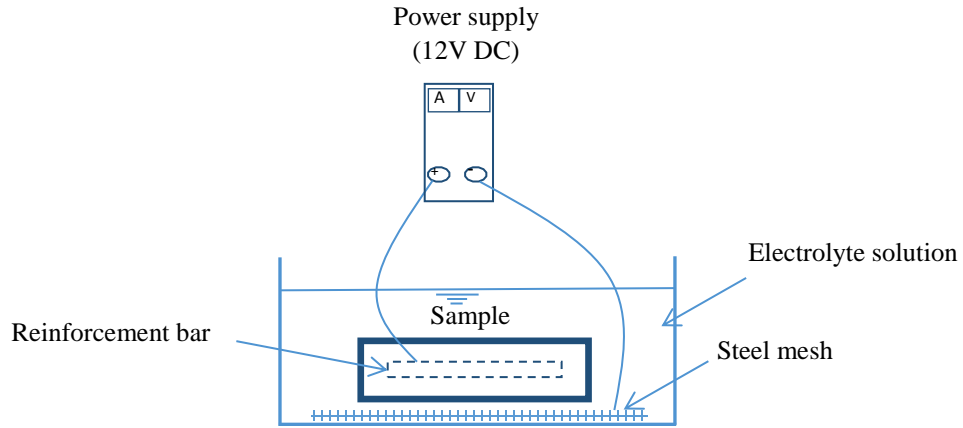


Figure 2.3 Accelerated Corrosion Schematic

Table 2.4 Description of Different Curing Techniques

Curing Technique	Description
1	28 days in air at 23° C
2	28 days in water at 23° C
3	3 days in water then air both at 23° C
4	7 days in water then air both at 23° C
5	3 days in water at 23° C then air at 3-5° C
6	7 days in water at 23° C then air at 3-5° C
7	28 days in air at 3-5° C
8	1 day in water at 50° C then water at 23° C
9	3 days in water at 50° C then water at 23° C
10	7 days in water at 50° C then water at 23° C

Table 2.5 Properties of Various Concrete Qualities

Concrete Quality	Curing Technique (Defined in Table 2.4)	Mixture Type	28-Day f_c' (MPa)	28-Day f_t (MPa)	28-Day D_a x 10^{-12} (m ² /sec)	RCPT (Coulombs)
1	2	20% MK	93.61	10.57	1.91	303
2	2	12.5% MK	84.53	8.61	2.50	553
3	2	6.5% MK	78.04	7.93	3.01	965
4	2	Normal Concrete	76.16	7.81	7.52	2072
5	6		69.21	7.64	7.85	2100
6	5		65.85	7.42	7.99	2130
7	4		75.44	7.45	8.32	2432
8	3		73.33	7.49	8.86	2596
9	1		53.16	5.65	9.33	3000
10	7		47.45	5.68	9.62	3120
11	8		58.91	5.95	12.21	3093
12	9		59.38	6.69	15.02	3633
13	10		57.88	6.37	18.01	3700

Half-cell potential test (ASTM C876 1991) using a reference copper–copper sulphate electrode was performed every 12 hours (at the same time the reading of the current was taken) up to the end of the initiation period only (**Figure 2.4**). The power supply was disconnected and the samples were allowed to depolarize prior to the half-cell potential readings. Besides, all sample readings were taken at the same time and in the same moist surface conditions in order to ensure fair comparison between all specimens. Once the corrosion initiation was detected, the samples were drilled and concrete dust was collected to determine the chloride content at the surface of steel bar using a Chlorimeter, following the procedures stated in ASTM C1556 standard (2011).



Figure 2.4 Half-Cell Potentials Test

2.6 Experimental Results and Discussions

The results of the 28-day compressive strength (f_c') and splitting tensile strength (f_t) for the 13 concrete qualities evaluated in this paper are shown in **Table 2.5**. It was found that the highest f_c' and f_t , and lowest D_a were associated with the mixture with 20% MK followed by 12.5% MK and 6.5% MK, represented by qualities 1, 2, and 3, respectively. At the end of the accelerated corrosion tests, all tested samples were broken and the corroded steel bars were extracted. The bars were then cleaned and the amount of steel mass loss was determined as per the ASTM G1 standard method (2011). The percentages of steel mass losses at both propagation and damage stages for all tested specimens are shown in **Table 2.6**.

Table 2.6 Service Lifetimes Calculated from the Accelerated Corrosion Tests of all Samples

Sample No.	Initial Current (mA)	Half-Cell (mV)	T_i (h)	Standard Deviation (T_i)	Chloride Threshold (% wt. of Concrete)	T_p (h)	Standard Deviation (T_p)	Mass Loss at Propagation (%)	Mass Loss at Damage (%)	T_d (h)	T_p/T_i
20S1	69.7	-524	140	5.66	0.576	211	1.41	1.89	8.69	137	1.51
20S2	76.4	-544	107	1.41	0.445	150	0.00	1.66	8.01	140	1.40
20S3	82.1	-539	96	0.00	0.393	117	4.24	1.49	5.69	129	1.21
20S4	94.8	-557	62	2.83	0.440	54	0.00	1.48	6.92	112	0.87
20S5	95.6	-550	60	0.00	0.345	44	2.83	1.19	4.20	128	0.73
20S6	98.9	-536	60	0.00	0.400	46	5.66	1.24	5.08	124	0.77
20S7	102.9	-540	58	2.83	0.288	48	8.49	1.29	3.98	98	0.83
20S8	104.2	-553	38	2.83	0.181	36	0.00	1.16	10.24	56	0.95
20S9	105.9	-570	58	2.83	0.160	44	2.83	1.61	5.08	126	0.76
20S10	109.9	-580	56	5.66	0.114	40	2.83	1.51	10.17	132	0.71
20S11	110.3	-585	56	5.66	0.114	44	2.83	1.37	8.47	80	0.79
20S12	112.2	-590	38	2.83	0.087	34	2.83	1.50	9.75	108	0.89
20S13	113.2	-570	56	5.66	0.016	48	0.00	1.35	3.81	100	0.86
30S1	49.2	-507	350	2.83	0.775	466	5.66	3.19	10.88	150	1.33
30S2	56.1	-510	280	5.66	0.695	325	1.41	2.90	9.09	137	1.16
30S3	60.9	-469	233	7.07	0.679	249	4.24	2.44	8.22	120	1.07
30S4	75.2	-460	150	0.00	0.662	114	0.00	2.25	7.67	180	0.76
30S5	77.8	-502	144	0.00	0.655	92	2.83	1.95	7.12	136	0.64
30S6	82.2	-480	136	2.83	0.628	124	2.83	2.56	9.35	182	0.91
30S7	85.9	-442	134	1.41	0.541	116	5.66	2.39	9.56	170	0.87
30S8	86.1	-511	130	2.83	0.459	94	2.83	2.13	3.50	76	0.72
30S9	93.2	-480	132	0.00	0.411	90	0.00	2.33	7.69	102	0.68
30S10	94	-514	132	0.00	0.358	102	0.00	2.42	6.38	66	0.77
30S11	98.4	-476	130	1.41	0.235	98	5.66	2.57	8.11	124	0.75
30S12	98.8	-507	102	0.00	0.124	74	4.24	1.96	8.01	80	0.73
30S13	104.1	-540	84	0.00	0.107	66	0.00	1.72	7.38	110	0.79
40S1	32.3	-403	1156	5.66	0.838	1090	5.66	5.13	15.02	196	0.94
40S2	41.5	-377	980	2.83	0.819	929	7.07	4.55	13.12	183	0.95
40S3	46.2	-379	802	5.66	0.775	745	1.41	3.96	11.69	167	0.93
40S4	51.2	-396	378	0.00	0.775	228	0.00	3.19	10.04	179	0.60
40S5	62.2	-350	376	2.83	0.743	230	5.66	3.69	8.57	150	0.61
40S6	66.2	-325	320	5.66	0.710	228	0.00	3.93	8.71	162	0.71
40S7	68.8	-360	308	7.07	0.669	220	2.83	3.86	6.22	156	0.71
40S8	75.9	-335	336	0.00	0.473	228	0.00	4.52	12.64	148	0.68
40S9	76.4	-350	284	2.83	0.447	208	2.83	4.14	11.16	162	0.73
40S10	80.9	-460	285	4.24	0.478	215	1.41	4.06	8.20	182	0.75
40S11	83.7	-520	260	5.66	0.423	168	0.00	3.64	7.20	128	0.65
40S12	86.4	-490	170	2.83	0.208	130	2.83	2.91	7.83	100	0.76
40S13	89.1	-476	156	0.00	0.202	132	0.00	3.01	5.83	88	0.85

2.6.1 Effects of Cover Thickness on the Corrosion Initiation/Propagation Periods

Table 6 presents the results of the corrosion initiation periods in the 20, 30, and 40 mm concrete cover specimens. The 20 mm specimens developed an average initiation period of 68 hours, compared to the 30 and 40 mm specimens, which showed a higher initiation pattern with an average of 164 and 447 hours, respectively. The propagation period was attained by visual inspection of all samples at the time of first crack detection (**Table 2.6**). At the end of the propagation period, all tested specimens experienced one longitudinal hair crack extending along the length of the bar. The crack widths for all specimens at the end of the propagation periods ranged from 0.01 mm to 0.05 mm. Again, all larger concrete cover samples showed longer propagation periods compared to the smaller cover samples, irrespective of concrete qualities or mixture proportions. The 20 mm cover samples showed an average propagation period of 70 hours, while the 30 and 40 mm cover samples showed a higher propagation period with an average of 155 and 365 hours, respectively. **Figure 2.5** shows the relationship between T_i and T_p versus cover thickness for all tested samples. The figure indicates that increasing cover thickness (20 to 40 mm) yielded larger values of T_i and T_p at all concrete qualities (1 through 13). The results also indicated that as the thickness of the concrete cover increased, the corrosion initiation period increased slightly more than the increase of the propagation period. For example, the average initiation period of all tested samples increased 6.57 times when the concrete cover increased from 20 to 40 mm, while the average propagation period increased 5.19 times. This can also be observed from **Table 2.6**; the average values of T_p/T_i were smaller at larger concrete cover. The average T_p/T_i ratios of all 20, 30, and 40 mm samples were as follows: 0.94, 0.86, and 0.76, respectively. These results may suggest that the increase of cover thickness yielded an

almost linear reduction trend in the ratios of T_p/T_i . Nevertheless, further experiments including larger values of cover thicknesses (> 40 mm) are needed to generalize this trend.

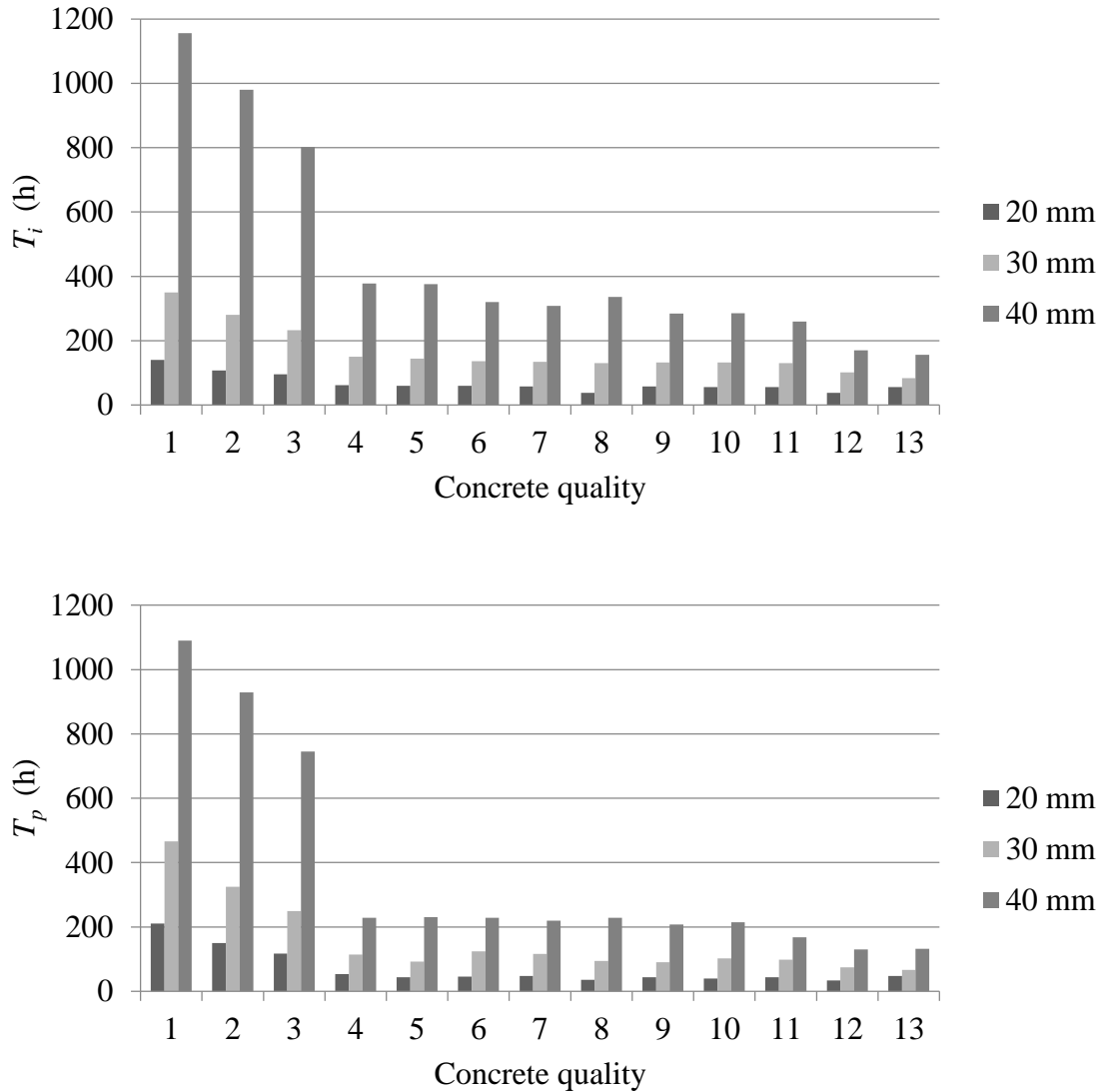


Figure 2.5 Relationship between Cover Thickness and Initiation/Propagation Periods: a) T_i and b) T_p

2.6.2 Effects of Concrete Quality on the Corrosion Initiation and Propagation Periods

When the concrete samples were connected to the power supply, the electrical current flowed through the concrete between the anodic (embedded bar) and cathodic (steel mesh)

sites due to the migration of ions. Low quality concrete (high chloride diffusion coefficients) has low resistance and should have higher currents passing through it. Therefore, the samples that had the highest initial current and high chloride diffusion in this investigation were assumed to have the lowest concrete quality and were expected to have the shortest corrosion period. **Table 2.6** presents the results of corrosion periods for all tested samples. As expected, both the initiation and propagation times increased as the initial current decreased. The initial current also decreased (indicating higher concrete resistivity in terms of chloride permeability/diffusion) as the concrete cover was increased from 20 to 40 mm. **Figure 2.6** shows the relationship between the initial current and both T_i and T_p at the three concrete covers for the 60 specimens with the normal concrete mixtures (qualities ranged from 4 to 13). It is clear from this figure that the concrete quality (as assessed through initial current measurements) had an effect on both the initiation and propagation periods. Unlike the effect of cover thickness on the T_p/T_i ratio (which decreased by using thicker concrete covers), different concrete qualities showed no clear influence on the T_p/T_i ratio. It can also be observed from **Table 2.6** that T_p/T_i ratios of MK samples were larger than 1.0 in both 20 and 30 mm and almost 1.0 in 40 mm cover samples compared with all other samples less than 1.0. This trend may indicate that MK samples resulted in longer propagation than initiation periods in most cases, unlike normal concrete specimens. However, further tests on different MK mixtures are warranted to confirm this observation. On the other hand, as seen in **Table 2.6**, the values of steel mass loss at the end of the propagation period were measured for all tested samples; different concrete qualities had no significant effect on the percentage of mass loss in the same concrete cover. However, concrete with 40 mm concrete cover showed higher average ratio of steel mass loss

compared to concrete with 30 and 20 mm concrete covers (3.89% in 40 mm, 2.37% in 30 mm, and 1.44% in 20 mm). This increase in the percentage of steel mass loss with higher concrete cover thickness is possibly related to the longer time required for cracks to become visible in thicker samples, as seen from T_p results in **Table 2.6**.

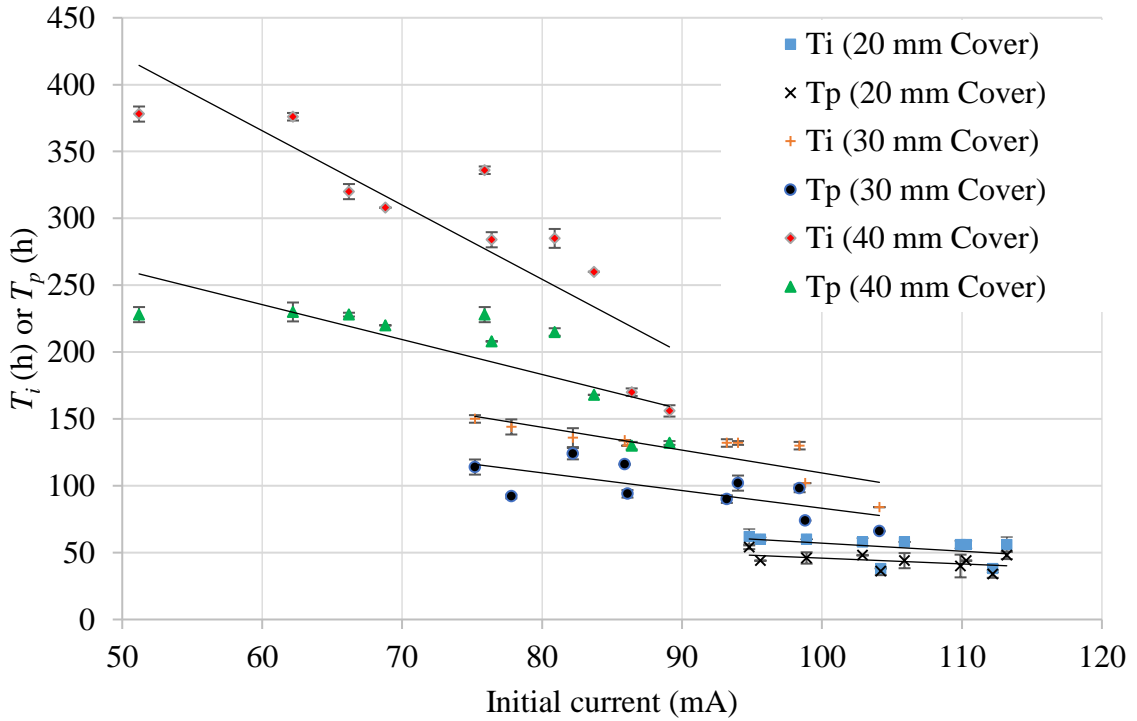


Figure 2.6 Initiation and Propagation Periods vs. Initial Current

The results from the RCPT and chloride diffusion indicated a significant effect of the curing techniques (concrete quality) and MK replacement on the chloride permeability. It is clear from **Table 2.6** that a minimum chloride diffusion coefficient of $1.91 \times 10^{-12} \text{ m}^2/\text{sec}$ was associated with the sample that had the minimum RCPT coulombs. Moreover, a maximum value of chloride diffusion of $18.0 \times 10^{-12} \text{ m}^2/\text{sec}$ was also associated with the highest RCPT results, which indicated the maximum chloride permeability. Concrete quality was

also reflected in the chloride threshold measured at the end of initiation period. In **Table 2.6**, it can be seen that increasing the concrete quality increased the required chlorides to start corrosion. This trend can be attributed to the impact of concrete quality on the pH of the pore solution, which warrants an increase in the critical chloride content required to initiate corrosion in steel (Justnes, 1998). In addition, this effect may be related to the influence of the possible changes in chloride binding capacity as a result of variable concrete qualities (Panesar and Chidiac, 2011). Nevertheless, the effect of chloride binding capacity is outside the scope of this investigation. **Figure 2.7** represents the relation between the RCPT and chloride threshold, it can be seen that as RCPT increase, the chloride threshold decrease.

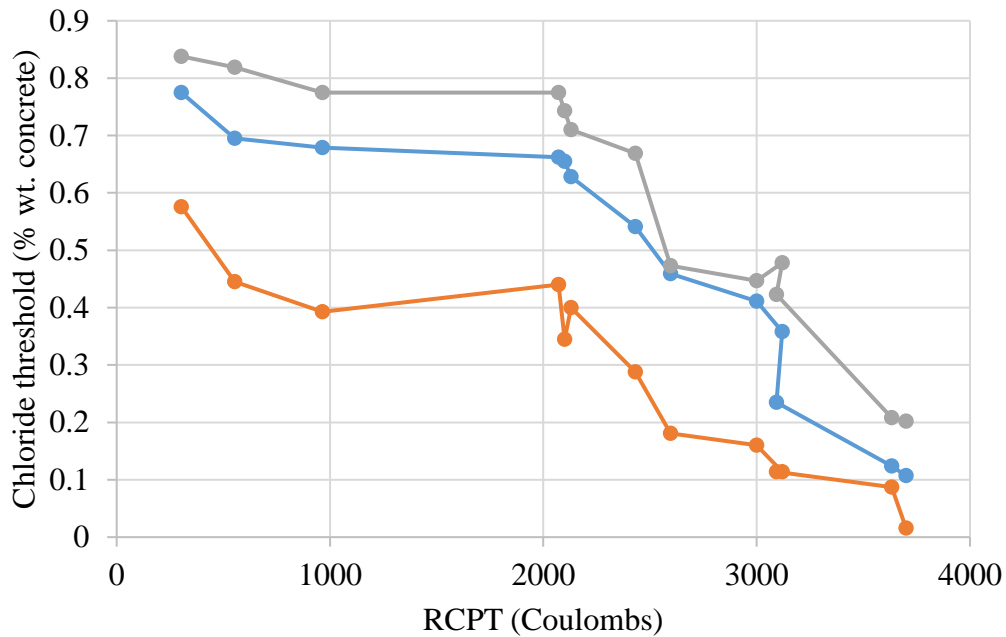


Figure 2.7 Concrete Quality vs. Chloride Threshold

2.6.3 Effect of MK Replacement on the Corrosion Initiation and Propagation Periods

By comparing the normal concrete mixtures with their MK counterpart specimens, as shown in **Table 2.6**, it can be seen that the inclusion of MK yielded a significant effect on both initiation and propagation periods and the corresponding T_p/T_i ratio (average values of samples with MK mixtures compared to the average of samples with normal concrete mixture). **Table 2.6** indicates that increasing the MK replacement level from 0 to 20% resulted in a general increase in both initiation and propagation periods at all values of cover thicknesses. For instance, increasing the MK percentage in the 20 mm cover samples from 0 to 6.5%, 12.5%, and 20% resulted in 55%, 73%, and 126% higher initiation periods and 117%, 178%, and 291% longer propagation periods, respectively. Similar increasing trends in both initiation and propagation periods were also seen when using higher MK replacements in the 30 and 40 mm cover samples. This overall increase in the initiation periods due to the MK replacement is attributed to the minimized chloride permeability and diffusion coefficients of MK mixtures compared to normal concrete mixtures (see **Table 2.5**). On the other hand, the increase in the propagation periods as a result of increasing the MK percentage may be related to the overall higher tensile strength of concrete containing higher MK replacement, as shown in **Table 2.5**.

It can also be noticed from **Table 2.6** that all mixtures containing MK exhibited longer average initiation and propagation periods than those obtained from normal concrete mixture regardless of curing technique or cover thickness. For example, the average initiation time of the 20 mm samples cast with MK mixtures was 111% higher than that obtained from the samples constructed with normal concrete mixtures. Similarly, the

average propagation period of the 20 mm MK samples was 264% higher than the average propagation period of normal concrete samples, as demonstrated in **Table 2.6**. This was also the case for other samples with 30 and 40 mm covers. This significant increase in the initiation and propagation stages was expected from the incorporation of MK in the mixture, which resulted in denser microstructure and overall low chloride penetrability of these mixtures.

It can also be observed from **Figure 2.8** that the corrosion initiation and propagation time with chloride penetrability and chloride diffusion of concrete are closely related to each other. The analysis of results showed that there is a good correlation between corrosion initiation time and total charge and chloride diffusion coefficient passed through concrete specimens, same trend is followed in propagation period. It is clear also that increasing the resistivity of concrete mixture (in terms of chloride permeability/diffusion) increases the propagation and initiation period compared with lower resistivity concrete.

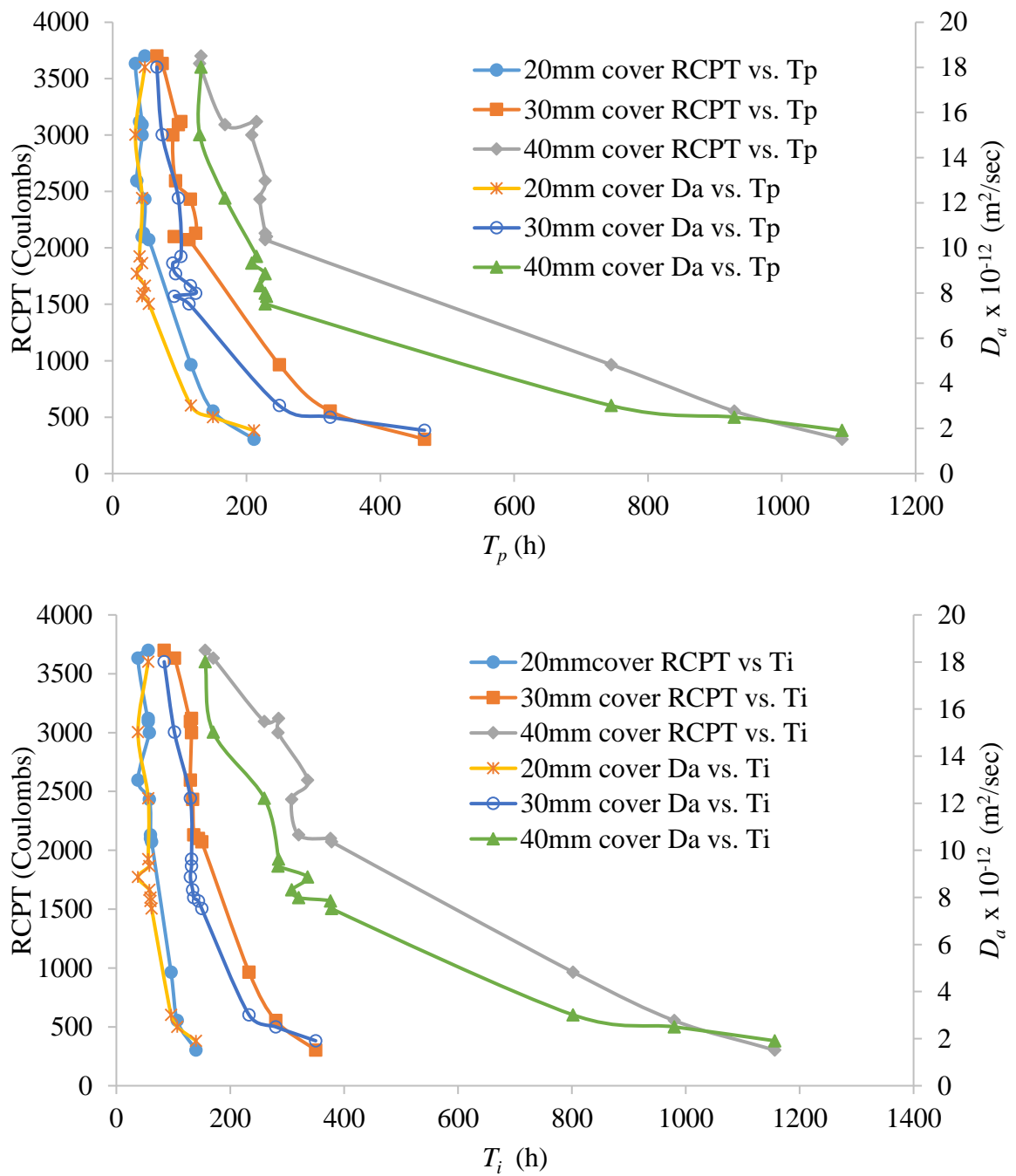


Figure 2.8 Relationship between RCPT/Chloride Diffusion Coefficient (D_a) and: a) T_i and b) T_p

2.6.4 Damage Period

Table 2.6 presents the results of the damage periods of all tested samples. As seen from this table, the variation of the results of this period was somehow high. In this investigation,

the damage period was obtained at the time of the formation of a 4 mm crack. As a result, these relatively high variations in the damage periods may be related to the changes in the number of cracks and crack patterns having the same crack width (4 mm). In addition, the corrosion that caused this 4 mm crack could be either localized or uniformly distributed. The occurrence of localized corrosion can result in a shorter 4 mm crack than that seen from well-distributed corrosion.

The results of this investigation indicated that the damage period does not seem to be significantly affected by the concrete quality (in terms of varied curing technique and mixture proportions) or cover thickness. This finding was further confirmed after performing an analysis of variance (ANOVA) on the results of the damage period. The ANOVA results for the effects of the concrete quality and cover thickness on the damage period are presented in **Table 2.7**. It was found that both concrete quality and cover thickness have a statistically non-significant effect on the length of the damage period based on a 5% significance level. It can also be concluded that the cover thickness has a greater effect on the damage period than concrete quality does according to the F values of those two factors (**Table 2.7**). This can be noticed from the slight increase in the average damage periods when cover thickness was increased from 20 to 40 mm. The average damage periods of the 20 mm cover samples were 113.1 hours while those for the 30 and 40 mm covers were 125.6 and 153.9, respectively. Meanwhile, the average mass losses of the same covers were 6.93, 7.92, and 9.71% for the 20, 30, and 40 mm concrete cover samples, respectively. This slight increase in the damage periods may have resulted from the longer amount of time it took the 4 mm crack to show on a higher cover thickness. In addition, the damage period seems to be independent of the initiation or propagation periods.

Table 2.7 ANOVA Results for the Effect of Different Factors on the Damage Period

Factor	Sum of Squares	df	Mean Square	F-Value	p-Value Prob > F	Significance
Concrete Quality	20625.12	12	1718.76	1.48	0.22	not significant
Concrete Cover	7718.87	2	3859.43	3.36	0.05	not significant

2.6.5 Half-Cell Potential Readings

The half-cell potential measurement was used to indicate the probability of corrosion of the steel reinforcement. In general, the half-cell potential readings followed the same trend of variation as those of the current readings during the entire test. The half-cell potential readings at the end of the initiation period for all tested samples are presented in **Table 2.6**. Despite the small variation in the results at the end of the initiation period for all tested samples, the results can secure an average reading for each concrete cover. The half-cell potential readings at the end of the initiation period showed an average of -556, -492, and -402 mV for the 20, 30, and 40 mm concrete cover samples, respectively. **Figure 2.9** shows the half-cell potential readings for the tested samples (qualities ranged from 1 to 13) of 20, 30, and 40 mm cover samples separately. This figure indicates that the half-cell potential readings increased (moved toward less negative values) as the quality of the concrete improved. This was clear from the slope of the trend line of the readings for each concrete cover. The figure also indicated that the results of the half-cell potentials became more scattered as the concrete cover increased, indicating less accuracy with higher concrete covers. As the size of concrete cover increased, the reading increased (moved toward small negative values).

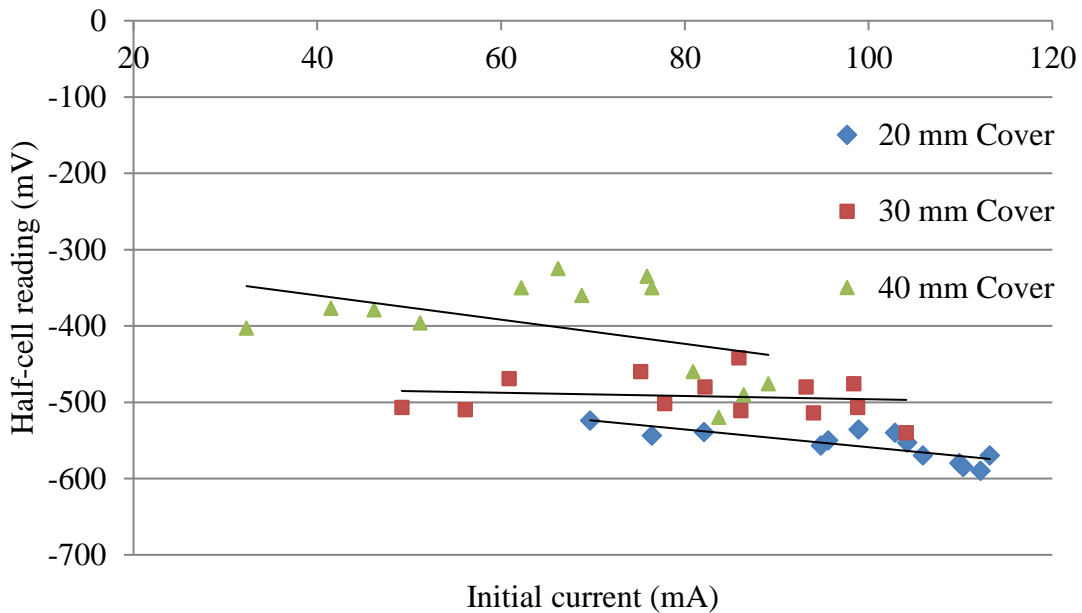


Figure 2.9 Half-Cell Potential Readings

2.6.6 Theoretical Comparison between Experimental Data and Prediction Models

2.6.6.1 Prediction of Initiation Period

The initiation period was estimated using one of the available models from the literature (based on a Monte Carlo simulation) for the purpose of comparing it with the initiation period obtained from the experimental results, considering only variable concrete qualities (cover thickness was constant). Probabilistic analysis, similar to that performed by Bentz (Bentz, 2003) and Val and Trapper (Val and Trapper, 2008), was employed using the Monte Carlo simulation to obtain the probability of corrosion initiation. 50,000 iterations were utilized until the chloride concentration at the embedded bar surface reached a critical value of 0.05% (percentage weight of concrete) as given in the literature (Trejo and Pillai, 2003). The probability of corrosion initiation (P_i) was then based on the time taken to reach the specified chloride concentration (C_{th}) of 0.05% at the surface of the bar (Val and Trapper

2008). The chloride content at the concrete surface (C_s) was assumed as 0.5% of the weight of concrete. Also, the diffusion decay index (m) was kept at a constant value of 0.33, which indicates the reduction in the magnitudes of the chloride diffusion coefficients versus concrete age. **Table 2.8** summarizes the assumptions, variables and coefficient of variation (COV) for each factor used to calculate P_i for all tested 40 mm cover samples (Gjørsv 2009). The P_i of all the specimens was calculated as previously described to evaluate the effect of concrete qualities on the probability of corrosion initiation. An example of the variation of P_i versus the predicted time in years is presented in **Figure 2.10** for all concrete qualities of the 40 mm samples.

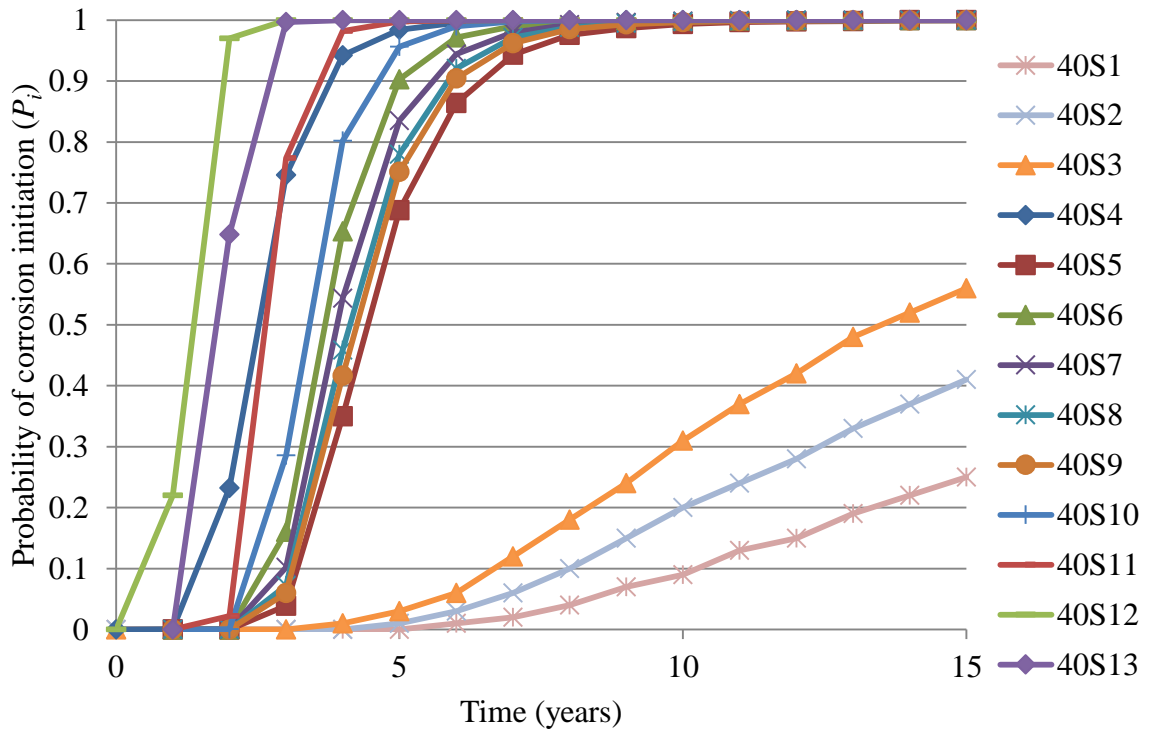


Figure 2.10 Probabilities of Corrosion Initiation for 40 mm Cover Samples

Table 2.8 Summary of Variables for Calculating P_i (Gjørv 2009)

Factor	Average Value	Units	COV %
C_s	0.5	% wt. of concrete	30%
D_a	Table 5	$\text{m}^2/\text{sec} \times 10^{-12}$	20%
m	0.33	-	10%
Cover Thickness	40	mm	8%
C_{th}	0.05	% wt. of concrete	20%

As seen from **Figure 2.10**, different concrete qualities (1 to 13) have a considerable effect on the probability of corrosion initiation. The lowest probability of corrosion initiation was obtained from 40S1, which had the highest concrete quality due to the largest replacement of MK (20%). The lower the MK replacement (qualities 2 and 3), the higher the probability that corrosion initiation had started, as shown in **Figure 2.10**. The trend was also seen from other concrete qualities' and probability of corrosion (4 to 13). Furthermore, the figure shows that the addition of MK in the mixture (represented by 40S1, 40S2, and 40S3) resulted in a significant decline in the values of initiation probability compared to those of the normal concrete mixtures (40S4 to 40S13). It is worth noting that this effect also manifested in all other tested samples cast with 20 and 30 mm covers. These results matched the experimental results in the form of the impact of various concrete qualities on the length of the corrosion initiation period at all values of concrete cover thicknesses. These trends indicated that the experimental results were reliable in identifying the influence of concrete qualities on the corrosion initiation period using a relatively simple and short test procedure.

2.6.6.2 Prediction of Propagation Period

The propagation period was predicted using the model developed by El Maaddawy and Soudki (El Maaddawy and Soudki, 2007) to calculate the time from the initiation to first cracking in the concrete cover. This model is based on a relationship between the value of steel mass loss and the corresponding internal radial pressure resulting from the expansive nature of corrosion products. Therefore, the amount of steel mass loss that causes cover cracking can be predicted based on the bar diameter, concrete mechanical properties, cover thickness, and electrical current. The time to cracking can then be estimated by means of Faraday's law (using the values of electrical current). This model was utilized to calculate the time to cracking (defined here as the propagation period) for all tested samples. The modulus of elasticity (E) of concrete used in this model was calculated using **Eq. (2.1)**, according to CSA A23.3 standard (CSA 2014). The average values of the propagation period predicted using this model for 20, 30, and 40 mm cover samples were calculated for each concrete quality and compared to the average values obtained from the experiment in

Figure 2. 11.

$$E = \left[3300\sqrt{f'_c} + 6900 \right] \left(\frac{\gamma_c}{2300} \right)^{1.5} \quad (\text{Eq. 2.1})$$

Where: f'_c = 28-day compressive strength of concrete (MPa) and γ_c = density of the concrete (kg/m^3).

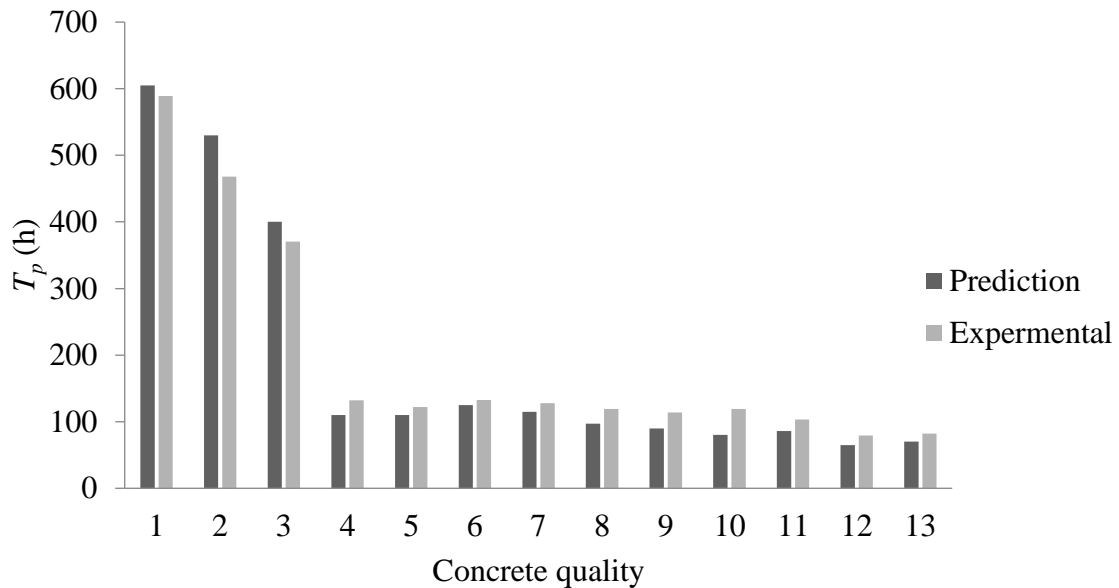


Figure 2.11 Comparison between the Model Predicted Propagation Period and Experiment

It can be observed from **Figure 2. 11** that the results of the average predicted propagation periods were in agreement with the experimental results. A similar trend of variations can be noticed from different concrete qualities in both the measured and predicted propagation times. The predicted propagation times increased as a result of increasing concrete qualities from 13 to 1. However, the figure indicated that a slightly higher difference between the measured and predicted times existed in concrete qualities 1, 2, and 3 (which incorporated MK). These variations may be related to the effect of MK replacement in these mixtures, an effect that needs to be taken into consideration in the model developed by El Maaddawy and Soudki (2007). Further investigations dealing with the influence of MK percentage on the expected time to corrosion cracking are needed to obtain more precise predictions and enhance the accuracy of the available models.

2.7 Conclusions

This paper presented the results of an experimental investigation focusing on determining three stages of service lifetime of RC structures subjected to reinforcement corrosion. The results of 78 prism samples with variable curing conditions, cover thicknesses, and mixture proportions were analyzed to identify the corrosion initiation, propagation, and damage periods. The results of initiation and propagation periods obtained from the experiments were validated (on a comparative basis in terms of concrete quality rank) using currently available models from the literature. Based on the results of this study, the following conclusions can be drawn:

- The increase of cover thickness significantly increased both the initiation period (T_i) and propagation period (T_p) regardless of curing condition or mixture composition. The average ratios between propagation and initiation time (T_p/T_i) decreased as a result of the increase in cover thickness. The average length of the damage period witnessed a slight increase due to increased cover thickness. In addition, increasing cover thickness yielded higher average values of mass loss of steel at both propagation and damage stages.
- Better curing condition (28 days of water curing in this study) in mixtures without MK resulted in both longer initiation and propagation periods, irrespective of cover thickness. Also, better curing condition increased the chloride threshold required to start corrosion process. In contrast, it was found that changing curing conditions had non-significant effects on the ratios of T_p/T_i ,

percentage of steel mass loss (at propagation and damage stages), and length of the damage period at all values of cover thickness.

- The increase in the MK replacement from 0 to 20% significantly extended both the initiation and propagation periods at all values of cover thickness. Using higher percentages of MK resulted in a slight increase in the T_p/T_i ratios and the length of the damage period.
- The results of the half-cell potential test at the time of detecting corrosion initiation showed less accurate readings at higher cover thicknesses. On the other hand, the results indicated that using better curing technique and larger cover thickness resulted in slightly higher average half-cell potential readings (less negative) at corrosion initiation. Nonetheless, additional tests are essential to confirm this finding and to prove its applicability in actual concrete structures.
- The results of probability of corrosion initiation obtained from Monte Carlo simulation showed a similar trend of variation to that obtained from the experiments in all tested samples. Better curing techniques (28 days of water curing in this study) were found to lead to lower probabilities of corrosion initiation and vice versa. Moreover, incorporating MK into the mixtures resulted in a very low probability of corrosion initiation compared to mixtures without MK.
- The results of propagation period obtained from the experiments were found to have a fair agreement with the results predicted by one of the available models

to estimate the time from the initiation to first cracking. Nonetheless, a slight difference was found in the results between the measured and predicted times in concrete mixtures containing MK. Thus further validation of this model is suggested to take into account the effect of MK percentage on the length of the propagation period.

2.8 Reference

- ANDRADE, C. 1993. Calculation of chloride diffusion coefficients in concrete from ionic migration measurements. *Cem. Concr. Res.*, 23, 724-742.
- ANDRADE, C. 2015. Prediction of service life of reinforced concrete by considering the initiation and the propagation periods. *ACI*, SP 305-4, 1–10.
- BAZANT, Z. P. 1979. Physical model for steel corrosion in concrete sea structures--theory. *Journal of the Structural Division*, 105.
- BENTZ, E. C. 2003. Probabilistic Modeling of Service Life for Structures Subjected to Chlorides. *ACI Materials Journal*, 100, 391-397.
- BROWNE, R. D. 1982. Design Prediction of the Life for Reinforced Concrete in Marine and Other Chloride Environments. *Durability of Building Materials*, 1, 113-25.
- CADY, P. D. & WEYERS, R. E. 1979. Deterioration rates of concrete bridge decks. *J. Transport. Eng.*, 110, 34-44.
- CADY, P. D. & WEYERS, R. E. 1983. Chloride Penetration and the Deterioration of Concrete Bridge Decks, Cement, Concrete, and Aggregates. *CCAGDP*, 5, 81-87.
- CORNET, I., ISHIKAWA, T. & BRESLER, B. 1968. The mechanism of steel corrosion in concrete structure. *Materials Protection*, 7, 44–7.
- EL MAADDAWY, T. & SOUDKI, K. 2007. A model for prediction of time from corrosion initiation to corrosion cracking. *Cement and Concrete Composites*, 29, 168–175.
- GJØRV, O. E. 2009. *Durability Design of Concrete Structures in Severe Environments*. Taylor & Francis, N.Y., USA. .
- HASSAN, A. A. A., HOSSAIN, K. M. A., & LACHEMI, M. 2010. Structural assessment of corroded self-consolidating concrete beams. *Eng. Struct.*, 32(3), 874–885.
- HASSAN, A. A. A., HOSSAIN, K. M. A. & LACHEMI, M. 2009. Corrosion Resistance of Self-Consolidating Concrete in Full-Scale Reinforced Beams. *Cement and Concrete Composites*, 31, 29-38.
- JUSTNES, H. 1998. A review of chloride binding in cementitious systems. *Nordic Concrete Research, Publication No. 21. 1/98*, Nordic Concrete Federation, Norsk Betongforening, Oslo, 48–63.

- LIFE-365 2015. Life-365 Service Life Prediction Model and Computer Program for Predicting the Service Life and Life-Cycle Cost of Reinforced Concrete Exposed to Chlorides Version 2.2.2.
- LIU, Y. & SHI, X. 2012. Stochastic modeling of service life of concrete structures in chloride-laden environments. *J. Mater. Civ. Eng.*, 24, 381-390.
- LIU, Y. & WEYERS, R. E. 1998. Modeling the Time-to-Corrosion Cracking in Chloride Contaminated Reinforced Concrete Structures. *ACI Materials Journal*, 95, 675-681.
- MAAGE, M., HELLAND, S., POULSEN, E., VENNESLAND, Ø. & CARLSEN, J. E. 1996. Service life prediction of existing concrete structures exposed to marine environment. *ACI Materials Journal*, 93, 602-8.
- MAHESWARAN, T. & SANJAYAN, J. G. 2004. A semi-closed-form solution for chloride diffusion in concrete with time-varying parameters. *Magazine of Concrete Research*, 56, 359-366.
- MEHTA, P. K. & MONTEIRO, P. J. M. 1993. *Concrete: Structure, Properties and Materials*, New Jersey, U.S.A., Prentice Hall
- MORINAGA, S. 1990. Prediction of service lives of reinforced concrete buildings based on the corrosion rate of reinforcing steel. *Proc., Building Materials and Components*, 5-16.
- PANESAR, D. K. & CHIDIAC, S. E. 2011. Effect of cold temperature on the chloride-binding capacity of cement. *J. Cold Reg. Eng.*, 25, 133-144.
- SANGOJU, B., PILLAI, R. G., GETTU, R., BHARATKUMAR, B. H. & IYER, N. R. 2015. Use of portland pozzolana cement to enhance the service life of reinforced concrete exposed to chloride attack. *J. Mater. Civ. Eng.*, 27.
- SHAIKH, F. U. A., MIHASHI, H. & KOBAYAKAWA, A. 2015. Corrosion durability of reinforcing steel in cracked high-performance fiber-reinforced cementitious composite beams. *J. Mater. Civ. Eng.*, 27.
- TREJO, D. & PILLAI, R. G. 2003. Accelerated chloride threshold testing: Part I - ASTM A 615 and A 706 reinforcement. *ACI Mater. J.*, 100, 519-527.
- TUUTTI, K. 1982. Corrosion of steel in concrete. *Research Report, Swedish Cement and Concrete Research Institute, Stockholm, Sweden.*
- VAL, D. V. & TRAPPER, P. A. 2008. Probabilistic evaluation of initiation time of chloride-induced corrosion. *Reliab. Eng. Syst. Safe.*, 93, 364-372.
- WANG, Y., LI, Q. & LIN, C. 2016. Chloride diffusion analysis of concrete members considering depth-dependent diffusion coefficients and effect of reinforcement presence. *J. Mater. Civ. Eng.*, 28.

3. A study on the effect of curing temperature and duration on rebar corrosion using wet-dry cycle corrosion test

3.1 Abstract

This investigation aimed to study the corrosion activity in reinforced concrete exposed to different curing temperatures and durations using wet-dry cycle corrosion test. The study also tested reinforced concrete samples under an impressed current accelerated corrosion test for comparison. A total of ten curing techniques were conducted by varying curing temperature (hot, normal, and cold) and curing duration (one, three, seven, and 28 days). The ten curing techniques were evaluated based on the results of wet-dry cycle, accelerated corrosion, rapid chloride permeability, and chloride diffusion tests. The chloride threshold, pH value, current measurement, half-cell, mass loss, and crack width readings were assessed during wet-dry cycle and impressed current corrosion tests. Heat-cured samples showed the highest chloride diffusion/permeability, shortest corrosion periods, and had the lowest chloride threshold and pH values. This was followed by cold-cured samples (28-day at 3–5°C) and then air-cured samples (28-day at 23°C). Curing samples in water for 28 days at 23°C proved to be the best curing technique. The results also showed that the impressed current accelerated corrosion test can be used effectively to evaluate and compare corrosion activities in different concrete qualities, but it cannot be used after the initiation of the first crack.

3.2 Introduction

The durability of reinforced concrete is directly linked to the resistivity of concrete towards the ingress of harmful substances. There are many forms of deterioration of concrete such

as acidic attack, sulfate attack, freeze and thaw, alkali-aggregate reaction, and corrosion of steel rebars (Hooton and McGrath, 1995). Corrosion of rebars is the most significant cause of deterioration of reinforced concrete structures. The concrete pore solution contains saturated calcium hydroxide solution with small percentages of other alkali ions, such as sodium and potassium ions, that maintain a pH balance of between 12.5 and 13.5. Steel rebars are protected from corrosion in concrete by a passive film that is formed due to the high pH values (alkalinity) of concrete pore solutions (Verbeck, 1975, Townsend et al., 1981). Breaks in the passive film are usually caused by high concentrations of chloride ions (chloride threshold) or a decrease in concrete alkalinity (Shamsad, 2003). The formation of a cement-rich layer (cover) at the rebar-concrete interface stabilizes the high pH and contributes to the passivity of steel rebar in concrete (Page, 1975). On the other hand, the chloride threshold required to break the passive film is still debatable as it depends on various factors including steel surface condition, quality of concrete, relative humidity, temperature, and the pH of concrete pore solutions (Angst et al., 2009, Manera et al., 2008, Hope, 1987).

The service life of the concrete structure is defined as “the time during which concrete fulfills its performance requirements, without non-intended maintenance” (Newman and Choo, 2003). Service life models are generally conducted by estimating two main periods: the initiation period and propagation period (Tuutti, 1982). The corrosion initiation period is the time it takes the chlorides from the external environment to penetrate through the concrete cover and accumulate at the rebar surface in sufficient amounts to break down its protective passive layer and initiate corrosion (Mehta and Monteiro, 1993). The propagation period starts after the breakdown of the protective layer around the reinforcing

bar (initiation period) and continues until the initiation of the first crack (Cabrer, 1996). The corrosion prediction models based on Fick's law are mostly used to estimate the initiation period, while models based on internal pressure produced by rust are commonly used to estimate the propagation period (Liu and Weyers, 1998, El Maaddawy and Soudki, 2007, Jang and Oh, 2010).

Concrete structures frequently exposed to rain, snow, and water contaminated by chloride solutions are highly vulnerable to corrosion attack (Crumpton et al., 1989, Hooton et al., 2001). Some of these exposure conditions are cyclic in nature, such as wetting and drying cycles (ocean waves) or freezing and thawing cycles (frost weathering). The wetting and drying cycles facilitate deeper ingress of aggressive ions in concrete, which leads to higher probability of corrosion (Moukwa, 1990, Morris et al., 2002, Cheewaket et al., 2012). The rate of chloride penetration depends on the wetting and drying periods. In the wetting period, the chlorides penetrate the concrete surface under diffusion. The water then evaporates in the drying period, leaving the chloride precipitated in concrete. The consequent wetting process dissolves the precipitated chlorides and transports them further into the concrete until they reach the rebar surface. The corrosion process is initiated when chlorides accumulating at the surface of the steel rebar exceed a certain limit (threshold value). Drying the concrete for enough time facilitates the ingress of chloride to deeper depths and provides enough oxygen to accelerate the corrosion process (Neville, 1996). Although chlorides are directly responsible for the initiation of corrosion, they have a limited role in the rate of corrosion after initiation. Many researchers have pointed out other factors affecting the rate of corrosion besides the chlorides content, such as the availability

of oxygen, temperature, relative humidity, concrete electrical resistivity, and the pH value of the pore solution (Alonso et al., 1988, Gjrv et al., 1977, Monfore, 1968).

Curing condition is one of the main factors affecting the durability of concrete (Rasheeduzzafar et al., 1989, CEB, 1985). According to previous studies, curing conditions influence the surface layer of concrete, which is the first line of defense (Gneyisi et al., 2007, Alizadeh et al., 2008, Khanzadeh-Moradllo et al., 2015). Adequate moist-curing makes the surface of fresh concrete stronger, impermeable, crack-free, and durable (Gonnerman and Shuman, 1928, Al-Gahtani, 2010, Ibrahima et al., 2013). On the other hand, poor curing conditions lead to restricted hydration in the surface layers, which results in higher porosity and permeability (Mangat and Limbachiya, 1999). Researchers have pointed out that concrete with an insufficient/improper curing regime indicates a high-corrosive activity, while concrete with a sufficient and proper curing regime indicates a low-corrosive activity (Hassan et al., 2009b, Detwiler et al., 1991). Hooton et al. showed that mixture composition and curing regimes significantly affect the chloride diffusion coefficients and, consequently, the predicted times to corrosion (Hooton et al., 2002). Similarly, Chen et al. tested concrete samples for chloride penetrability and found that air-cured specimens had considerably lower chloride permeability compared to specimens sufficiently cured in water (Chen et al., 2012). Zhao et al. also found that water-cured specimens had denser interfacial zones and higher anti-carbonation ability compared to air-cured specimens (Zhao et al., 2016).

One of the most commonly used accelerated corrosion tests is the impressed-current-based technique. In this technique, the corrosion of steel bars is induced by applying an electrical

potential current. The steel bar in the concrete sample is connected to a positive power supply while a stainless-steel mesh submerged in an electrolytic solution is connected to a negative power supply. The direction of the current is arranged so that the steel bar acts as an anode and the stainless-steel mesh acts as a cathode. The corrosion degree can be controlled by varying the current density and/or the time of the impressed current. The advantages of adopting this technique are the ability to achieve a high degree of corrosion quickly and the ease of controlling the desired degree of corrosion. On the other hand, the disadvantage is the artificial formation and distribution of the corrosion rust products. The steel bars in this technique corrode in an accelerated fashion due to electric force driving the chlorides into concrete (Yuan et al., 2007, Austin et al., 2004). Also, in the impressed current method, gaseous evolution may be present, which could influence the composition and spatial distribution of the corrosion products (Pourbaix, 1974). On the other hand, under natural corrosion conditions, the corrosion is generally initiated only on the side of the bar closest to the concrete surface, and corrosion products diffuse into the pores and cracks of the surrounding concrete before building up a pressure inside the structure.

The main objective of this investigation was to study the corrosion activity in reinforced concrete samples exposed to different curing techniques. Ten curing techniques were investigated experimentally using a wet-dry corrosion cycle test to study their corrosion activities. The same tested samples were also investigated using impressed current accelerated corrosion test for comparison in order to evaluate the effectiveness of this technique in monitoring the corrosion activity in reinforced concrete. The effect of curing techniques on chloride permeability, chloride diffusion coefficient, chloride threshold

level, concrete pH values, concrete electrical resistivity, corrosion periods, and rebars mass loss were studied in this investigation.

3.3 Research significance

Limited research has investigated the effect of concrete curing conditions on the corrosion activity of reinforced concrete, especially investigating different curing temperatures and durations. Moreover, most of the available literature has divided the corrosion activity in reinforced concrete into two periods only: initiation and propagation periods. And, the investigation of the propagation period (time to crack) in the literature was usually conducted using impressed current accelerated corrosion testing. However, researchers have expressed concerns that the impressed current accelerated corrosion test may not be suitable in evaluating corrosion activity as it does not monitor a natural corrosion. In this investigation, wet-dry corrosion testing was conducted on reinforced concrete samples subjected to ten curing techniques with variable temperatures and durations. The investigation was also conducted to identify and study three corrosion periods rather than only two. The investigation also included comparison between the results of the wet-dry and impressed current tests to evaluate the effectiveness of the impressed current corrosion test in evaluating corrosion activity in reinforced concrete samples.

3.4 Materials and mixture proportions

All tested specimens were made from one concrete mixture. They were similar in terms of mixture proportions and type of materials used. After casting, however, the tested specimens were cured using different curing techniques. Type GU Canadian Portland cement similar to ASTM Type I was used in this investigation; the chemical and physical

properties of this cement are shown in **Table 3.1**. Natural sand and stone with a maximum size of 10 mm were used as fine and coarse aggregates, respectively. The coarse and fine aggregates (**Table 3.2**) each had a specific gravity of 2.60 and water absorption of 1%. A 20M (20-mm diameter) bar was used in all tested specimens. The mixture proportions are shown in **Table 3.3**.

Table 3.1 Chemical and physical properties of cement

Chemical properties %	Cement
SiO ₂	19.64
Al ₂ O ₃	5.48
Fe ₂ O ₃	2.38
FeO	-
TiO ₂	-
C	-
P ₂ O ₅	-
SO ₄	-
CaO	62.44
MgO	2.48
Na ₂ O	-
C ₃ S	52.34
C ₂ S	16.83
C ₃ A	10.5
C ₄ AF	7.24
K ₂ O	-
Loss on ignition	2.05
Physical properties	
specific density	3.15
Color	gray
Grain size (µm)	45
Surface area(m ² /kg)	320-400
Blaine fineness(m ² /kg)	410

Table 3.2 Sieve analysis

Sieve size (mm)	20 mm coarse aggregate (% passing)	Sieve size	10 mm coarse aggregate (% passing)	Sieve size	Fine aggregate passing (% passing)
28	100	14	100	10	100
20	65.1	10	95.8	5	99.4
14	64.6	5	21	2.5	79.4
10	34.4	2.5	2.9	1.25	55.4
5	3.8	1.25	0	0.63	35.2
2.5	1.4	0.63	-	0.32	18.6
1.25	-	0.32	-	0.16	7.3
0.63	-	0.16	-	0.08	2.2

Table 3.3 Mixture proportions for Concrete mixture

Cement (Kg/m ³)	W/C	Coarse aggregate (Kg/m ³)	Fine aggregate (Kg/m ³)	Water (Kg/m ³)	HRWR (L/m ³)
450	0.4	834	926.6	180	4.5

3.5 Accelerated corrosion sample detail

All samples had a 60-mm width, 60-mm depth, and 250-mm length and contained one 20M steel bar embedded in the center (**Figure 3.1**). The reinforcing steel was placed carefully in the center of each sample to ensure 20-mm equal covers in all directions (**Figure 3.1**). Two wires were attached to the embedded steel bar; the first wire was connected to the half-cell or the power supply to measure the passing current. The second wire was intended to be a spare wire in case the first wire was slashed or torn during pouring of concrete. The second wire was also intended to check the connectivity of the main wire with the embedded steel bar (by reading the resistance between the two wires) after concrete was

poured. The specimens were designated according to the curing technique (C1 to C10) and the type of corrosion testing (wet-dry (W) or impressed current (I)). For example, a specimen with a curing technique of 4 using the wet-dry cycle corrosion test was designated as C4W.

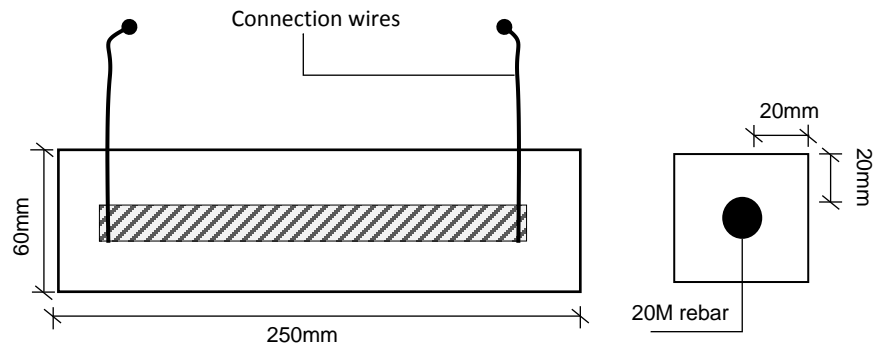


Figure 3.1 Sample Cross-section detail

3.6 Testing program

The research program described herein was undertaken to investigate the effects of using different curing techniques on the corrosion activity in reinforced concrete. All specimens were made from one concrete mixture (**Table 3.3**). The fresh properties tests for this mixture included air content according to ASTM C 231 and slump according to ASTM C 143. After mixing and completing the fresh properties tests, 60 concrete prisms 60 x 60 x 250 mm with embedded steel bars and 90 concrete cylinders 100 x 200 mm were prepared and cured according to their designated curing technique. The curing techniques were as following:

1. Curing technique 1: 28 days in water after mixing at 23°C.

2. Curing technique 2: 7 days in water after mixing at 23°C followed by 21 days refrigerated at 3–5°C.
3. Curing technique 3: 3 days in water after mixing at 23°C followed by 25 days refrigerated at 3–5°C.
4. Curing technique 4: 7 days in water after mixing followed by 21 days in air, both at 23°C.
5. Curing technique 5: 3 days in water after mixing followed by 25 days in air, both at 23°C.
6. Curing technique 6: 28 days in air after mixing at 23°C.
7. Curing technique 7: 28 days refrigerated after mixing at 3–5°C.
8. Curing technique 8: 1 day in water after mixing at 50°C followed by 27 days in water at 23°C.
9. Curing technique 9: 3 days in water after mixing at 50°C followed by 25 days in water at 23°C.
10. Curing technique 10: 7 days in water after mixing at 50°C followed by 21 days in water at 23°C.

The sequence of numbering from 1 to 10 was selected based on the resulting concrete quality. Curing techniques that resulted in a higher concrete quality (lower chloride diffusion/permeability values) were given a higher number while those associated with lower concrete quality were given a lower number.

The 90 prepared concrete cylinders were used to test the compressive strength (ASTM C39), splitting tensile strength (ASTM C496 / C496M), chloride diffusion coefficient (ASTM 1556), and rapid chloride permeability test (RCPT) (ASTM 1202C). On the other

hand, of the 60 prepared prisms, 30 were used for the impressed current accelerated corrosion test and the other 30 were used for the wet-dry cycle corrosion test. The 30 samples in each corrosion test were further divided into three groups of ten samples. Each group of ten samples was tested under the above ten curing conditions. The impressed current accelerated corrosion test setup used in this study consisted of a tank, electrolytic solution (5% NaCl by the weight of water), and a stainless-steel mesh placed at the bottom of the tank. All tested samples were fully submerged in the electrolytic solution and connected to a constant 12V DC power supply so that the reinforcing bar in each sample acted as anode while the stainless-steel mesh acted as cathode. The wet-dry corrosion test setup consisted of a tank, electrolytic solution (5% NaCl by the weight of water), and a timer power circuit (**Figure 3.2**). The timer power circuit was used to regulate the wet-dry cycles by controlling submerged pumps to fill and empty the tanks with the electrolytic solution every cycle. A 1-day wet-dry cycle was chosen in this investigation to represent a daily application of de-icing salts that a reinforced concrete structure might experience during winter (Hooton, 1999, Angst et al., 2009). The length of the wetting and drying periods was chosen as 6 and 18 hours, respectively (1-day cycle) (Hong, 1998). The wet-dry cycle and impressed current corrosion tests were divided into two stages: stage 1 (set 1 samples) started immediately after the end of the curing periods, and stage 2 (sets 2 and 3 samples) started 30 days after stage 1 (in order to estimate the initiation/propagation periods for sets 2 and 3 from the results of set 1).

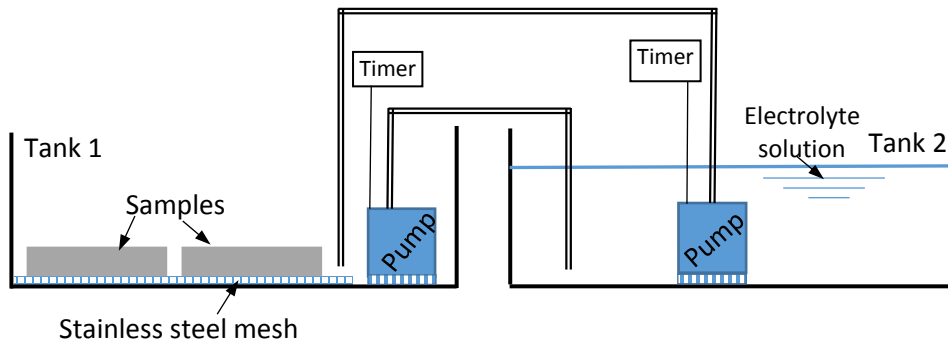


Figure 3.2 Wet-dry cycles schematic diagram

3.7 Readings and measurements

The current readings, half-cell potential measurements, and crack widths (once detected) were carefully taken every 12 hours during the impressed current accelerated corrosion test. Meanwhile, the same readings (current, half-cell, and crack widths) were taken every 3 cycles/days during the wet-dry cycle test. The current readings were taken during the wet-dry cycle in order to monitor the corrosion activity throughout the test. This was done by connecting the sample to a 12V power supply (when the tank was filled with the electrolytic solution) during the time of current reading only (to measure the current passed) and then disconnected right after the readings were taken. All half-cell measurements stopped being taken after the end of the initiation period, as they were only used to indicate the probability of corrosion initiation and had no value after the corrosion took place.

The drop of the initial current in the beginning of the test indicated the formation of the passive film around the reinforcing bar, which protected the steel from corrosion (**Figure 3.3**). On the other hand, the gradual increase of the current after reaching the lowest point indicated the de-passivation of the protective film (Cornet et al., 1968). The corrosion initiation period in this study was identified as the time taken to reach the lowest point in the current-cycles curve. Meanwhile, the corrosion propagation period was identified as the time taken from the end of the initiation period until the appearance of the first crack (**Figure 3.3**).

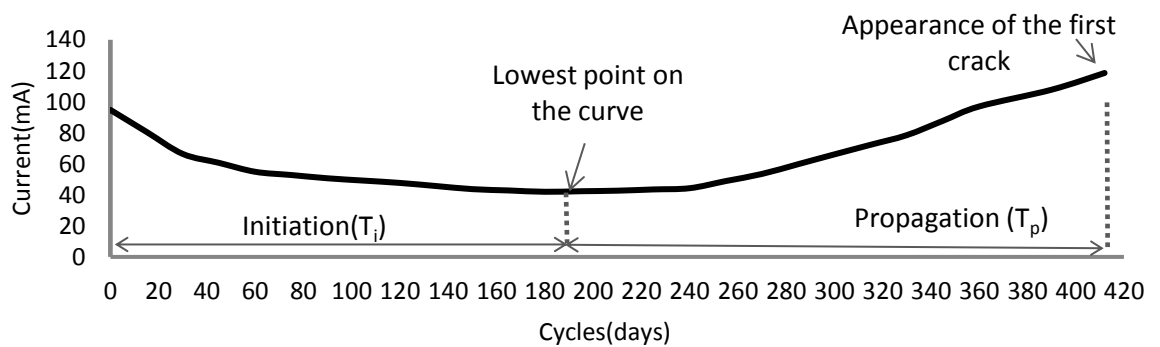


Figure 3.3 Typical current vs. time curve

For each of the impressed current and wet-dry corrosion tests, the plotted current-cycle graph for set 1 in the first stage was used to predict the end of the initiation period for the other two sets. After identifying the initiation period from set 1, the samples of set 2, which started 30 days after set 1, were removed from the tank (at the same initiation period as set 1); drilled and tested for chloride content; and then cut into halves to test the pH values using a full rainbow pH scale (ASTM 710) (**Figure 3.4** and **Figure 3.5**). At this time, the wet-dry cycles were still running on the other two sets (sets 1 and 3) until they reached the

propagation period (set 3) and the damage period (set 1). Immediately after the end of initiation period for set 3, the samples were periodically monitored to detect the appearance of the first crack to determine the propagation period (**Figure 3.6a**). Once the propagation period was detected, the test was terminated for this set and the samples were taken out of the tank. The corroded rebars were then removed from the samples and cleaned using a wire brush and then their mass losses were calculated using ASTM G102 (**Figure 3.7**). On the other hand, after the appearance of the first crack for set 1, the crack widths were monitored and measured using a microscope with a graduated scale of 0.002-mm increments until any of the cracks reached 4 mm; this was done to record the end of the damage period (**Figure 3.6b**). At this stage, the test was terminated for set 1 and the mass loss for the embedded bars was calculated similar to set 3.



Figure 3.4 Chloride threshold extraction

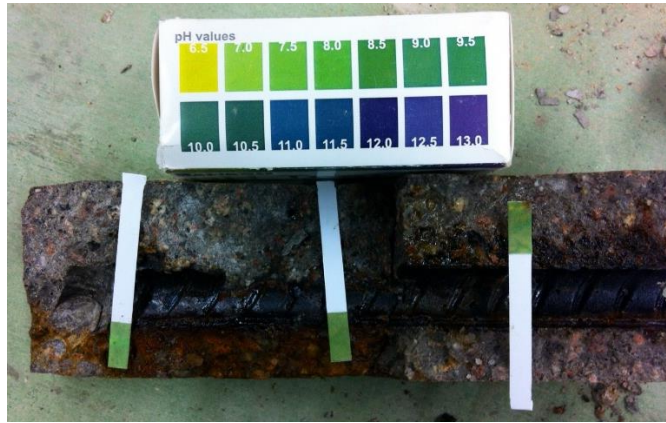
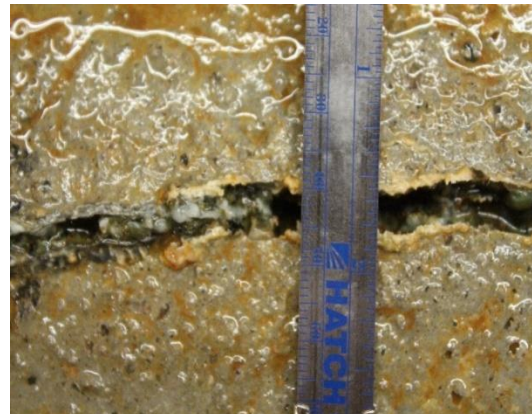


Figure 3.5 pH reading from concrete sample



a) Propagation period crack (hair crack)



b) Damage period crack(4-5mm width)

Figure 3.6 Crack width at different



Figure 3.7 Rebar mass loss (from top initiation stage, propagation stage and bottom damage stage)

3.8 Experimental Results and Discussion

The results of the 28-day compressive strength (f_c'), splitting tensile strength (f_t), chloride diffusion (D_a), and RCPT for the ten concrete curing techniques are presented in **Table 3.4**.

Wet-dry cycle results for initiation period (T_i), propagation period (T_p), damage period (T_d), chloride threshold (C_{th}), pH value, current measurement, half-cell reading, and mass loss % are presented in **Table 3.5**.

Table 3.4 Mechanical and chloride resistivity test results

Curing technique	28-day f_c' (MPa)	28-day f_t (MPa)	28-day $D_a \times 10^{-12}$ (m ² /sec)	28-RCPT (Coulombs)
1	76.16	7.81	7.52	2072
2	69.21	7.64	7.85	2100
3	65.85	7.42	7.99	2130
4	75.44	7.45	8.32	2432
5	73.33	7.49	8.86	2596
6	53.16	5.65	9.33	3000
7	58.91	5.68	12.2	3093
8	47.45	5.95	9.62	3120
9	59.38	6.69	15	3633
10	57.88	6.37	18	3700

Table 3.5 Wet-dry cycles corrosion tests results

Sample No.	Initial current (mA)	Half-cell (mV)at initiation	T _i (Days)	Chloride threshold(C _{th}) (%wt. concrete)	pH at initiation	T _p (Days)	Mass loss at propagation (%)	Mass loss at damage (%)	T _d (Days)	T _p /T _i
C1W	94.2	-524	249	0.67	11	390	2.25	10.05	237	1.57
C2W	95.3	-544	240	0.65	11	357	2.05	9.5	201	1.49
C3W	99.1	-539	231	0.59	10	315	1.98	8.53	177	1.36
C4W	102.3	-557	210	0.54	10	285	1.9	7.26	162	1.36
C5W	104.3	-550	204	0.34	10	246	1.84	6.19	150	1.21
C6W	106	-536	198	0.32	10	240	1.8	7.07	135	1.21
C7W	109.5	-540	186	0.24	10	237	1.81	5.28	123	1.27
C8W	110.6	-553	150	0.32	9	180	1.72	5.3	96	1.2
C9W	112.8	-570	129	0.29	9	156	1.7	5.06	81	1.21
C10W	113	-580	90	0.2	9	108	1.24	4.4	63	1.2

3.8.1 Effect of curing technique on corrosion activity

As seen from **Table 3.4**, curing technique 10 (7 days in water at 50°C then water at 23°C) showed the lowest chloride resistance (highest chloride diffusion coefficients and highest RCPT charge pass) while curing technique 1 (28 days in water at 23°C) had the highest chloride resistance. In addition, samples of curing technique 10 showed the lowest concrete resistivity (highest initial current) while samples of curing technique 1 showed the highest resistivity (lowest initial current) (**Table 3.5**). In general, applying heat-curing (50°C in curing techniques 8–10) gave the lowest chloride resistance. This was followed by complete curing time in a cold environment (3–5°C in curing technique 7), then complete curing time in air at 23°C (curing technique 6). Different curing techniques also appeared to affect the corrosion periods. As seen in **Figure 3.8**, corrosion initiation, propagation, and damage periods increased with higher concrete quality, which was associated with better

curing techniques. Similar to the results of the chloride diffusion/permeability, the results of the RCPT and initial current indicated that all samples with elevated curing temperatures (techniques 8–10) had the shortest corrosion periods (initiation, propagation, and damages), while those cured in 23°C water for 28 days had the longest corrosion periods. The results also showed that improving the concrete quality by using better curing techniques slightly affected the damage period and significantly affected the propagation period. As seen in **Table 3.5**, when the concrete quality improved (from curing technique 10 to 1), the ratio of T_p/T_i increased from 1.2 to 1.57, indicating an increase in the propagation time. A similar trend can also be seen for the damage period; the distance between initiation and damage curves in **Figure 3.8** slightly decreased (from curing technique 1 to 10). Unlike the propagation period, the damage period was measured from the time of the crack initiation until the crack opened 4-mm wide. During this period, the corrosion activity was more affected by the ingress of the aggressive ions through the opening of the crack rather than the uncracked body of the concrete. Therefore, the concrete quality had a minimal effect on the length of the damage period.

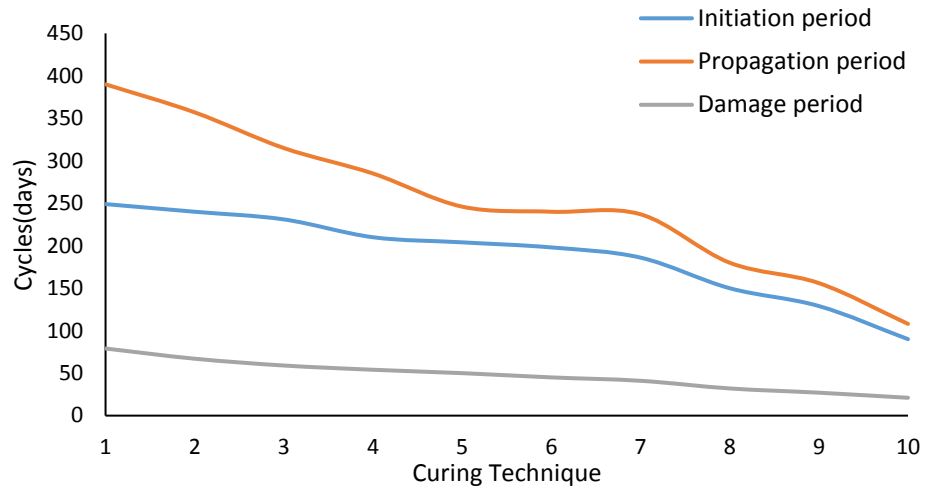


Figure 3.8 Curing technique-cycles relation

The pH readings at the initiation period for all tested samples are presented in **Table 3.5**. Despite the small variations in pH results, a clear relationship between the pH values and curing techniques can be seen. **Figure 3.9** and **Table 3.5** show that curing technique 10 had the lowest pH value, while the full 28-day water-cured samples had the highest pH value. It should be noted that better cured concrete has higher concrete quality and likely higher cement hydrated product such as portlandite, which increases the pH value of concrete (Lothenbach et al., 2007, Ballester et al., 2009, Bediako et al., 2015).

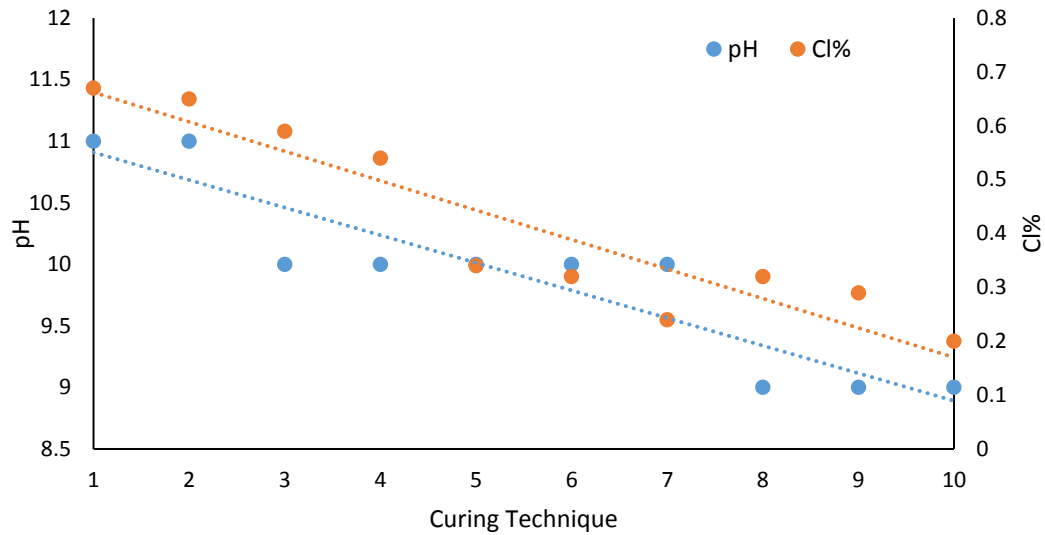


Figure 3.9 pH vs curing technique and chloride threshold

3.8.2 Effect of curing technique on chloride threshold

The chloride threshold values at the end of the initiation period were measured for all tested samples (set 2); it was found that different concrete curing techniques had a significant effect on the percentage of chloride threshold at the rebar surface (**Table 3.5**). It can be seen from **Figure 3.9** that better cured sample required more chloride to start the corrosion process (higher chloride threshold). It should be noted that poor quality concrete (poor curing) influences the concentration of the free chloride and affects the chloride binding capacity, which in turn decreases the chloride threshold required for the de-passivation of the bar's protective film (Pettersson, 1995, Hansson and Sørensen, 1990, Glass et al., 2000). **Figure 3.10** shows the relationship between chloride threshold versus the diffusion coefficient and the amount of charge passed in the RCPT. As can be seen from the plot, samples with higher chloride permeability seem to have a lower chloride threshold. There is a general downward relationship between increasing the chloride diffusion coefficients

or increasing the RCPT and the chloride threshold. It is also observed from the **Figure 3.10** that the chloride permeability and chloride diffusion of concrete are closely related. It is clear that the concrete samples with low RCPT values have low diffusion coefficients and both have higher chloride thresholds required to start the corrosion process. It can also be seen in **Figure 3.9** that increasing the pH value of concrete increased the critical level of chloride at the bar surface that was required to initiate corrosion (chloride threshold). It should be noted that the alkalinity of the pore solution contributed to the passivation of protective film around the steel bar. In concrete with higher pH value, higher concentrations of chloride ions would be required to destroy the passive film and cause the onset of corrosion (Erlin and Verbeck, 1975, Hausmann, 1967).

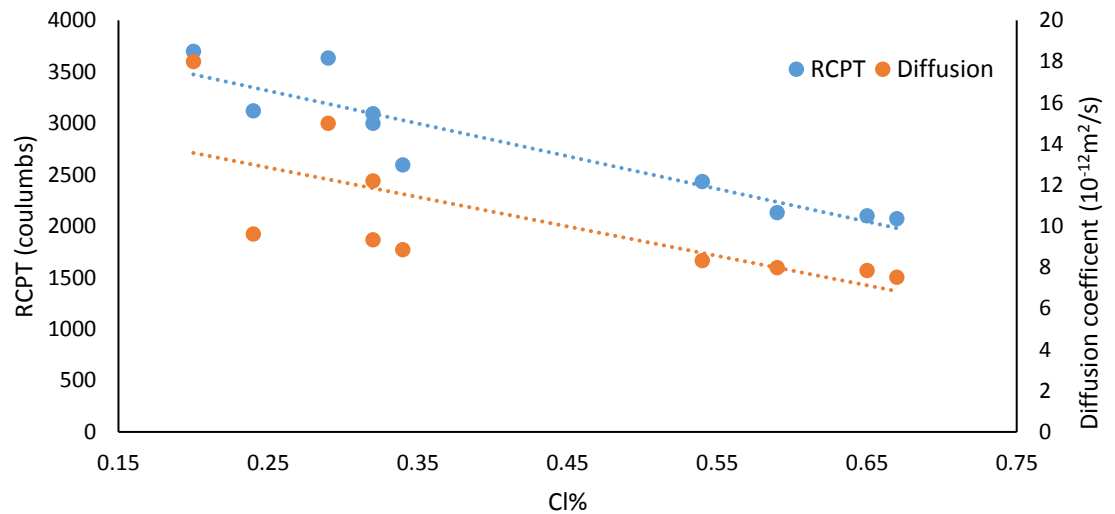


Figure 3.10 Chloride threshold vs. RCPT and diffusion coefficient

3.8.3 Effect of curing technique on rebar mass loss

The values of steel mass loss at the end of the propagation and damage periods were measured for all tested samples (Table 3.5). In this investigation, the propagation period was judged to be terminated when a hair width crack was formed, while a 4-mm crack was needed for the damage period to be terminated. Concrete cured for 28 days in water at 23°C showed a higher average ratio of steel mass loss compared to air- or hot-water curing. As seen in Figure 3.11, the mass loss, in general, showed an upward trend with better curing techniques in both propagation and damage periods. It is also clear from the figure that the mass loss in the damage period was more affected by the curing technique compared to the propagation period. Higher mass loss was required to cause the 4-mm crack in better-cured concrete compared to poorer-cured concrete (Figure 3.11). This result may be due to the fact that better concrete quality (better-cured concrete) can provide higher resistance for the cracks to open wider. However, the exact relation between mass loss and crack widths involves many factors and cannot be simply predicted in this investigation.

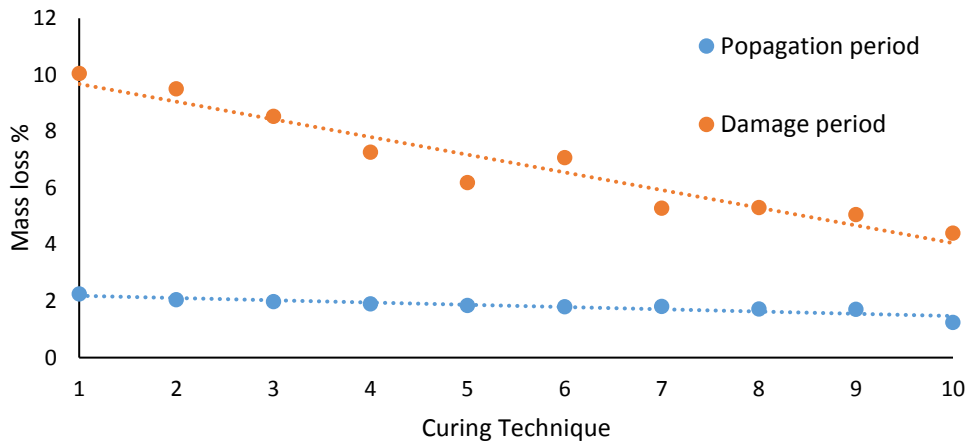


Figure 3.11 Concrete curing technique and mass loss

3.8.4 Comparison between wet-dry cycle and impressed current corrosion tests

The results of wet-dry cycle and impressed current corrosion tests are presented in **Table 3.5** and **Table 3.6**. In general, the impressed current corrosion test seemed to be a reliable technique for monitoring the rebar corrosion in the tested samples. The results of the impressed current corrosion test followed the same trend of variation as those of the wet-dry cycle test. Similar to the wet-dry cycle test, each of initial current, initiation period, propagation period, pH value, and chloride threshold values appeared to decrease with poorer curing techniques (from 1 to 10). The results of the half-cell in the impressed current test also showed similar trend variation compared to that of the wet-dry test, indicating high probability of corrosion at the corrosion initiation. However, the values of each of the chloride threshold and pH values in the impressed current test appeared to be lower than those found in the wet-dry test. It should be noted that the wet-dry test took around two and half years while the impressed current test lasted around ten days. The relatively longer time to complete the wet-dry test allowed the samples to reach higher hydration stage and therefore showed slightly higher pH values. And since the chloride threshold is affected by the pH level of the concrete, the values of the chloride threshold in the impressed current test also appeared to be less than those in the wet-dry test. Unlike the initiation and propagation periods, the results of the damage period in the impressed current test did not show a similar trend of variation as that of the wet-dry test (from curing technique 1 to 10). As seen from **Table 3.6**, when the curing technique changed from 1 to 10, the damage periods in the impressed current test changed randomly from 2.33 to 5.5 days. The damage period was calculated from the time of the initiation of the first crack until the crack reached a width of 4 mm. Unlike the wet-dry test, after the initiation of the crack in the impressed

current test, the salt solution was in direct contact with the rebar, causing sudden increase in the current and concentrated corrosion at the area of the rebar exposed to the salt solution. This corrosion process is more related to the crack size and width than the concrete quality. Therefore, the damage period in the impressed current test did not show dependence on the curing technique. This was also confirmed by looking at the mass losses of the damage period, which also showed random results in the impressed current test compared to the wet-dry test.

Table 3.6 Impressed current accelerated corrosion tests results

Sample No.	Initial current (mA)	Half-cell (mV) at initiation	T _i (Days)	Chloride threshold (C _{th}) (%wt. concrete)	pH	T _p (Days)	Mass loss at propagation (%)	Mass loss at damage (%)	T _d (Days)	T _p /T _i
C1I	94.8	-557	2.58	0.44	10	2.25	1.48	6.92	4.67	0.87
C2I	95.6	-550	2.5	0.4	10	1.83	1.19	4.2	5.33	0.73
C3I	98.9	-536	2.5	0.34	10	1.92	1.24	5.08	5.17	0.77
C4I	102.9	-540	2.42	0.28	9	1.83	1.29	3.98	4.08	0.76
C5I	104.2	-570	2.42	0.18	9	1.83	1.16	10.24	5.25	0.76
C6I	105.9	-580	2.33	0.16	9	1.67	1.01	5.08	5.5	0.72
C7I	109.9	-585	2.33	0.11	8	1.83	1.21	10.17	3.33	0.79
C8I	110.3	-570	2.33	0.11	8	1.67	1.37	8.47	4.17	0.72
C9I	112.2	-553	2.08	0.08	8	1.5	1.0	9.75	2.33	0.72
C10I	113.2	-590	2.08	0.01	8	1.42	1.05	3.81	4.5	0.68

3.9 Conclusion

Based on the results of this study, the following conclusions can be drawn:

- Heat-cured samples (50°C) showed the highest chloride diffusion/permeability, lowest concrete electrical resistance, and the shortest corrosion initiation, propagation, and damage periods. This was followed by samples completely cured in a cold environment (3–5°C) and then samples completely cured in air at 23°C.

On the other hand, curing samples in water at 23°C for 28 days showed the lowest chloride diffusion/permeability, longest corrosion periods, and highest concrete electrical resistance.

- The propagation period in the wet-dry corrosion test was more affected by the curing technique (concrete quality) compared to the damage period. Better curing technique (higher concrete quality) seemed to significantly increase the propagation period and slightly extend the damage period.
- Higher concrete quality associated with better curing technique required higher levels of chloride at the bar surface to initiate corrosion (higher chloride threshold). Also, concrete with higher chloride permeability (represented by the RCPT) and/or higher chloride diffusion had lower chloride thresholds. Concrete with high pH values also required higher concentrations of chloride ions at the bar surface to destroy the passive film around the steel bar and initiate corrosion.
- Better curing technique improved the concrete quality and increased the resistance for the cracks to open wider. The steel bar mass loss in concrete with better curing technique (28 days in water at 23°C) seemed higher than concrete with poorer curing technique (air- or hot-water curing). Also, the effect of curing technique on the steel mass loss was more pronounced in the damage period compared to the propagation period.
- The impressed current accelerated corrosion test can be considered a reliable technique to compare the corrosion activates in different concrete types/qualities up to the initiation of the first crack (propagation period). The impressed current

corrosion test showed a similar trend of variation as that of the wet-dry test, indicating lower chloride diffusion/permeability, higher concrete electrical resistance, and the shortest corrosion initiation and propagation periods with better curing techniques (1 to 10).

- Because wet-dry test takes relatively long time that allows the samples to reach higher degree of hydration, the chloride threshold and pH values appeared to be slightly higher in the wet-dry test compared to the impressed current test.

The impressed current corrosion test proved to be unreliable at evaluating the corrosion damage period. The damage periods in this test did not show a clear correlation with the curing technique used (concrete quality). This is because once the crack opened in the impressed current test, the salt solution came in direct contact with the rebar, causing a sudden increase in the current and concentrated corrosion at the opened crack area.

3.10 Reference

- AL-GAHTANI, A. S. 2010. Effect of curing methods on the properties of plain and blended cement concretes. *Cement and Concrete Composites*, 24, 308–314.
- ALIZADEH, R., GHODS, P., CHINI, M., HOSEINI, M., GHALIBAFIAN, M. & SHEKARCHI, M. 2008. Effect of Curing Conditions on the Service Life Design of RC Structures in the Persian Gulf Region. *Journal of Materials in Civil Engineering*, 20, 2-8.
- ALONSO, C., ANDRADE, C. & GONZÁLEZ, J. A. 1988. Relation Between Concrete Resistivity and Corrosion Rate of the Reinforcements in Carbonated Mortar Made with Several Cement Types. *Cement and Concrete Research*, 687-698.
- ANGST, U., BERNHARD ELSENER, CLAUS K. LARSEN & ØYSTEIN VENNESLAND 2009. Critical chloride content in reinforced concrete — A review. *Cement and Concrete Research*, 39, 1122–1138.
- AUSTIN, S. A., LYONS, R. & ING, M. J. 2004. Electrochemical Behavior of Steel-Reinforced Concrete During Accelerated Corrosion Testing. *Corrosion - NACE*, 60, 203-212.
- BALLESTER, P., HIDALGO, A., MÁRMOL, I., MORALES, J. & SÁNCHEZ, L. 2009. Effect of Brief Heat-Curing on Microstructure and Mechanical Properties in Fresh Cement Based Mortars. *Cement and Concrete Research*, 39, 573-579.

- BEDIAKO, M., KEVERN, J. T. & AMANKWAH, E. O. 2015. Effect of Curing Environment on the Strength Properties of Cement and Cement Extenders. *Materials Sciences and Applications*, 6, 33-39.
- CABRER, J. G. 1996. Deterioration of concrete due to reinforcement steel corrosion. *Cement and Concrete Composites Journal*, 18, 47–59.
- CEB 1985. Guide to Durable Concrete Structures. *Comité Euro-International du Beton, Lausanne, Switzerland*.
- CHEEWAKET, T., JATURAPITAKKUL, C. & CHALEE, W. 2012. Initial corrosion presented by chloride threshold penetration of concrete up to 10 year-results under marine site, *Constr. . Build. Mater*, 37, 693-698.
- CHEN, H.-J., HUANG, S.-S., TANG, C.-W., MALEK, M. A. & EAN, L.-W. 2012. Effect of curing environments on strength, porosity and chloride ingress resistance of blast furnace slag cement concretes: A construction site study. *Construction and Building Materials*, 35, 1063-1070.
- CORNET, I., ISHIKAWA, T. & BRESLER, B. 1968. The mechanism of steel corrosion in concrete structure. *Materials Protection*, 7, 44–7.
- CRUMPTON, C. F., SMITH, B. J. & JAYAPRAKASH, G. P. 1989. Salt Weathering of Limestone Aggregate and Concrete Without Freeze-Thaw. *Transportation Research Record 1250 Transportation Research Board*, 8-16.
- DETWILER, R. J., KJELLEN, K. O. & GJORV, O. E. 1991. Resistance to chloride intrusion of concrete cured at different temperatures. *Materials Journal*, 88, 19-24.
- EL MAADDAWY, T. & SOUDKI, K. 2007. A model for prediction of time from corrosion initiation to corrosion cracking. *Cement and Concrete Composites*, 29, 168–175.
- ERLIN, B. & VERBECK, G. J. 1975. Corrosion of metals in concrete-needed research. *Special Publication*, 49, 39-46.
- GJØRV, O. E., SORENSON, S. I. & ARNESEN, A. 1977. Notch Sensitivity and Fracture Toughness of Concrete *Cement and Concrete Research*, 7, 333-344.
- GLASS, G., REDDY, B. & BUENFELD, N. 2000. The participation of bound chloride in passive film breakdown on steel in concrete. *Corrosion Science*, 42, 2013-2021.
- GONNERMAN, H. F. & SHUMAN, E. C. 1928. Flexure and Tension Tests of Plain Concrete., *Major Series 171, 209, and 210 Report of the Director of Research, Portland Cement Association*, 149-163.
- GÜNEYISI, E., OZTURAN, T. & GESOGLU, M. 2007. Effect of initial curing on chloride ingress and corrosion resistance characteristics of concretes made with plain and blended cements. *Journal of Building and Environment*, 42, 2676–2685.
- HANSSON, C. M. & SØRENSEN, B. 1990. The threshold concentration of chloride in concrete for the initiation of reinforcement corrosion. *Corrosion rates of steel in concrete*. ASTM International.
- HASSAN, A. A. A., HOSSAIN, K. M. A. & LACHEMI, M. 2009. Corrosion Resistance of Self-Consolidating Concrete in Full-Scale Reinforced Beams. *Cement and Concrete Composites*, 31, 29-38.
- HAUSMANN, D. 1967. Steel corrosion in concrete--How does it occur? *Materials protection*.
- HONG, K. 1998. *Cyclic wetting and drying and its effects on chloride ingress in concrete*. National Library of Canada= Bibliothèque nationale du Canada.

- HOOTON, R. D. 1999. Advances in Cement and Concrete. *Engineering Foundation, New York*.
- HOOTON, R. D., GEIKER, M. R. & BENTZ, E. C. 2002. Effects of Curing on Chloride Ingress and Implications on Service Life. *ACI Materials Journal* 99, 201-206.
- HOOTON, R. D. & MCGRATH, P. F. 1995. Issues Related to Recent Developments in Service Life Specifications for Concrete Structures. *Chloride Penetration into Concrete, International RILEM Workshop St. Remy - Les Chevreuse*, 10.
- HOOTON, R. D., THOMAS, M. D. A. & STANISH, K. 2001. Prediction of Chloride Penetration in Concrete. Federal Highway Administration.
- HOPE, B. I. A. 1987. Chloride corrosion threshold in concrete. *ACI Materials Journal* 84, 306-313.
- IBRAHIMA, M., SHAMEEMA, M., AL-MEHTHEL, M. & MASLEHUDDINAM. 2013. Effect of curing methods on strength and durability of concrete under hot weather conditions. *Cement and Concrete Composites*, 41, 60-69.
- JANG, B. S. & OH, B. H. 2010. Effects of non-uniform corrosion on the cracking and service life of reinforced concrete structures. *Cement and Concrete Research* 40, 1441-1450.
- KHANZADEH-MORADLLO, M., MESHKINI, M., ESLAMDOOST, E., SADATI, S. & SHEKARCHI, M. 2015. Effect of Wet Curing Duration on Long-Term Performance of Concrete in Tidal Zone of Marine Environment. *International Journal of Concrete Structures and Materials*, 9, 487-498.
- LIU, Y. & WEYERS, R. E. 1998. Modeling the Time-to-Corrosion Cracking in Chloride Contaminated Reinforced Concrete Structures. *ACI Materials Journal*, 95, 675-681.
- LOTHENBACH, B., WINNEFELD, F., ALDER, C., WIELAND, E. & LUNK, P. 2007. Effect of Temperature on the Pore Solution, Microstructure and Hydration Products of Portland Cement Pastes. *Cement and Concrete Research*, 37, 483-491.
- MANERA, M., VENNESLAND, O. & BERTOLINI, L. 2008. Chloride threshold for rebar corrosion in concrete with addition of silica fume. *CORROSION SCIENCE*, 50, 554-560.
- MANGAT, P. S. & LIMBACHIYA, M. C. 1999. Effect of initial curing on chloride diffusion in concrete repair materials. *cement and concrete research*, 29, 1475-1485.
- MEHTA, P. K. & MONTEIRO, P. J. M. 1993. *Concrete: Structure, Properties and Materials*, New Jersey, U.S.A., Prentice Hall
- MONFORE, G. E. 1968. Electrical Resistivity of Concrete. *JPCA Res Develop Lab*, 2, 35-48.
- MORRIS, W., VICO, A., VAZQUEZ, M. & DE SANCHEZ, S. R. 2002. Corrosion of reinforcing steel evaluated by means of concrete resistivity measurements. *Corrosion Science*, 44, 81-99.
- MOUKWA, M. 1990. Characteristics of the attack of cement paste by MgSO₄ and MgCl₂ from the pore structure measurements. *Cem. Concr. Res.*, 20, 148-158.
- NEVILLE, A. M. 1996. *Properties of Concrete*, New York, NY USA.
- NEWMAN, J. B. & CHOO, B. S. 2003. Advanced Concrete Technology: Concrete Properties. *Butterworth-Heinemann*.

- PAGE, C. L. 1975. Mechanism of corrosion protection in reinforced concrete marine structures. *Nature*, 258, 514–515.
- PETTERSSON, K. 1995. Chloride threshold value and the corrosion rate in reinforced concrete. *In Proc. of the Nordic Seminar. Lund.* , 257-266.
- POURBAIX, M. 1974. Atlas of Electrochemical Equilibria in Aqueous Solutions. *National Association of Corrosion Engineers*.
- RASHEEDUZZAFAR, A. S. AL-GAHTANI & AL-SAADOUN, S. S. 1989. Influence of Construction Practices on Concrete Durability. *Materials Journal*, 86, 566-575.
- SHAMSAD, A. 2003. Reinforcement Corrosion in Concrete Structures, its Monitoring and Service Life Prediction – A Review. *Journal of Cement and Concrete Composites*, 25, 459-471.
- TOWNSEND, H. E., CLEARY, H. J. & ALLEGRA, L. 1981. Breakdown of Oxide films in Steel Exposure to Chloride Solutions. *Corrosion - NACE*, 37, 384-391.
- TUUTTI, K. 1982. Corrosion of steel in concrete. *Research Report, Swedish Cement and Concrete Research Institute, Stockholm, Sweden*.
- VERBECK, G. J. 1975. Mechanism of Corrosion in Concrete. *In Corrosion of Metals in Concrete International ACI SP-49*.
- YUAN, Y., JI, Y. & SHAH, S. P. 2007. Comparison of two accelerated corrosion techniques for concrete structures. *ACI Structural Journal*, 104, 344–347.
- ZHAO, Q., HE, X., ZHANG, J. & JIANG, J. 2016. Long-age wet curing effect on performance of carbonation resistance of fly ash concrete. *Construction and Building Materials*, 127, 577-587.

4. Refined statistical modeling for chloride permeability and strength of concrete containing metakaolin

4.1 Abstract

An experimental investigation was conducted to develop design tools using refined statistical analysis to optimize chloride permeability and strength of concrete containing metakaolin (MK). The study adopts the design of experiments (DOEs) to test 53 concrete mixtures based on enhanced response surface method (RSM). Three factors were considered: total binder content (binder), percentage of metakaolin (MK%), and water-to-binder ratio (W/B). The mixtures were examined based on the rapid chloride permeability test (RCPT), chloride diffusion test, compressive strength (f_c), modulus of elasticity (MOE), splitting tensile strength (STS), flexural strength (FS), and cost of mixture per cubic meter. The developed statistical models and design charts are valid for concrete with W/B ratios ranging from 0.3 to 0.5, MK from 0% to 25%, and total binder content from 350 kg/m³ to 600 kg/m³. The results endorse that the obtained derived models and design charts are useful for understanding the influence of the key factors on concrete mechanical and durability properties. These models and design charts are beneficial for predicting and selecting the optimum mixture proportions for a given application in a simple and accurate way. This paper's recommendations can be of special interest to designers considering the use of concrete containing MK in structural applications.

4.2 Introduction

Optimizing concrete mixtures has become essential in recent years, with various supplementary cementing materials (SCM) and admixtures being added to concrete. Statistical design technique is an efficient tool for optimizing concrete mixtures as it provides statistical models, which helps researches to understand the interactions between parameters that have been modelled and optimized (Ghezal and Khayat, 2002). There are numerous models used for optimizing concrete mixtures such as response surface methodology (RSM), factorial design, and fractional factorial design (Sonebi, 2004, Nehdi and Summer, 2002, Soudki et al., 2001, Akalin et al., 2010, Rougeron and P.C. Aitcin, 1994, Khayet et al., 2011). Design of experiments method relies on analysis of variance (Montgomery 2012, Speed, 1987) ; this method selects a few points out of the full factorial set that can represent accurate information about the response space.

Central composite design (CCD) and face-centered composite design (FCCD) are RSM design techniques applied in numerous civil engineering fields (Bayramov et al., 2004a, Wong et al., 2005, Chen et al., 2010, Kang et al., 2010). CCD and FCCD are a compilation of mathematical and statistical techniques used for developing, refining, and optimizing processes, and can be used to evaluate the relative significance of numerous factors, even in complex interactions. Both CCD and FCCD methods divide the experimental space into three parts: the factorial part (2^k , where k = number of influencing factors), axial part, and central part (Schmidt and Launsby, 1994, Montgomery 2012). The main difference between the two methods is the location of the axial points (**Figure 4.1**). The sampling axial point in the CCD method is located outside the design space by distance $\alpha = \sqrt[4]{2^m}$ (m = factorial factors), whereas in the FCCD method the axial points lay on the boundary of the design

space. **Figure 4.1** shows the location of the points in both CCD and FCCD methods. The number of points for each method is fifteen: 8 vertices points, 6 axial points, and 1 central point.

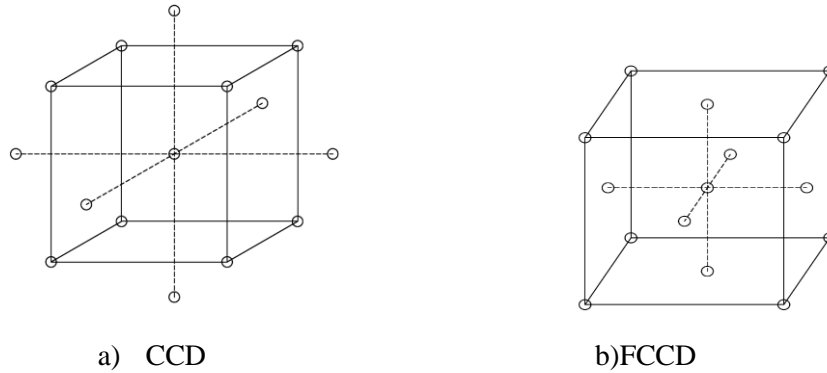


Figure 4.1 CCD and FCCD point arrangement

Utilizing MK as SCM in concrete is receiving great attention nowadays. MK improves the mechanical and durability properties of concrete compared to concrete without SCM. MK also makes the concrete environmentally friendly as it does not emit CO₂ and requires lower manufacturing temperatures compared to cement. In precast concrete industry, mixtures with up to 25% MK proved to have enhanced mechanical and durability properties (Cassagnabère et al., 2010, Cassagnabère et al., 2009). According to previous studies, incorporating MK in concrete mixtures increases strength and rate of strength gain and improves the overall mixture durability (Justice et al., 2005b, Akalin et al., 2010, Madandoust and Mousavi, 2012). Concrete mixtures containing 0%–20% MK showed a noticeable increase in the compressive strength (f_c) (Paiva et al., 2012, Hassan et al., 2012b). The ideal MK replacement level was found to be approximately 20%–25% and any further increase in the MK percentage showed no effect on the f_c (Vu et al., 2001, Paiva et al., 2012, Khatib and Hibbertb, 2005). On the other hand, adding MK was also found to

improve the concrete splitting tensile strength (STS), flexural strength (FS), and modulus of elasticity (MOE) [20-22]

The prediction of chloride ingress in reinforced concrete structures has become a crucial part in service life prediction and the maintenance of new and existing structures (Hassan et al., 2009a, Ehlen et al., 2009, Hooton et al., 2002). The resistivity of concrete to chloride ingress is expressed by the chloride permeability property. The assessment of chloride permeability can be performed using RCPT (ASTM C1202) and/or a chloride bulk diffusion test (ASTM C1556). The corrosion occurs when the chloride level at the rebar exceeds the normal threshold. (Cheewaket et al., 2012, Liang et al., 2002). The addition of MK in concrete proved to reduce the chloride permeability and increase the pH of the mixture (Barnes et al., 2003, Coleman and Page, 1997). Therefore, mixtures containing MK can be expected to provide a high degree of protection against corrosion. However, the overall strength and durability of MK mixtures are greatly affected by the physical and chemical properties of the MK (Bonakdar et al., 2005b, Sabir et al., 2001a, Justice et al., 2005b).

Limited research has been undertaken that considers the statistical analysis in optimizing the chloride permeability and strength of MK mixtures (Razak and Wong, 2005, Mehdipour et al., 2016, Dhinakaran et al., 2012, Erhan Güneyisi et al., 2014). In addition, most of the available studies utilized a traditional statistical analysis with minimum number of points representing the response space. The main objective of this investigation was to utilize an enhanced statistical analysis to develop more precise models and design charts for concrete containing metakaolin. The variables were total binder content, water-to-binder ratio, and

percentage of MK. The models' responses were rapid chloride permeability, chloride diffusion, compressive strength, modulus of elasticity, splitting tensile strength, flexural strength, and cost per cubic meter. Design of experiments approach was also used to present the most significant factors affecting each variable in the mixture and to develop prediction models for each test result. In addition, a numerical optimization tool was utilized to select an optimized mixture achieving the balance between high mechanical/durability properties and lower cost. This mixture was then tested experimentally using the same procedure to validate the prediction models.

4.3 Development of Refined Response Surface Method

Three factors were considered in the developed enhanced CCD model: total binder content, W/B ratio, and the percentage of MK. The effect of each factor was evaluated at five different levels corresponding to coded values of -1, -0.5, 0, +0.5, and +1 to establish nonlinear models (**Eq. 4.1**). The developed CCD model in this investigation considered more points on the block surface than the commonly used points in standard CCD (**Figure 4.1**). In this study a quadratic model was selected with 8 vertices points, 12 centers of edges, 6 constrain plane centroids, 8 axial check points, 18 interior points, and 1 overall centroid (**Figure 4.2**). These points give a total of 53 points to develop the optimization models compared to 15 points using the standard CCD model (see **Figure 4.1**). The developed models had three independent factors: X_1 , X_2 , and X_3 . X_1 represents the total binder content, X_2 represents the W/B ratio, and X_3 represents the percentage of MK. The derived statistical models are valid for concrete mixtures made with total binder content ranging from 350 kg/m³ (-1) to 600 kg/m³ (+1); W/B ratio from 0.3 (-1) to 0.5 (+1); and percentage of MK

from 0% (-1) to 25% (+1). The selected range for each of the binder content, W/B ratio, and MK percentage were chosen based on the literature and practical considerations and to cover a wide range of possible mixture proportions.

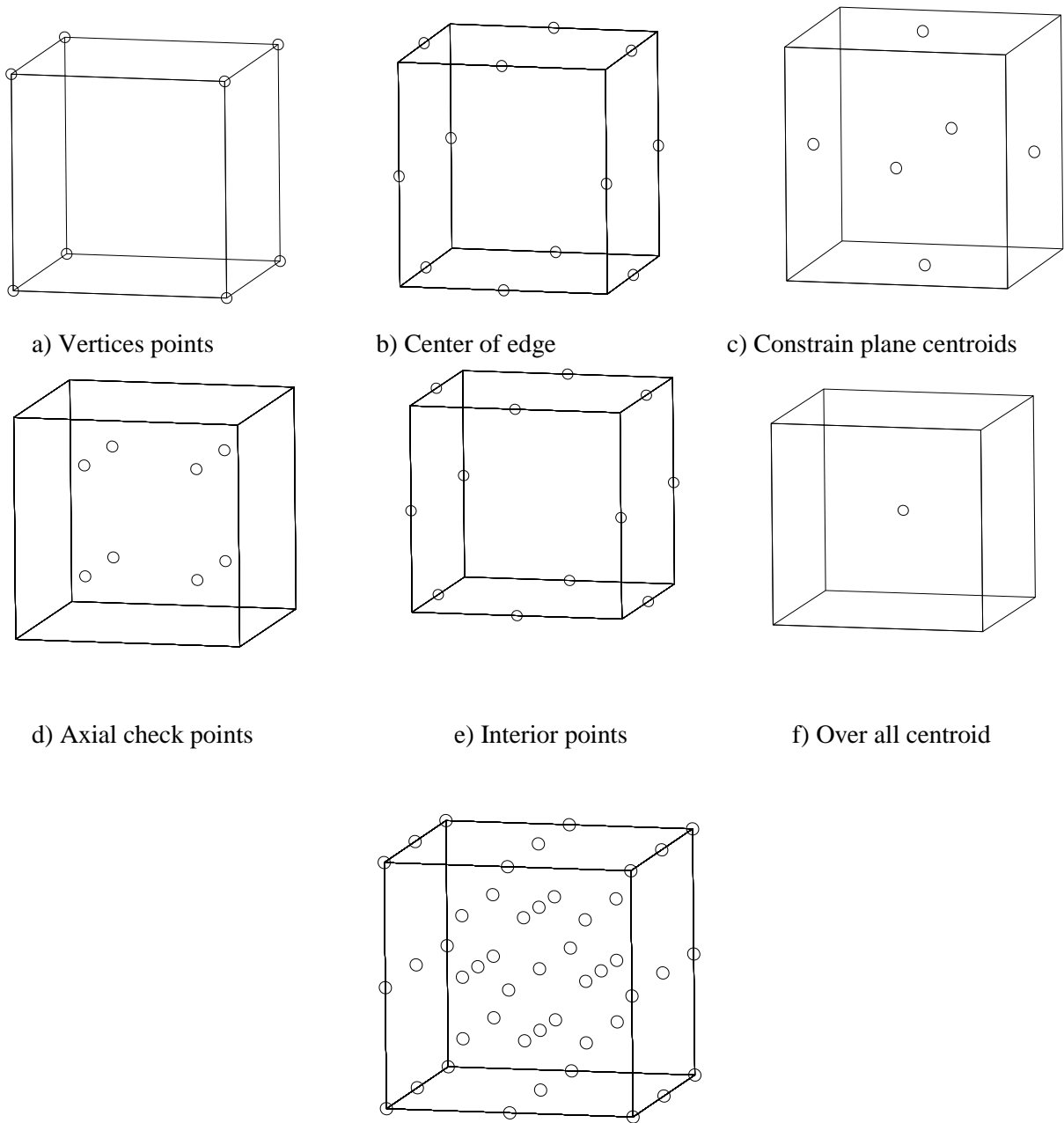


Figure 4.2 Modified CCD points

The coded values are expressed according to **Eq.4.1**:

$$Coded\ Value = \frac{\text{absolute value} - \text{central value}}{0.5 \times \text{range between maximum and minimum values}} \quad (\text{Eq.4.1})$$

A polynomial function was fitted to correlate independent factors and responses using **Eq. 4.2**. The measured responses were compressive strength (Y1), flexural strength (Y2), modulus of elasticity (Y3), splitting tensile strength (Y4), rapid chloride permeability (Y5), chloride diffusion coefficient (Y6), and cost per cubic meter (Y7).

$$Y = \beta_0 + \sum \beta_i X_i + \sum \beta_{ij} X_i X_j + \sum \beta_{ii} X_i^2 \quad (\text{Eq.4.2})$$

Where Y is the predicted response, X_i is the independent factor, β_0 is the constant coefficient of the model (intercept), β_i ($i = 1,2,3$), β_{ij} ($i = 1,2,3; j = 1,2; i > j$), and β_{ii} represents linear, interaction, and quadratic effect of the model, respectively.

A commercially available program for experimental design using statistical analysis method was used to analyze the outcomes from each test (2012a). This program performs nonlinear regression analysis for each response (test result) based on the input values (variables). Eventually, the program yields to equations of the response and obtains response surface diagrams. The developed equations were based only on the most significant variables (factors) and their interactions. The equation may be linear or nonlinear depending on the behavior of the response throughout the range of variables. Linear equations contain main variables and their interactions, while nonlinear equations include higher-order variables (quadratic or cubic). The significance of the variables and their connections was determined after compiling the analysis of variance (ANOVA). The

analysis of variance tests the probability values (Probability > F); the factor is significant if its probability value is less than 0.05 (Montgomery 2012). In addition, the degree of significance among the significant factors can be determined based on the F-value for each factor. The factor with a higher F-value is considered more significant than factors with lower F-values. On this basis, the significant variables for each response were selected to form the prediction equations. These equations exhibited some coefficients, which depend on the contribution of each factor. The factor with lower value of probability > F is preceded by higher coefficients in the respective equation. The selection of these equations was limited to obtain a possible higher value of correlation coefficient R^2 for each model. A high R^2 value for the selected equation, such as 0.90, implies that the factors varied systematically with the experimentation. After many trials in the utilized software, best-fit models were then obtained for each response. The equations can be interpreted in the form of coded values or actual values of significant variables (**Table 4.1**). For simplifying the equations, in this paper the form of actual values of each variable was used for models and plotted for simpler use. Design charts were plotted based on the equations developed for each response. Each response contains 5 charts representing different W/B ratio, binder content, and percentage of MK. **Figure 4.3** illustrates a general flow chart on the usage of the charts presented in this research.

Table 4.1 Coded and absolute values of investigated parameters

Variable		Level				
		-1	-0.5	0	+0.5	+1
Binder (kg/m ³)	X ₁	350	412.5	475	537.5	600
W/B	X ₂	0.3	0.35	0.4	0.45	0.5
MK%	X ₃	0	6.25	12.5	18.75	25

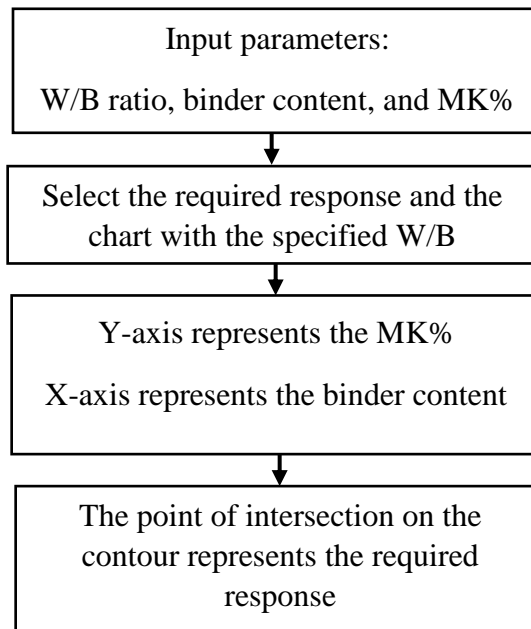


Figure 4.3 General flow chart on using the design charts

4.4 Research Significance

Although there are research papers on the use of MK in concrete mixtures, there has been little research studying the combined effect of the total binder content, water-to-binder ratio, and percentage of MK on the overall performance of the mixture. In addition, modelling the chloride permeability and chloride diffusion in MK mixtures is missing from the literature. Moreover, the current statistical analysis for optimizing concrete mixtures lacks high precision as researchers only use a minimum number of points on the response space. In this paper an enhanced statistical analysis with more precise models was

developed with the aid of an extensive experimental investigation to optimize concrete mixtures containing MK. The developed models account for the effects of total binder content, water-to-binder ratio, and percentage of MK on the chloride permeability and mechanical properties of the mixture. This paper exclusively develops design charts to help select the optimum concrete mixture with specific target strength, chloride permeability, and/or total cubic meter cost. The authors believe that this investigation will strongly contribute to understanding, optimizing, and designing concrete containing MK as an SCM.

4.5 Experimental Program

4.5.1 Materials

Type GU Canadian Portland cement similar to ASTM Type I, with a specific density of 3.15, was used for all 53 mixtures. Metakaolin, with a specific gravity of 2.56, was used in all concrete mixtures (**Table 4. 2**). Superplasticizer similar to ASTM Type F (ASTM C494) (ASTM 2013) with specific gravity, volatile weight, and pH of 1.2, 62%, and 9.5, respectively, was used to achieve the required slump of the mixtures. Natural sand and 10 mm maximum size stone were used as fine and coarse aggregates, respectively (**Table 4. 3**). The coarse and fine aggregates each had a specific gravity of 2.60 and water absorption of 1%.

Table 4.2 Chemical and physical properties

Chemical properties %	Cement	MK
SiO ₂	19.64	51-53
Al ₂ O ₃	5.48	42-44
Fe ₂ O ₃	2.38	<2.2
FeO	-	-
TiO ₂	-	<3
C	-	-
P ₂ O ₅	-	<0.2
SO ₄	-	<0.5
CaO	62.44	<0.2
MgO	2.48	<0.1
Na ₂ O	-	<0.05
C ₃ S	52.34	-
C ₂ S	16.83	-
C ₃ A	10.5	-
C ₄ AF	7.24	-
K ₂ O	-	<0.4
Loss on ignition	2.05	<0.5
Physical properties		
Specific density	3.15	2.56
Color	gray	pink
Grain size (μm)	45	60
Surface area(m ² /kg)	320-400	650-1250
Blaine fineness(m ² /kg)	410	19000

Table 4.3 Sieve analysis

Sieve size	10 mm coarse aggregate (% passing)	Sieve size	Fine aggregate passing (% passing)
14	100	10	100
10	95.8	5	99.4
5	21	2.5	79.4
2.5	2.9	1.25	55.4
1.25	0	0.63	35.2
0.63	-	0.32	18.6
0.32	-	0.16	7.3
0.16	-	0.08	2.2

4.5.2 Mixture Proportioning and Casting

Based on the selected points of the refined response surface method, 53 concrete mixtures were selected (**Table 4.4**). The coarse-to-fine aggregate ratio was maintained constant with a ratio of 1.2 for all (Bai et al., 1999, Paiva et al., 2012). This percentage was chosen to assure improved workability for all mixtures to alleviate the drop of the slump resulted from the addition of MK. Given the type and size of the tested aggregates in this investigation, it is believed that the effect of coarse-to-fine aggregate ratio on the mixture strength is minor compared to the other tested variables [39]. Therefore, the coarse-to-fine aggregate ratio was not included as a variable in the investigation. The mixture ingredients were blended in a mechanical rotary mixer. Sufficient amounts of superplasticizer were added to the concrete mixtures until they reached the required workability, which is determined by slump test to achieve a slump of 50 ± 10 mm. The freshly mixed concrete was tested for slump according to ASTM C 143. After completing the fresh properties tests, a number of concrete cylinders and concrete prisms were cast for the chloride permeability and hardened strength tests. After 24 hours of casting, all cylinders and prisms were demolded and cured in a temperature-controlled moist curing room for 28 days at 21 °C.

Table 4.4 Mixture proportions

RUN number (mixture number)	Coded value			Actual value			Fine aggregate (kg/m ³)	Coarse aggregate (kg/m ³)
	X ₁	X ₂	X ₃	Binder (kg/m ³)	W/B	MK%		
1	1	1	1	600	0.5	25	589.2	707.0
2	-1	1	-1	350	0.5	0	843.7	1012.4
3	-1	-1	-1	350	0.3	0	926.4	1111.7
4	1	1	-1	600	0.5	0	602.2	722.6
5	-1	-1	1	350	0.3	25	918.8	1102.6
6	1	-1	-1	600	0.3	0	744.0	892.8
7	1	-1	1	600	0.3	25	731.0	877.2
8	-1	1	1	350	0.5	25	836.1	1003.3
9	1	1	0	600	0.5	12.5	595.7	714.8
10	0	-1	1	475	0.3	25	824.9	989.9
11	1	-1	0	600	0.3	12.5	737.5	885.0
12	1	0	1	600	0.4	25	660.1	792.1
13	-1	0	-1	350	0.4	0	885.1	1062.1
14	0	1	-1	475	0.5	0	722.9	867.5
15	0	1	1	475	0.5	25	712.7	855.2
16	-1	-1	0	350	0.3	12.5	922.6	1107.2
17	1	0	-1	600	0.4	0	673.1	807.7
18	-1	1	0	350	0.5	12.5	839.9	1007.9
19	-1	0	1	350	0.4	25	877.5	1053.0
20	0	-1	-1	475	0.3	0	835.2	1002.2
21	-1	0	0	350	0.4	12.5	881.3	1057.5
22	1	0	0	600	0.4	12.5	666.6	799.9
23	0	-1	0	475	0.3	12.5	830.1	996.1
24	0	1	0	475	0.5	12.5	717.8	861.4
25	0	0	-1	475	0.4	0	779.1	934.9
26	0	0	1	475	0.4	25	768.8	922.6
27	0.5	0.5	-0.5	537.5	0.45	6.25	691.4	829.7
28	0.5	-0.5	-0.5	537.5	0.35	6.25	754.9	905.9
29	-0.5	-0.5	0.5	412.5	0.35	18.75	849.7	1019.7
30	0.5	0.5	0.5	537.5	0.45	18.75	685.6	822.7
31	0.5	-0.5	0.5	537.5	0.35	18.75	749.1	898.9
32	-0.5	0.5	0.5	412.5	0.45	18.75	801.0	961.2
33	-0.5	0.5	-0.5	412.5	0.45	6.25	805.5	966.5
34	-0.5	-0.5	-0.5	412.5	0.35	6.25	854.2	1025.0
35	-0.5	-0.5	0	412.5	0.35	12.5	852.0	1022.4
36	-0.5	0	-0.5	412.5	0.4	6.25	829.8	995.8
37	0.5	0.5	0	537.5	0.45	12.5	688.5	826.2
38	0	0.5	0.5	475	0.45	18.75	743.3	892.0
39	0	-0.5	0.5	475	0.35	18.75	799.4	959.3
40	0	-0.5	0	475	0.35	12.5	802.0	962.4
41	0	0	0.5	475	0.4	18.75	771.4	925.6
42	0	-0.5	-0.5	475	0.35	6.25	804.6	965.5

Table 4.4 (Continued) Mixture proportions

RUN number (mixture number)	Coded value			Actual value			Fine aggregate (kg/m ³)	Coarse aggregate (kg/m ³)
	X ₁	X ₂	X ₃	Binder (kg/m ³)	W/B	MK%		
43	0.5	0	0	537.5	0.4	12.5	720.3	864.3
44	-0.5	0	0	412.5	0.4	12.5	827.6	993.1
45	0	0.5	-0.5	475	0.45	6.25	748.4	898.1
46	0.5	0	0.5	537.5	0.4	18.75	717.4	860.8
47	0.5	0	-0.5	537.5	0.4	6.25	723.2	867.8
48	0	0.5	0	475	0.45	12.5	745.9	895.0
49	-0.5	0.5	0	412.5	0.45	12.5	803.2	963.9
50	-0.5	0	0.5	412.5	0.4	18.75	825.4	990.4
51	0.5	-0.5	0	537.5	0.35	12.5	752.0	902.4
52	0	0	-0.5	475	0.4	6.25	776.5	931.8
53	0	0	0	475	0.4	12.5	773.9	928.7

4.5.3 Test Procedures

Three concrete cylinders 100 mm diameter x 200 mm high were prepared from each mixture to test the 28-day f_c (ASTM C39). The indirect splitting tensile strength (STS) test was performed according to ASTM 496 on three concrete cylinders 100 mm diameter x 200 mm high for each tested mixture. The MOE for each mixture was calculated according to ASTM C469 using two concrete cylinders 100 mm diameter x 200 mm high. Each cylinder had two strain gages glued to each side of the cylinder, which were connected to a data acquisition system that recorded the stress versus strain during the whole history of the test. Three concrete prisms 100 x 200 mm were cast for each tested mixture according to ASTM C78 to test the FS. The prisms were tested under three-point flexural testing using a universal testing machine. The chloride permeability of the 53 mixtures was evaluated by means of the RCPT using ASTM C1202. The chloride diffusion test was also used to evaluate the chloride permeability of the concrete samples based on the bulk diffusion test. To verify the results of the RCPT and chloride diffusion tests, two samples were tested for

each of tested mixtures. The chloride content profile (chloride content versus diffusion depth) for each mixture was used to determine the apparent chloride diffusion coefficient (D_a) by analysis using Fick's second law of diffusion, as per ASTM C1556. After collecting the experimental results, a refined statistical analysis was executed on the data and prediction models and design charts were generated.

4.6 Results and Discussion

Table 4.5 shows the results of the experimental work for all tested samples. These results were used in the developed refined statistical analysis to obtain models for each response.

Table 4.6 shows the standard deviation and relative errors, with 95% confidence limit of measured responses. **Table 4.7** shows the derived models for all responses using the RSM.

For simplifying the equations, the form of actual values of each variable was applied. Based on the derived equations obtained from the results of the 53 concrete mixtures, a set of charts was plotted for each response. For all charts, the x-axis represents the binder content, which varied from 350 to 600 kg/m³, and the y-axis represents the percentage of MK, which varied from 0% to 25%. Each curve was plotted on a specific W/B ratio based on the five levels used in the mixture design (0.3, 0.35, 0.4, 0.45, and 0.5).

Table 4.5 Experimental results

Mixture	f_c (MPa)	STS (kN)	FS (kN)	MOE (GPa)	$D_{a,x} 10^{-12}$ (m ² /s)	RCPT (coulombs)	Cost (CAD*)
1	67	6.6	6.00	65	1.385	1192	265.9
2	35	3.3	2.72	33	6.526	4545	187.5
3	51	4.9	4.40	47	2.484	788	193.8
4	54	5.7	5.70	53	3.825	3144	256.4
5	83	8	9.17	82	1.227	455	199.4
6	84	10.88	9.42	82.98	0.798	400	267.3
7	108	12.47	10.48	108	0.200	203	315.7
8	58	5.5	5.80	53	2.309	1460	193
9	58	6.1	5.85	58	2.771	1901	261.1
10	90	10.27	9.77	86.98	0.724	254	238.1

Table 4.5 (Continued) Experimental results

Mixture	f_c (MPa)	STS (kN)	FS (kN)	MOE (GPa)	$D_a \times 10^{-12}$ (m ² /s)	RCPT (coulombs)	Cost (CAD*)
11	92	12.28	10.12	87.29	0.399	300	272
12	85	8	9.80	81.22	0.479	420	271.3
13	47	3.32	3.20	48.85	4.408	1763	190.6
14	40	3	3.35	42.6	4.366	4181	221.9
15	65	6.4	6.10	61.486	2.626	1267	229.4
16	80	7	8.10	80	2.087	520	196.6
17	65	5.94	6.00	68.61	3.175	1091	261.8
18	40	5.1	3.16	40	5.547	2546	190.2
19	77.5	8.8	7.07	76.87	1.474	590	196.2
20	77	6.3	6.20	74	1.584	450	230.6
21	68	6.19	5.05	65.94	2.734	1228	193.4
22	82	6.7	9.13	79.35	1.265	500	266.6
23	87	7.1	8.30	82	1.242	410	234.3
24	50	3.16	4.70	45	4.268	2231	225.7
25	50	4.4	3.60	53.2	2.320	1314	226.2
26	80	8.5	8.00	71.59	1.394	540	233.8
27	52	4.2	3.90	49	3.386	2273	243.7
28	76	7.8	7.56	73.197	1.722	470	248.6
29	82	8.5	7.94	76.339	1.421	388	215.2
30	68	8.21	7.63	65	1.391	1146	248.0
31	90	10.86	8.75	89.93	0.418	350	252.9
32	43.8	5.99	5.00	41.79	3.237	1890	211.5
33	38	3.22	2.84	31	5.027	3540	208.2
34	68	6.5	6.89	67.45	2.129	604	212.0
35	70	7.3	7.40	75.09	2.127	494	213.6
36	63	4.18	4.39	59.33	3.407	1125	210.1
37	60	5.47	6.36	57	2.332	1566	245.8
38	64	6.2	5.60	57	1.983	1190	229.7
39	89.7	9	8.70	83	1.222	382	234.0
40	80	7.7	7.50	75	1.775	480	232.2
41	79	7.1	7.52	68	1.809	643	231.9
42	78	7.4	7.04	74.56	2.393	553	230.3
43	78	7.91	6.90	64	1.585	694	248.3
44	72	6.5	6.40	66.7	3.301	864	211.7
45	49	3.85	3.53	46	3.567	2554	226.0
46	81	9.68	7.90	80.17	1.077	625	250.4
47	72	6.5	6.00	57.42	3.170	958	246.2
48	50	4	3.90	46	2.527	1973	227.8
49	40	4.16	3.64	38.13	3.604	2474	209.8
50	73	6.7	7.43	68	2.707	665	213.3
51	84	10.15	8.64	82.39	1.122	405	250.7
52	67	5	4.54	57	1.947	1076	228.1
53	55	5.3	6.72	55	3.263	810	230.0

*CAD = Canadian Dollar

Table 4.6 Experimental error (fc, STS, FS, and MOE)

Factor	f_c			STS			FS			MOE		
	standard Error	Low	High	standard Error	Low	High	standard Error	Low	High	standard Error	Low	High
Intercept	1.308	65.271	70.593	0.167	6.047	6.725	0.135	5.980	6.528	1.204	60.538	65.439
X ₁ -Binder	3.608	6.254	20.935	0.460	1.274	3.144	0.371	0.538	2.049	3.323	4.304	17.823
X ₂ -W/B	3.608	-39.529	-24.848	0.460	-4.730	-2.860	0.371	-4.304	-2.792	3.323	-41.003	-27.483
X ₃ -MK%	3.608	4.687	19.368	0.460	2.063	3.934	0.371	1.664	3.175	3.323	6.782	20.302
X ₁ X ₂	1.595	-4.575	1.916	0.203	-1.333	-0.507	0.164	-0.456	0.212	1.469	-3.844	2.133
X ₁ X ₃	1.595	-5.300	1.191	0.203	-0.844	-0.017	0.164	-0.837	-0.169	1.469	-5.075	0.902
X ₂ X ₃	1.595	-3.930	2.561	0.203	-0.534	0.293	0.164	-0.511	0.157	1.469	-4.650	1.327
X ₁ ²	2.017	-2.345	5.864	0.257	0.186	1.231	0.208	0.124	0.969	1.858	0.327	7.886
X ₂ ²	2.017	-5.886	2.323	0.257	-0.371	0.675	0.208	-0.271	0.574	1.858	-4.738	2.821
X ₃ ²	2.017	-4.278	3.931	0.257	-0.636	0.410	0.208	-0.660	0.186	1.858	-2.836	4.724
X ₁ X ₂ X ₃	1.998	-4.155	3.976	0.255	-0.489	0.547	0.206	-0.282	0.555	1.840	-3.541	3.947
X ₁ ² X ₂	2.826	-4.753	6.746	0.360	-0.813	0.652	0.291	-0.747	0.437	2.602	-5.246	5.344
X ₁ ² X ₃	2.826	-5.304	6.195	0.360	-1.301	0.164	0.291	-0.970	0.214	2.602	-2.422	8.167
X ₁ X ₂ ²	2.826	-2.281	9.218	0.360	0.520	1.985	0.291	-0.961	0.222	2.602	-0.931	9.658
X ₁ X ₃ ²	2.826	-3.912	7.587	0.360	-0.542	0.923	0.291	-0.817	0.366	2.602	-1.711	8.878
X ₂ ² X ₃	2.826	-8.144	3.355	0.360	-1.397	0.068	0.291	-1.339	-0.155	2.602	-4.948	5.641
X ₂ X ₃ ²	2.826	-1.820	9.679	0.360	-0.544	0.921	0.291	-0.103	1.081	2.602	-1.955	8.635
X ₁ ³	4.808	-18.276	1.289	0.613	-3.164	-0.671	0.495	-0.580	1.434	4.428	-16.660	1.358
X ₂ ³	4.808	3.289	22.854	0.613	0.569	3.062	0.495	0.508	2.522	4.428	7.466	25.483
X ₃ ³	4.808	-8.816	10.749	0.613	-1.934	0.559	0.495	-1.143	0.871	4.428	-14.535	3.482

Table 4. 6 (continued) **Experimental error (Da, RCPT, and Cost)**

Factor	Da			RCPT			Cost		
	standard Error	Low	High	standard Error	Low	High	standard Error	Low	High
Intercept	0.066	2.230	2.497	0.609	29.261	31.741	0.755	229.216	232.251
X ₁ -Binder	0.102	-1.088	-0.679	1.681	-8.684	-1.843	1.159	35.981	40.638
X ₂ -W/B	0.102	1.095	1.504	1.681	23.129	29.970	1.159	-8.382	-3.725
X ₃ -MK%	0.102	-1.245	-0.836	1.681	-12.495	-5.654	1.159	3.163	7.821
X ₁ X ₂	0.135	-0.474	0.069	0.743	-2.113	0.912	0.000	0.000	0.000
X ₁ X ₃	0.135	-0.105	0.438	0.743	-0.313	2.711	0.000	0.000	0.000
X ₂ X ₃	0.135	-0.760	-0.217	0.743	-7.047	-4.022	0.000	0.000	0.000
X ₁ ²	0.000	0.000	0.000	0.940	-2.566	1.259	0.000	0.000	0.000
X ₂ ²	0.000	0.000	0.000	0.940	2.694	6.519	0.000	0.000	0.000
X ₃ ²	0.000	0.000	0.000	0.940	-1.778	2.047	0.000	0.000	0.000
X ₁ X ₂ X ₃	0.000	0.000	0.000	0.931	-1.069	2.720	0.000	0.000	0.000
X ₁ ² X ₂	0.000	0.000	0.000	1.317	-3.618	1.740	0.000	0.000	0.000
X ₁ ² X ₃	0.000	0.000	0.000	1.317	-2.543	2.816	0.000	0.000	0.000
X ₁ X ₂ ²	0.000	0.000	0.000	1.317	-2.248	3.110	0.000	0.000	0.000
X ₁ X ₃ ²	0.000	0.000	0.000	1.317	-2.076	3.282	0.000	0.000	0.000
X ₂ ² X ₃	0.000	0.000	0.000	1.317	-3.748	1.611	0.000	0.000	0.000
X ₂ X ₃ ²	0.000	0.000	0.000	1.317	-1.514	3.844	0.000	0.000	0.000
X ₁ ³	0.000	0.000	0.000	2.241	-3.760	5.357	0.000	0.000	0.000
X ₂ ³	0.000	0.000	0.000	2.241	-17.003	-7.886	0.000	0.000	0.000
X ₃ ³	0.000	0.000	0.000	2.241	-2.687	6.430	0.000	0.000	0.000

Table 4.7 Derived statistical models

coefficient	f_c	STS	FS	MOE	D_a	RCPT ^{0.5}	Cost
β_0	-530.44	-58.25	-55.8896	-812.53	-2.84	765.4709	103.8792
β_1	-2.16	-0.55	0.027594	-1.99	0.000	0.150435	0.306476
β_2	7195.03	1176.46	501.6519	9093.53	25.6	-6045.24	-60.5335
β_3	3.04	-0.97	-0.64253	9.1	0.02	2.01481	0.439343
β_{12}	-2.93	-0.83	0.310289	-2.91	-0.02	0.180835	0.000
β_{13}	-0.01	0.000	0.001455	-0.02	0.000	-0.00278	0.000
β_{23}	8.76	3.77	3.443503	-9.51	-0.39	-1.96386	0.000
β_{11}	0.01	0.000	-0.00021	0.01	0.000	-0.00039	0.000
β_{22}	-16942.5	-2572.68	-1587.98	-21557.93	0.000	15337.18	0.000
β_{33}	-0.16	0.000	-0.00595	-0.06	0.000	-0.07957	0.000
β_{123}	0.000	0.000	0.000873	0.000	0.000	0.005284	0.000
β_{112}	0.000	0.000	-9.90E-05	0.000	0.000	-0.0006	0.000
β_{113}	0.000	0.000	-1.90E-06	0.000	0.000	6.99E-07	0.000
β_{122}	2.77	1	-0.29563	3.49	0.000	0.344906	0.000
β_{133}	0.000	0.000	-1.20E-05	0.000	0.000	3.09E-05	0.000
β_{223}	-19.16	-5.31	-5.97826	2.77	0.000	-8.54747	0.000
B_{233}	0.25	0.01	0.031311	0.21	0.000	0.07456	0.000
β_{111}	0.000	0.000	2.19E-07	0.000	0.000	4.09E-07	0.000
β_{222}	13071.45	1815.13	1515.214	16474.44	0.000	-12444.6	0.000
β_{333}	0.000	0.000	-7.00E-05	0.000	0.000	0.000958	0.000

Response(Y)= $\beta_0 + \beta_1 X_1 + \beta_2 X_2 + \beta_3 X_3 + \beta_{12} X_1 X_2 + \beta_{13} X_1 X_3 + \beta_{23} X_2 X_3 + \beta_{11} X_1^2 + \beta_{22} X_2^2 + \beta_{33} X_3^2 + \beta_{123} X_1 X_2 X_3 + \beta_{112} X_1^2 X_2 + \beta_{113} X_1^2 X_3 + \beta_{122} X_1 X_2^2 + \beta_{133} X_1 X_3^2 + \beta_{223} X_2^2 X_3 + \beta_{233} X_2 X_3^2 + \beta_{111} X_1^3 + \beta_{222} X_2^3 + \beta_{333} X_3^3$

4.6.1 Compressive Strength (f_c)

The 28-day f_c results of the tested mixtures are shown in **Table 4.5**. As seen from the Table 4., at a given binder content and W/B ratio the 28-day f_c increased as the percentage of MK increased. For example, **Table 4.5** shows that, for mixtures 12, 17, and 22 where the binder content and W/B ratio were constant at 600 kg/m³ and 0.4, respectively, increasing the MK from 0% to 25% increased the f_c from 65 MPa to 85 MPa. This result agrees with other researchers' results which show that increasing the percentage of MK up to a maximum of 25% exhibited the highest compressive strengths (Paiva et al., 2012, Badogiannis and Tsivilis, 2009, Poon et al., 2006). The results in **Table 4.5** also show that increasing the

W/B ratio decreased the 28-day f_c . Increasing the W/B ratio from 0.3 to 0.5 yielded a drop in the f_c by 30% to 60%. Mixtures 9, 11, and 22 (in **Table 4.5**), which have a 600 kg/m³ binder content and a 12.5% MK, showed that increasing the W/B ratio from 0.3 to 0.5 reduced the 28-day f_c from 92 MPa to 58 MPa. The binder content also affected the f_c : as the binder content increased, the f_c increased. For example, at a constant percentage of MK of 12.5% and a constant W/B ratio of 0.3 (mixtures 11, 16, and 23), increasing the binder content from 350 to 600 kg/m³ increased the f_c from 80 MPa to 92 MPa (**Table 4.5**).

An analysis of variance was completed for the 53 mixtures, based on the 28-day f_c results, to select the most significant factors affecting f_c . These factors were X_2 , X_1 , and X_3 , respectively, in order of significance. The W/B ratio (X_2) was the most significant factor, followed by the metakaolin replacement (factor X_3) and then the total binder content (factor X_1) (**Table 4.8**). Five contour charts were plotted (**Figure 4.4**) based on the developed model with R^2 of 0.926 (**Table 4.8**) for the different levels of the W/B ratios (0.5, 0.45, 0.4, 0.35, and 0.3). The plotted contour charts simplify the design and optimization process and give a better understanding of the interaction between a mixture's parameters and responses. By looking at the charts, it can be seen that decreasing the W/B ratio or increasing the MK/binder content increases the 28-day f_c . The charts also give a good understanding of how the three parameters (binder, MK, and W/B ratio) are related to each other and how they affect the f_c .

Table 4.8 Analysis of variance for significant parameters (F-value and P-value)

Response	Significant factor						Model R ²
	Binder (A)		W/B (B)		MK% (C)		
	F-value	P-value	F-value	P-value	F-value	P-value	
f_c	14.20	0.0006	79.59	< 0.0001	11.11	0.0021	0.926
STS	23.09	< 0.0001	68.16	< 0.0001	42.55	< 0.0001	0.937
FS	12.12609	0.0014	91.2196	< 0.0001	42.417	< 0.0001	0.912
MOE	11.09	0.0021	106.22	< 0.0001	16.61	0.0003	0.935
D _a	75.74	< 0.0001	163.84	< 0.0001	105.02	< 0.0001	0.887
RCPT	9.802157	0.003638	249.3721	< 0.0001	29.135	< 0.0001	0.973
Cost	1092.914	< 0.0001	27.28765	< 0.0001	22.45955	< 0.0001	0.959

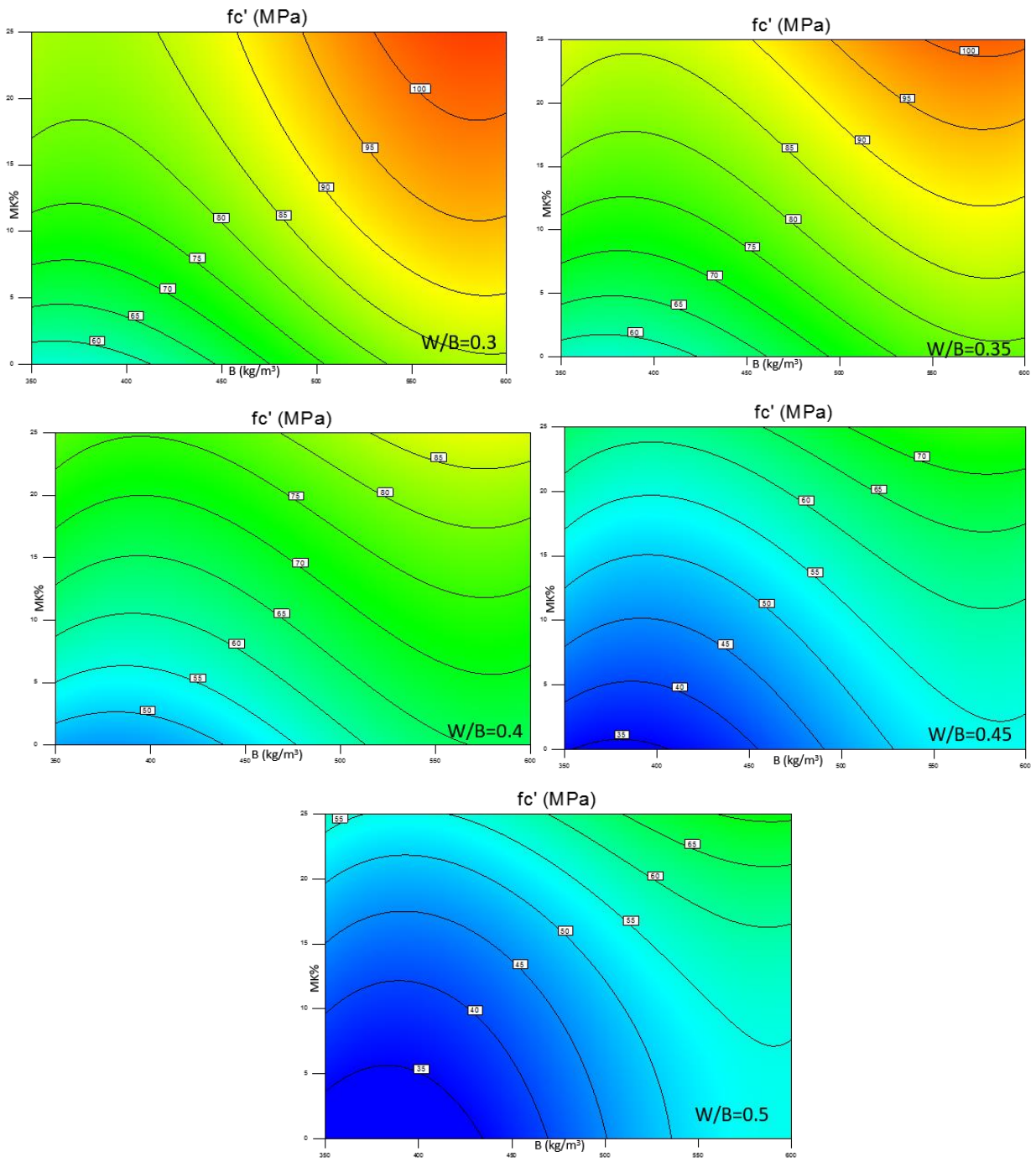


Figure 4.4 Compression strength charts with variance W/B content

4.6.2 Splitting Tensile Strength (STS)

All concrete performs poorly under tensile stress and a low strain capacity (Mindess et al., 2003). The tensile strength of concrete is typically estimated around 10% of the compressive strength. The results of STS are presented in **Table 4.5**. It can be observed that the STS increased as the MK increased. For example, increasing the percentage of MK from 0% to 25% at a W/B ratio of 0.45 and a binder content of 475 kg/m^3 (mixtures 38, 45, and 48 in **Table 4.5**) increased the STS from 3.85 kN to 6.2 kN. Güneyisi et al. (Güneyisi et al., 2008) also found similar result when testing concrete with MK ranges from 0% to 20%. It can also be observed that the STS decreased when the W/B ratio was increased from 0.3 to 0.5 (**Table 4.5**). As an example, mixtures 16, 18, and 20, with 350 kg/m^3 binder content and 12.5% MK, show that increasing the W/B ratio from 0.3 to 0.5 reduced the STS from 7 kN to 5.1 kN. The results in **Table 4.5** also indicated that increasing the binder content increased the STS. Moreover, in mixtures 1, 8, and 15, which have similar W/B ratio and percentage of MK (0.5 and 25%, respectively), the STS increased from 5.5 kN to 6.6 kN when the binder content increased from 350 kg/m^3 to 600 kg/m^3 . The above effects of MK, W/B ratio, and binder content on the STS matched the results from other investigations (Güneyisi and Mermerdaş, 2007).

After performing the analysis of variance, factors X_2 (W/B), X_3 (MK), and X_1 (binder content), respectively in terms of significance, were found to be the most significant factors governing the STS (**Table 4.8**). The developed model of the STS (**Table 4.7**) showed an R^2 of 0.937 (**Table 4.7**). A set of five contour charts were plotted based on the derived model with different W/B ratios (**Figure 4.5**). The charts express the relationships between the STS results and the three parameters (W/B ratio, binder content, and MK). The charts

also give a better view of the interaction between the three parameters and of how they are related to each other.

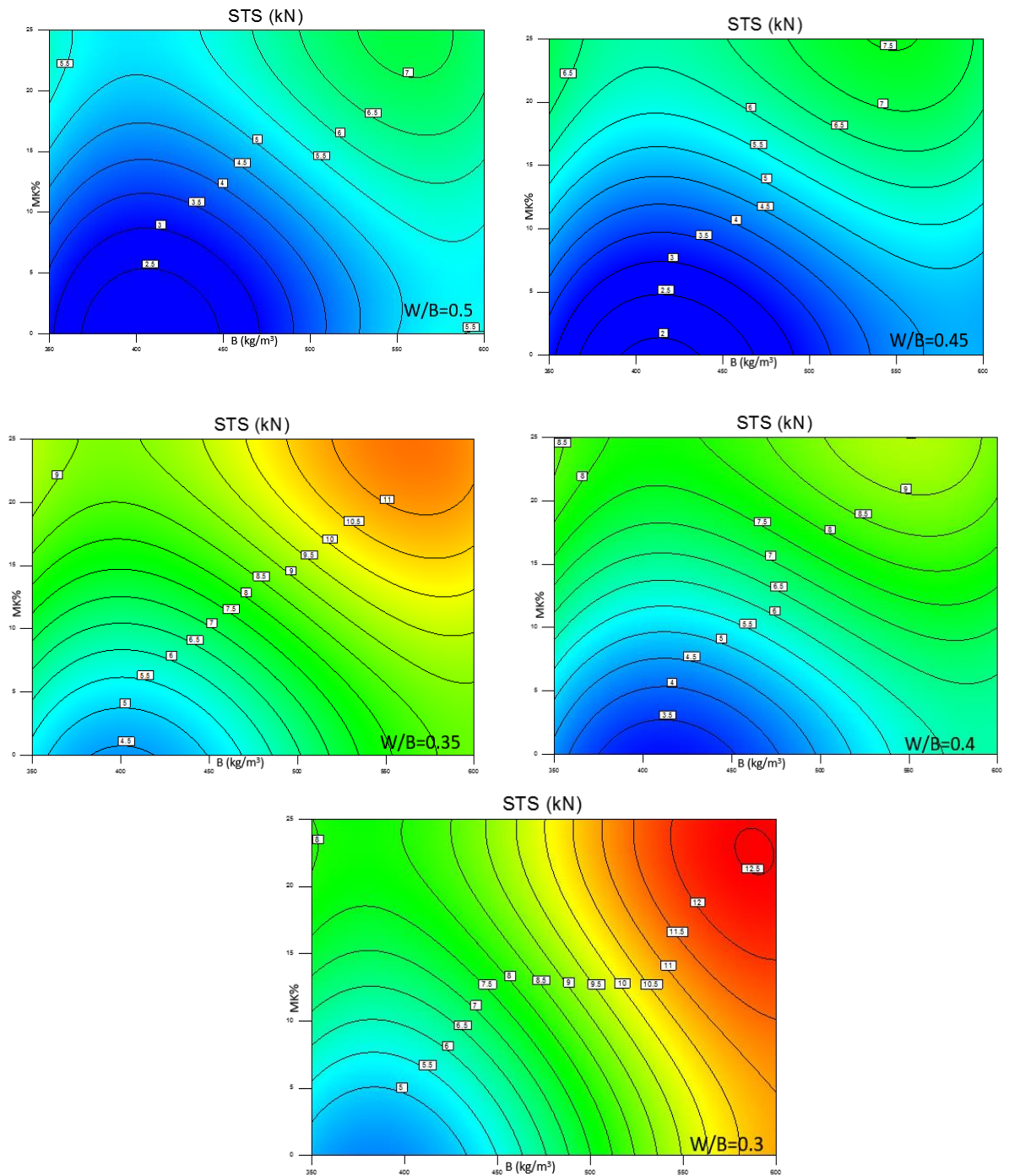


Figure 4.5 Splitting tensile strength charts with variance W/B content

4.6.3 Flexural Strength (FS)

As shown in **Table 4.5**, it can be observed that mixtures containing a higher content of MK exhibited higher flexural strength compared to mixtures with lower MK content. By comparing mixtures 10, 20, and 23 in **Table 4.5** (both with W/B = 0.3 and binder content = 475 kg/m³), it can be noted that increasing the MK from 0% to 25% increased the FS from 6.2 kN to 9.77 kN. Qian and Li also found the same enhancement of the FS when testing high performance concrete with increased percentage of MK (Qian and Li, 2001). It can also be observed from **Table 4.5** that decreasing the W/B ratio or increasing the binder content increased the FS. For example, in mixtures 23, 24, 40, 48, and 53 the FS increased from 3.9 kN to 8.3 kN by varying the W/B ratio from 0.3 to 0.5 while fixing the binder content and MK percentage to 475 kg/m³ and 12.5%, respectively. The results of the effects of MK, W/B ratio, and binder content on the FS are similar to those found by other studies (Qian and Li, 2001, Dubey and Banthia, 1998).

After completing the analysis of variance on the FS test results, the significant factors were found to be X₂ (W/B), X₃ (MK), and X₁ (binder content), respectively, in order of significance (**Table 4.8**). A model was derived based on the FS results with R² = 0.912 showing a good correlation between the FS and the three variables (**Table 4.7**). In addition, five contour charts were plotted (**Figure 4.6**) for each level of the W/B content. The contour charts clarify how the three factors (binder, MK%, and W/B) are interconnected and affect the FS. Also, the charts (**Figure 4.6**) illustrate that the FS increases by both increasing the percentage of MK and/or the binder content and decreasing the W/B ratio.

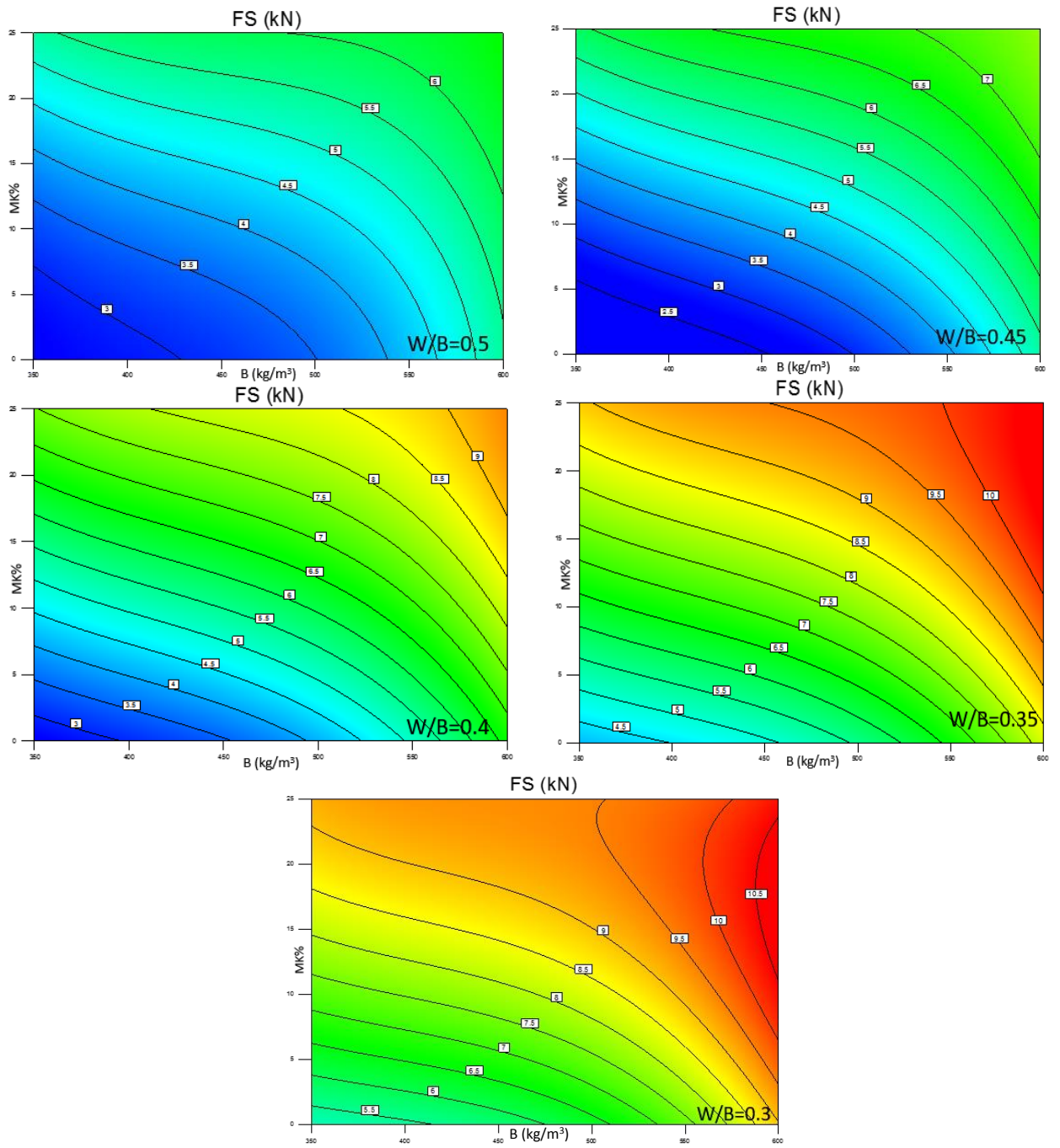


Figure 4.6 Flexural strength charts with various W/B ratios

4.6.4 Modulus of Elasticity (MOE)

All mixtures with MK showed higher MOE compared to mixtures with no MK. From **Table 4.5**, it can be observed that in mixtures 24, 25, 52, and 53 with a fixed W/B ratio and binder content of 0.4 and 475 kg/m³, respectively, varying the percentage of MK from 0% to 25% increased the MOE from 45 GPa to 57 GPa. On the other hand, decreasing the W/B ratio or increasing the binder content increased the MOE (Qian and Li, 2001). For example, mixtures 1, 7, and 12 (600 kg/m³ binder content and 25% MK) show that varying the W/B ratio from 0.5 to 0.3 increased the MOE from 65 GPa to 108 GPa. These results of the MOE were in accordance with what has been reported by previous investigations (Qian and Li, 2001, Khatib and Clay, 2004).

The results from the analysis of variance for the MOE indicated that the most significant factors affecting the mixture elasticity were X₂ (W/B), X₃ (MK%), and X₁ (binder content), respectively, in order of significance (**Table 4.7**). A model with R² of 0.935 (**Table 4.7**) was developed to predict the MOE for various W/B ratios, binder contents, and percentages of MK (**Table 4.7**). **Figure 4.7** also presents the developed model in five contour charts for each W/B ratio. These charts provide a suitable interpretation on how the three parameters interact (binder, MK%, and W/B) and how their interaction effects on the MOE. The charts offer a simple way to predict the response values without dealing with long formulas.

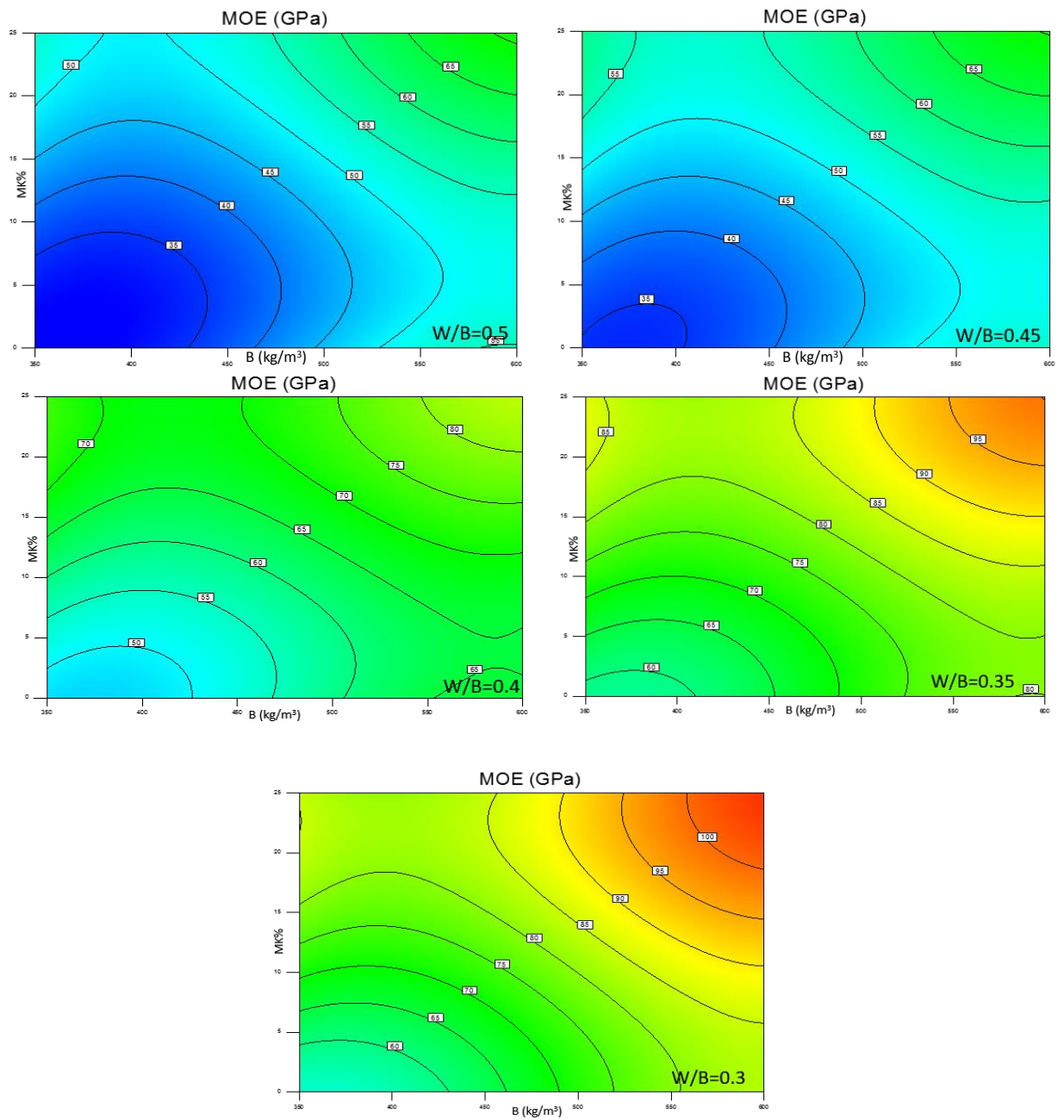


Figure 4.7 Modulus of elasticity charts

4.6.5 Rapid Chloride Permeability Test (RCPT)

It has been proven that adding SCM improves the resistance to chloride ion penetration (Rodriguez and Hooton, 2003). Moreover, mixtures containing higher replacement of MK provide lower chloride permeability compared to mixtures with low/no MK (Hassan et al., 2012b, Poon et al., 2006). This lower chloride permeability is attributed to the pozzolanic reaction resulting from the addition of MK. **Table 4. 5** illustrates that increasing the percentage of MK from 0% to 25% at a W/B ratio of 0.3 and binder content of 350 kg/m³ (mixtures 3, 5, and 16 as an example) increased the resistivity from 788 to 455 coulombs. Decreasing the W/B ratio or increasing the binder content also increased the resistivity of concrete. For example, mixtures 5, 8, and 19, which had a constant binder content of 350 kg/m³ and a constant MK percentage of 25%, showed an increase in the concrete resistivity from 1460 to 455 coulombs, when the W/B ratio was increased from 0.3 to 0.5. However, mixtures 21, 22, 43, 44, and 53, which had a constant MK percentage of 12.5% and W/B ratio of 0.4 and varying binder content from 350 kg/m³ to 600 kg/m³, RCPT results decreased from 1228 to 500 coulombs.

The analysis of variance for the RCPT results showed that the most significant factors affecting the chloride resistivity were X₂ (W/B), X₃ (MK), and X₁ (binder content), respectively, in order of significance (**Table 4. 8**). The developed prediction model in **Table 4. 7** presents an equation ($R^2 = 0.973$) that correlates the binder content, W/B ratio, and MK content with the RCPT results. **Figure 4. 8** also presents five contour charts plotted with the five levels of the W/B ratio based on the developed model. The charts give a good presentation of how the three parameters (binder, MK%, and W/B) are linked to each other

and of how they clarify the effect of the W/B ratio, binder content, and percentage of MK on the RCPT results.

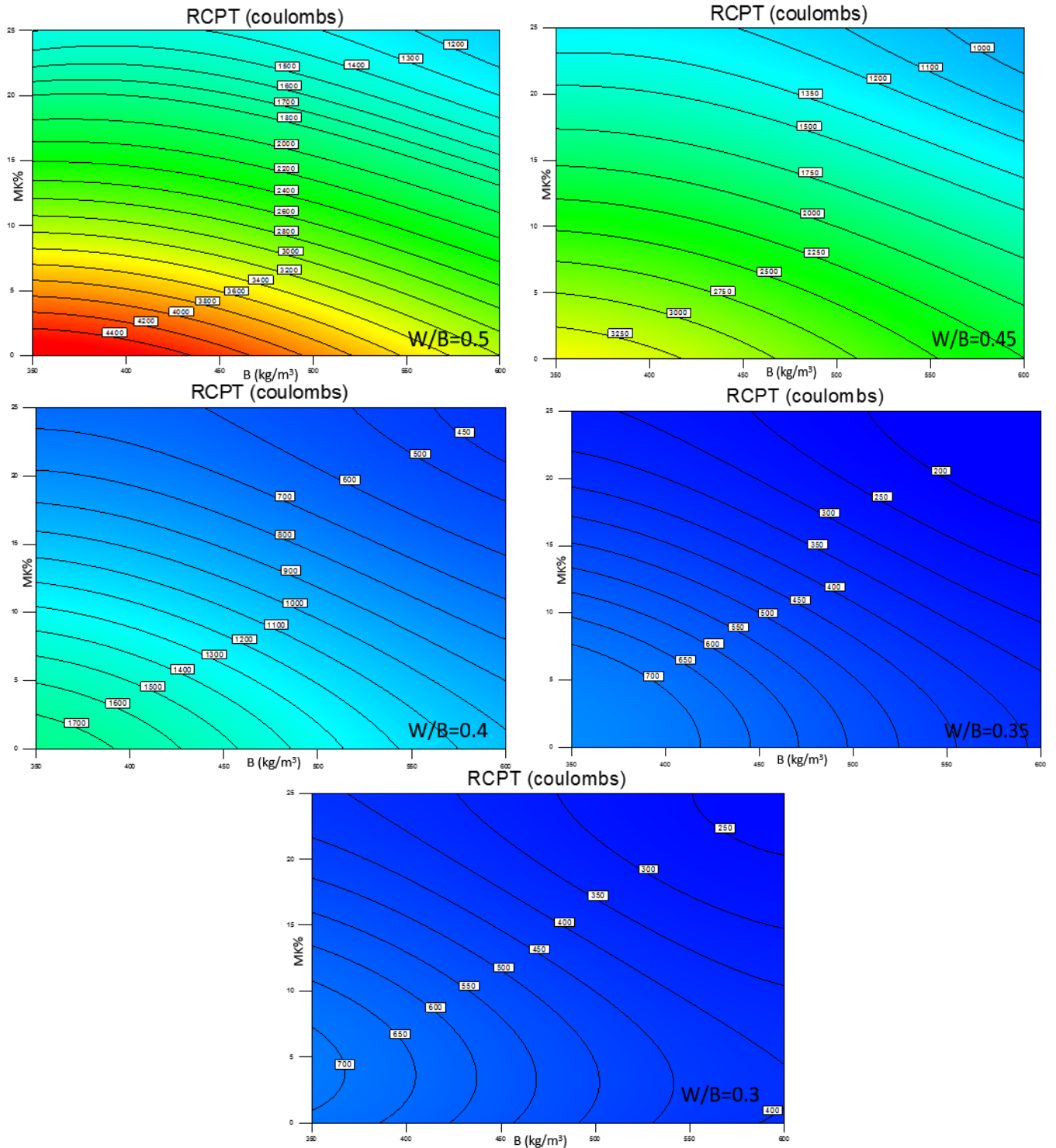


Figure 4.8 RCPT charts with various W/B ratios

4.6.6 Diffusion Coefficient (D_a)

As the chlorides are the most significant cause of the rebar corrosion, it is important to calculate the diffusion of chlorides in concrete. The apparent diffusion coefficient (D_a) is the most common presentation of the chloride diffusion in concrete. The results showed that the addition of MK decreased the chloride diffusion at different W/B ratios (Poon et al., 2006). This decrease is attributed to decreasing the pore size as a result of the pozzolanic reactivity of the MK mixture. Mixtures 3, 5, and 16 (in **Table 4. 5**), as an example, illustrate that varying the percentage of MK from 0% to 25% at a binder content of 350 kg/m^3 and a W/B ratio of 0.3 decreased the D_a from 2.484 to $1.227 \times 10^{-12}(\text{m}^2/\text{s})$. Meanwhile, in mixtures 1, 7, and 12, increasing the W/B ratio from 0.3 to 0.5 at a constant binder content of 600 kg/m^3 and constant MK of 25% increased the D_a from 0.2 to $1.385 \times 10^{-12}(\text{m}^2/\text{s})$. The results also showed that increasing the binder content at a given W/B ratio and MK content resulted in an increase in the D_a .

The most significant factors governing the results of this test were found to be X_2 (W/B), X_3 (MK), and X_1 (binder content), respectively, in order of significance (**Table 4. 8**). The developed model presented in **Table 4. 7** showed a good correlation with the collected data. Based on the developed model five contour charts were plotted (**Figure 4. 9**) with the five levels of the W/B ratio in order to clarify the effect of the three parameters (binder, MK%, and W/B) on the diffusion coefficient and to facilitate using the model in an easy and simple way.

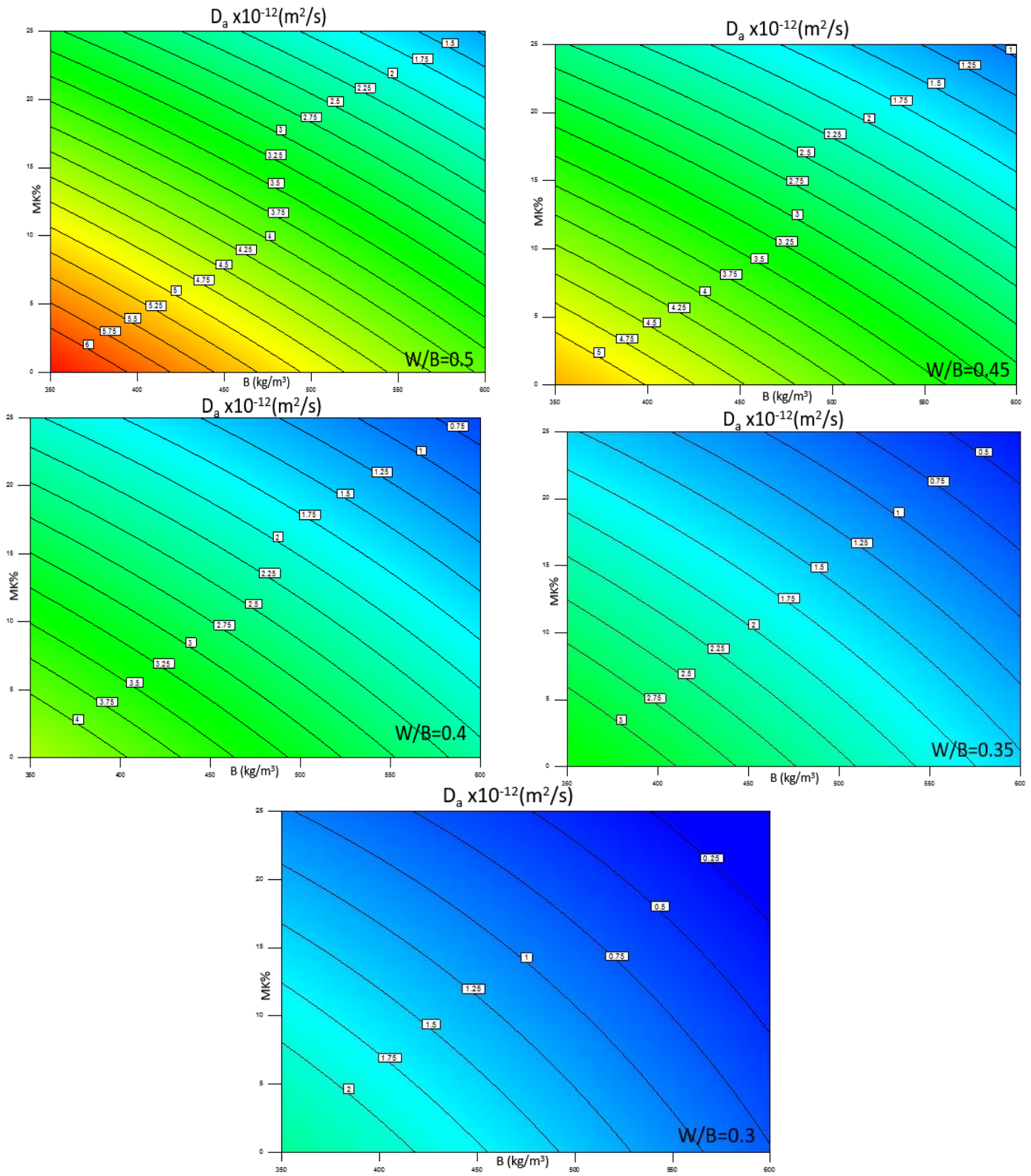


Figure 4.9 Diffusion coefficient charts with various W/B ratios

4.6.7 Cost Analysis

The cost of a cubic meter versus the mechanical and durability properties is a key factor in selecting the mixture required for a project. Choosing mixtures with the lowest cost possible and highest mechanical and durability properties is the target for designers and decision-making personnel. This cost analysis is based on the price of materials in Canada as of the date of this investigation. The costs of cement, MK, fine aggregate, coarse aggregate, and superplasticizer (in Canadian dollars) were found to be \$350/ton, \$420/ton, \$35/ton, \$35/ton, and \$6/liter, respectively. It can be seen that increasing the binder content or the percentage of MK improved the mechanical properties and reduced the chloride permeability but raised the cost per cubic meter. On the other hand, reducing the W/B ratio and/or increasing the percentage of MK also improved the mechanical properties and reduced the chloride permeability but increased the demand for superplasticizer and hence raised the total cost. Therefore, it was important to perform ANOVA analysis to optimize the cost of the mixture and to facilitate selecting the mixture variables that warrant lower cost and higher target response.

The analysis of variance indicated that the significant factors dominating the cost per cubic meter of each mixture of this analysis were X_1 (binder content), X_3 (MK), and X_2 (W/B ratio), respectively, in order of significance (**Table 4. 8**). The developed model listed in **Table 4. 7** shows a good correlation with the calculated data. Based on the developed model, five contour charts were plotted (**Figure 4. 10**) with the five levels of the W/B ratio in order to clarify the effect of the three parameters (binder, MK%, and W/B) on the concrete's cost per cubic meter and to facilitate using the model in an easy and simple way.

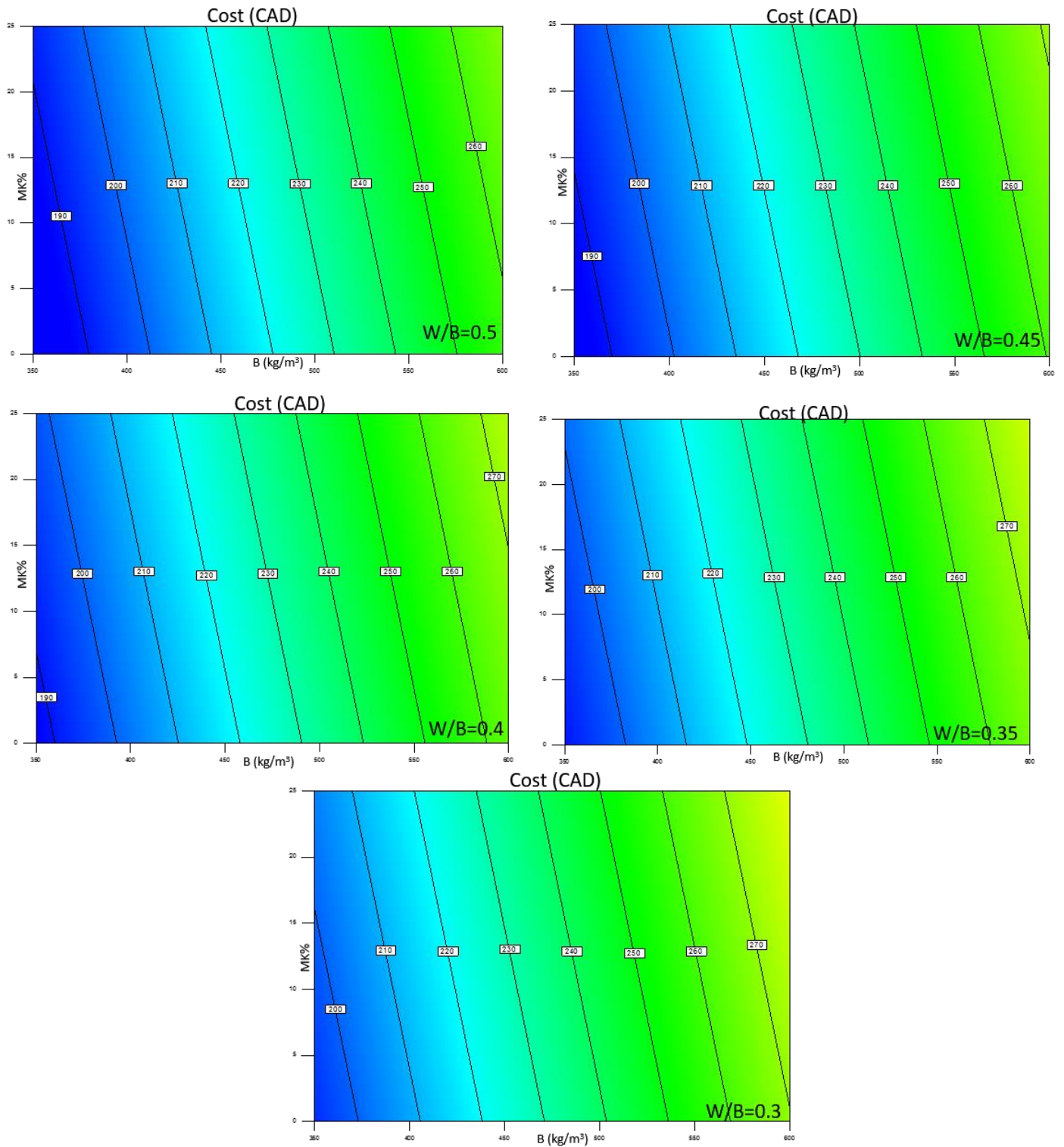


Figure 4.10 Cost charts with various W/B ratios

4.6.8 Optimization and Validation

By reviewing the results from the mechanical and durability properties tests of the 53 mixtures, the optimum mixture was found to be mixture 7, with a binder content of 600 kg/m³, W/B ratio of 0.3, and 25% MK. This was clear as the mixture with the lowest W/B ratio, highest binder content, and 25% MK should have minimum chloride permeability and maximum mechanical properties, as expected. Meanwhile, the lowest-cost mixture was found to be mixture 2, which had a W/B ratio of 0.5, a binder content of 350 kg/m³, and 0% MK. However, mixture 2 had the minimum chloride permeability and strength. Therefore, in order to obtain one mixture with high mechanical/durability properties and lower cost, a numerical optimization tool was utilized. This tool is available with the RSM as commercially used software. The target in this technique was established to maximize the compressive strength, modulus of elasticity, splitting tensile strength, and flexural strength, and to minimize the chloride permeability, chloride diffusion, and total cost of the mixture. In this optimization, the developed prediction models were used along with the predefined targets in a number of trials, which maintained the desired criteria. The results yielded an optimum mixture with the following ingredients: X₁ (binder content = 544.81 kg/m³), X₂ (W/B ratio = 0.32), and X₃ (MK% = 24.42%), with the following mechanical/durability properties and cost: 102.71 MPa, 99.29 GPa, 10.16 kN, 12.03 kN, 0.39x10⁻¹²(m²/s), 165.92 coulombs, 262.19 CAD, *f_c*, MOE, FS, STS, D_a, RCPT, and cost, respectively.

The optimum mixture was tested under the same procedure to validate the prediction models (**Table 4. 9**). The results obtained from the prediction models are quite close to the actual test results (**Table 4. 9**). It should be mentioned that the differences are still in

tolerance of $\pm 10\%$ from the actual predicted models, indicating a good correlation between models and actual results.

Table 4.9 Validation of the statistical models

Test	Predicted	Tested	Tolerance
f_c (MPa)	102.71	99.3	-3.43%
STS (kN)	12.03	12.1	0.58%
FS (kN)	10.16	9.7	-4.74%
MOE (GPa)	99.29	98.7	-0.60%
Da (m ² /s)	0.39×10^{-12}	0.36×10^{-12}	-8.33%
RCPT(coulombs)	165.92	170	2.40%
Cost (CAD)	262.19	262.19	0.00%

4.7 Conclusion

The chloride permeability and mechanical properties of 53 mixtures were studied. The parametric study investigated the effect of MK%, binder content, and W/B ratio. The chloride permeability included RCPT and chloride diffusion tests, while the mechanical properties included 28-day f_c , FS, STS, and MOE tests. The investigation also included optimization based on cost analysis and validation of the developed statistical models. From the results described in this paper, the following conclusions can be drawn:

- The developed prediction models and design charts can be used as a fast and useful tool to design an optimum MK mixture with target chloride permeability and strength. These design tools predict the RCPT, chloride diffusion factor, f_c , MOE, STS, FS, and cost based on total binder content, percentage of MK, and W/B ratio of the mixture.
- Increasing the binder content from 350 kg/m³ to 600 kg/m³, reducing the W/B ratio from 0.5 to 0.3, and/or increasing the percentage of MK from 0% to 25% resulted

in a lower chloride permeability/diffusion factor and an increase in the 28-day f_c , MOE, STS, and FS.

- The W/B ratio (factor X_2) showed the most significant effect on the chloride permeability and strength of the tested mixtures, followed by MK (factor X_3) and total binder content (factor X_1). Meanwhile, the binder content (factor X_1), followed by MK (factor C) and W/B ratio (factor B) were the most significant factors affecting the cost per cubic meter of the mixture.
- The results obtained from the numerical optimization yielded an optimum mixture that achieved a balance between high mechanical/durability properties and lower cost. This optimum mixture contained a total binder of 548.01 kg/m³, W/B ratio of 0.32, and MK replacement of 24.42%.
- Testing validation mixtures and comparing the results from the prediction models showcased the usefulness of these models for estimating the chloride permeability, strength, and cost of MK mixtures.

4.8 Reference

2012. Design Expert. 9 ed. Minneapolis: Design-Ease® Software
- AKALIN, O., ULAS, A. K. & BAHAR, S. 2010b. Self-consolidating high-strength concrete optimization by mixture design method. *ACI Materials Journal*, 107, 357–364.
- BADOGIANNIS, E. & TSIVILIS, S. 2009. Exploitation of poor Greek kaolins: Durability of metakaolin concrete. *Cement and Concrete Composites*, 31, 128-133.
- BAI, J., WILD, S., SABIR, B. B. & KINUTHIA, J. M. 1999. Workability of concrete incorporating pulverized fuel ash and metakaolin. *Magazine of Concrete Research*, 51, 207-216.
- BARNES, P., BENSTED, J. & JONES, T. R. 2003. Metakaolin as pozzolanic addition to concrete. *Structure and performance of cements*. 2 ed. England: CRC press.

- BAYRAMOV, F., TAŞDEMİR, C. & TAŞDEMİR, M. A. 2004. Optimisation of steel fibre reinforced concretes by means of statistical response surface method. *Cement & Concrete Composites*, 26, 665–675.
- BONAKDAR, M., M. BAKHSHI & GHALIBAFIAN, M. 2005. Properties of high-performance concrete containing high reactivity metakaolin. *ACI-SP*, 228, 287-296.
- CASSAGNABÈRE, F., ESCADEILLAS, G. & MOURET, M. 2009. Study of the reactivity of cement/metakaolin binders at early age for specific use in steam cured precast concrete. *Construction and Building Materials*, 23, 775-784.
- CASSAGNABÈRE, F., MOURET, M., ESCADEILLAS, G., BROILLIARD, P. & BERTRAND, A. 2010. Metakaolin, a solution for the precast industry to limit the clinker content in concrete: Mechanical aspects. *Construction and Building Materials*, 24, 1109-1118.
- CHEEWAKET, T., JATURAPITAKKUL, C. & CHALEE, W. 2012. Initial corrosion presented by chloride threshold penetration of concrete up to 10 year-results under marine site, *Constr. . Build. Mater*, 37, 693-698.
- CHEN, J., XU, Q., LI, J. & FAN, S. 2010. Improved response surface method for anti-slide reliability analysis of gravity dam based on weighted regression. *J. Zhejiang Univ.- Sc A.*, 11, 432-439.
- COLEMAN, J. & PAGE, C. L. 1997. Aspects of the pore solution chemistry of hydrated cement pastes containing metakaolin. *Cement and concrete research*, 27, 147-154.
- DHINAKARAN , G., THILGAVATHI, S. & VENKATARAMANA, J. 2012. Compressive strength and chloride resistance of metakaolin concrete. *KSCE Journal of Civil Engineering*, 16, 1209-1217.
- DUBEY, A. & BANTHIA, N. 1998. Influence of high-reactivity metakaolin and silica fume on the flexural toughness of high-performance steel fiber-reinforced concrete. *ACI Materials Journal*, 95, 284-292.
- EHLEN, M. A., THOMAS, M. D. A. & BENTZ, E. C. 2009. Life-365 Service Life Prediction Model™ Version 2.0. *Concrete International*, 31, 41-46.
- ERHAN GÜNEYİSİ, GESOĞLU, M., AKOI, A. O. M. & MERMERDAŞ, K. 2014. Combined effect of steel fiber and metakaolin incorporation on mechanical properties of concrete. *Composites Part B: Engineering*, 56, 8-91.
- GHEZAL, A. & KHAYAT, K. H. 2002. Optimizing Self-Consolidating Concrete with Limestone Filler by Using Statistical Factorial Design Methods. *ACI Materials Journal*, 99, 264-272.
- GÜNEYİSİ, E., GESOĞLU, M. & MERMERDAS, K. 2008. Improving strength, drying shrinkage, and pore structure of concrete using metakaolin. *Materials and Structures*, 41, 937–949.
- GÜNEYİSİ, E. & MERMERDAŞ, K. 2007. Comparative study on strength, sorptivity, and chloride ingress characteristics of air-cured and water-cured concretes modified with metakaolin. *Materials and Structures*, 40, 1161-1171.
- HASSAN, A. A. A., HOSSAIN, K. M. A. & LACHEMI, M. 2009. Corrosion Resistance of Self-Consolidating Concrete in Full-Scale Reinforced Beams. *Cement & Concrete Composites*, 31, 29-38.

- HASSAN, A. A. A., HOSSAIN, K. M. A. & LACHEMI, M. 2012. Effect of Metakaolin and Silica Fume on the Durability of Self-Consolidating Concrete. *Cement & Concrete Composites*, 34, 801-807.
- HOOTON, R. D., GEIKER, M. R. & BENTZ, E. C. 2002. Effects of Curing on Chloride Ingress and Implications on Service Life. *ACI Materials Journal* 99, 201-206.
- JUSTICE, J. M., KENNSION, L. H., MOHR, B. J., BECKWITH, S. L., MCCORMICK, L. E., WIGGINS, B., ZHANG, K. Z. Z. & KURTIS, E. Comparison of two metakaolins and a silica fume used as supplementary cementitious materials. Proc. Seventh International Symposium on Utilization of High-Strength/High Performance Concrete, 2005 Washington D.C.
- KANG, S. C., KOH, H. M. & CHOO, J. F. 2010. An efficient response surface method using moving least squares approximation for structural reliability analysis. *Probab. Eng. Mech*, 25, 365-371.
- KHATIB, J. M. & CLAY, R. M. 2004. Absorption characteristics of metakaolin concrete. *Cement and Concrete Research*, 34, 19-29.
- KHATIB, J. M. & HIBBERT, J. J. 2005. Selected engineering properties of concrete incorporating slag and metakaolin. *Construction and Building Materials*, 19, 460-472.
- KHAYET, M., COJOCARU, C. & ESSALHI, M. 2011. Artificial neural network modeling and response surface methodology of desalination by reverse osmosis. *Journal of Membrane Science*, 368, 202–14.
- LIANG, M., LIN, L. & LIANG, C. 2002. Service life prediction of existing reinforced concrete bridges exposed to chloride environment. *Journal of Infrastructure Systems*, 8, 76-85.
- MADANDOUST, R. & MOUSAVI, S. Y. 2012. Fresh and Hardened Properties of Self-Compacting Concrete Containing Metakaolin. *Construction and Building Materials*, 35, 752-760.
- MEHDIPOUR, I., VAHDANI, M., AMINI, K. & SHEKARCHI, M. 2016. Linking stability characteristics to material performance of self-consolidating concrete-equivalent-mortar incorporating fly ash and metakaolin. 105, 206–217.
- MINDESS, S., YOUNG, F. J. & DARWIN, D. 2003. *Concrete*, Upper Saddle River, Prentice Hall.
- MONTGOMERY, A. D. 2012. *Design and analysis of experiments* New York, Wiley.
- NEHDI, M. L. & SUMMER, J. 2002. Optimization of ternary cementitious mortar blends using factorial experimental plans. *Materials and Structures*, 35, 495–503.
- PAIVA, H., VELOSA, A., CACHIM, P. & FERREIRA, V. M. 2012. Effect of metakaolin dispersion on the fresh and hardened state properties of concrete. *Cement and Concrete Research*, 42, 607-612.
- POON, C. S., KOU, S. C. & LAM, L. 2006. Compressive strength, chloride diffusivity and pore structure of high performance metakaolin and silica fume concrete. *Journal of Construction and Building Materials*, 20, 858–865.
- QIAN, X. Q. & LI, Z. J. 2001. The relationships between stress and strain for high performance concrete with metakaolin. *Cement and Concrete Research*, 31, 1607-1611.

- RAZAK, H. A. & WONG, H. S. 2005. Strength estimation model for high-strength concrete incorporating metakaolin and silica fume. *Cement and Concrete Research*, 35, 688–695.
- RODRIGUEZ, O. G. & HOOTON, R. D. 2003. Influence of cracks on chloride ingress into concrete. *ACI Materials Journal*, 100, 120-126.
- ROUGERON, P. & P.C. AITCIN 1994. Optimization of the Composition of a High-Performance Concrete. *Cement, Concrete and Aggregates*, 16, 115-124.
- SABIR, B. B., WILD, S. & BAI, J. 2001. Metakaolin and calcined clays as pozzolans for concrete: a review. *Cement & Concrete Composites*, 23, 441-454.
- SCHMIDT, S. R. & LAUNSBY, R. G. 1994. *Understanding Industrial Designed Experiments*, Colorado Springs, Colorado, Air Academic Press.
- SONEBI, M. 2004. Medium strength self-compacting concrete containing fly ash: modelling using factorial experimental plans. *Cement and Concrete Research*, 34, 1199–1208.
- SOUDKI, K., EL-SALAKAWY, E. & ELKUM, N. 2001. Full factorial optimization of concrete mix design for hot climates. *Journal of materials in civil engineering*, 13, 427-433.
- SPEED, T. P. 1987. What is an analysis of variance? (with discussion). *Annals of Statistics*, 15, 885–941.
- VU, D. D., STROEVEN, P. & BUI, V. B. 2001. Strength and durability aspects of calcined kaolin-blended Portland cement mortar and concrete. *Cement and Concrete Composites*, 23, 471-478.
- WONG, S. M., HOBBS, R. E. & ONOF, C. 2005. An adaptive response surface method for reliability analysis of structures with multiple loading sequences. *Structure safety*, 27, 287-308.

5. Time-Dependence of Chloride Diffusion for Concrete Containing Metakaolin

5.1 Abstract

Chloride diffusion coefficient depends on many variables including concrete quality, environmental conditions, and time. In this investigation, the concrete quality and time were studied while maintaining the environmental conditions constant. Fifty-three concrete mixtures were tested based on a refined statistical analysis. Enhanced response surface method (RSM) was used to present the most significant factors affecting the chloride diffusion at different ages. The tested mixtures contained various water-to-binder (W/B) ratios (0.3 to 0.5), metakaolin (MK) replacement (0% to 25 %), and total binder content (350 kg/m³ to 600 kg/m³). Bulk diffusion test was adopted for two years to determine the time-dependent coefficient m of chloride diffusion for all mixtures based on the error function solution to Fick's law. This coefficient was calculated based on two different bulk diffusion test methods: total and average methods. Design charts were developed to facilitate the optimization of mixture proportions for designers/engineers. The investigation also included some experimental relationships between the rapid chloride permeability test (RCPT), chloride diffusion coefficient, and compressive strength results. The results showed that the values of the chloride diffusion indicated a general reduction from 28 days to 760 days of testing. As the percentage of MK or binder content increased or as the W/B ratio decrease, the chloride diffusion reduction coefficients, m_{total} and m_{avr} , were found to increase. Based on the analysis of variance (ANOVA) from the statistical model, MK was found to be the most significant factor affecting the chloride diffusion at late ages (360 and 720 days), while the

W/B ratio was the most significant factor affecting early ages of chloride diffusion (28 and 90 days). The developed models and design charts in this paper can be of special interest to designers/engineers by aiding prediction of service life of concrete containing MK.

5.2 Introduction

Enhancing protection and prediction of service life for reinforcing concrete structures strongly impacts economic and ecological sustainability. Rebar corrosion is one of the main problems affecting the durability of reinforced concrete structures. Service life time of reinforced concrete structures can be drastically reduced if the chloride ions near the rebar surface exceed the chloride threshold level in a short time (Andrade et al., 2011). Concrete cover is considered the first barrier for chloride ion penetration to reach the rebar surface. Chloride ions diffuse slowly through deeper cover thickness, thus improving the structure's service life. Once the chloride threshold is exceeded at the rebar surface, corrosion may start. The concrete cover protecting the rebars can be cracked due to the expansive nature of rust products. The cracking of concrete covers significantly increases the ingress of chlorides and other deleterious substances, causing strength reduction of the structural element and acceleration of the corrosion process (Kato and Uomoto, 2005, Boulfiza et al., 2003). Predicting the time of corrosion initiation is determined by the rate of chloride ingress (diffusion coefficient), environmental loading, and chloride threshold level (Stewart and Rosowsky, 1998, Erdogdu et al., 2004, Song et al., 2008). The rate of chloride diffusion is affected by concrete quality due to the size and volume of pore structure, and by time due to the blockage and reduction of the capillary pore structure from the hydration process. Concrete is not a static material, as the concrete continues to hydrate with time, the volume

of capillary pores decreases, which reduces the diffusion rate with time. The concrete quality depends mainly on binder content, water-to-binder (W/B) ratio, and any supplementary cementing material (SCM), where they are the primary controlling factors for concrete quality. On the other hand, aggregates in concrete generally have negligible permeability and consequently have an insignificant effect on the transport mechanism of chloride through concrete.

Metakaolin (MK) as a SCM in concrete is receiving a lot of attention recently. The use of MK as a SCM can considerably improve the performance of concrete structures by improving their durability properties (Gruber et al., 2001a, Asbridge et al., 2001, Courard et al., 2003, Hassan et al., 2012b). Utilizing MK also improves mechanical properties such as compressive strength, flexural strength, and modulus of elasticity of concrete compared to concrete without any SCM (Akalın et al., 2010, Justice et al., 2005b, Hassan et al., 2012b). The incorporation of MK in concrete mixtures not only enhances the durability properties and the mechanical properties of concrete, it also significantly reduces CO₂ emissions as it requires lower manufacturing temperatures compared to cement (Malhotra, 2000).

Diffusion is the prime chloride ingress mechanism, where chloride ions are transported from high concentration to lower concentration in a semi-finite medium (concrete matrix). The prediction and optimization of chloride ingress in reinforced concrete structures has become a crucial part in service life prediction and maintenance of new and existing structures (Hassan et al., 2009a, Ehlen et al., 2009, Hooton et al., 2002). Diffusion of chloride is modeled by using the error function solution to Fick's second law of diffusion (**Eq.5**).

1)(Crank, 1956), which has been studied by numerous researchers (Díaz et al., 2006, Lizarazo-Marriaga and Claisse, 2009, Vedalakshmi et al., 2008, Hooton et al., 2002).

$$C(x, t) = C_s \left(1 - \operatorname{erf} \frac{x}{2\sqrt{D_a t}} \right) \quad (\text{Eq. 5.1})$$

Where $C(x, t)$ = chloride concentration measured at depth x and exposure time t (mass %); C_s = surface chloride concentration, (mass %); x = depth below the exposed surface (to the middle of a layer) (m); D_a = chloride diffusion coefficient (m^2/s); and t = the exposure time (s).

The main weakness of **Eq. 5.1** is the assumption of constant diffusion over time. As a consequence, a single value of the chloride diffusion coefficient can never be obtained from the measured concentration profiles, particularly if the measurements are performed over a long time period. This is because concrete is a hydraulic material that will continually hydrate if there is moisture available. The hydration process will cause refining of the pore structure and subsequently will lower the chloride diffusion coefficient with time (Halamiczkova et al., 1995, Young, 1988).

Statistical design technique is an efficient tool for optimizing concrete mixtures. It provides statistical models, which help researchers understand the interactions between parameters that have been modeled and optimized (Ghezal and Khayat, 2002). Response surface method (RSM) design techniques are applied in numerous civil engineering fields (Bayramov et al., 2004a, Wong et al., 2005, Chen et al., 2010, Kang et al., 2010). The RSM is a compilation of mathematical and statistical techniques used for developing, refining, and optimizing

processes, and it can be used to evaluate the relative significance of numerous factors even in complex interactions. RSM relies on ANOVA, a method that selects a few points out of the full factorial set that can represent efficient information about the response space.

Limited research has been undertaken that considers statistical analysis in developing models to predict and optimize the chloride diffusion and time dependent coefficient of concrete containing MK. In addition, most of the available studies relate only one factor in the prediction equation based on either the water-to-cement ratio (W/C ratio) or the SCM used. Moreover, most of the available studies utilized a traditional statistical analysis with minimum member points representing the response space. The main objectives of this investigation were divided into two stages: the first stage focused on developing enhanced prediction models for the chloride diffusion coefficient for 53 concrete mixtures at different ages (28, 90, 180, 360, and 760 days). The models incorporated the effects of the three experimental variables: total binder content, W/B ratio, and percentage of MK. The second stage of this investigation focused on predicting the time reduction coefficient (m) for chloride diffusion based on the three experimental variables. RSM was used in this investigation to present the most significant factors affecting chloride diffusion and chloride reduction coefficients in the 53 mixtures, and to develop prediction models for both stages. More points were used in the RSM to enhance the statistical analysis and to develop more precise models for predicting chloride diffusion in concrete containing MK. Design charts were also developed to aid designers/engineers to optimize mixture proportions. In addition, empirical relationship models were established based on the experimental results of chloride diffusion coefficient, chloride permeability test (RCPT), and compressive strength. Finally,

a verification mixture was tested under compression strength, RCPT, and chloride diffusion to assess the performance of the prediction models.

5.3 Research significance

Although there are some available research papers studying chloride diffusion in concrete containing MK, there is limited research that covers the time-dependence effect of chloride diffusion in MK mixtures. The literature also lacks research on the combined effect of the total binder content, W/B ratio, and percentage of MK on the chloride diffusion at different ages; as well as modeling chloride diffusion using statistical analysis in MK mixtures. In this paper an enhanced statistical analysis with more points on the response surface is used in order to develop more precise models, which combine all factors in one equation. The models presented in this paper were developed with the aid of RSM based on an extensive experimental investigation designed to predict the chloride diffusion at different ages and chloride diffusion reduction coefficient in concrete mixtures containing MK. The developed models account for the effects of total binder content, W/B ratio, and percentage of MK. Moreover, unique empirical relationship models based on the results of chloride diffusion coefficient, RCPT, and compressive strength were also developed in this paper. The authors believe that the design charts developed in this investigation will help designers/engineers optimize their concrete mixtures and also strongly contribute to enhancing service life prediction for concrete containing MK.

5.4 Development of response surface method

In this study, three factors were considered in the development of the enhanced RSM: total binder content, W/B ratio, and the percentage of MK. The derived statistical models are valid

for concrete mixtures made with total binder content ranging from 350kg/m^3 (-1) to 600kg/m^3 (+1), W/B ratios from 0.3 (-1) to 0.5 (+1), and percentage of MK from 0% (-1) to 25% (+1). The selected range for each of these variables was chosen based on literature and practical considerations. The developed RSM in this investigation considered extra points on the block surface than the common number of points used in standard RSM. In this study, a quadratic model was selected with 8 vertices points, 12 centers of edges, 6 constrain plane centroids, 8 axial check points, 18 interior points, and 1 overall centroid. These points give a total of 53 points to develop the optimization models compared to 15 points used in the standard RSM (see **Fig. 5.1**).

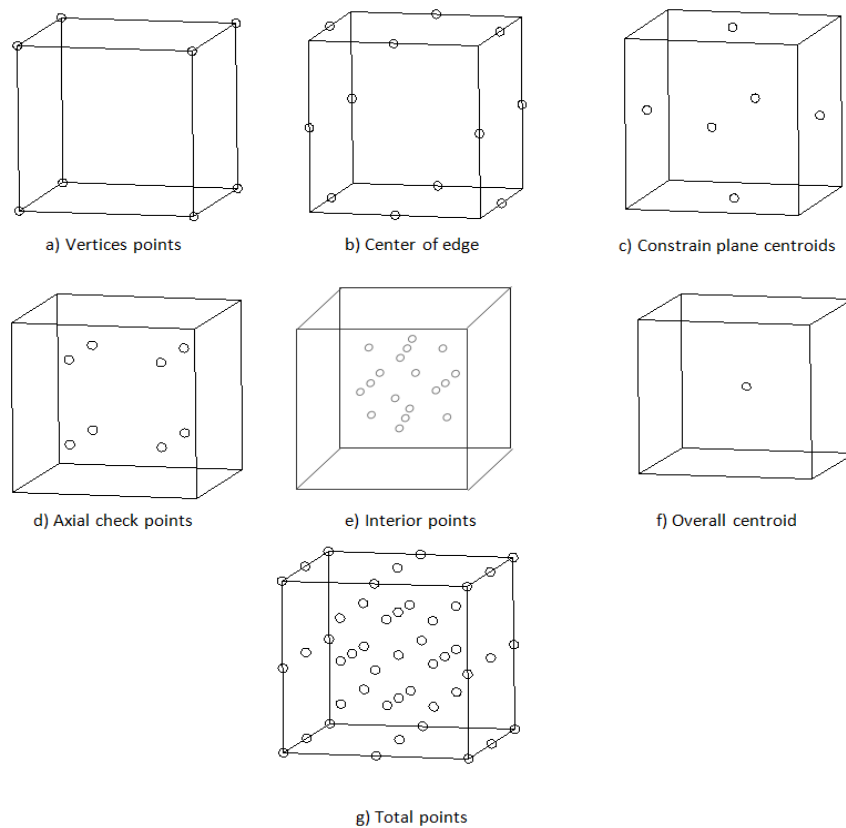


Figure 5.1 Modified RSM points

The coded values are expressed according to **Eq.5.2**:

$$\text{Coded Value} = \frac{\text{absolute value} - \text{central value}}{0.5 \times \text{range between maximum and minimum values}} \quad (\text{Eq.5.2})$$

The significance of the variables and their connections were determined after compiling the ANOVA, which tests the probability values (Probability > F) and indicates that the factor is significant if its probability value is less than 0.05. Also, the factor with the higher F-value is considered the most significant factor. The prediction equations can be interpreted in forms of coded values or actual values of significant variables. For simplifying the equations, the form of actual values of each variable was sensible for models. Graphs were also plotted to help predict the chloride diffusion reduction coefficients.

5.5 Chloride diffusion reduction coefficient calculation (m)

The reduction of chloride ionic ingress through concrete with time is beneficial in delaying the onset of chloride-induced corrosion and thus enhancing the corrosion-free life of structures. Various assumptions have been used to determine the chloride reduction coefficient based on the maturity of concrete. This coefficient is an important property of the concrete as it is used in the service life prediction models; for example, the model presented in the Life365 software (2012b). The chloride diffusion reduction coefficient (m) is determined by linear regression of chloride diffusion values calculated using Cranks solution to Fick's laws with time on a log-log scale. **Fig. 5.2** shows a typical chloride diffusion coefficient versus time on a log-log scale (sample 26 as an example).

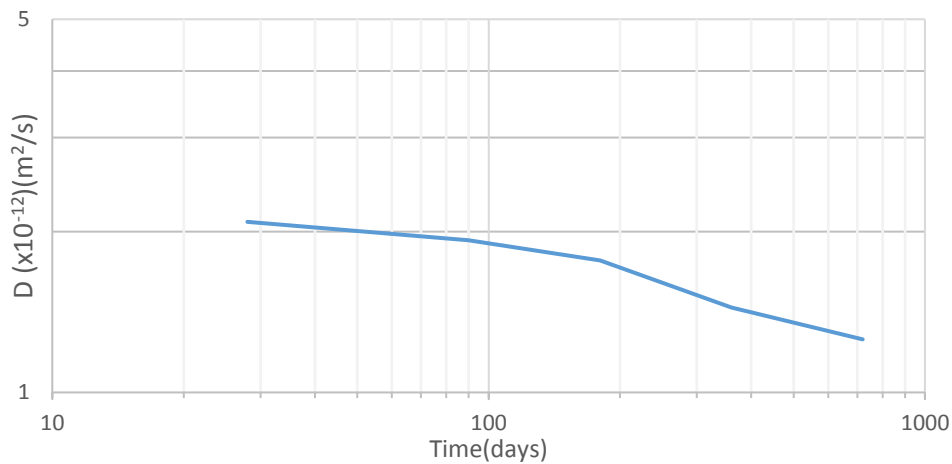


Figure 5.2 Typical chloride diffusion coefficient vs. time (log-log scale)

Eq. 5.3 presents the rate of reduction of chloride diffusion over time, which was established in laboratory tests and mathematically captured using a power function equation (Mangat and Molloy, 1994, Takewaka and Matsumoto, 1988, Tang and Nilsson, 1992).

$$D_a = D_0 \left(\frac{t_0}{t} \right)^m \quad \text{Eq. 5.3}$$

Where D_a is the chloride diffusion coefficient at time t ; D_0 is the chloride diffusion coefficient at reference time (t_0); and m is the chloride diffusion reduction coefficient. In this paper, two assumptions will be studied for calculating the diffusion reduction coefficient m . The first assumption, m_{total} , uses the concrete maturity as the time basis versus the calculated diffusion coefficient. The second assumption, m_{avr} , considers the average age of the concrete during the exposure period versus the calculated diffusion coefficient. The time used to calculate

m_{total} , for a sample that has been cured for 28 days and exposed to chloride for 90 days, would be 118 days (**Eq. 5.4**).

$$t_{total} = t_1 + t_2 \quad (\text{Eq. 5.4})$$

Where t_{total} is the total age; t_1 is the 28-day curing period; and t_2 is the chloride exposure period.

Meanwhile, for the same sample, the time used to calculate m_{avr} would be 59 days (with an average exposure period between 28 and 90 days), as seen in **Eq. 5.5**.

$$t_{avr} = \frac{t_1 + t_2}{2} \quad (\text{Eq. 5.5})$$

Where t_{avr} is the average exposure period; t_1 is the 28-day curing period; and t_2 is the chloride exposure period.

The negative slope m is calculated based on a linear relation of the chloride diffusion coefficient plotted versus time on a log-log scale. The slope m is calculated based on the relation in **Eq. 5.6**.

$$m = \frac{\log D_1 - \log D_2}{\log t_1 - \log t_2} \quad (\text{Eq. 5.6})$$

Where m is the slope of the linear relation; D_1 is the chloride diffusion coefficient at the exposure age t_1 ; and D_2 is the chloride diffusion coefficient at the exposure age t_2 .

5.6 Experimental program

5.6.1 Materials

Type GU Canadian Portland cement similar to ASTM Type I, with a specific gravity of 3.15, was used for the 53 concrete mixtures. Metakaolin with a specific gravity of 2.56 was used in all concrete mixtures (**Table 5.1**).

Table 5.1 Chemical and physical properties

Chemical properties %	Cement	MK	Physical properties	Cement	MK
SiO ₂	19.64	51-53	Specific gravity	3.15	2.56
Al ₂ O ₃	5.48	42-44	Color	Gray	Pink
Fe ₂ O ₃	2.38	<2.2	Grain size (μm)	45	60
FeO	-	-	Surface area(m ² /kg)	320- 400	650- 1250
TiO ₂	-	<3	Blaine fineness (m ² /kg)	410	19000
C	-	-			
P ₂ O ₅	-	<0.2			
SO ₄	-	<0.5			
CaO	62.44	<0.2			
MgO	2.48	<0.1			
Na ₂ O	-	<0.05			
C ₃ S	52.34	-			
C ₂ S	16.83	-			
C ₃ A	10.5	-			
C ₄ AF	7.24	-			
K ₂ O	-	<0.4			
Loss on ignition	2.05	<0.5			

Natural sand and 10 mm maximum size stone were used as fine and coarse aggregates, respectively (**Table 5.2**). The coarse and fine aggregates each had a specific gravity of 2.60 and water absorption of 1%. A superplasticizer similar to ASTM Type F (ASTM C494) with

specific gravity, volatile weight, and pH of 1.2, 62%, and 9.5, respectively, was used to achieve the required slump of the mixtures.

Table 5.2 Sieve analysis

Sieve size (mm)	10 mm coarse aggregate (% passing)	Sieve size (mm)	Fine aggregate passing (% passing)
14	100	10	100
10	95.8	5	99.4
5	21	2.5	79.4
2.5	2.9	1.25	55.4
1.25	0	0.63	35.2
0.63	-	0.32	18.6
0.32	-	0.16	7.3
0.16	-	0.08	2.2

5.6.2 Mixture proportioning and casting

Based on the selected points of the refined RSM, 53 concrete mixtures were selected (**Table 5.3**). The coarse-to-fine aggregate ratio was maintained constant at 1.2 for all mixtures. The mixture ingredients were blended in a mechanical rotary mixer. Slump test was conducted according to ASTM C 143 for all tested mixtures. Sufficient amounts of superplasticizer were added to the concrete mixtures until they reached the required workability by achieving a slump of 50 ± 10 mm. After mixing the concrete, a number of concrete cylinders were cast and prepared for the RCPT, chloride diffusion, and compressive strength tests, with dimensions of 100 mm diameter x 200 mm height. After 24 hours of casting, all cylinders were demolded and cured in a temperature-controlled curing room for 28 days at 21 °C.

Table 5.3 Mixture proportions and results

RUN number	Coded value			Actual value			Results	
	A	B	C	Binder (Kg/m ³)	W/B	MK%	f'_c (MPa)	RCPT (coulombs)
1	1	-1	1	600	0.3	25	108	203
2	1	-1	0	600	0.3	12.5	92	300
3	0.5	-0.5	0.5	537.5	0.35	18.75	90	350
4	1	0	1	600	0.4	25	85	420
5	0	-1	1	475	0.3	25	90	254
6	1	-1	-1	600	0.3	0	84	400
7	0.5	0	0.5	537.5	0.4	18.75	81	625
8	0.5	-0.5	0	537.5	0.35	12.5	84	405
9	0	-0.5	0.5	475	0.35	18.75	89.7	382
10	-1	-1	1	350	0.3	25	83	455
11	0	-1	0	475	0.3	12.5	87	410
12	1	0	0	600	0.4	12.5	82	500
13	1	1	1	600	0.5	25	67	1192
14	0.5	0.5	0.5	537.5	0.45	18.75	68	1146
15	0	0	1	475	0.4	25	80	540
16	-0.5	-0.5	0.5	412.5	0.35	18.75	82	388
17	-1	0	1	350	0.4	25	77.5	590
18	0	-1	-1	475	0.3	0	77	450
19	0.5	0	0	537.5	0.4	12.5	78	694
20	0.5	-0.5	-0.5	537.5	0.35	6.25	76	470
21	0	-0.5	0	475	0.35	12.5	80	480
22	0	0	0.5	475	0.4	18.75	79	643
23	0	0	-0.5	475	0.4	6.25	67	1076
24	0	0.5	0.5	475	0.45	18.75	64	1190
25	-1	-1	0	350	0.3	12.5	80	520
26	-0.5	-0.5	0	412.5	0.35	12.5	70	494
27	-0.5	-0.5	-0.5	412.5	0.35	6.25	68	604
28	-1	1	1	350	0.5	25	58	1460
29	0	0	-1	475	0.4	0	50	1314
30	0.5	0.5	0	537.5	0.45	12.5	60	1566
31	0	-0.5	-0.5	475	0.35	6.25	78	553
32	-1	-1	-1	350	0.3	0	51	788
33	0	0.5	0	475	0.45	12.5	50	1973
34	0	1	1	475	0.5	25	65	1267
35	-0.5	0	0.5	412.5	0.4	18.75	73	665
36	-1	0	0	350	0.4	12.5	68	1228
37	1	1	0	600	0.5	12.5	58	1901
38	0.5	0	-0.5	537.5	0.4	6.25	72	958
39	1	0	-1	600	0.4	0	65	1091

Table 5.3 (Continued) Mixture proportions and results

RUN number	Coded value			Actual value			Results	
	A	B	C	Binder (Kg/m ³)	W/B	MK%	f_c (MPa)	RCPT (coulombs)
40	-0.5	0.5	0.5	412.5	0.45	18.75	43.8	1890
41	0	0	0	475	0.4	12.5	55	810
42	-0.5	0	0	412.5	0.4	12.5	72	864
43	0.5	0.5	-0.5	537.5	0.45	6.25	52	2273
44	-0.5	0	-0.5	412.5	0.4	6.25	63	1125
45	0	0.5	-0.5	475	0.45	6.25	49	2554
46	-0.5	0.5	0	412.5	0.45	12.5	40	2474
47	1	1	-1	600	0.5	0	54	3144
48	0	1	0	475	0.5	12.5	50	2231
49	0	1	-1	475	0.5	0	40	4181
50	-1	0	-1	350	0.4	0	47	1763
51	-0.5	0.5	-0.5	412.5	0.45	6.25	38	3540
52	-1	1	0	350	0.5	12.5	40	2546
53	-1	1	-1	350	0.5	0	35	4545

5.6.3 Test methods

All mixture samples were tested after 28 days of curing to determine their compressive strengths, as per ASTM C39, by testing a minimum of three cylinders of each concrete mixture. The chloride permeability was primarily evaluated by means of the RCPT as per ASTM C1202. To study the chloride diffusion reduction coefficient for the 53 concrete mixtures, a bulk diffusion test (ASTM C1556) was selected because it measures the actual ingress of chloride ions over time (Stanish et al., 2000). The bulk diffusion test is based on immersing cylinder samples in a 16.5% NaCl solution for 28 days. Limewater was used to saturate the sample for 28 days, instead of being air-dried, to prevent initial sorption effect when chloride solution is introduced. The cylinder samples were coated with epoxy on all surfaces except for the top surface. After the immersion period, powder samples were extracted at different depths from the exposed surface for analysis of chloride contents. After

being stored for 24 hours in bottles of a specific extraction liquid, the chloride ion content of the collected powder samples was measured using a chloride meter device. The chloride content profile (chloride content versus diffusion depth) for each mixture was plotted and used to determine the chloride diffusion coefficient (D_a) by analysis against the error function solution to Fick's second law of diffusion (**Eq. 5.1**) as stated in ASTM C1556. The goodness of curve fit was evaluated by the R^2 value (coefficient of multiple determination). A value of 1 for R^2 indicates a curve with a perfect fit passing through all data points, while a value of 0 indicates a poor fit. After collecting the experimental results, statistical analysis was executed on the data and prediction models were developed.

5.7 Results and discussion

5.7.1 Experimental results

The compressive strength and RCPT at 28 days were reported for the 53 mixtures, as shown in **Table 5.3**. The chloride diffusion coefficients for all tested mixtures at 28, 90, 180, 360, and 720 days of exposure were also determined (**Table 5.4**) Relationships were noted between RCPT, chloride diffusion, and compressive strength based on the results of the 53 concrete mixtures. Based on the chloride diffusion results for each mixture, a linear relation was plotted on a log-log scale between chloride diffusion and time of exposure to calculate the chloride reduction coefficient (m) (**Table 5.4**).

Table 5.4 Chloride diffusion and chloride diffusion reduction coefficient

Mixture	D_{28} $\times 10^{-12}(\text{m}^2/\text{s})$	D_{90} $\times 10^{-12}(\text{m}^2/\text{s})$	D_{180} $\times 10^{-12}(\text{m}^2/\text{s})$	D_{360} $\times 10^{-12}(\text{m}^2/\text{s})$	D_{720} $\times 10^{-12}(\text{m}^2/\text{s})$	m_{total}	m_{avr}
1	0.199601	0.1905	0.181	0.111768	0.09	0.30729	0.278419
2	0.399202	0.3595	0.32	0.263578	0.109581	0.498757	0.451896
3	0.417695	0.3995	0.381	0.261383	0.199785	0.284528	0.257795
4	0.479042	0.4015	0.324	0.260164	0.149805	0.448468	0.406333
5	0.724086	0.689	0.654	0.426186	0.366562	0.262627	0.237952
6	0.798404	0.591	0.384	0.312477	0.246989	0.452642	0.410114
7	1.076952	0.859547	0.642094	0.62405	0.381067	0.400808	0.36315
8	1.121781	0.9295	0.737	0.58537	0.490393	0.319232	0.289239
9	1.22218	1.036691	0.851382	0.440998	0.429654	0.403314	0.365421
10	1.227386	1.205	1.183	0.922475	0.699904	0.2167	0.196341
11	1.241549	1.076	0.91	0.53985	0.055684	0.309345	0.280281
12	1.264747	1.064	0.863	0.433311	0.322877	0.526747	0.477257
13	1.385477	1.3005	1.216	0.977924	0.890917	0.170347	0.154342
14	1.391222	1.181	0.971	0.551156	0.412538	0.468976	0.424914
15	1.394162	1.2005	1.007	0.614373	0.297255	0.596229	0.540211
16	1.421167	1.2445	1.068	0.705878	0.660992	0.295323	0.267576
17	1.474135	1.284	1.094	0.716952	0.18681	0.79695	0.722073
18	1.584063	1.4265	1.269	0.942696	0.633547	0.353548	0.32033
19	1.585078	1.3985	1.212	0.850463	0.543065	0.413248	0.374422
20	1.722403	1.552	1.382	1.045935	1.049505	0.191123	0.173167
21	1.775135	1.605	1.435	1.10137	1.078994	0.192067	0.174022
22	1.809131	1.6265	1.444	1.098262	1.019646	0.221211	0.200428
23	1.947276	1.718711	1.537421	1.193106	1.098527	0.220852	0.200102
24	1.983162	1.7655	1.584	1.241095	1.191908	0.196422	0.177968
25	2.087334	1.7905	1.598	1.243964	1.265804	0.192967	0.174837
26	2.126746	1.9275	1.768	1.442417	1.257212	0.202811	0.183756
27	2.129116	1.956	1.785	1.449899	1.382477	0.166598	0.150945
28	2.309129	1.958	1.787	1.451805	1.258612	0.234124	0.212127
29	2.320239	2.2625	2.216	1.957913	1.895756	0.077951	0.070627
30	2.331575	2.135	1.95	1.604493	1.377538	0.203023	0.183948
31	2.392797	2.136	1.94	1.589253	1.497431	0.180827	0.163837
32	2.484175	2.2185	2.044	1.69844	1.662392	0.154967	0.140408
33	2.526548	2.317	2.15	1.805745	1.605536	0.174918	0.158484
34	2.625889	2.33226	2.13752	1.77312	1.675409	0.173362	0.157074
35	2.707107	2.113	1.6	1.000132	0.854207	0.445	0.40319
36	2.734494	2.517952	2.328904	1.960614	1.756001	0.170871	0.154817
37	2.770954	2.544	2.354	1.984943	1.972111	0.131204	0.118877
38	3.170156	2.564	2.357	1.976188	1.936797	0.190099	0.172238
39	3.17499	2.969937	2.769874	2.371449	2.375227	0.111962	0.101443

Table 5.4 (Continued) Chloride diffusion and chloride diffusion reduction coefficient

Mixture	D_{28} $\times 10^{-12}(\text{m}^2/\text{s})$	D_{90} $\times 10^{-12}(\text{m}^2/\text{s})$	D_{180} $\times 10^{-12}(\text{m}^2/\text{s})$	D_{360} $\times 10^{-12}(\text{m}^2/\text{s})$	D_{720} $\times 10^{-12}(\text{m}^2/\text{s})$	m_{total}	m_{avr}
40	3.23698	2.9725	2.77	2.375824	2.310992	0.129999	0.117785
41	3.263482	3.028	2.819	2.412862	2.330496	0.129902	0.117698
42	3.300712	3.09732	2.89364	2.485737	2.311873	0.137374	0.124467
43	3.385899	3.173	2.96	2.543372	2.517679	0.114304	0.103565
44	3.406876	3.2	2.993	2.577737	2.49497	0.120182	0.108891
45	3.566791	3.349084	3.131168	2.700764	2.707534	0.106336	0.096345
46	3.603937	3.385008	3.166016	2.732801	2.690357	0.112788	0.102191
47	3.824736	3.293	2.761	2.192507	1.975226	0.254936	0.230984
48	4.26797	4.0225	3.777	3.289617	3.104111	0.122841	0.1113
49	4.365514	4.141	3.916	3.426945	3.393626	0.097157	0.088029
50	4.408358	4.168	3.928	3.432232	3.347181	0.106242	0.09626
51	5.026756	4.76	4.493	3.942748	3.935018	0.094465	0.08559
52	5.547025	5.256	4.965	4.369545	4.275756	0.100423	0.090988
53	6.526384	5.997	5.468	4.763006	4.765563	0.121308	0.109911

Statistical analysis was then used to obtain models for each result of the chloride diffusion coefficient and chloride diffusion reduction coefficient to identify significant factors and prediction models. To simplify the prediction models, the form of actual values of each variable was applied in **Table 5.5**. **Eq.5.7** is used to predict the diffusion coefficient and the diffusion reduction coefficient based on the factors stated in **Table 5.5**. Finally, a number of charts were developed to represent a simplified method to predict the chloride reduction coefficient.

$$Y(\text{response}) = A + B * \text{Binder} + C * \text{W/B} + D * \text{MK}\% + E * \text{Binder} * \text{W/B} + F * \text{Binder} * \text{MK}\% + G * \text{W/B} * \text{MK}\% + H * \text{Binder}^2 + I * \text{W/B}^2 + J * \text{MK}\%^2 + K * \text{Binder} * \text{W/B} * \text{MK}\% + L * \text{Binder}^2 * \text{W/B} + M * \text{Binder}^2 * \text{MK}\% + N * \text{Binder} * \text{W/B}^2 + O * \text{Binder} * \text{W/B}^2 * \text{MK}\% + P * \text{Binder} * \text{MK}\%^2 + Q * \text{W/B} * \text{MK}\%^2 + R * \text{Binder}^3 + S * \text{W/B}^3 + T * \text{MK}\%^3$$

(Eq.5.7)

Table 5.5 Derived statistical model

	D ₂₈	D ₉₀	D ₁₈₀	D ₃₆₀	D ₇₂₀	$m_{avr}^{0.5}$	$m_{total}^{0.5}$	factor
A	-2.83919	-9.87576	-9.58769	-6.41679	-11.9886	3.640028	3.824104	
B	-0.00191	0.116607	0.102085	0.057124	0.059486	-0.00369	-0.00387	* Binder(kg/m ³)
C	25.58516	-47.1859	-40.1342	-17.9747	19.59767	-14.2871	-15.0096	* W/B
D	0.022369	0.043778	0.244744	0.35963	0.459566	-0.27824	-0.29231	* MK%
E	-0.01622	0.132869	0.163032	0.184453	0.304869	-0.04906	-0.05155	* Binder(kg/m ³) * W/B
F	0.000107	0.001739	0.001255	0.000798	0.001022	0.000104	0.00011	* Binder(kg/m ³) * MK%
G	-0.3907	-1.81411	-2.45081	-2.59571	-3.44745	1.327575	1.394711	* W/B * MK%
H	0	-0.00034	-0.00032	-0.00022	-0.00028	2.74E-05	2.87E-05	* Binder(kg/m ³) ²
I	0	96.79056	69.20823	1.892847	-151.299	49.16957	51.65607	* W/B ²
J	0	-0.011	-0.00866	-0.00758	-0.00688	0.000262	0.000275	* MK% ²
K	0	0.001152	0.001166	0.00116	0.001239	3.09E-06	3.25E-06	* Binder(kg/m ³) * W/B * MK%
L	0	-4.1E-06	-3.5E-05	-8.4E-05	-0.00015	1.93E-05	2.03E-05	* Binder(kg/m ³) ² * W/B
M	0	-2.5E-06	-2E-06	-1.5E-06	-1.8E-06	-2.8E-08	-3E-08	* Binder(kg/m ³) ² * MK%
N	0	-0.19954	-0.20058	-0.172	-0.25158	0.03519	0.036969	* Binder(kg/m ³) * W/B ²
O	0	1.38E-05	1.29E-05	1.39E-05	1.64E-05	-4.3E-06	-4.5E-06	* Binder(kg/m ³) * MK% ²
P	0	1.783631	2.682339	2.928647	4.008054	-1.73695	-1.82479	* W/B ² * MK%
Q	0	-0.02219	-0.02486	-0.02517	-0.02789	0.003127	0.003285	* W/B * MK% ²
R	0	2.68E-07	2.52E-07	1.97E-07	2.59E-07	-2.2E-08	-2.3E-08	* Binder(kg/m ³) ³
S	0	-1.93714	12.6032	54.46539	203.2459	-41.7753	-43.8878	* W/B ³
T	0	0.000317	0.000298	0.000265	0.00024	2.05E-05	2.15E-05	* MK% ³

Y(response) = A+B * Binder+C* W/B+ D* MK%+E * Binder* W/B+F* Binder* MK%+ G* W/B* MK%+ H* Binder²+ I* W/B²+J* MK%²+K* Binder* W/B* MK%+ L* Binder² * W/B+M* Binder² * MK%+M* Binder* W/B²+N* Binder* W/B²+O* Binder* MK%²+P * Binder* MK%²+Q* W/B* MK%²+R* Binder³+ S* W/B³+T * MK%³

5.7.2 Chloride permeability and chloride diffusion coefficients results

The RCPT and bulk diffusion test were replicated for the 53 mixtures at 28 days. In addition, the bulk diffusion test was repeated at 90, 180, 360, and 720 days for all tested mixtures. The results from different testing exposure periods are shown in **Tables 5.3, 4**. The results showed that the addition of MK decreased the chloride permeability and chloride diffusion. Test results for all chloride diffusion coefficients are compared in **Figure 5.3**. It is clear from the figure that all mixtures exhibited a significant decrease in the chloride diffusion coefficient values from 28 days to 760 days, as expected. These results are attributed to the effect of the hydration process, which decreased the permeability of the concrete (Courard et al., 2003). **Fig.5.3** and **Table 5.3, 5.4** also show a decrease in the chloride permeability and chloride diffusion as the percentage of MK or binder content increased or as the W/B ratio decreased. For example, mixtures 1, 2, and 6 in **Table 5.4** illustrate that varying the percentage of MK from 0% to 25%, at a binder content of 600 kg/m^3 and a W/B ratio of 0.3, decreased the D_{28} from 0.79×10^{-12} to 0.199×10^{-12} . Meanwhile, mixtures 3, 7, and 14 confirm that increasing the W/B ratio from 0.35 to 0.45, at a constant binder content of 537.5 kg/m^3 and constant MK of 18.75%, increased the D_{28} from 0.417×10^{-12} to 1.39×10^{-12} . It can also be confirmed from **Table 5.4** that increasing the binder content from 350 kg/m^3 to 600 kg/m^3 in mixtures 4, 15, and 17, which had a W/B ratio of 0.4 and MK replacement of 25%, decreased the D_{28} from 1.47×10^{-12} to $0.479 \times 10^{-12} (\text{m}^2/\text{s})$. **Table 5.4** also shows that the reduction of the chloride diffusion with increased percentages of MK from 0% to 25% was more pronounced at lower W/B ratio and/or higher binder content. Looking at the results in **Table 5.4**, the reduction of D_{28} in mixtures 6 to 1 (0.3 W/B ratio and 600 kg/m^3) as a result of increasing MK from 0 to

25% was 75% while the same reduction was 64% in mixtures 47 to 13 (0.5 W/B ratio and 600 kg/m³). Similarly, the reduction of D_{28} in the same mixtures 6 to 1 (0.3 W/B ratio and 600 kg/m³) as a result of increasing MK from 0 to 25% showed 75% while the same reduction was 50% in mixtures 32 to 10 (0.3 W/B ratio and 350 kg/m³). Similar to previous studies, incorporating MK in concrete mixtures decreased the diffusion coefficient and increased chloride resistivity (Gruber et al., 2001a, Poon et al., 2006, Dhinakaran et al., 2012).

The ANOVA analysis for the chloride diffusion coefficient showed that the most significant factors governing the results of the 28- and 90-day chloride diffusion coefficients were B (W/B), C (MK), and A (binder content), in order of significance. At 180 days, both MK (factor C) and W/B ratio (factor B) were nearly equally significant factors. On the other hand, at 360 and 720 days, the most significant factors governing the chloride diffusion coefficients were C (MK), B (W/B), and A (binder content), in order of significance (**Table 5.6**). The equations in **Table 5.5** can be utilized to estimate the chloride diffusion coefficient D_a for concrete with different binder content, percentage of MK, and W/B ratio at 28, 90, 180, 360, and 720 days with $R^2 = 0.89, 0.93, 0.93, 0.92,$ and 0.92 , respectively. It should be noted that the use of these equations is limited to the range of the factors studied in the current research.

Table 5.6 Significant factors for statistical models

Response	Significant factor						Model R ²
	Binder (A)		W/B (B)		MK% (C)		
	F-value	P-value	F-value	P-value	F-value	P-value	
D ₂₈	75.7371	2.78E-11	163.842	9.11E-17	105.0188	1.86E-13	0.89
D ₉₀	25.66345	1.52E-05	30.79635	3.64E-06	28.02032	7.76E-06	0.93
D ₁₈₀	23.82221	2.62E-05	30.27839	4.18E-06	30.42485	4.02E-06	0.93
D ₃₆₀	19.46685	0.000103	28.01426	7.77E-06	30.22744	4.24E-06	0.92
D ₇₂₀	20.05944	8.49E-05	24.65397	2.04E-05	30.16075	4.32E-06	0.92
<i>m_{avr}</i>	6.650813	0.014558	3.510476	0.069861	16.58262	0.000274	0.82
<i>m_{total}</i>	6.650813	0.014558	3.510476	0.069861	16.58262	0.000274	0.82

5.7.3 Chloride diffusion reduction coefficient *m* for concrete containing metakaolin

The values of chloride diffusion reduction coefficient m_{total} and m_{avr} for the 53 concrete mixtures were determined using methods outlined in Section 5.5. The effect of time on the chloride diffusion coefficient of the various mixtures can be seen in **Table 5.4** and **Fig. 5.3**. As seen, there is a general decreasing trend of the chloride diffusion coefficients after 28 days. This decrease is due to the continuous hydration of cement and binding material, which causes densification of concrete. The improvement in pore structure with time was more pronounced in mixtures with higher MK content. **Table 5.4** summarizes the chloride reduction coefficient m calculated using different time basis. All results showed similar range of m as given by other researchers where $0 < m < 1$ (Boddy et al., 2001, Mangat and Molloy, 1994). In general, varying the concrete mixtures affected the chloride reduction coefficient value. Mixtures 11, 21, 33, 41, and 48, which have 475 kg/m³ binder content and 12.5% MK replacement, show that increasing the W/B ratio from 0.3 to 0.5 reduced m_{total} and m_{avr} from 0.31 to 0.12 and from 0.28 to 0.11, respectively. On the other hand, the values of m_{total} and m_{avr} were found to increase as the percentage of MK or binder content increased, indicating

more reduction of the chloride diffusion with time (**Eq. 5.3**). For example, increasing the percentage of MK from 0% to 25% in mixtures 10, 25, and 32, which have a constant W/B ratio of 0.3 and binder content of 350 kg/m^3 , increased m_{total} and m_{avr} from 0.15 to 0.22 and from 0.14 to 0.2, respectively. The results in **Table 5.4** also indicate that the chloride diffusion reduction coefficient showed lower values when calculated using m_{total} compared to when calculated using m_{avr} . The results follow the same trend as previous studies which indicated that the addition of MK decreased the chloride diffusion and diffusion coefficient with time (Boddy et al., 2001, Thomas MDA and PB., 1999, Andrade et al., 2011).

In addition, the prediction models for the m_{avr} and m_{total} were developed for the 53 samples based on ANOVA analysis. The models showed the most significant factors governing m_{avr} and m_{total} values; namely, C (MK), A (binder content), and B (W/B), in order of significance, as shown in **Table 5.6** ($R^2 = 0.82$ for both models). For simplifying the equations, the form of actual values of each variable was applied.

Based on the derived equations obtained from the results of the 53 concrete mixtures, a set of charts was plotted for each response. For all charts, the x-axis represents the binder content which varied from 350 kg/m^3 to 600 kg/m^3 and the y-axis represents the percentage of MK which varied from 0% to 25%. Each curve is plotted on a specific W/B ratio, based on the five levels used in this investigation (0.3, 0.35, 0.4, 0.45, and 0.5) (**Figure 5.4** and **5.5**). The charts represent a simplified method of predicting the chloride reduction coefficient m . The following steps demonstrate how to use the developed charts to predict m_{total} for mixtures with 0.35 W/B ratio, 400 kg/m^3 binder, and 15% MK.

Step 1: Select the chart with 0.35 W/B ratio (labeled on the bottom right of the chart)

Step 2: Draw a vertical line from the 400 kg/m^3 crossing the contour lines (**Figure 5.4**)

Step 3: Draw a horizontal line from the 15% MK replacement

The intersection of both the horizontal and the vertical lines represent the m_{total} , which is equal to 0.2 in this example.

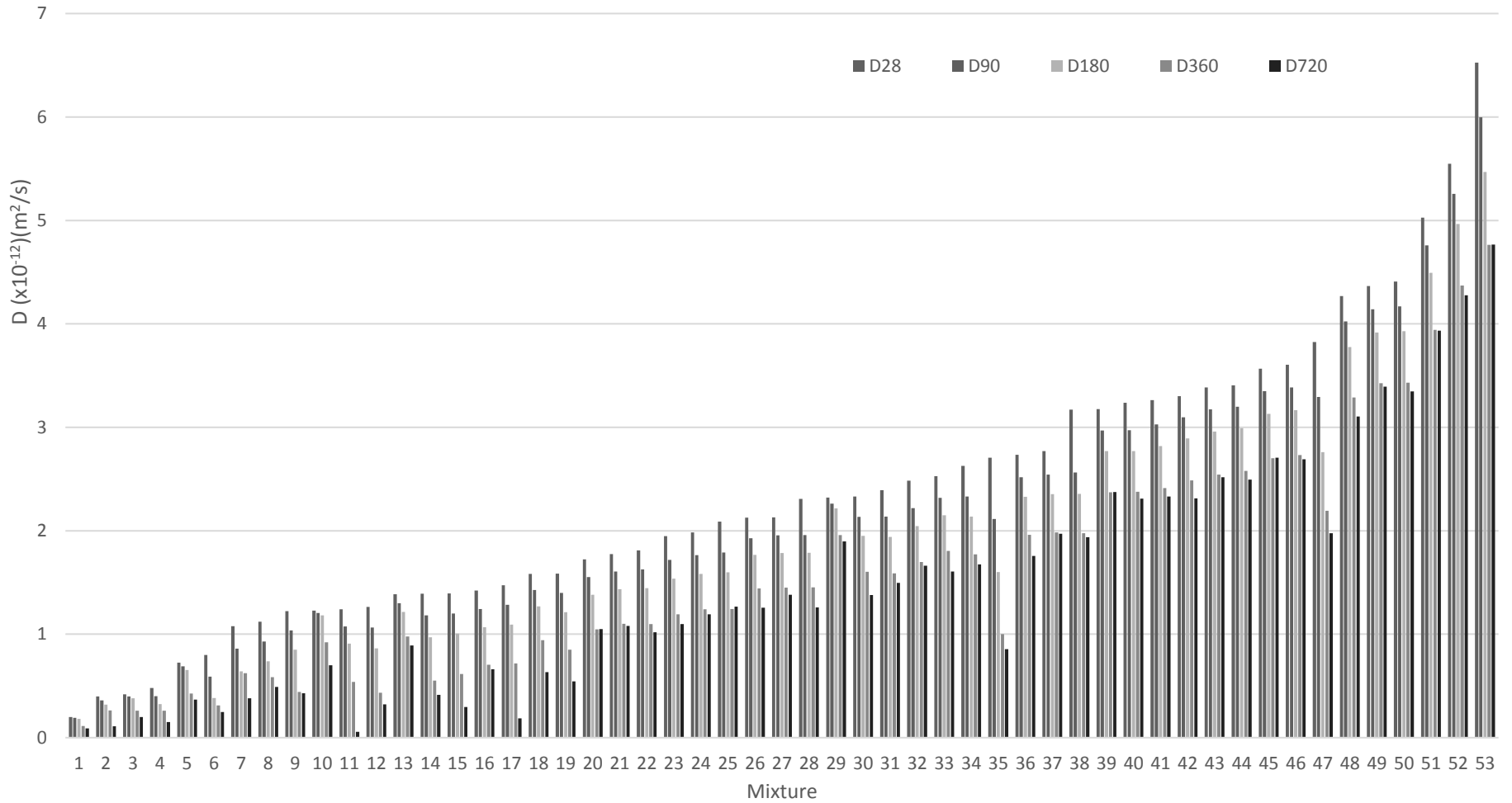


Figure 5.3 Chloride diffusion coefficients at 28, 90, 180, 360, and 720 days

1
2
3

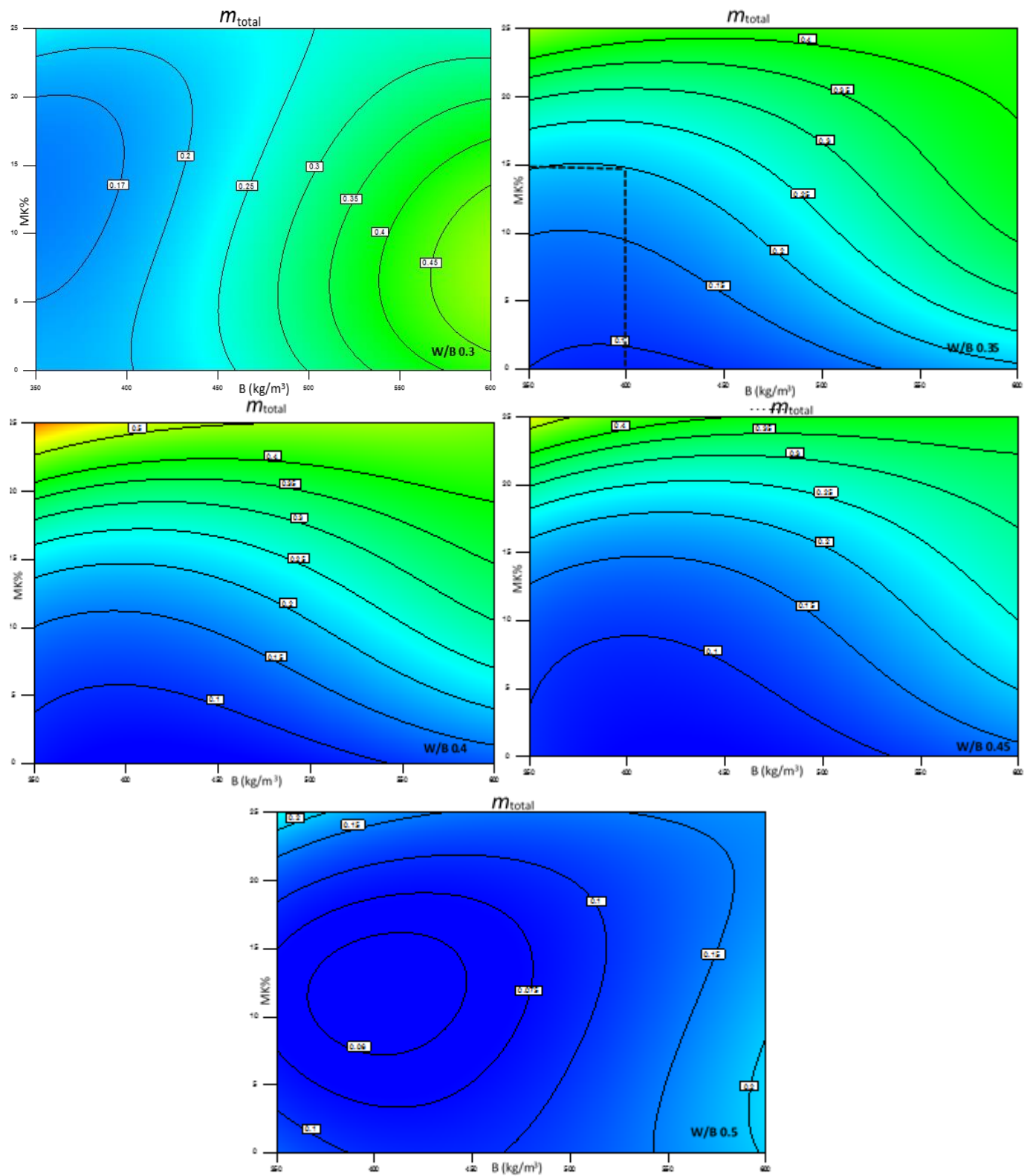


Figure 5.4 m_{total} charts with different W/B ratios

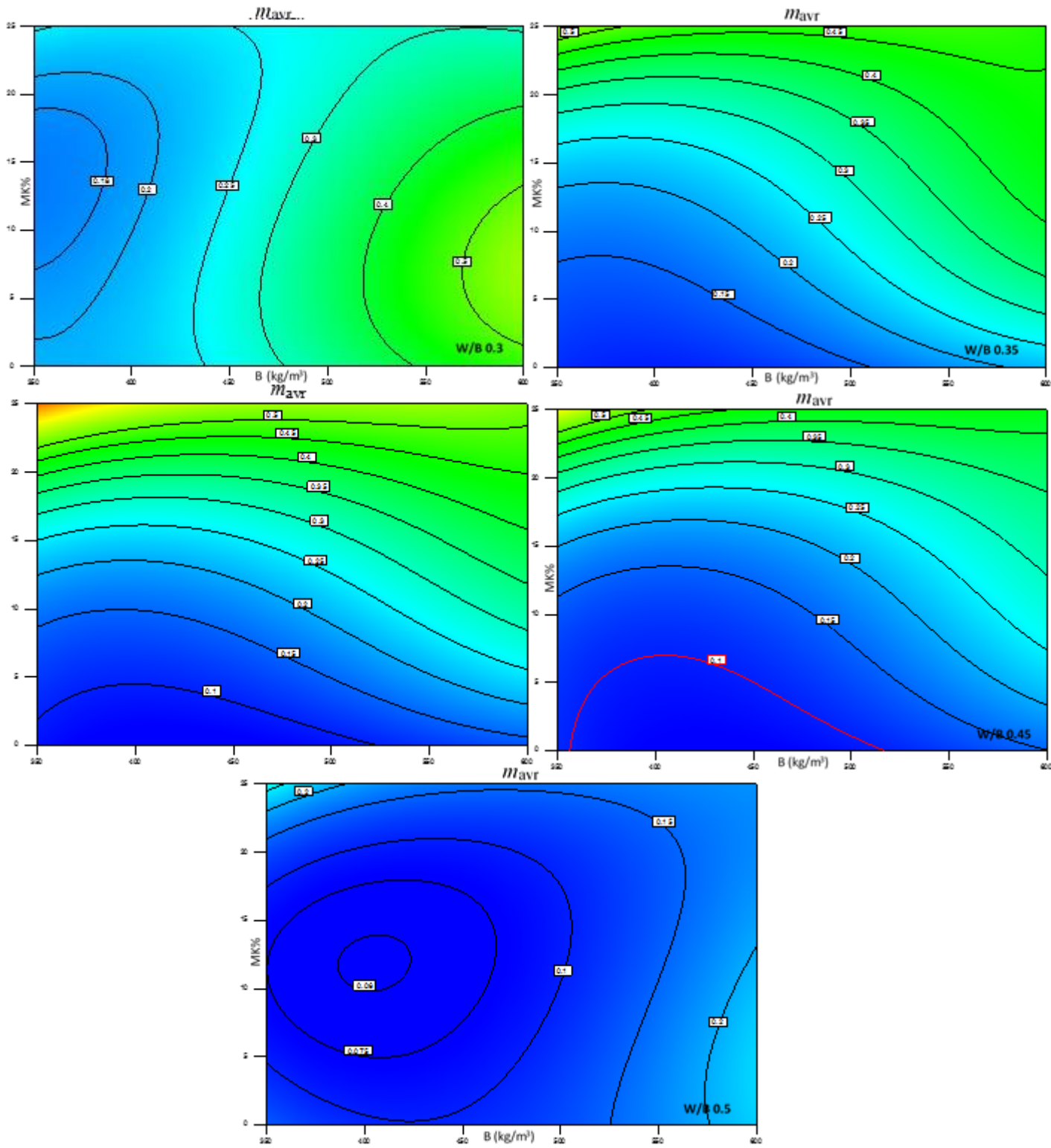


Figure 5.5 mavr charts with different W/B ratios

5.7.4 Development of empirical relationships for chloride diffusion coefficient, RCPT, and compressive strength

Fig. 5.6 shows the relationship between the chloride diffusion coefficient and the amount of charge passed of the RCPT. As seen from the figure, there is a general upward relationship between the chloride diffusion coefficient and the charge passed. It is obvious from the figure that a non-linear relationship exists for the tested samples. As a result, a non-linear equation was developed to predict the chloride diffusion coefficient D_{28} by substituting the RCPT value. This equation can be used for a quick estimation of the chloride diffusion after obtaining the RCPT test results, which only requires 6 hours to be measured compared to 35 days or more for chloride diffusion.

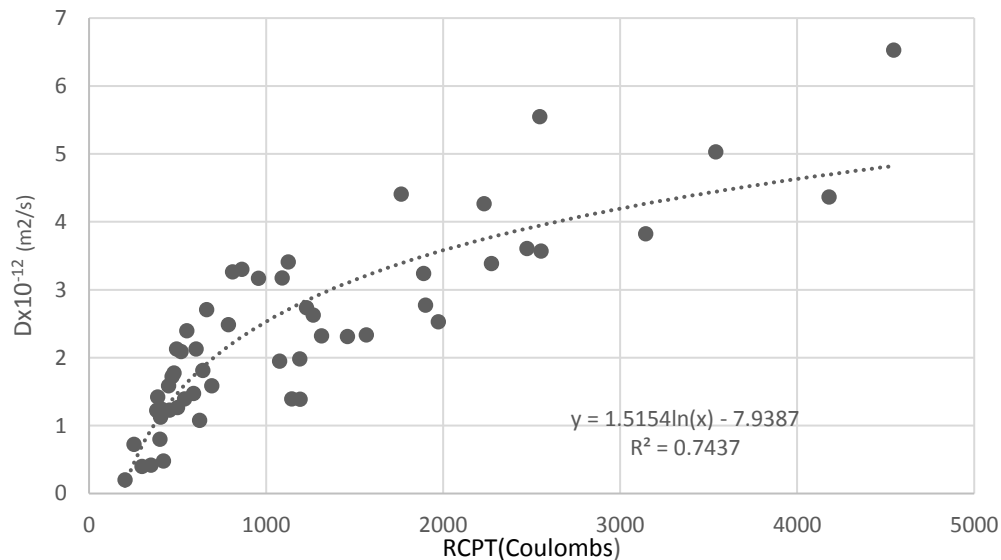


Figure 5.6 Chloride diffusion coefficient vs. RCPT

Eq. 5.8 can be utilized to estimate the chloride diffusion coefficient D_{28} (m^2/s) for concrete containing MK as a function of the RCPT (coulombs) with $R^2 = 0.74$. It should be noted that the use of this equation is limited to the range of factors studied in this research.

$$D_{28}(m^2/s) = 1.5154 * \ln(\text{RCPT}(\text{coulombs})) - 7.9387 \quad \text{Eq. 5.8}$$

Fig. 5.6 illustrates the relationship between the compressive strength and the 28-day chloride diffusion coefficient. In general, lower D_{28} values corresponded to the higher compressive strength values, as both indicate high quality of concrete. Additionally, such good correlation holds across all the mixtures with variable binder content, percentage of MK, and/or W/B ratio.

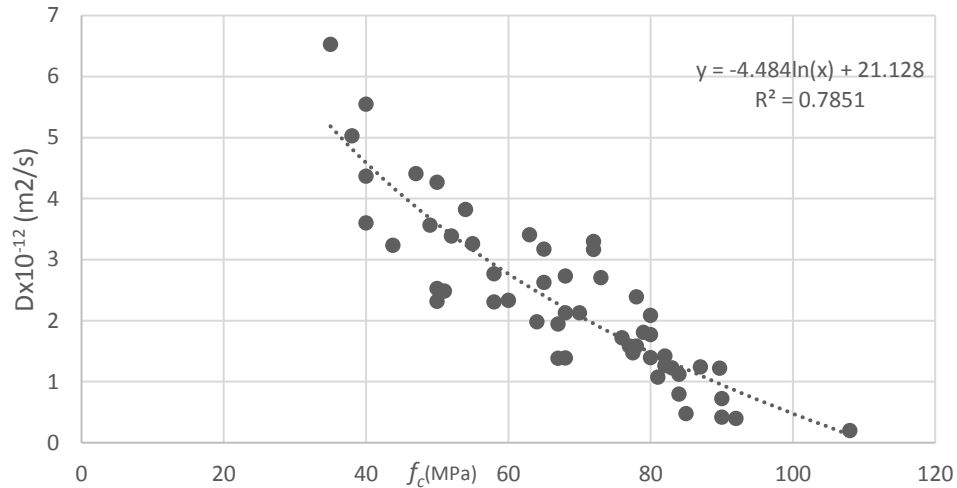


Figure 5.7 Chloride diffusion coefficient vs. compressive strength

Eq. 9 can be utilized to estimate the chloride diffusion coefficient D_{28} as a function of the compressive strength f_c for concrete mixtures containing MK with $R^2 = 0.78$.

$$D_{28} (\text{m}^2/\text{s}) = -4.484 * \ln(f_c (\text{MPa})) + 21.128 \quad \text{(Eq.5.9)}$$

Fig.5.8 shows the relationship between the 28-day compressive strength and the amount of charge passed of the RCPT. It can be seen from the plot that there is a general downward relationship between the compressive strength and the charge passed. It is obvious from the figure that a non-linear relationship exists for the tested samples. Based on the results of the 28-day compressive strength, the RCPT can be predicted using **Eq. 5.10** with R^2 of 0.878.

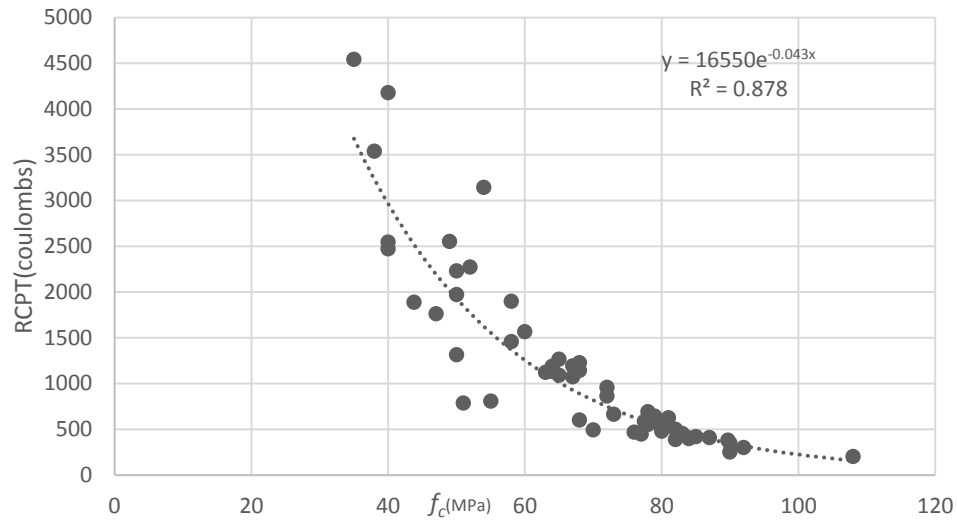


Figure 5.8 RCPT vs. compressive strength

$$RCPT \text{ (coulombs)} = 16550 * e^{-0.043f_c \text{ (MPa)}}$$

Eq. 10

5.7.5 Models' performance assessment

A random mixture was selected with a maximum replacement of MK to validate the prediction models. This mixture consisted of 544.81 kg/m³ binder, 0.32 W/B ratio, and 25% MK replacement. The validation mixture was tested for chloride diffusion test at various ages (28, 90, 180, 360, and 720 days). The test results for the selected mixtures are presented in **Table 5.7**. It can be seen that the results obtained from the prediction models are quite close to the actual test results, especially at early ages (D₂₈, D₉₀, and D₁₈₀). It should be mentioned that the differences are still in tolerance of $\pm 10\%$ from the actual predicted models, indicating a good agreement between the developed models and actual results.

Table 5.7 Validation of the statistical models

Test	Predicted	Tested
D ₂₈ (m ² /s)	0.41 xE ⁻¹²	0.37 xE ⁻¹²
D ₉₀ (m ² /s)	0.31 xE ⁻¹²	0.32 xE ⁻¹²
D ₁₈₀ (m ² /s)	0.24 xE ⁻¹²	0.26 xE ⁻¹²
D ₃₆₀ (m ² /s)	0.14xE ⁻¹²	0.2xE ⁻¹²
D ₇₂₀ (m ² /s)	0.08 xE ⁻¹²	0.13xE ⁻¹²
<i>m</i> _{total}	0.401	0.404
<i>m</i> _{avr}	0.358	0.366

5.8 Conclusions

The following conclusions can be drawn from the results described in this paper:

- The 28-day chloride permeability (measured by the RCPT) and chloride diffusion (measured by the bulk diffusion test) continued to reduce as the percentage of MK increased from 0% to 25%. This reduction was more pronounced in mixtures with lower W/B ratios and/or higher binder content compared to mixtures with higher W/B ratios and/or lower binder content. The reduction of chloride permeability/diffusion with increasing the MK content can be attributed to the pozzolanic activity of MK which improves the pore structure and densifies the whole concrete matrix.
- The results of the chloride diffusion showed a general reduction from 28 days to 760 days of testing. The chloride diffusion reduction coefficients, *m*_{total} and *m*_{avr}, were found to increase as the percentage of MK or binder content increased or as the W/B ratio decrease, indicating more reduction of the chloride diffusion with time. On the other hand, the chloride diffusion reduction coefficient calculated using total time (*m*_{total}) showed lower values than when it was calculated using average time (*m*_{avr}).

- Based on the analysis of variance (ANOVA), the most significant factors affecting the chloride diffusion at early ages (28 and 90 days) were the W/B ratio followed by the percentage of MK and binder content. On the other hand, the most significant factors affecting the chloride diffusion at late ages (360 and 720 days) were the percentage of MK followed by the W/B ratio and binder content. The ANOVA also showed that the most significant factor affecting m_{avr} and m_{total} was the percentage of MK.
- Based on the relationship between the D_{28} and the RCPT results in this investigation, it is possible to predict the 28-day chloride diffusion using the results of the RCPT. The developed equation can give a quick estimation of the chloride diffusion in a shorter amount of time using the results of 6 hours of testing (RCPT) compared to the results of the regular bulk diffusion test, which can take 35 days or more. Moreover, the developed relationship between the compressive strength and D_{28} in this investigation can provide easier prediction of the diffusion coefficient compared to RCPT.
- The developed prediction models and design charts can be used as a fast and useful tool to predict the service life of MK mixtures. These design tools predict the chloride reduction coefficients and the chloride diffusion at different ages based on the total binder content, percentage of MK, and W/B ratio of the mixture.
- Testing validation mixture and comparing the results from the prediction models confirmed the usefulness of these models for estimating the chloride diffusion and the chloride reduction coefficients in mixtures containing MK.

5.9 Reference

2012. Life-365 Service Life Prediction Model and Computer Program for Predicting the Service Life and Life-Cycle Cost of Reinforced Concrete Exposed to Chlorides Version 2.1.
- AKALIN, O., ULAS, A. K. & BAHAR, S. 2010. Self-consolidating high-strength concrete optimization by mixture design method. *ACI Materials Journal*, 107, 357–364.
- ANDRADE, C., CASTELLOTE, M. & D'ANDREA, R. 2011. Measurement of ageing effect on chloride diffusion coefficients in cementitious matrices. *Nuclear Materials* 412, 209–216.
- ASBRIDGE, A. H., CHADBOURN, G. A. & PAGE, C. L. 2001. Effects of metakaolin and the interfacial transition zone on the diffusion of chloride ions through cement mortars. *Cement and Concrete Research*, 31, 1567-1572.
- BAYRAMOV, F., TAŞDEMİR, C. & TAŞDEMİR, M. A. 2004. Optimisation of steel fibre reinforced concretes by means of statistical response surface method. *Cement & Concrete Composites*, 26, 665–675.
- BODDY, A., HOOTON, R. D. & GRUBER, K. A. 2001. Long-term testing of the chloride penetration resistance of concrete containing high-reactivity metakaolin. *Cement and Concrete Research*, 31, 759-765.
- BOULFIZA, M., SAKAI, K., BANTHIA, N. R. & YOSHIDA, H. 2003. Prediction of Chloride Ions Ingress in Uncracked and Cracked Concrete. *Materials journal*, 100, 38-48.
- CHEN, J., XU, Q., LI, J. & FAN, S. 2010. Improved response surface method for anti-slide reliability analysis of gravity dam based on weighted regression. *J. Zhejiang Univ.-Sc A.*, 11, 432-439.
- COURARD, L., DARIMONT, A., SCHOUTERDEN, M., FERAUCHE, F., WILLEM, X. & DEGEIMBRE, R. 2003. Durability of mortars modified with metakaolin. *Cement and Concrete Research*, 33, 1473-1479.
- CRANK, J. 1956. *Mathematics of diffusion*, bristol, clarendon press.
- DHINAKARAN , G., THILGAVATHI, S. & VENKATARAMANA, J. 2012. Compressive strength and chloride resistance of metakaolin concrete. *KSCE Journal of Civil Engineering*, 16, 1209-1217.
- DÍAZ, B., NOVOA, X. R. & PEREZ, M. C. 2006. Study of the chloride diffusion in mortar: A new method of determining diffusion coefficients based on impedance measurements. *Cement and Concrete Composites*, 28, 237–245.
- EHLEN, M. A., THOMAS, M. D. A. & BENTZ, E. C. 2009. Life-365 Service Life Prediction Model™ Version 2.0. *Concrete International*, 31, 41-46.
- ERDOGDU, S., KONDRATOVAL, I. L. & BREMNER , T. W. 2004. Determination of chloride diffusion coefficient of concrete using open-circuit potential measurements. *Cement and Concrete Research*, 34, 603-609.

- GHEZAL, A. & KHAYAT, K. H. 2002. Optimizing Self-Consolidating Concrete with Limestone Filler by Using Statistical Factorial Design Methods. *ACI Materials Journal*, 99, 264-272.
- GRUBER, K., RAMLOCHAN, T., BODDY, A., HOOTON, R. D. & THOMAS, M. D. A. 2001. Increasing concrete durability with high-reactivity metakaolin. *Cem Concr Compos*, 23, 479-484.
- HALAMICKOVA, P., DETWILER, R. J., BENTZ, D. P. & GARBOCZI, E. J. 1995. Water Permeability and Chloride Ion Diffusion in Portland Cement Mortars: Relationship to Sand Content and Critical Pore Diameter. *Cem. and Conc. Res.*, 25, 790-802
- HASSAN, A. A. A., HOSSAIN, K. M. A. & LACHEMI, M. 2009. Corrosion Resistance of Self-Consolidating Concrete in Full-Scale Reinforced Beams. *Cement & Concrete Composites*, 31, 29-38.
- HASSAN, A. A. A., HOSSAIN, K. M. A. & LACHEMI, M. 2012. Effect of Metakaolin and Silica Fume on the Durability of Self-Consolidating Concrete. *Cement & Concrete Composites*, 34, 801-807.
- HOOTON, R. D., GEIKER, M. R. & BENTZ, E. C. 2002. Effects of Curing on Chloride Ingress and Implications on Service Life. *ACI Materials Journal* 99, 201-206.
- JUSTICE, J. M., KENNSION, L. H., MOHR, B. J., BECKWITH, S. L., MCCORMICK, L. E., WIGGINS, B., ZHANG, K. Z. Z. & KURTIS, E. Comparison of two metakaolins and a silica fume used as supplementary cementitious materials. Proc. Seventh International Symposium on Utilization of High-Strength/High Performance Concrete, 2005 Washington D.C.
- KANG, S. C., KOH, H. M. & CHOO, J. F. 2010. An efficient response surface method using moving least squares approximation for structural reliability analysis. *Probab. Eng. Mech*, 25, 365-371.
- KATO, Y. & UOMOTO, T. 2005. Modeling of effective diffusion coefficient of substances in concrete considering spatial properties of composite materials. *Advanced Concrete Technology* 3, 241-251.
- LIZARAZO-MARRIAGA, J. & CLAISSE, P. 2009. Determination of the concrete chloride diffusion coefficient based on an electrochemical test and an optimization model. *Materials Chemistry and Physics*, 117, 536-543.
- MALHOTRA, V. M. 2000. Role of supplementary cementing materials in reducing greenhouse gas emissions. In: O.E. GJORN & SAKAI, K. (eds.) *Concrete Technology for a Sustainable Development in the 21st Century*. London, UK: E & FN Spon.
- MANGAT, P. S. & MOLLOY, B. T. 1994. Prediction of long term chloride concentration in concrete. *Materials and Structures* 27, 338-346.
- POON, C. S., KOU, S. C. & LAM, L. 2006. Compressive strength, chloride diffusivity and pore structure of high performance metakaolin and silica fume concrete. *Journal of Construction and Building Materials*, 20, 858-865.
- SONG, H., LEE, C. & ANN, K. 2008. Factors influencing chloride transport in concrete structures exposed to marine environments *Cement & Concrete Composites*, 30, 113-121.

- STANISH, K. D., HOOTON, R. D. & THOMAS, M. D. A. 2000. Testing the Chloride Penetration Resistance of Concrete: A Literature Review. Federal Highway Administration.
- STEWART, M. G. & ROSOWSKY, D. 1998. Time-dependent reliability of deteriorating reinforced concrete bridge decks. *Structural Safety*, 20, 91–109.
- TAKEWAKA, K. & MATSUMOTO, S. Quality and cover thickness of concrete based on the estimation of chloride penetration in marine environments. *In: MALHOTRA, V. M., ed. 2nd International Conference of Concrete in Marine Environment, 1988. ACI, 381-400.*
- TANG, L. & NILSSON, L. 1992. Chloride diffusivity in high strength concrete at different ages. *Nordic Concrete Research, Nordic Concrete Federation, Nordic Concrete Research, Nordic Concrete Federation, 162-171.*
- THOMAS MDA & PB., B. 1999. Modelling chloride diffusion in concrete: effect of fly ash and slag. *Cem Concr Res*, 29, 487–95.
- VEDALAKSHMI, R., DEVI, R., EMMANUEL, B. & PALANISWAMY, N. 2008. Determination of diffusion coefficient of chloride in concrete: an electrochemical impedance spectroscopic approach. *Materials and Structures* 41 1315–1326.
- WONG, S. M., HOBBS, R. E. & ONOF, C. 2005. An adaptive response surface method for reliability analysis of structures with multiple loading sequences. *Structure safety*, 27, 287-308.
- YOUNG, J. F. 1988. Review of the Pore Structure of Cement Paste and Concrete and its Influence on Permeability. *American Concrete Institute SP-108*, 1-18.

6. Probabilistic and statistical modeling of chloride-induced corrosion for concrete containing metakaolin

6.1 Abstract

This paper presents new models for computing the chloride-induced corrosion period based on combining Monte Carlo Simulation and statistical analysis methods. The study is divided into two parts. The first part utilized Monte Carlo simulation to predict the probability of corrosion (1 to 200 years) for concrete containing metakaolin (MK) with different mixture proportions and concrete covers. Also, the effect of different mixture parameters (percentage of MK, binder content, and water-to-binder ratio) on the probability of corrosion was studied in this part. The second part adopted statistical analysis to develop models predicting the chloride-induced corrosion period (time to reach 10% probability of corrosion initiation) in various MK mixtures and identified the most significant factors affecting this period. Design charts were also developed using statistical analysis to facilitate and simplify the prediction of the chloride-induced corrosion period. The results showed that the probability of corrosion decreased as the percentage of MK increased. Also, using lower W/B ratio or higher binder content in MK mixtures improved the effectiveness of MK to reduce the probability of corrosion. The results also showed that the most significant factor affecting the chloride-induced corrosion period was found to be MK replacement, W/B ratio, and binder content respectively, in order of significance. The developed models and design charts in this paper will help designers and engineers to better understand the influence and the

importance of various mix design parameters of MK mixtures on the chloride-induced corrosion period estimation.

6.2 Introduction

The deterioration of reinforced concrete (RC) structures in harsh marine environments is mainly due to chloride-induced corrosion of rebar in concrete. For both new and existing RC structures questions arise—how safe and how long is the structure able to sustain its function? It is reported that the costs of repair and maintenance of corroded structures exceeds billions of dollars per year (Cusson and Isgor, 2004). For this reason, it is very important to enhance and improve the prediction methods for service lifetime of structures. Service life is defined as “the time during which concrete fulfils its performance requirements, without non-intended maintenance” (Newman and Choo, 2003). A service period of more than 120 years may be specified for important concrete infrastructures (Gjørsv., 2009, Ghali et al., 2016). Service life design is carried out mainly by considering initiation and propagation of reinforcement corrosion. One of the first service life models, developed by Tuutti (Tuutti, 1982), divided the service life of RC structures into two phases: the initiation phase (t_i) and the propagation phase (t_p). The initiation phase is also known as the chloride-induced corrosion period, which is the time required for chloride ions to penetrate the concrete cover and reach the rebar surface. The corrosion occurs when the chloride level at the rebar exceeds the normal threshold (Cheewaket et al., 2012, Liang et al., 2002). Up till now, a universal chloride threshold value does not exist due to its dependency on many factors such as: type of binder, temperature, the surface condition of steel, availability of oxygen,

electrochemical potential, etc.(Angst et al., 2009). The second phase, the propagation period, is where corrosion of the reinforcement steel initiates and continue until the first crack occurs on the concrete cover surface (Amleh, 2000). The cracking of concrete cover significantly increases the ingress of chlorides and other deleterious substances, reducing the strength of the structural element and accelerating the corrosion process (Kato and Uomoto, 2005, Boulfiza et al., 2003).

The chloride-induced corrosion period of concrete structures can be extended by improving the durability characteristics of concrete mixtures (Cady and Weyers, 1983, Ramezani-pour et al., 2015, Thomas and Bamforth, 1999). Adding supplementary cementing material (SCM) enhances the concrete durability, which can increase the chloride-induced corrosion period of the structure (Ehlen et al., 2009, Hooton et al., 2002, Mehta and Monteiro, 1993). Metakaolin (MK) is receiving a lot of attention nowadays. Using MK as an SCM can considerably improve the performance of concrete structures by improving chlorides resistivity properties (Gruber et al., 2001b, Asbridge et al., 2001, Courard et al., 2003, Hassan et al., 2012a). The addition of MK in concrete proved to reduce the chloride permeability, corrosion process by carbonation, and decrease the *Alkali-silica reaction* of mixtures (Barnes et al., 2003, Coleman and Page, 1997, Ramlochan et al., 2000, McPolin et al., 2009). The reduction of chloride permeability is due to the high pozzolanic and micro filler characteristics of MK which reduce the porosity in the concrete mixture (Poon et al., 2001, Wild et al., 1996). MK has been used in the precast concrete industry and glass fibre reinforced cement composites to enhance the mechanical and durability properties of concrete members (Cassagnabère et al., 2010, Cassagnabère et al., 2009, Marikunte et al., 1997).

The incorporation of MK into concrete mixtures not only enhances the durability properties and the mechanical properties of concrete, it also leads to a significant reduction in CO₂ emissions into the environment as it requires lower manufacturing temperatures compared to cement (Malhotra, 2000), which makes MK a more environmentally friendly product.

The corrosion mechanism is complex and greatly affected by the environment and concrete material properties. One of the problems facing the prediction of service life for RC structures is the scatteredness in mechanical and durability properties. Even for the same structural member, mechanical and durability properties may vary from one point to another. Therefore, the sources of variation for environmental and material uncertainties should be considered in service life performance assessment. Probability analysis of the structure plays an important role in the performance of its serviceability (Kirkpatrick et al., 2002, Enright and Frangopol, 1998, Marsh and Frangopol, 2008). There are several methods for determining the reliability of structures' performance due to the variation of concrete mechanical and durability properties (Quanwang et al., 2015, McNally and Sheils, 2012). An acceptable probability of failure for corrosion initiation of reinforcing steel may be taken as 10% (Fluge, 2001). Monte Carlo Simulation (MCS) method is a powerful method for reliability analysis that can take different probabilistic parameters into account simultaneously (MAREK and BROZZETTI, 2001, Ann et al., 2010). This method uses a sampling of random variables to construct a set of values that aims to describe the failure and safe spaces. Monte Carlo analysis can be described as a repeated statistical sampling process (Marek et al., 1993).

Statistical design technique is an efficient tool for developing design models for corrosion and durability properties of concrete (Nieves-Mendoza et al., 2012, Cabrera et al., 1995, Xuemei et al., 2015). Statistical models help in understanding the interactions between parameters that have been modeled and optimized (Ghezal and Khayat, 2002). One of the statistical techniques is the response surface method (RSM), which is applied in numerous civil engineering fields (Bayramov et al., 2004b, Wong et al., 2005, Chen et al., 2010, Kang et al., 2010). The RSM is a compilation of mathematical and statistical techniques used for developing, refining, and optimizing processes, and it can be used to evaluate the relative significance of numerous factors, even in complex interactions. RSM relies on analysis of variance, selecting a few points out of the full factorial set that can represent efficient information about the response space as presented in **Figure 6.1**.

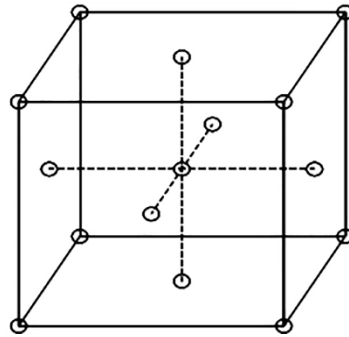


Figure 6.1 Statistical method point arrangement

The prediction of the chloride-induced corrosion period is necessary to ensure long-term safety and sustainability of RC structures subjected to severe environmental conditions. The probabilistic analysis of structures has an extensive literature (Sudret, 2008, Bastidas-Arteaga et al., 2011). However, limited research has been conducted on the probability of chloride-induced corrosion for concrete containing MK based on

mixture proportions. Moreover, research combining the statistical analysis with the probabilistic method is even less frequent. The main objective of this investigation was to combine statistical and probabilistic analyses to develop enhanced chloride-induced corrosion prediction models for concrete containing MK with different mixture proportions. In the first part of this investigation, probabilistic models were developed using MCS to predict the probability of corrosion (1 to 200 years) in different MK mixtures with different concrete covers. This part also investigated the effect of W/B ratio, MK replacement, and total binder content on the probability of corrosion. The second part of the investigation used statistical analysis to develop models predicting the chloride-induced corrosion period (time to reach 10% probability of corrosion initiation) in concrete containing MK with different covers. These models considered three mixture variables: W/B ratio (0.3–0.5), MK replacement (0%–25%), and total binder content (350 kg/m³–600 kg/m³). Additionally, the statistical analysis in the second part was used to investigate the most significant factors affecting the chloride-induced corrosion period. The investigation also included developing design charts to predict the chloride-induced corrosion period based on the developed models. These charts can assist designers and decision makers in predicting the corrosion period in concrete containing MK.

6.3 Research Significance

Although there are research papers modeling the corrosion in RC structures, predicting the chloride-induced corrosion period in concrete containing MK is missing from the literature. This research work is mainly conducted to predict the chloride-induced

corrosion period in MK concrete mixtures with different mixture proportions (different w/b ratio, MK content, and binder content). In addition, estimating the chloride-induced corrosion period using traditional deterministic approaches is a challenge due to the inherent randomness of corrosion model parameters. In this study, combined probabilistic and statistical approaches were used to develop chloride-induced corrosion prediction models for concrete containing MK based on mixture proportions and concrete cover thickness. The developed models in this investigation took into account the uncertainty in concrete chloride resistivity and environmental conditions. The outcome of this paper can be of special interest for designers considering the use of concrete containing MK in structural applications exposed to chloride attack.

6.4 Methodology

6.4.1 Chloride-Induced Corrosion Prediction

Diffusion is the prime chloride ingress mechanism, where chloride ions are transported from higher to lower concentration in a semi-finite medium (concrete matrix). The prediction and optimization of chloride ingress in reinforced concrete structures have become a crucial part in corrosion prediction and maintenance of new and existing structures (Hassan et al., 2009b, Ehlen et al., 2009, Hooton et al., 2002). Chloride diffusion is modeled using Fick's second law of diffusion (**Eq.6.1**) (Crank, 1956), which has been studied by numerous researchers (Diaz et al., 2006, Lizarazo-Marriaga and Claisse, 2009, Vedalakshmi et al., 2008, Hooton et al., 2002).

$$C(x, t) = C_s \left(1 - \operatorname{erf} \frac{x}{2\sqrt{Dt}} \right) \quad (\mathbf{Eq.6.1})$$

Where $C(x,t)$ = chloride concentration, measured at depth x and exposure time t ; C_s = surface chloride concentration, (mass %); x = depth below the exposed surface (to the middle of a layer) (m); D = chloride diffusion coefficient (m^2/s); and t = the exposure time (s).

Equation 6.2 presents the rate of reduction of diffusion over time, which was established in laboratory tests and mathematically captured using a power function equation (Mangat and Molloy, 1994, Takewaka and Matsumoto, 1988, Tang and Nilsson, 1992).

$$D_a = D_{28} \left(\frac{t_0}{t} \right)^m \quad \text{(Eq.6.2)}$$

Where D_a is the chloride diffusion coefficient at time t ; D_{28} is the chloride diffusion coefficient at 28-days (t_{28}); and m is the chloride diffusion reduction coefficient. Various assumptions have been used to determine the chloride diffusion reduction coefficient ' m ' based on the maturity of concrete. This is because concrete is a hydraulic material that continuously hydrates with the availability of moisture. The hydration process causes refining of the pore structure and subsequently lowers the diffusion coefficient over time (Halamickova et al., 1995, Young, 1988).

The calculations of the 28-day chloride diffusion coefficient (D_{28}) and chloride diffusion reduction coefficient (m) in this investigation are based on models previously developed and validated by the authors for different MK mixtures. The detailed study of the diffusion coefficient and chloride diffusion reduction coefficient can be found elsewhere (Al-Alaily and Hassan, 2016b). These developed models account for three

variables: W/B ratio (0.3–0.5), percentage of MK (0%–25%), and binder content (350kg/m³–600 kg/m³), as seen in **Table 6.1**.

Table 6.1 Chloride diffusion and chloride diffusion reduction models used

Coefficient	D ₂₈	m ^{0.5}
β ₀	-2.83919	3.640028
β ₁	-0.00191	-0.00369
β ₂	25.58516	-14.2871
β ₃	0.022369	-0.27824
β ₁₂	-0.01622	-0.04906
β ₁₃	0.000107	0.000104
β ₂₃	-0.3907	1.327575
β ₁₁	0	2.74E-05
β ₂₂	0	49.16957
β ₃₃	0	0.000262
β ₁₂₃	0	3.09E-06
β ₁₁₂	0	1.93E-05
β ₁₁₃	0	-2.80E-08
β ₁₂₂	0	0.03519
β ₁₃₃	0	-4.30E-06
β ₂₂₃	0	-1.73695
B ₂₃₃	0	0.003127
β ₁₁₁	0	-2.20E-08
β ₂₂₂	0	-41.7753
β ₃₃₃	0	2.05E-05

Response (D₂₈ or m^{0.5}) =

$$\beta_0 + \beta_1 X_1 + \beta_2 X_2 + \beta_3 X_3 + \beta_{12} X_1 X_2 + \beta_{13} X_1 X_3 + \beta_{23} X_2 X_3 + \beta_{11} X_1^2 + \beta_{22} X_2^2 + \beta_{33} X_3^2 + \beta_{123} X_1 X_2 X_3 + \beta_{112} X_1^2 X_2 + \beta_{113} X_1^2 X_3 + \beta_{122} X_1 X_2^2 + \beta_{133} X_1 X_3^2 + \beta_{223} X_2^2 X_3 + \beta_{233} X_2 X_3^2 + \beta_{111} X_1^3 + \beta_{222} X_2^3 + \beta_{333} X_3^3$$

Note: X₁ = Water-to-binder ratio X₂ = Binder content X₃ = Percentage of MK

6.4.2 Monte Carlo Simulation (MCS)

MCS is based on the limit states philosophy evaluating the random interaction of load effects S and resistance R (Nowak and Collins, 2000). The chloride concentration at the level of reinforcement C_x represents the load effect S , while the chloride threshold (C_{th}) represents the resistance R . The reliability function (RF) can be written as follows (3):

$$RF = R - S = C_{th} - C_x \quad (\text{Eq.6.3})$$

The reliability function was analyzed using Monte Carlo techniques. The random variables can be described by the coefficient of variations (Gjørsv., 2009) presented in Table 2. The measure of reliability is expressed by the probability of failure P_f (Eq.6.4). The most common recommended limit for the *probability of failure* for the chloride-induced corrosion period is 10% corrosion probability (Gjørsv., 2009).

$$P_f = P (C_{th} - C_x < 0) \quad (\text{Eq.6.4})$$

Where P_f is the probability of failure and P is probability of $(C_{th} - C_x < 0)$.

6.5 Scope of Work

6.5.1 Monte Carlo Simulation Modeling (First Part)

The modeling started by choosing an MK mixture with a selected W/B ratio (a number between 0.3 and 0.5), binder content (a value between 350kg/m³ and 600 kg/m³), and percentage of MK (a percentage between 0% and 25%). The computer then used equations from Table 1 to calculate the chloride diffusion coefficient (D_{28}) and the chloride diffusion reduction coefficient (m). Based on the average values and covariance found in the literature (Gjørsv., 2009, Bentz, 2003) (presented in **Table 6.2**), the program then generated 50,000 random numbers for the D_{28} , m , C_s , x , and C_{th} . In the following step, the chloride concentration at the level of reinforcement, C_x , was calculated based on the 50,000 random numbers (D_{28} , m , C_s , x , and C_{th}) at year one using equations 1 and 2. The probabilities of failure were then calculated based on equations 3 and 4. The computer repeated the loop until it reached the required number of years (200 years in our study). After finishing the loop, the calculations were repeated to calculate the probability of corrosion for another MK mixture with different

values of W/B, binder contents, and percentage of MK. The computer program in each mixture plotted the probability of corrosion (failure) (P_f) on the y-axis and the years on the x-axis. **Figure 6.2** represents a flowchart showing the procedure used to develop the probability models, and **Figure 6.3** presents a sample of the program output.

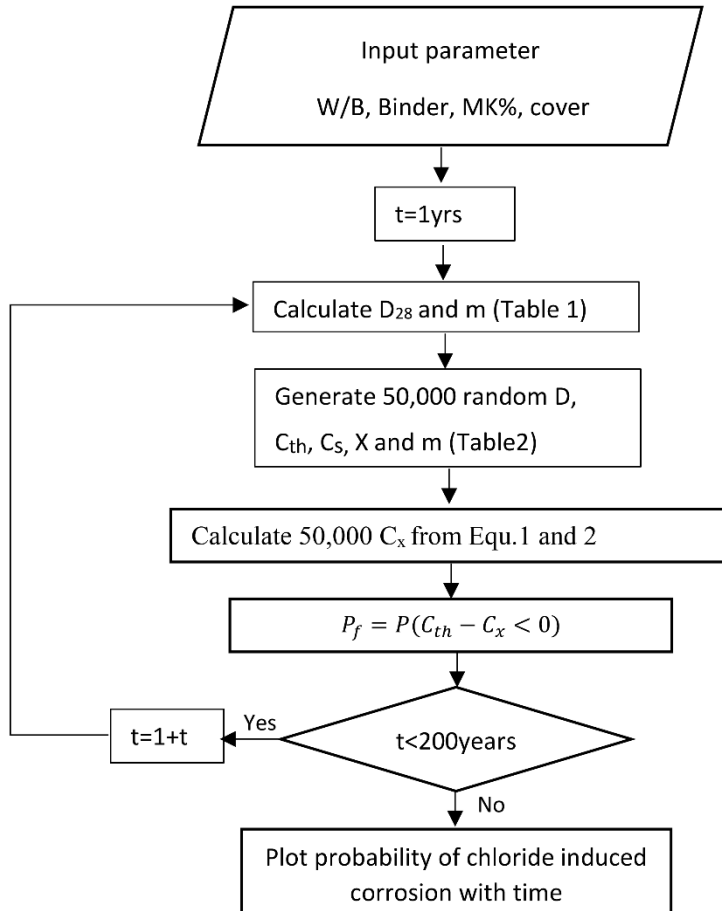


Figure 6.2 Program flowchart

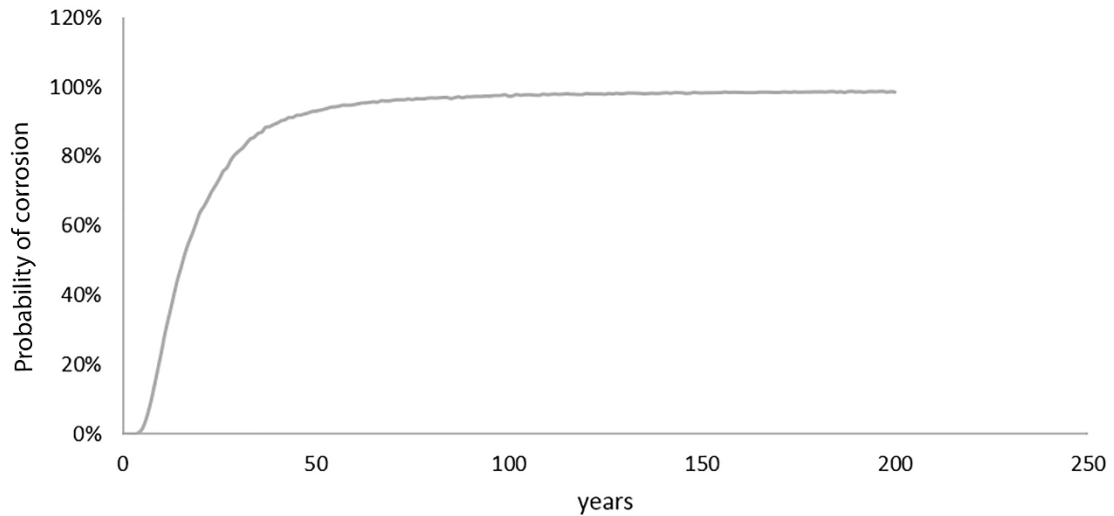


Figure 6.3 Sample of program output plot

Table 6.2 Input parameter for probabilistic analysis

Factor	Average value	Units	*COV %
C_s	0.5	% cement	30%
D	Table 1	$m/s * 10^{-12}$	20%
m	Table 1	-	10%
x	30,40,60	mm	8%
C_{th}	0.05	% cement	20%

* (Bentz, 2003, GjØrv., 2009)

6.5.2 Chloride-Induced Corrosion Period Statistical Analysis (Second Part)

In the second part, statistical analysis was applied to develop equations that predict the time for chloride-induced corrosion (time associated with 10% probability of corrosion initiation) for different MK mixtures with different concrete covers. Three factors were used to develop the prediction equations: W/B ratio (0.3–0.5), binder content (350 kg/m^3 –600 kg/m^3), and percentage of MK (0%–25%). The prediction equations were developed for three concrete covers: 30 mm, 40 mm and 60 mm. Based on the selected points of the statistical analysis method, 17 concrete mixtures were selected (as seen in **Table 6.3**). At each selected mixture in Table 3, and for each concrete cover (30 mm,

40 mm, and 60 mm) the year associated with the 10% probability of corrosion initiation was found through MCS and recorded in the table. Statistical analysis was then conducted using the data in **Table 6.3**, and the chloride-induced corrosion prediction (chloride that causes 10% probability of corrosion initiation) equations were developed for each concrete cover (**Table 6.4**). The most significant factors affecting the chloride-induced corrosion period were also identified using statistical analysis. Finally, for the three concrete covers, prediction charts were developed based on the developed statistical analysis equations. The x-axis in these charts represents the binder content, varied from 350 kg/m³ to 600 kg/m³, and the y-axis represents the percentage of MK, varied from 0% to 25%. Each curve in the chart is plotted on a specific W/B ratio based on the five levels used in the mixtures (0.3, 0.35, 0.4, 0.45, and 0.5).

Table 6.3 Mixture proportions

Mixture	W/B	Binder (kg/m ³)	MK%	time for 10% corrosion probability		
				30-mm cover (years)	40-mm cover (years)	60-mm cover (years)
1	0.3	350	12.5	11	27	60
2	0.4	475	12.5	16	35	79
3	0.5	350	12.5	2	4	12
4	0.4	475	12.5	16	35	79
5	0.4	600	25	181	320	717
6	0.4	475	12.5	16	35	79
7	0.5	600	12.5	15	34	76
8	0.5	475	25	10	26	56
9	0.5	475	0	2	9	19
10	0.3	475	0	37	65	144
11	0.3	600	12.5	183	325	735
12	0.4	350	25	157	281	632
13	0.4	475	12.5	16	35	79
14	0.4	600	0	9	22	52
15	0.4	350	0	2	5	15
16	0.4	475	12.5	16	35	79
17	0.3	475	25	50	87	195

Table 6.4 Chloride-induced corrosion prediction equations

coefficient	30 mm	40 mm	60 mm
β_0	-0.025056276	1.513437543	1.58503502
β_1	-6.619038244	-7.808094123	-4.616669864
β_2	0.015569978	0.011726279	0.013232341
β_3	0.091581304	0.121762296	0.100162124
β_{12}	-0.015933757	-0.006958443	-0.013193985
β_{13}	0.261666564	0.153870222	0.155545291
β_{23}	-0.000217892	-0.000216262	-0.000178721

$$\text{Response Ln(chloride-induced corrosion period)} = \beta_0 + \beta_1 X_1 + \beta_2 X_2 + \beta_3 X_3 + \beta_{12} X_1 X_2 + \beta_{13} X_1 X_3 + \beta_{23} X_2 X_3$$

Note: X1 = Water-to-binder ratio X2 = Binder content X3 = Percentage of MK

6.6 Results and Discussion

6.6.1 Effect of W/B Ratio on the Probability of Corrosion

Based on the models developed in the first part, a parametric analysis was conducted with varied binder content (350 kg/m³ to 600 kg/m³), W/B ratio (0.3 to 0.5), and MK replacement (0% to 25%) to show the effect and sensitivity of each parameter on the probability of corrosion separately. **Figure 6.4** compares five mixtures with constant binder content and constant percentage of MK (400 kg/m³ and 0% MK, respectively) to show the effect of the W/B ratio on the probability of corrosion. The concrete cover thickness was also kept constant at 40 mm in all mixtures, compared in **Figure 6.4**. It should be noted that the results of the parametric analysis showed that the effect of W/B ratio on the probability of corrosion did not depend on the percentage of MK, binder content, and/or cover thickness. Therefore, **Figure 6.4** only presents one example of the effect of W/B ratio in mixtures with any constant values of each of binder content, percentage of MK, and cover thickness (400 kg/m³, 0% MK, and 40-mm concrete cover were chosen as an example). By looking at **Figure 6.4** it can be seen that increasing the W/B ratio from 0.3 to 0.5 increased the probability of corrosion. It can also be noticed

that the probability of corrosion is greatly reduced when 0.3 W/B ratio was used compared to a higher W/B ratio. There is a huge jump in the curve when the W/B ratio was increased from 0.3 to 0.35. And when the W/B ratio was higher than 0.4, a similar probability of corrosion was obtained (close to 100% probability of corrosion after 40 years).

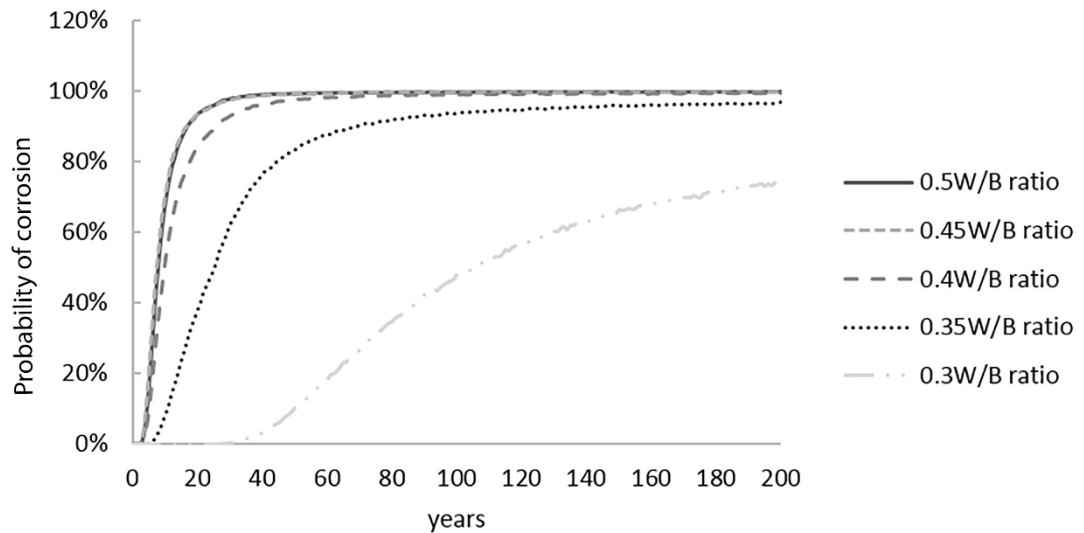


Figure 6.4 Effect of W/B ratio on the probability corrosion (0% MK, 400 kg/m³binder, and 40-mm concrete cover)

6.6.2 Effect of the Percentage of MK on the Probability of Corrosion

To study the effect of MK on the probability of corrosion, five MK replacement levels were selected (0%, 5%, 10%, 15%, 20%, and 25%) while the other variables (W/B ratio, binder content, and cover thickness) were kept constant. As seen in **Figure 6.5**, by increasing the percentage of MK from 0% to 25%, at a constant binder content and constant W/B ratio, the probability of corrosion significantly decreased. For example, adding 25% MK in the mixture with 600 kg/m³ binder and 0.35 W/B ratio decreased the probability of corrosion at 200 years from 71% to 3% (**Figure 6.5**). The effect of

MK on the probability of corrosion was also investigated in mixtures with variable W/B ratios and binder contents (**Figure 6.6**) in order to study the influence of different water and/or cement contents on the reactivity of MK. **Figure 6.6** shows the probability of corrosion of a mixture with 25% MK with varied W/B ratios/binder contents and a constant concrete cover (40 mm). Increasing the W/B ratio from 0.3 to 0.5 at a constant binder content of 350 kg/m³ or 600 kg/m³ in this mixture decreased the effect of MK on reducing the probability of corrosion, as seen in **Figure 6.6**. Also, increasing the binder content from 350 kg/m³ to 600 kg/m³ at a constant W/B ratio of 0.3 or 0.5 enhanced the effect of MK on reducing the probability of corrosion (**Figure 6.6**).

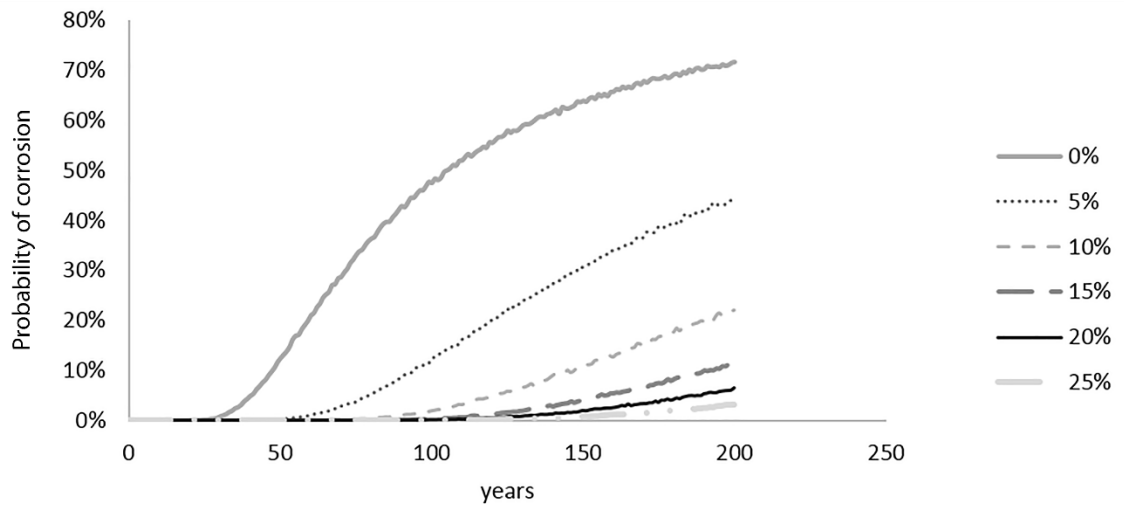


Figure 6.5 Effect of MK replacement on the probability of corrosion (600 kg/m³ binder, 0.35 W/B ratio, and 40-mm concrete cover)

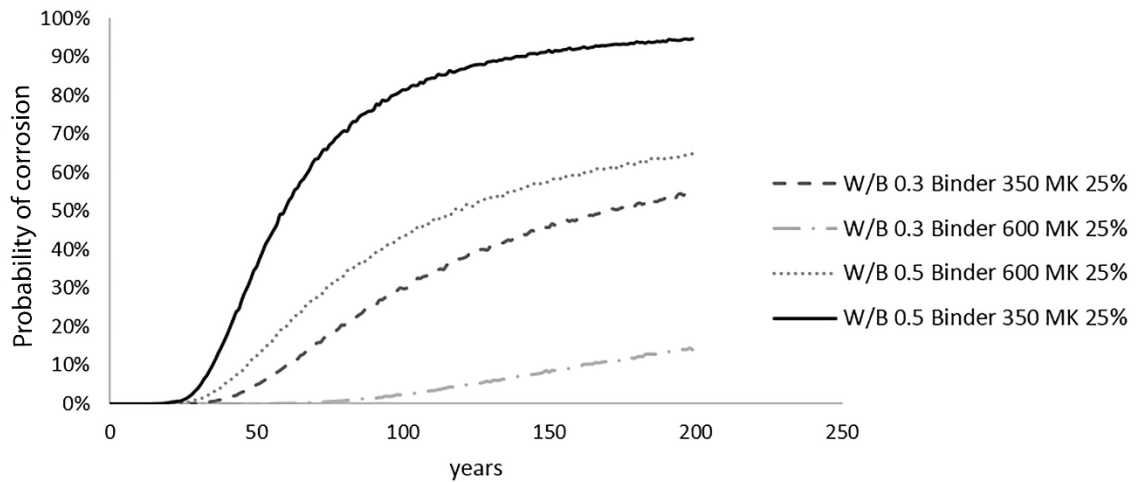


Figure 6.6 Effect of MK replacement at different binder and W/B contents on the probability of corrosion (25% MK and 40-mm concrete cover)

6.6.3 Effect of Binder Content on the Probability of Corrosion

Five concrete mixtures with constant percentage of MK, W/B ratio, and concrete cover thickness (**Figure 6.7**) were selected to investigate the effect of binder content on the probability of corrosion. As seen from the figure, increasing the binder content from 350 kg/m³ to 600 kg/m³ reduced the probability of corrosion. It can also be noted that increasing the binder content from 350 kg/m³ to 500 kg/m³ had an insignificant effect on the probability of corrosion in the first 50 years, while binder contents of 550 kg/m³ to 600 kg/m³ showed a noticeable decrease in the probability of corrosion. It should be noted that increasing cement content reduces the permeability and leads to a denser concrete matrix, which intern reduces the chloride diffusion and probability of corrosion (Gjørsv., 2009, Ferreira and Jalali, 2006, Shamsad et al., 2012).

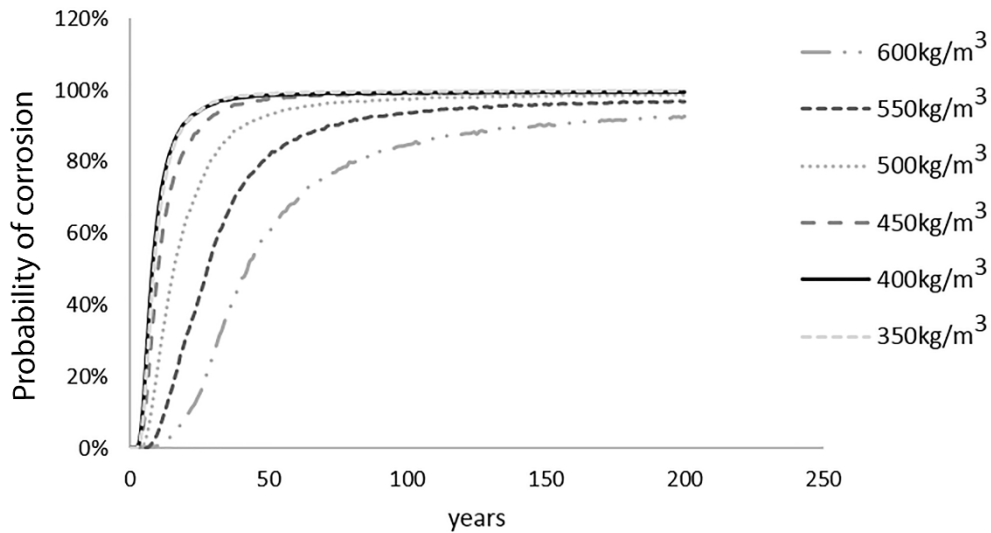


Figure 6.7 Effect of binder content on the probability of corrosion (0% MK, 0.4 W/B ratio, and 40-mm concrete cover)

6.6.4 Statistical Analysis Prediction Equations

As mentioned before, in the second part, statistical analysis was utilized to develop equations to predict the chloride-induced corrosion period (at 10% probability of corrosion initiation) and to identify the most significant factor affecting this period. Three prediction equations having R^2 of 0.81, 0.78, and 0.78 (Table 4) were developed to predict the corrosion time (10% probability corrosion) for MK concrete with 30-mm, 40-mm, and 60-mm concrete covers, respectively. **Table 6.5** also shows the analysis of variance (ANOVA) for the 17 selected MK mixtures (**Table 6.3**). The significance of variables and their interactions was determined after performing the ANOVA by applying the least-square approach. The degree of significance among the significant factors was determined based on the F-value for each factor. The factor with a higher F-value is considered more significant than other factors with lower F-values. As seen from the table, the most significant factors affecting the chloride-induced corrosion

period (in the three concrete covers) were the percentage of MK (factor X_3), followed by the W/B ratio (factor X_2) and then the total binder content (factor X_1) respectively, in order of significance.

Table 6.5 ANOVA for significant parameters (F-value and P-value)

Cover	W/B (X_1)		Binder (X_2)		MK% (X_3)		R^2
	F-value	P-value	F-value	P-value	F-value	P-value	
30-mm	15.841	0.002601	8.701843	0.014537	17.86667	0.001752	0.81
40-mm	12.045	0.006014	8.676315	0.014646	14.47226	0.003462	0.78
60-mm	12.147	0.005869	7.772625	0.019187	14.26034	0.003624	0.78

Based on the equations developed from the statistical analysis (**Table 6.4**), a set of charts were plotted. In all charts, the x-axis represents the binder content varied from 350 kg/m^3 to 600 kg/m^3 , and the y-axis represents the percentage of MK varied from 0% to 25%. Each chart is plotted for a specific W/B ratio based on the five levels used in the mixture design (0.3, 0.35, 0.4, 0.45, and 0.5) (**Figs.6, 8, 9, and 10**). These charts represent a simplified method of predicting the chloride-induced corrosion period of concrete containing MK with variable concrete covers (30 mm, 40 mm, and 60 mm). The following example demonstrates how to use the developed charts to predict the chloride-induced corrosion period of a mixture with a 30-mm concrete, 0.35 W/B ratio, 450 kg/m^3 binder content, and 15% MK replacement.

6.6.5 Steps of design

- i. Select 30-mm concrete cover charts (Figure 8)
- ii. Select the chart with 0.35 W/B ratio
- iii. X-axis represents the binder content (450 kg/m^3)
- iv. Y-axis represents the percentage of MK (15%)

- v. The point of intersection on the contour represents time to reach 10% probability of corrosion initiation (40 years)

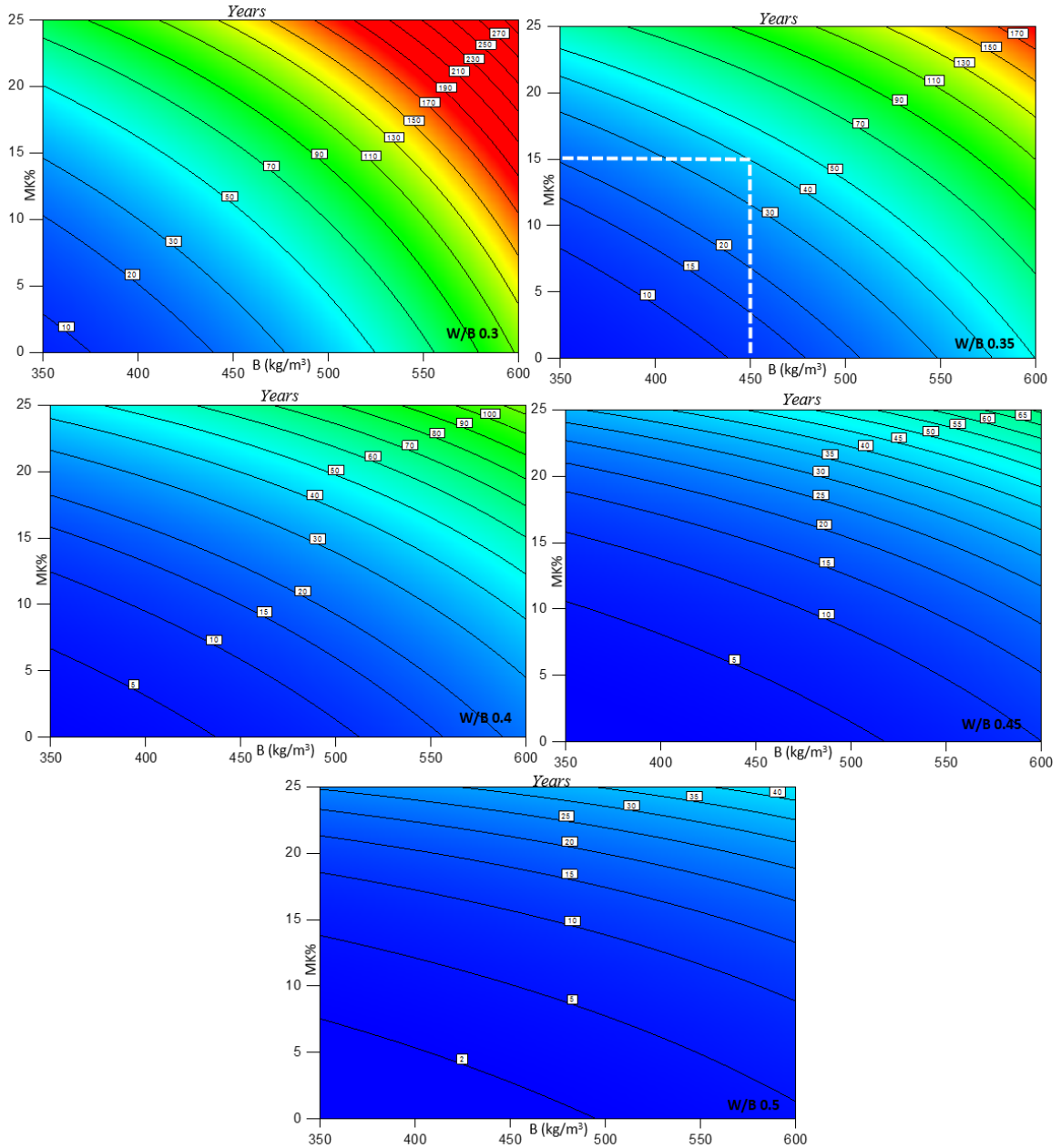


Figure 6.8 Chloride-induced corrosion period (at 10% probability of corrosion initiation) for 30-mm cover

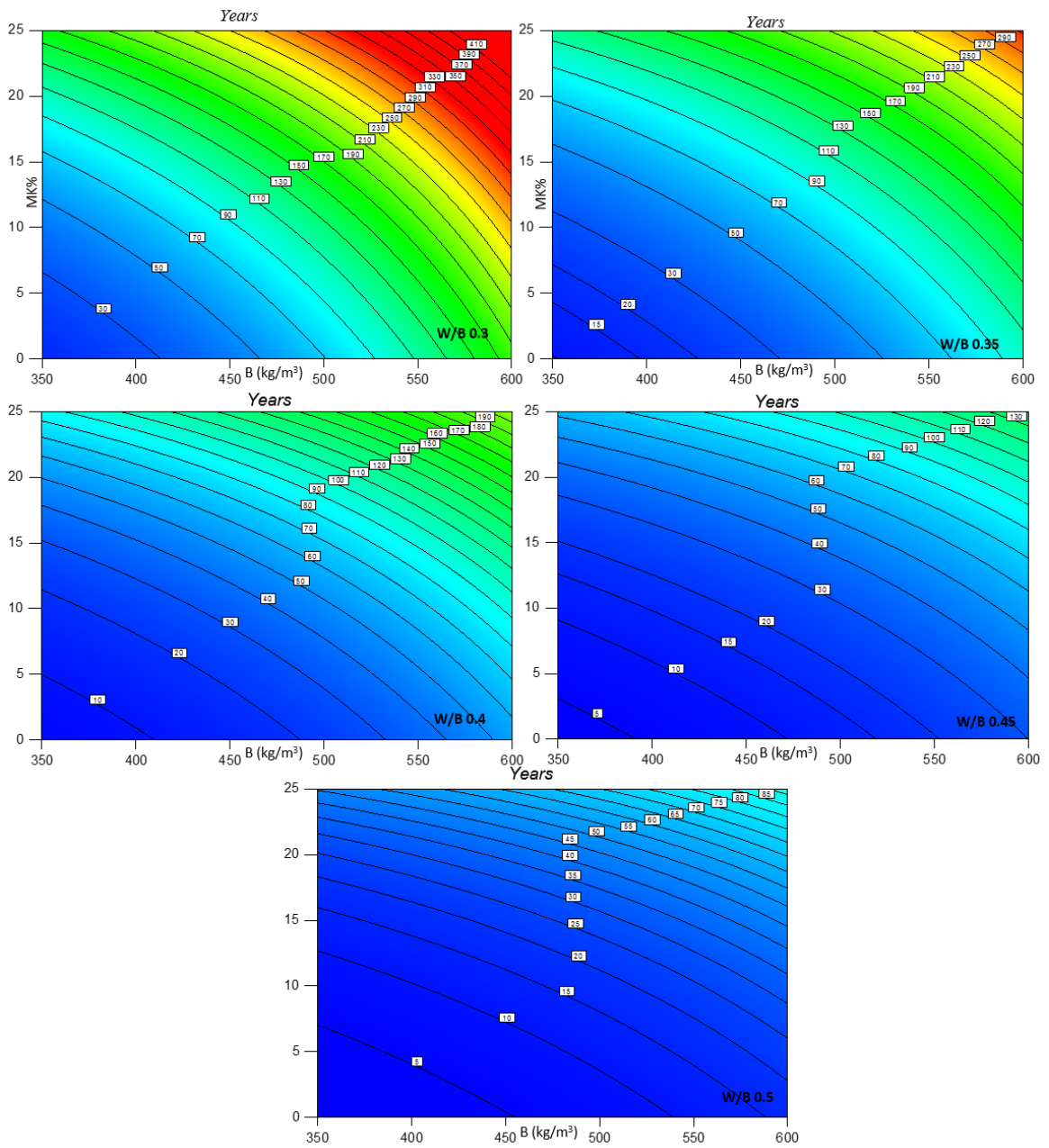


Figure 6.9 Chloride-induced corrosion period (at 10% probability of corrosion initiation) for 40 mm cover

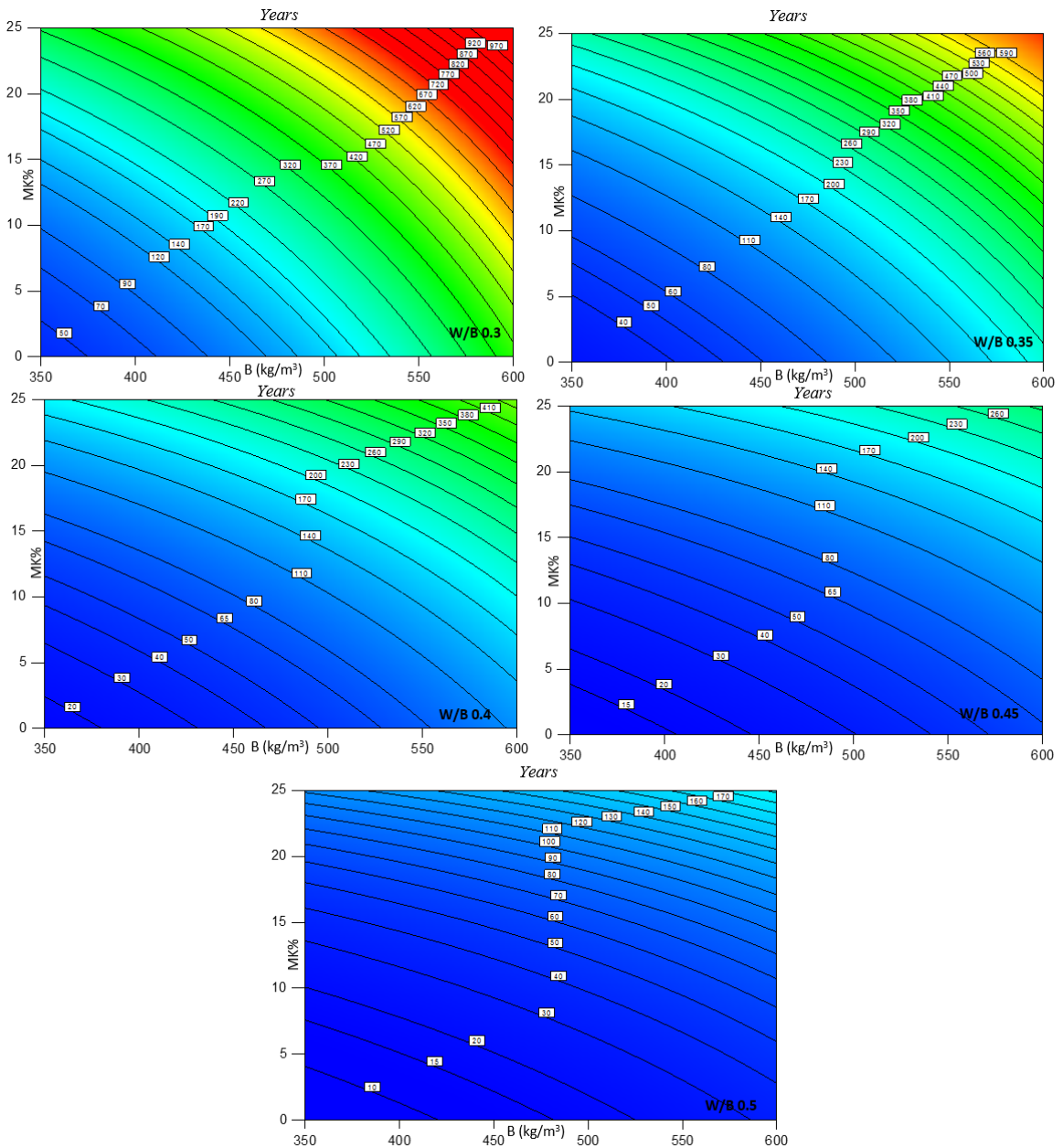


Figure 6.10 Chloride-induced corrosion period (at 10% probability of corrosion initiation) for 60-mm

6.7 Conclusion

From the results described in this paper, the following conclusions can be drawn:

- Increasing the binder content or MK replacement and/or decreasing the W/B ratio decreased the probability of corrosion. Also, the probability of corrosion

was greatly reduced when 0.3 W/B ratio was used compared to a higher W/B ratio.

- Decreasing the W/B ratio significantly affected the reactivity of MK and its ability to reduce the probability of corrosion. MK mixtures with a lower W/B ratio (0.3) had a reduced probability of corrosion compared to MK mixtures with a higher W/B ratio (0.5). Also, increasing the binder content from 350 kg/m³ to 600 kg/m³ had a positive effect on MK's ability to reduce the probability of corrosion.
- Using binder content of 350 kg/m³ to 500 kg/m³ showed insignificant differences in the probability of corrosion (especially after 50 years). On the other hand, using binder content above 500 kg/m³ showed a noticeable effect on increasing the probability of corrosion.
- The most significant factors affecting the chloride-induced corrosion time (time for 10% probability of corrosion initiation) in 30-mm, 40-mm, and/or 60-mm cover MK mixtures were found to be the percentage of MK, W/B ratio, and binder content, respectively, in order of significance.
- The design charts developed with different concrete covers provided a good understanding of how the three MK mixture parameters (binder content, percentage of MK, and W/B ratio) are related to each other in the chloride-induced corrosion period prediction. These charts can be used effectively and easily, instead of using long equations, to predict the chloride-induced corrosion

period of MK mixtures based on the binder content, percentage of MK, and W/B ratio.

6.8 Reference

- AL-ALAILY, H. S. & HASSAN, A. A. A. 2016. Time-Dependence of Chloride Diffusion for Concrete Containing Metakaolin. *Journal of Building Engineering* 7, 159–169.
- AMLEH, L. B. 2000. Deterioration of reinforcing steel in concrete due to corrosion. A thesis submitted to the Faculty of Graduate Studies and Research in partial fulfillment of requirements for the degree of Doctor of Philosophy, McGill University, Montreal, Canada.
- ANGST, U., BERNHARD ELSENER, CLAUS K. LARSEN & ØYSTEIN VENNESLAND 2009. Critical chloride content in reinforced concrete — A review. *Cement and Concrete Research*, 39, 1122–1138.
- ANN, K. Y., PACK, S. W., HWANG, J.-P., SONG, H. W. & KIM, S. H. 2010. Service life prediction of a concrete bridge structure subjected to carbonation. *construction and building materials*, 24, 1494-1501.
- ASBRIDGE, A. H., CHADBOURN, G. A. & PAGE, C. L. 2001. Effects of metakaolin and the interfacial transition zone on the diffusion of chloride ions through cement mortars. *Cement and Concrete Research*, 31, 1567-1572.
- BARNES, P., BENSTED, J. & JONES, T. R. 2003. Metakaolin as pozzolanic addition to concrete. *Structure and performance of cements*. 2 ed. England: CRC press.
- BASTIDAS-ARTEAGA, E., CHATEAUNEUF, A., SÁNCHEZ-SILVA, M., BRESSOLETTE, P. & SCHOEFS, F. 2011. A comprehensive probabilistic model of chloride ingress in unsaturated concrete. *Engineering Structures*, 33, 720-730.
- BAYRAMOV, F., TAŞDEMİR, C. & TAŞDEMİR, M. A. 2004. Optimisation of steel fibre reinforced concretes by means of statistical response surface method. *Cement and Concrete Composites*, 26, 665–675.
- BENTZ, E. C. 2003. Probabilistic Modeling of Service Life for Structures Subjected to Chlorides. *ACI Materials Journal*, 100, 391-397.
- BOULFIZA, M., SAKAI, K., BANTHIA, N. R. & YOSHIDA, H. 2003. Prediction of Chloride Ions Ingress in Uncracked and Cracked Concrete. *Materials journal*, 100, 38-48.
- CABRERA, J. G., CLAISSE, P. A. & HUNT, D. N. 1995. A statistical analysis of the factors which contribute to the corrosion of steel in Portland cement and silica fume concrete. *construction and Building Materials*, 9, 105-113.
- CADY, P. D. & WEYERS, R. E. 1983. Chloride Penetration and the Deterioration of Concrete Bridge Decks, Cement, Concrete, and Aggregates. *CCAGDP*, 5, 81-87.
- CASSAGNABÈRE, F., ESCADEILLAS, G. & MOURET, M. 2009. Study of the reactivity of cement/metakaolin binders at early age for specific use in steam cured precast concrete. *Construction and Building Materials*, 23, 775-784.

- CASSAGNABÈRE, F., MOURET, M., ESCADEILLAS, G., BROILLIARD, P. & BERTRAND, A. 2010. Metakaolin, a solution for the precast industry to limit the clinker content in concrete: Mechanical aspects. *Construction and Building Materials*, 24, 1109-1118.
- CHEEWAKET, T., JATURAPITAKKUL, C. & CHALEE, W. 2012. Initial corrosion presented by chloride threshold penetration of concrete up to 10 year-results under marine site, *Constr. . Build. Mater*, 37, 693-698.
- CHEN, J., XU, Q., LI, J. & FAN, S. 2010. Improved response surface method for anti-slide reliability analysis of gravity dam based on weighted regression. *J. Zhejiang Univ.- Sc A.*, 11, 432-439.
- COLEMAN, J. & PAGE, C. L. 1997. Aspects of the pore solution chemistry of hydrated cement pastes containing metakaolin. *Cement and concrete research*, 27, 147-154.
- COURARD, L., DARIMONT, A., SCHOUTERDEN, M., FERAUCHE, F., WILLEM, X. & DEGEIMBRE, R. 2003. Durability of mortars modified with metakaolin. *Cement and Concrete Research*, 33, 1473-1479.
- CRANK, J. 1956. *Mathematics of diffusion*, bristol, clarendon press.
- CUSSON, D. & ISGOR, B. 2004. Durability of concrete structures: prevention, evaluation, inspection, repair and prediction. *canadian civil engineer*, 21, 4-5.
- DÍAZ, B., NOVOA, X. R. & PEREZ, M. C. 2006. Study of the chloride diffusion in mortar: A new method of determining diffusion coefficients based on impedance measurements. *Cement and Concrete Composites*, 28, 237-245.
- EHLEN, M. A., THOMAS, M. D. A. & BENTZ, E. C. 2009. Life-365 Service Life Prediction Model™ Version 2.0. *Concrete International*, 31, 41-46.
- ENRIGHT, M. P. & FRANGOPOL, D. M. 1998. Probabilistic analysis of resistance degradation of reinforced concrete bridge beams under corrosion. *Eng. Struct.*, 20, 960-971.
- FERREIRA, R. M. & JALALI, S. 2006. Probability-based durability design of concrete structures in marine environment. *Concrete Repair, Rehabilitation and Retrofitting*.
- FLUGE, F. 2001. Marine chlorides – A probabilistic approach to derive provisions for EN 206-1. *Third DuraNet Workshop on Service life design of concrete structures, from theory to standardisation*.
- GHALL, A., GAYED, R. B. & KROMAN, J. 2016. Sustainability of Concrete Infrastructures. *Journal of Bridge Engineering*, 21.
- GHEZAL, A. & KHAYAT, K. H. 2002. Optimizing Self-Consolidating Concrete with Limestone Filler by Using Statistical Factorial Design Methods. *ACI Materials Journal*, 99, 264-272.
- GJØRV., O. E. 2009. *Durability Design of Concrete Structures in Severe Environments*, New york, Taylor & Francis.
- GRUBER, K. A., RAMLOCHAN, T., BODDY, A., HOOTON, R. D. & THOMAS, M. D. A. 2001. Increasing concrete durability with high-reactivity metakaolin. *Cement and Concrete Composites*, 23, 479-484.
- HALAMICKOVA, P., DETWILER, R. J., BENTZ, D. P. & GARBOCZI, E. J. 1995. Water Permeability and Chloride Ion Diffusion in Portland Cement Mortars: Relationship to Sand Content and Critical Pore Diameter. *Cem. and Conc. Res.* , 25, 790-802

- HASSAN, A. A. A., HOSSAIN, K. M. A. & LACHEMI, M. 2009. Corrosion Resistance of Self-Consolidating Concrete in Full-Scale Reinforced Beams. *Cement and Concrete Composites*, 31, 29-38.
- HASSAN, A. A. A., HOSSAIN, K. M. A. & LACHEMI, M. 2012. Effect of Metakaolin and Silica Fume on the Durability of Self-Consolidating Concrete. *Cement and Concrete Composites*, 34, 801-807.
- HOOTON, R. D., GEIKER, M. R. & BENTZ, E. C. 2002. Effects of Curing on Chloride Ingress and Implications on Service Life. *ACI Materials Journal* 99, 201-206.
- KANG, S. C., KOH, H. M. & CHOO, J. F. 2010. An efficient response surface method using moving least squares approximation for structural reliability analysis. *Probab. Eng. Mech*, 25, 365-371.
- KATO, Y. & UOMOTO, T. 2005. Modeling of effective diffusion coefficient of substances in concrete considering spatial properties of composite materials. *Advanced Concrete Technology* 3, 241-251.
- KIRKPATRICK, T. J., WEYERS, R. E., ANDERSON-COOK, C. M. & SPRINKEL, M. M. 2002. Probabilistic model for the chloride-induced corrosion service life of bridge decks. *Cem. Concr. Res.*, 32, 1943–1960.
- LIANG, M., LIN, L. & LIANG, C. 2002. Service life prediction of existing reinforced concrete bridges exposed to chloride environment. *Journal of Infrastructure Systems*, 8, 76-85.
- LIZARAZO-MARRIAGA, J. & CLAISSE, P. 2009. Determination of the concrete chloride diffusion coefficient based on an electrochemical test and an optimization model. *Materials Chemistry and Physics*, 117, 536–543.
- MALHOTRA, V. M. 2000. Role of supplementary cementing materials in reducing greenhouse gas emissions. In: O.E. GJORN & SAKAI, K. (eds.) *Concrete Technology for a Sustainable Development in the 21st Century*. London, UK: E & FN Spon.
- MANGAT, P. S. & MOLLOY, B. T. 1994. Prediction of long term chloride concentration in concrete. *Materials and Structures* 27, 338-346.
- MAREK, P. & BROZZETTI, J. 2001. Probabilistic Assessment of Structures using Monte Carlo simulation. *GUŠTAR, M. Basics, Exercises, Software, ITAM Academy of Sciences Czech Republic*.
- MAREK, P., GUŠTAR, M. & TIKALSKY, P. J. 1993. Monte Carlo Simulation - Tool for Better Understanding of LRFD. *Journal of Structural Engineering*, 119, 1586-1599.
- MARIKUNTE, S., ALDEA, C. & SHAH, S. P. 1997. Durability of Glass Fiber Reinforced Cement Composites: Effect of Silica Fume and Metakaolin. *Advanced Cement Based Materials*, 5, 100-108.
- MARSH, P. S. & FRANGOPOL, D. M. 2008. Reinforced concrete bridge deck reliability model incorporating temporal and spatial variations of probabilistic corrosion rate sensor data. *Reliab. Eng. Syst. Saf.*, 93, 394–409.
- MCNALLY, C. & SHEILS, E. 2012. Probability-based assessment of the durability characteristics of concretes manufactured using CEM II and GGBS binders. *construction and Building Materials*, 30, 22-29.

- MCPOLIN, D. O., BASHEER, P. A. & LONG, A. E. 2009. Carbonation and pH in Mortars Manufactured with Supplementary Cementitious Materials. *Journal of Materials in Civil Engineering*, 21, 217-225.
- MEHTA, P. K. & MONTEIRO, P. J. M. 1993. *Concrete: Structure, Properties and Materials*, New Jersey, U.S.A., Prentice Hall
- NEWMAN, J. B. & CHOO, B. S. 2003. *Advanced Concrete Technology: Concrete Properties*. Butterworth-Heinemann.
- NIEVES-MENDOZA, D., GAONA-TIBURCIO, C., HERVERT-ZAMORA, H. L., TOBIAS, R. J., CASTRO-BORGES, P., COLAS, O. R., ZAMBRANO, R. P., MARTÍNEZ-VILLAFÁÑE, A. & ALMERAYA-CALDERÓN, F. 2012. Statistical Analysis of Factors Influencing Corrosion in Concrete Structures. *International journal of electrochemical science*, 7, 5495-5509.
- NOWAK, A. S. & COLLINS, K. R. 2000. *Reliability of structures*, Michigan, McGraw Hill.
- POON, C. S., LAM, L., KOU, S. C., WONG, Y. L. & WONG, R. 2001. Rate of pozzolanic reaction of metakaolin in high-performance cement pastes. *Cement and Concrete Research*, 31, 1301–1306.
- QUANWANG, L., KEFEI, L., XINGANG, Z., QINMING, Z. & ZHIHONG, F. 2015. Model-based durability design of concrete structures in Hong Kong–Zhuhai–Macau sea link project. *Structural Safety*, 53, 1-12.
- RAMEZANIANPOUR, A. A., KAZEMIAN, A., MOGHADDAM, M. A., MOODI, F. & RAMEZANIANPOUR, A. M. 2015. Studying effects of low-reactivity GGBFS on chloride resistance of conventional and high strength concretes. *Materials and Structures*, 1-13.
- RAMLOCHAN, T., THOMAS, M. & GRUBER, K. A. 2000. The effect of Metakaolin on alkali-silica reaction in concrete. *Cement and Concrete Research*, 30, 339-344.
- SHAMSAD, A., ABUL KALAM, A. & KEVIN, F. L. 2012. Effect of the Key Mixture Parameters on Tortuosity and Permeability of Concrete. *Journal of Advanced Concrete Technology*, 10 86-94.
- SUDRET, B. 2008. Probabilistic models for the extent of damage in degrading reinforced concrete structures. *Reliability Engineering and System Safety*, 93, 410-422.
- TAKEWAKA, K. & MATSUMOTO, S. Quality and cover thickness of concrete based on the estimation of chloride penetration in marine environments. *In: MALHOTRA, V. M., ed. 2nd International Conference of Concrete in Marine Environment*, 1988. ACI, 381-400.
- TANG, L. & NILSSON, L. 1992. Chloride diffusivity in high strength concrete at different ages. *Nordic Concrete Research, Nordic Concrete Federation*, Nordic Concrete Research, Nordic Concrete Federation, 162-171.
- THOMAS, M. D. A. & BAMFORTH, P. B. 1999. Modelling chloride diffusion in concrete: effect of fly ash and slag. *Cem Concr Res*, 29, 487–95.
- TUUTTI, K. 1982. Corrosion of steel in concrete. *Research Report, Swedish Cement and Concrete Research Institute, Stockholm, Sweden*.
- VEDALAKSHMI, R., DEVI, R., EMMANUEL, B. & PALANISWAMY, N. 2008. Determination of diffusion coefficient of chloride in concrete: an electrochemical impedance spectroscopic approach. *Materials and Structures* 41 1315–1326.

- WILD, S., KHATIB, J. M. & JONES, A. 1996. Relative strength, pozzolanic activity and cement hydration in superplasticised metakaolin concrete. *Cement and Concrete Research*, 26, 1537–1544.
- WONG, S. M., HOBBS, R. E. & ONOF, C. 2005. An adaptive response surface method for reliability analysis of structures with multiple loading sequences. *Structure safety*, 27, 287-308.
- XUEMEI, L., HONGJIAN, D. & MIN-HONG, Z. 2015. A model to estimate the durability performance of both normal and light-weight concrete. *construction and Building Materials*, 80, 255-261.
- YOUNG, J. F. 1988. Review of the Pore Structure of Cement Paste and Concrete and its Influence on Permeability. *American Concrete Institute SP-108*, 1-18.

7. Use of eXtended FEM and statistical analysis for modelling the corrosion-induced cracking in reinforced concrete containing metakaolin

7.1 Abstract

This study presents an improved modelling to predict the time for corrosion-induced cracking in concrete containing metakaolin (MK) based on combining eXtended finite element model (XFEM) and statistical analysis. The prediction model was developed based on the percentage of MK in the mixture, binder content, water-to-binder (W/B) ratio, and concrete cover thickness. The developed model was also validated experimentally using an accelerated corrosion test. Moreover, design charts were developed in this study using statistical analysis to facilitate and simplify the use of the prediction model. The results indicated that the corrosion pressure required to crack the concrete cover increased with higher percentages of MK, higher binder content, and/or lower W/B ratio. The most significant factors affecting the time for corrosion-induced cracking was found to be the concrete cover, W/B ratio, MK replacement, and binder content, respectively, in order of significance. The results also indicated that the time required for corrosion-induced cracking obtained from the developed prediction model showed a good agreement with the experimental results of the accelerated corrosion samples. Also, the cracks predicted by the XFEM showed a similar trend of variation with that found in the accelerated corrosion samples.

7.2 Introduction

Corrosion models are mostly conducted by estimating two main periods: initiation and propagation (Tuutti, 1982). The initiation period is the time taken for chlorides to diffuse through the exterior surface and buildup at the steel bar surface in adequate amount (threshold) until it breaks down the steel bar protective passive layer and initiates corrosion (Mehta and Monteiro, 1993). The propagation period starts after the initiation period and ends with the appearance of the first crack. As defined by the American Concrete Institute (American Concrete Institute (ACI) Committee 222, 1975), the propagation period is the time needed for adequate corrosion to occur and cause an unacceptable level of damage to the reinforced concrete structure. The corrosion rate is not the main aspect affecting the duration of the propagation period but also by the interpretation of “unacceptable damage”. This unacceptable damage differs according to the requirements of the shareholder and the classification of the concrete structure. There are two approaches defining the acceptable damage. The first approach defines the damage based on the formation of first hair crack (Liu and Weyers, 1998, Torres-Acosta and Martinez-Madrid, 2003), while the other approach defines it based on the formation of a 0.3-mm crack (Andrade et al., 1993).

The use of supplementary cementitious materials (SCMs) such as fly ash, silica fume, and/or metakaolin (MK) in concrete mixtures has been proven to improve the overall service lifetime of concrete structures. MK has been widely used for the production of high-strength and high-performance concrete over the past two decades (Zeljkovic, 2009). Replacing cement with MK decreases the average pore size of cement paste and increases the concrete resistance to chemical attack and chloride permeability (Badogiannis and

Tsivilis, 2009, Duan et al., 2013). Batis et al. evaluated the chemical resistance of mortars samples submerged in 3.5% NaCl solution and found an enhancement in corrosion resistance when MK was added (Batis et al., 2004). Previous studies have indicated that increasing the percentage of MK up to 20% increases the concrete durability and chloride resistivity while using more than 20% either did not show further enhancement or slightly reduced the concrete durability (Bonakdar et al., 2005a, Sabir et al., 2001b, Justice et al., 2005b, Gruber et al., 2001b, Poon et al., 2006, Hassan et al., 2012a).

Most of the current corrosion detection methods depend on the propagation period by modelling the pressure resulting from growing the corrosion products around the steel bar (Liu and Weyers, 1998, Chernin and Val, 2011, Lu et al., 2011, Castoreña et al., 2008). This period is affected by many factors such as concrete cover thickness, availability of oxygen, concrete moisture content, steel bar size, type of structure, and environment of exposure (Hooton and McGrath, 1995, Browne, 1982, Hansson and Sørensen, 1990). The propagation period is usually modeled using either numerical or analytical method. The model in the numerical method (finite element) accounts for the geometry of the concrete member (Jang and Oh, 2010, Du et al., 2006). On the other hand, a thick-wall cylinder approach (Liu and Weyers, 1998, El Maaddawy and Soudki, 2007) is used in the analytical method. The concrete around the rebar in this method is modeled as a hollow concrete cylinder with a thickness equal on all sides to the concrete cover (**Figure 7.1**). The models assume that the cracks occur in the hollow concrete cylinder independently of the geometry of the concrete member.

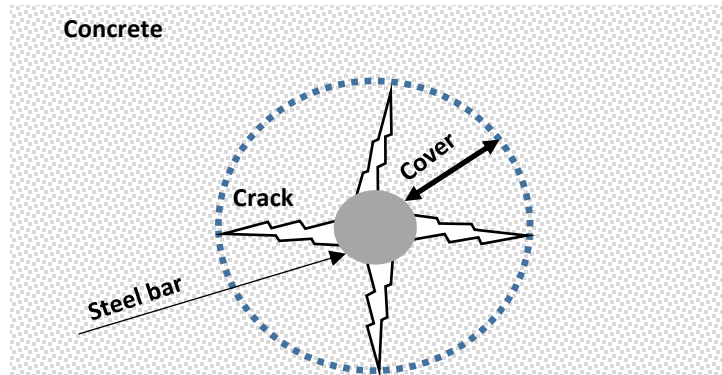


Figure 7.1 Crack modeling using a thick-wall cylinder approach

The extended finite element method (XFEM) was developed by Belytschko and Black (Belytschko and Black, 1999). This method has emerged as a powerful numerical procedure for analyzing crack propagation problems (Zhang and Bui, 2015, Unger et al., 2007). XFEM offers substantial advantages in the modelling of crack propagation compared to the conventional finite element. One of the main advantages of using XFEM is that there is no need to track the crack path with a new mesh, where the geometry of the discontinuities (crack) does not need to match the mesh (Simulia, 2013, Belytschko et al., 2009). Over the past few years, XFEM crack propagation modelling has been widely utilized in many fields for 2D and 3D problems (Pietruszczak and Haghghat, 2014, Möes et al., 2002, Sukumar et al., 2000). However, the application of XFEM for modelling reinforced concrete members is still very limited.

The statistical design technique is an effective tool in civil engineering fields (Bayramov et al., 2004b, Wong et al., 2005, Chen et al., 2010, Kang et al., 2010). There are several models used for modelling and optimizing concrete mixtures using statistical design technique (Sonebi, 2004, Soudki et al., 2001, Akalin et al., 2010, Nehdi and Summer, 2002,

Rougeron and P.C. Aitcin, 1994, Khayet et al., 2011, Al-Alaily and Hassan, 2016b). Statistical analysis includes the procedures of analysis of variance (ANOVA) for testing statistical significance of parameters and regression analysis for developing prediction models. Statistical models can be developed to predict the properties of concrete at different levels of the mixture variables and optimize the responses. It can also be used to understand the interactions between the parameters used and evaluate their relative significance, even in the presence of complex interactions (Montgomery 2012).

Limited research has been conducted to predict the corrosion-induced cracking in concrete containing MK, especially when the effect of mixture proportions (percentage of MK, binder content, and W/B ratio) was included. The main objective of this study was to estimate the corrosion-induced cracking period (propagation period) by combining XFEM modelling and statistical analysis. The significance of each of the MK replacement, binder content, and W/B ratio on the corrosion-induced cracking time was studied and analyzed. The developed prediction model was also verified experimentally in this investigation using accelerated corrosion testing for validation.

7.3 Research significance

Only a limited number of studies deal with the prediction of corrosion-induced cracking in concrete containing MK. Moreover, limited research has been undertaken that uses XFEM for modelling corrosion-induced cracking. The main objective of this investigation was to develop an enhanced corrosion-induced cracking prediction model for concrete containing MK using a combination of XFEM and statistical analysis. The developed model took into account the effects of the percentage of MK, binder content, W/B ratio, and concrete cover

thickness on the time for corrosion-induced cracking. The paper exclusively developed corrosion pressure prediction charts based on the developed model to help designers optimize their concrete mixtures and concrete covers. The authors believe that this investigation will enhance existing reinforcement corrosion prediction models and help designers/researchers to more accurately estimate the corrosion-induced cracking period for concrete containing MK.

7.4 Corrosion-induced cracking prediction approach

The numerical model used to simulate the damage and cracking in concrete cover based on a uniform corrosion is presented in the El maadawy model (**Eq.7.1**) (El Maaddawy and Soudki, 2007). This model was developed to estimate the time from the end of the corrosion initiation period to the appearance of the first crack (propagation period). The model is based on combining the thick-wall cylinder theory and Faraday's law, where Faraday's law has been taken by numerous researchers to estimate the weight loss of steel at different applied current density levels (Liu and Weyers, 1998, El Maaddawy and Soudki, 2007) and thick-wall cylinder theory has been used to calculate the radial pressure required to crack the concrete cover (Bazant, 1979).

$$T_{cr} = \left[\frac{7117.5 (D+\delta_0)(1+\nu+\psi)}{i E_{ef}} \right] + \left[P_{cr} + \frac{2\delta_0 E_{ef}}{(1+\nu+\psi)(D+2\delta_0)} \right] \quad (\text{Eq.7.1})$$

Where T_{cr} is the time to crack; D is the bar diameter in mm, $\psi = D'^2/2C (C + D')$ where C is concrete cover and $D' = D + 2 \delta_0$, δ_0 is the thickness of the porous zone, which is typically in the range of 10–20 μm (El Maaddawy and Soudki, 2007); E_{ef} is the effective elastic modulus of concrete which is equal to $[Ec/(1 + \phi_{cr})]$, where Ec is the elastic modulus of

concrete and ϕ_{cr} is the concrete creep coefficient (2.35 as per the CSA Standard A23.3-94 (Standard CSA, 1994)); ν is the Poisson's ratio of concrete (0.18); P_{cr} is the radial pressure required to crack the concrete cover; and i is the corrosion rate in mA/cm².

The El maadawy model simulates the expansion of corrosion products with the associated damage and cracking in concrete cover using thick-wall cylinder theory, in which the radial pressure required to crack the concrete cover P_{cr} is calculated as per **equation 7.2**:

$$P_{cr} = \frac{2Cf_{ct}}{D} \quad (\text{Eq.7.2})$$

Where C is the concrete cover, f_{ct} is the tensile strength, and D is the bar diameter.

In this investigation, a new radial pressure P_{cr} was developed based on XFEM and statistical analysis method. The new developed P_{cr} with the actual E_{ef} of concrete were substituted in equation 1 to calculate the corrosion-induced cracking time, which is the time from the end of the corrosion initiation period to the appearance of the first crack (corrosion propagation period).

7.5 Scope of work

The main objective of this study was to predict the time for corrosion-induced cracking for concrete containing MK. To calculate this time, the process of corrosion product expansion was first modeled using XFEM to predict the pressure required to crack the concrete section, P_{cr} . Statistical analysis was then applied to simplify the process by developing an equation to calculate P_{cr} based on the W/B ratio (0.3–0.5), percentage of MK (0%–25%), binder content (350 kg/m³–600 kg/m³) and concrete cover (20 mm–60 mm). Design charts were also developed to facilitate and simplify the use of the statistical analysis equation.

Finally, the developed model was tested experimentally using an accelerated corrosion test for validation.

7.5.1 XFEM description

The XFEM model is based on simulating the expansion pressure from the corrosion product by applying a uniform pressure load on a hollow concrete section. A two-dimensional model of the hollow concrete section was developed using ABAQUS software. The model geometry was drawn according to the concrete cover (20 mm, 40 mm, and 60 mm) using CPS4R element (**Figure 7.2a**) with a hollow section of 20 mm diameter representing the steel bar. The CPS4R element is used for two-dimension plane stress section modelling with 4-node bilinear, reduced integration, and hourglass control (Simulia, 2013). As shown in **Figure 7.2b**, the top side of the concrete model was taken as a fixed boundary condition (BC) while the other three sides were free BC. The top side BC for the model was taken five times farther away from the concrete cover to be sufficiently remote from the corrosion area such that there is negligible effect on the corrosion expansion process according to St. Venant's principle. The elements meshing aspect ratio were kept as constant as possible with a ratio of one. The concrete fracture energy, Poisson's ratio, tensile strength, compressive strength, and modulus of elasticity were inputs in the developed XFEM. Poisson's ratio was taken as 0.18 and the fracture energy was calculated based on the CEB-FIP model (Telford, 1993) (equation 3). On the other hand, the tensile strength, compressive strength, and modulus of elasticity were calculated based on equations developed previously by the authors (Al-alaily and Hassan, 2016a) for similar concrete types (as seen in **Table 7.1**). The mechanical properties in **Table 7.1** were based on the

W/B ratio (0.3–0.5), percentage of MK (0%–25%), and binder content (350 kg/m³–600 kg/m³). After developing the model, an internal pressure was applied to the hollow section representing the corrosion expansion of the steel bar.

$$G = G_{fo} \left(\frac{f_{cm}}{f_{cmo}} \right)^{0.7} \quad \text{(Eq.7.3)}$$

Where $f_{cmo} = 10$ MPa; and G_{fo} is interpolated depending on the maximum aggregate size, while f_{cm} is the mean compressive strength of concrete (Telford, 1993).

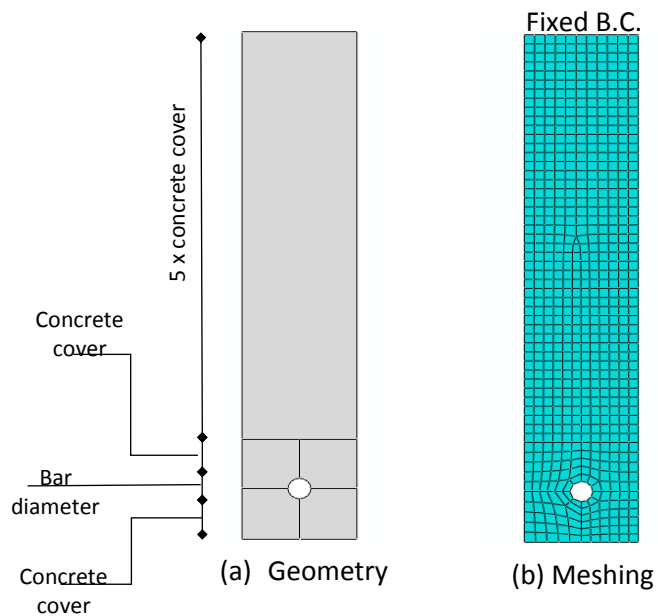


Figure 7.2 XFEM model

Table 7.1 Mechanical properties equations

	f_c	STS	MOE	Model factors
A	-530.44	-58.25	-812.53	Intercept
B	-2.16	-0.55	-1.99	A-Binder
C	7195.03	1176.46	9093.53	B-W/B
D	3.04	-0.97	9.1	C-MK%
E	-2.93	-0.83	-2.91	AB
F	-0.01	0	-0.02	AC
G	8.76	3.77	-9.51	BC
H	0.01	0	0.01	A ²
I	-16942.5	-2572.68	-21557.93	B ²
J	-0.16	0	-0.06	C ²
K	0	0	0	ABC
L	0	0	0	A ² B
M	0	0	0	A ² C
N	2.77	1	3.49	AB ²
O	0	0	0	AC ²
P	-19.16	-5.31	2.77	B ² C
Q	0.25	0.01	0.21	BC ²
R	0	0	0	A ³
S	13071.45	1815.13	16474.44	B ³
T	0	0	0	C ³

$$Y(\text{response}) = A + B * \text{Binder} + C * \text{W/B} + D * \text{MK\%} + E * \text{Binder} * \text{W/B} + F * \text{Binder} * \text{MK\%} + G * \text{W/B} * \text{MK\%} + H * \text{Binder}^2 + I * \text{W/B}^2 + J * \text{MK\%}^2 + K * \text{Binder} * \text{W/B} * \text{MK\%} + L * \text{Binder}^2 * \text{W/B} + M * \text{Binder}^2 * \text{MK\%} + N * \text{Binder} * \text{W/B}^2 + O * \text{Binder} * \text{MK\%}^2 + P * \text{Binder} * \text{MK\%}^2 + Q * \text{W/B} * \text{MK\%}^2 + R * \text{Binder}^3 + S * \text{W/B}^3 + T * \text{MK\%}^3$$

7.5.2 Statistical analysis and time-to-crack model enhancement

In this study, statistical analysis was applied to develop an equation to predict the pressure required to crack the concrete section of MK mixtures with different concrete covers and different mixture proportions. Statistical analysis was also applied to show the most significant factors affecting the pressure required to crack the concrete sections. The developed model had four independent factors, X_1 , X_2 , X_3 , and X_4 , which represent W/B ratio, total binder content, percentage of MK, and concrete cover, respectively (**Table 7.2**). Based on the selected points of the statistical analysis method, 29 concrete mixtures were selected (as seen in **Table 7.3**). For each selected mixture in **Table 7.3**, and for each concrete cover (20 mm, 40 mm, and 60 mm), the cracking pressure was found using XFEM

and recorded in the table. Statistical analysis was then conducted using the data in **Table 7.3**, and the cracking pressure (P_{cr}) prediction equation was developed. Finally, the time required for corrosion-induced cracking was calculated using the El maadawy equation (equation 1) after substituting equation 2 with the equation developed from the statistical analysis and substituting the modulus of elasticity with the modulus of elasticity found in **Table 7.1**.

Table 7.2 Parameter values used in analysis

Variable		Level		
		-1	0	1
W/B	X1	350	475	600
Binder (kg/m ³)	X2	0.3	0.4	0.5
MK%	X3	0	12.5	25
cover (mm)	X4	20	40	60

Table 7.3 Statistical analysis mixture proportions

Mixture	W/B	Binder (kg/m ³)	MK%	Cover (mm)	P _{cr} _{XFEM}
1	0.5	475	12.5	20	5
2	0.4	350	0	40	12
3	0.4	475	12.5	40	15
4	0.4	350	12.5	60	30
5	0.4	475	0	60	9
6	0.4	475	0	20	4
7	0.4	350	12.5	20	10
8	0.4	600	0	40	8
9	0.4	475	12.5	40	15
10	0.3	475	25	40	28
11	0.4	600	12.5	60	17
12	0.4	600	25	40	17
13	0.3	350	12.5	40	20
14	0.5	600	12.5	40	7
15	0.5	475	25	40	15
16	0.4	475	12.5	40	15
17	0.5	475	12.5	60	12
18	0.3	475	0	40	15
19	0.4	475	12.5	40	15
20	0.4	475	25	20	11
21	0.3	475	12.5	60	31
22	0.3	600	12.5	40	28
23	0.5	475	0	40	5
24	0.4	475	12.5	40	16
25	0.4	350	25	40	26
26	0.3	475	12.5	20	12
27	0.4	475	25	60	32
28	0.4	600	12.5	20	6
29	0.5	350	12.5	40	13

7.6 Model validation experimental program

Twelve concrete prisms were tested under an accelerated corrosion test to validate the developed model. The twelve prisms were made from four concrete mixtures with four percentages of MK (0%, 6.5%, 12.5%, and 20%). Each concrete mixture had three prisms with three concrete covers (20 mm, 30 mm, and 40 mm). The corrosion-induced cracking time (propagation period) at the appearance of the first crack on the sample's surface was recorded for all tested samples.

7.7 Materials

The tested mixtures were prepared with type GU-Portland cement with a specific gravity of 3.15. Metakaolin with a specific gravity of 2.56 was used as SCMs (**Table 7.4**). The fine and coarse aggregate both had a specific gravity of 2.6 and water absorption of 1%. **Table 7.5** show the sieve analysis that was conducted for both natural sand (fine aggregate) and 10-mm stone (coarse aggregate). ASTM type F superplasticizer was used to adjust the slump. This superplasticizer had a specific gravity of 1.2, volatile weight of 62% and pH of 9.5.

Table 7.4 Chemical and physical properties of cement

Chemical properties %	Cement	MK
SiO ₂	19.64	51-53
Al ₂ O ₃	5.48	42-44
Fe ₂ O ₃	2.38	<2.2
FeO	-	-
TiO ₂	-	<3
C	-	-
P ₂ O ₅	-	<0.2
SO ₄	-	<0.5
CaO	62.44	<0.2
MgO	2.48	<0.1
Na ₂ O	-	<0.05
C ₃ S	52.34	-
C ₂ S	16.83	-
C ₃ A	10.5	-
C ₄ AF	7.24	-
K ₂ O	-	<0.4
Loss on ignition	2.05	<0.5
Physical properties		
Specific density	3.15	2.56
Colour	gray	pink
Grain size (µm)	45	60
Surface area (m ² /kg)	320-400	650-1250
Blaine fineness (m ² /kg)	410	19000

Table 7.5 Aggregate sieve analysis

Sieve size (mm)	20-mm coarse aggregate (% passing)	Sieve size	10-mm coarse aggregate (% passing)	Sieve size	Fine aggregate passing (% passing)
28	100	14	100	10	100
20	65.1	10	95.8	5	99.4
14	64.6	5	21	2.5	79.4
10	34.4	2.5	2.9	1.25	55.4
5	3.8	1.25	0	0.63	35.2
2.5	1.4	0.63	-	0.32	18.6
1.25	-	0.32	-	0.16	7.3
0.63	-	0.16	-	0.08	2.2

7.8 Samples details

All tested specimens were 250 mm in length and had one 20M steel bar embedded in the center. The cross-sectional dimensions and the lengths of the bars were varied to maintain the required concrete cover for each specimen (**Figure 7.3**). The embedded bar was placed at the center of each sample to ensure equal cover in all directions (**Figure 7.3**). Two wires were attached to the embedded bar; one was connected to the power supply and the second was a spare wire in case the first wire's connection was damaged during concrete pouring. The second wire was also used to read the resistance between the two wires (after pouring the concrete) in order to confirm the connectivity of the main wire with the embedded bar. The specimens were designated according to their concrete cover (20 mm, 30 mm, or 40 mm) and MK percentage. For example, a specimen with a concrete cover of 20 mm and an MK replacement of 20% was designated as 20MK20.

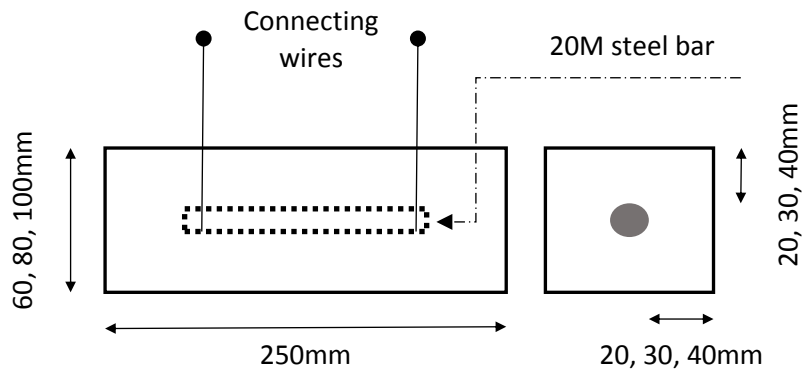


Figure 7.3 Test specimen details

7.9 Testing procedure

The accelerated corrosion test setup consisted of a tank, electrolyte solution (5% NaCl by the weight of water), and a stainless steel mesh placed at the bottom of the tank (**Figure 7.4**) (Hassan et al., 2009b, Hassan et al., 2012a). The twelve concrete prisms were placed at the bottom of the tank over the stainless steel mesh and fully submerged in the electrolyte solution. The concrete prisms were connected to a 12V power supply, where the stainless steel mesh served as a cathode while the embedded steel bar in each sample served as an anode. The propagation period was monitored by the appearance of the first visual crack on the surface of the specimen. The crack widths in each sample were monitored using a graduated scale microscope with 0.002-mm increments.

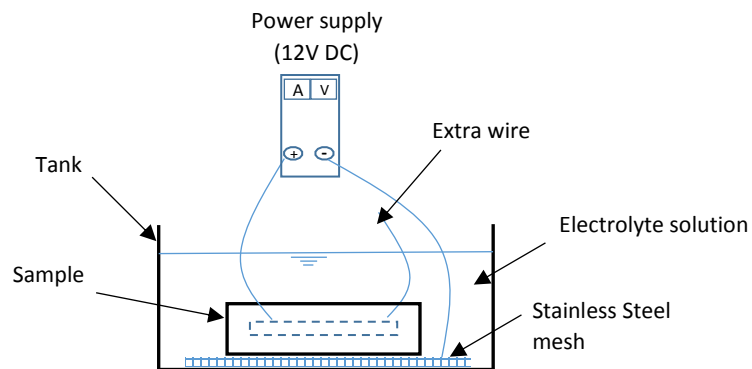


Figure 7.4 Accelerated corrosion schematic diagram

7.10 Results and discussion

7.10.1 Comparison between XFEM results and thick-wall theory

All XFEM results obtained from the developed model were compared with the results predicted by the thick-wall theory mathematical model. As seen in **Table 7.6**, the variation between the crack pressures calculated by XFEM ($P_{cr\ XFEM}$) and those calculated using thick-wall theory ($P_{cr\ thick\ wall}$) was acceptable. The highest variation of 25% difference was seen in mixture 25, while the minimum difference of 0.5% was seen in mixture 6. As the concrete cover over the bar increased, the ratio of $P_{cr\ XFEM}/P_{cr\ thick\ wall}$ decreased. **Table 7.6** shows that the average ratios of $P_{cr\ XFEM}/P_{cr\ thick\ wall}$ for 20-mm, 40-mm, and 60-mm concrete covers were 0.89, 0.87, and 0.78, respectively. This may be attributed to the fact that in the thick-wall theory, the nonlinear behavior of the concrete cover is assumed to behave in an elastic-perfectly plastic manner, which is a simplification of the actual behavior of concrete in tension. Hence, once the tensile stresses in the concrete cover reach the maximum tensile stresses, the behavior is assumed to be plastic until the cover is fully cracked. In the current XFEM analysis, a tension-softening model was adopted to represent the concrete behavior in tension. This is a more realistic representation of the actual concrete behavior. As a result of the difference in the concrete behavior modelling assumptions, the XFEM predictions of the cracking loads showed lower values compared to thick-wall theory, and this difference became more pronounced in higher concrete cover. The results of the XFEM analysis revealed that values of $P_{cr\ XFEM}$ increased as the ratio of C/D increased, as shown in **Figure 7.5**. This trend is in good agreement with the results of the finite element simulations by Chernin and Val (Chernin and Val, 2011).

Table 7.6 XFEM results for internal pressure

Mixture	P_{cr}	$P_{cr\ thick}$	$P_{cr\ XFEM}/P_{cr\ thick\ wall}$
1	5	5.265	0.950
2	12	14.183	0.846
3	15	17.847	0.840
4	30	36.219	0.828
5	9	12.056	0.747
6	4	4.019	0.995
7	10	12.073	0.828
8	8	8.867	0.902
9	15	17.847	0.840
10	28	32.336	0.866
11	17	20.989	0.810
12	17	19.711	0.862
13	20	24.305	0.823
14	7	7.683	0.911
15	15	17.031	0.881
16	15	17.847	0.840
17	12	15.795	0.760
18	15	17.985	0.834
19	15	17.847	0.840
20	11	13.367	0.823
21	31	39.566	0.783
22	28	31.538	0.888
23	5	4.616	1.083
24	16	17.847	0.896
25	26	31.671	0.821
26	12	13.189	0.910
27	32	40.102	0.798
28	6	6.996	0.858
29	13	15.177	0.857

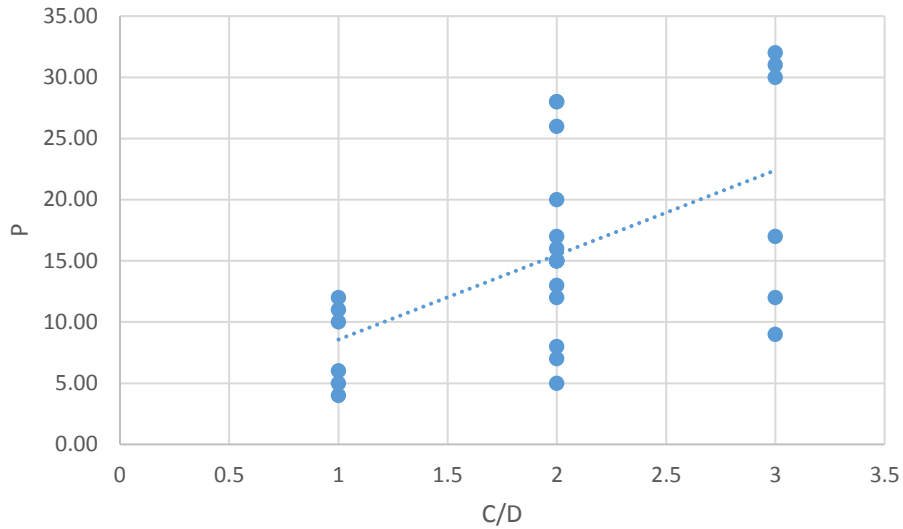


Figure 7.5 Relation between C/D to PcrXFEM

7.10.2 XFEM crack prediction

The accumulated corrosion products apply radial stresses on the concrete cover, and can be modeled as a uniform pressure load acting on a concrete ring. The radius of the concrete ring is taken as the thinnest of the concrete cover around the steel bar (Balafas and Burgoyne, 2010). This concrete ring has the shortest crack path from the steel bar to the concrete surface (Bazant, 1979). The XFEM formulation was used to calculate the pressure required to crack the concrete cover with an explicit-implicit crack description used in this study, where the enriched approximation of the displacements is given in **equation 7.4**.

$$u = \sum_{l=1}^N N_l(x) [u_l + H(x)a_l + \sum_{\alpha}^4 F_{\alpha}(x)b_l^{\alpha}] \quad (\mathbf{Eq.7.4})$$

The first part on the right-hand side describes the conventional FEM approximation with continuous shape functions $N_i(x)$ and nodal displacement u_i . The middle part accounts for the discontinuity in the displacement field across the crack path by incorporating the

discontinuity jump function $H(x)$ with additional nodal enriched degree of freedom vector a_I . The last part represents elastic asymptotic crack-tip functions $F_\alpha(x)$ and nodal enriched degree of freedom vector b_I^α .

The crack initiation starts by the degradation of the cohesive response at the enriched element, which is the stresses or the strains reaching a specified cracking initiation criteria (Simulia, 2013). In this study, the maximum principal stress criterion that was used to model the crack initiation was the tensile stress (f_t). Once the maximum principal stress is reached, the enrichment functions, which consist of the near-tip asymptotic functions, capture the singularity around the crack tip, and then the discontinuous function represents the jump in displacement across the crack surfaces. **Figure 7.6** shows an example of a concrete sample modeled using XFEM with a tensile strength of 3.8 Mpa. **Figure 7.6a** shows the hollow section when no load was applied. In **Figure 7.6b** the load was applied on the hollow section, and the principle stress reached 3.8 Mpa where the cracks started to initiate, reaching the cracking criteria. As the load increases, the stresses increase and the crack propagates until it reaches the concrete surface (**Figure 7.6c, d**).

Following the XFEM formulation, several obvious crack paths can be found (**Figure 7.6**), indicating possible crack propagations for the reinforced concrete sample under corrosion. On the other hand, in all specimens of the accelerated corrosion test, one main crack, which was found extended to the concrete surface, in addition to some secondary cracks, appeared after cutting the prism into slices. The main crack propagates following the shortest path to the concrete surface (**Figure 7.7**). In general, it was observed that the crack patterns agree

well with the expectation in **Figure 7.8**, which verifies the accuracy and practicability of the proposed simulation methodology.

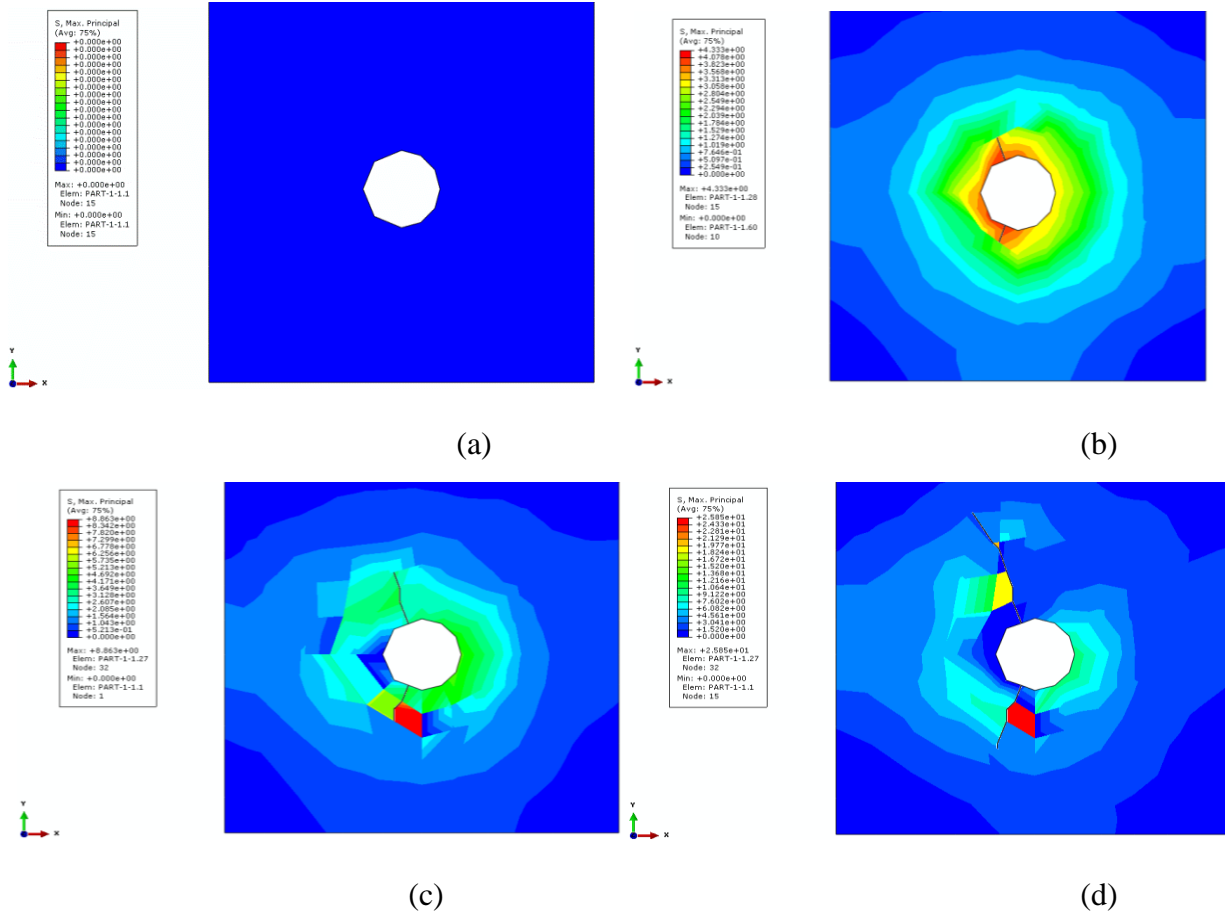


Figure 7.6 XFEM cracks propagation reaching concrete surface (principal stresses)



Figure 7.7 Propagation period surface crack

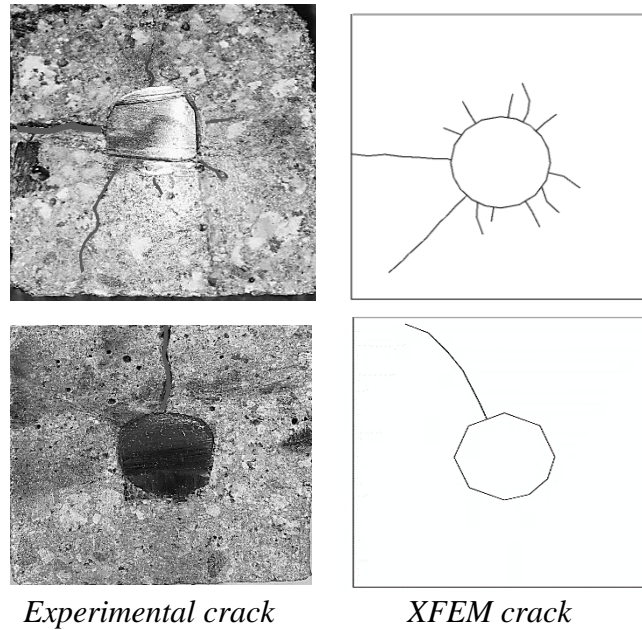


Figure 7.8 Samples of crack pattern from experiment and XFEM

7.10.3 Statistical analysis and most significant factor affecting cracks

An ANOVA analysis was completed for the radial corrosion pressure, P_{cr} , calculated for the 29 mixtures found in **Table 7.3**. The most significant factors affecting the internal corrosion pressure were found to be X4 (cover), X1 (W/B), X3 (MK), and X2 (binder), in order of significance (**Table 7.7**). In addition, the developed equation (equation 5) showed R^2 value of 0.95.

$$(P_{cr}) = -62.74943 + 136.33333 * X1 + 0.1360 * X2 + 0.48667 * X3 + 1.13000 * X4 - 0.28000 * X1 * X2 - 0.60000 * X1 * X3 - 1.50000 * X1 * X4 - 8.00000E-004 * X2 * X3 - 8.00000E-004 * X2 * X4 + 0.016000 * X3 * X4 \quad (\text{Eq7.5})$$

Table 7.7 ANOVA results

Factor	F-value	p-value
X1(w/b)	103.93	< 0.0001
X2(binder)	12.78	0.0022
X3(MK%)	101.24	< 0.0001
X4(cover)	123.68	< 0.0001

Based on the equations developed from the statistical analysis (**equation 7.5**), a set of charts was plotted. In all charts, the x-axis represents the W/B ratio varied from 0.3 to 0.5, and the y-axis represents the percentage of MK varied from 0% to 25%. Each set of charts is plotted for a specific concrete cover (20 mm, 40 mm, and 60 mm) based on five binder content levels (350 kg/m³, 412.5 kg/m³, 475 kg/m³, 537.5 kg/m³, and 600 kg/m³) (**Figs.7. 9, 10, and 11**). These charts represent a simplified method of predicting the radial corrosion pressure required to crack concrete cover for concrete containing MK. The following example demonstrates how to use the developed charts to predict the cracking pressure of a mixture with a 30-mm concrete cover, 0.45 W/B ratio, 600 kg/m³ binder content, and 12.5% MK replacement.

Steps of design

- vi. Select 30-mm concrete cover charts (**Figure 7.10**)
- vii. Select the chart with 600 kg/m³ binder content
- viii. X-axis represents the W/B ratio (0.45)
- ix. Y-axis represents the percentage of MK (12.5%)
- x. The point of intersection on the contour represents the pressure required to crack
- xi.
- xii. the concrete cover (13Mpa)

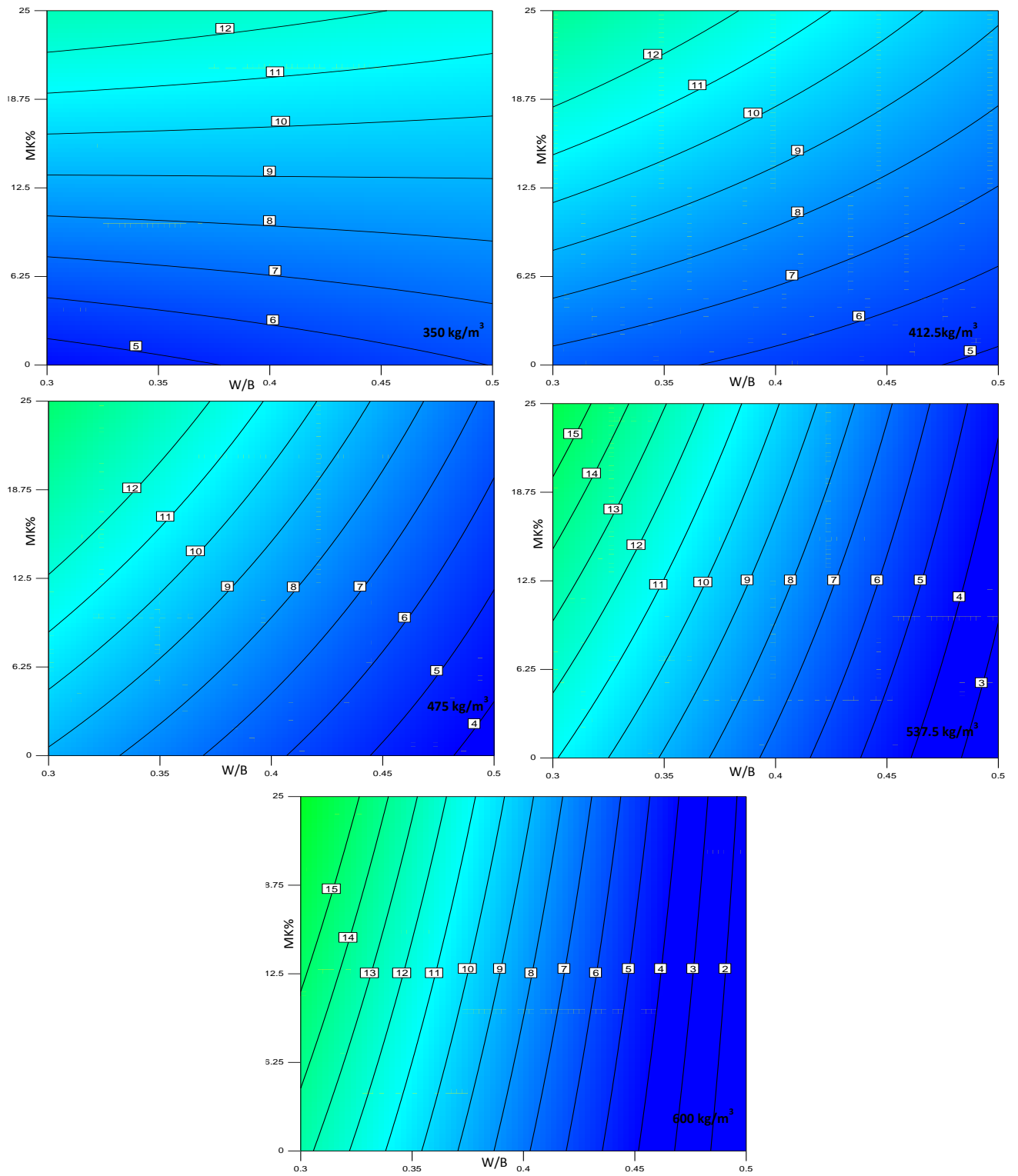


Figure 7.9 Corrosion cracking pressure for 20-mm cover

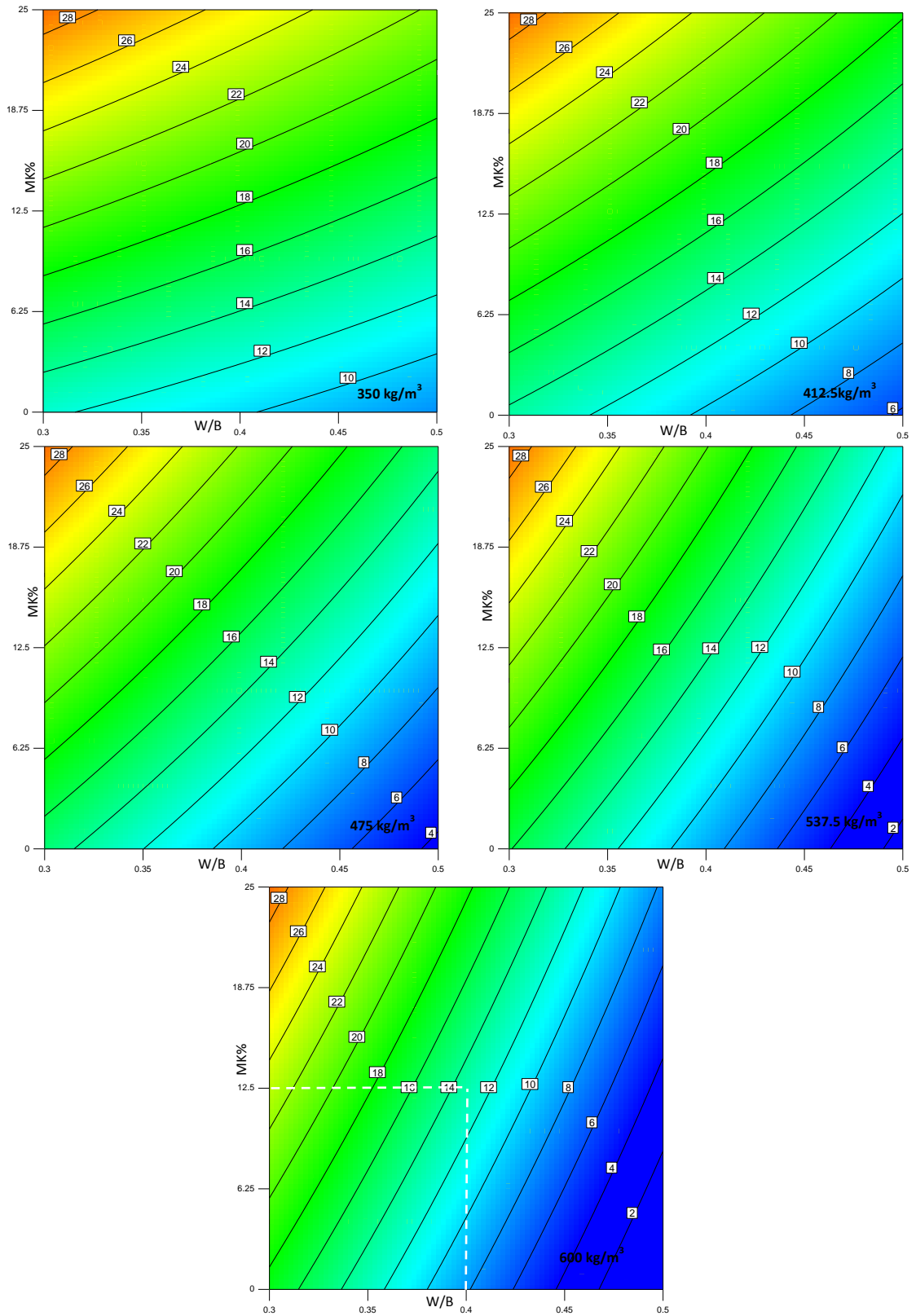


Figure 7.10 Corrosion cracking pressure for 30-mm cover

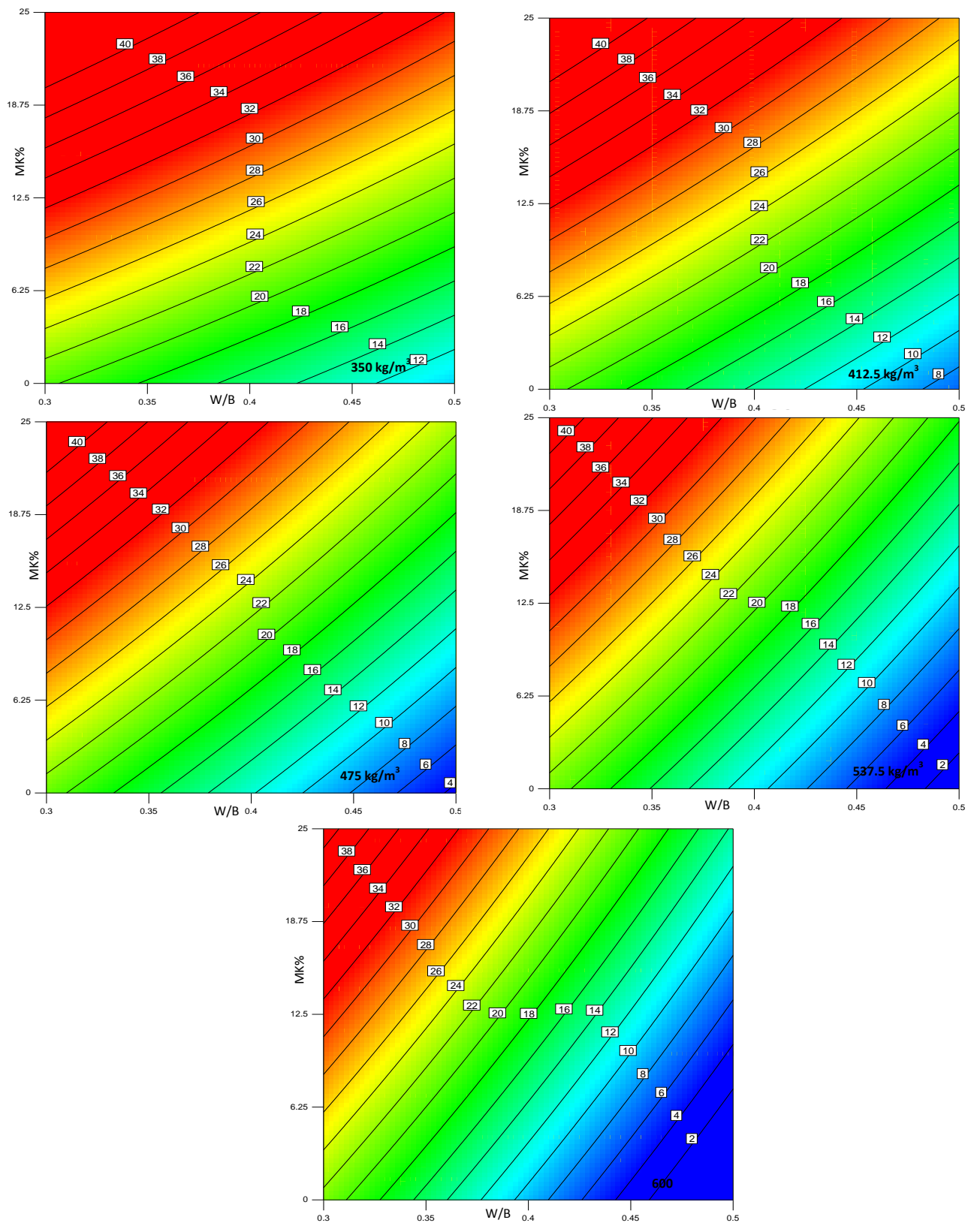


Figure 7.11 Corrosion cracking pressure for 40-mm cover

7.10.4 Model validation

The model introduced in this investigation replaces the internal pressure P_{cr} in the El maadawy model (Eq. 7.2) by the pressure developed in this investigation (Eq. 7.3). The results of the time to corrosion-induced crack period obtained from the experiments were found to agree with the results predicted by the developed model (Figure 7.12), where the upper and lower difference between the predicted and actual times was between $\pm 8\%$. The model was found to underestimate the time to corrosion-induced cracking for concrete with high percentages of MK and overestimate it for concrete with low percentages of MK. This could be due to the high density of concrete with high percentages of MK, which may actually require higher pressure to crack the concrete cover compared to concrete with low percentages of MK. However, further investigation is required to account for the corrosion rate for concrete containing MK.

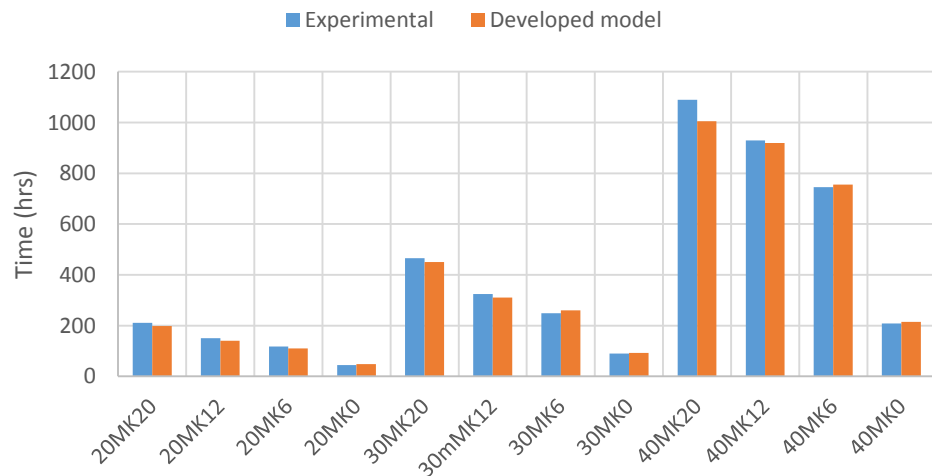


Figure 7.12 Time to corrosion-induced cracking experimental vs. developed model

7.11 Conclusion

From the results described in this paper, the following conclusions can be drawn:

- The developed model for concrete containing MK, with different mixture proportions and concrete covers, was found to be suitable for predicting the corrosion-induced cracking time. The results of the tested samples obtained from the accelerated corrosion test were in agreement with the results obtained from the developed model.
- Good correlation was found between the XFEM and the experimental results in terms of crack propagation pattern. Both the XFEM prediction and tested samples showed similar crack paths. Good correlation was also found between the XFEM and thick-wall theory in terms of internal pressure, especially in small cover/diameter ratio.
- The most significant factors affecting the time to corrosion-induced cracking in concrete containing MK was found to be the concrete cover, percentage of MK, W/B ratio, and binder content, respectively, in order of significance.
- The developed model confirmed that the corrosion-induced cracking time increased with higher binder content, higher percentage of MK, and/or with lower W/B ratio. Based on the tested parameters in this investigation, mixtures with 20% MK, 0.3 W/B ratio, and/or 600 kg/m³ showed the longest corrosion-induced cracking time.
- The developed chart in this investigation provided an easy and fast way to calculate the pressure required to crack the cover for concrete containing MK with different mixture proportions and concrete covers. These charts can be used

effectively and easily, instead of using long equations, to facilitate the prediction of corrosion-induced cracking time.

7.12 Reference

- AKALIN, O., ULAS, A. K. & BAHAR, S. 2010. Self-consolidating high-strength concrete optimization by mixture design method. *ACI Materials Journal*, 107, 357–364.
- AL-ALAILY, H. S. & HASSAN, A. A. A. 2016a. Refined statistical modeling for chloride permeability and strength of concrete containing metakaolin. *Construction and Building Materials*, 114, 564–579.
- AL-ALAILY, H. S. & HASSAN, A. A. A. 2016b. Time-Dependence of Chloride Diffusion for Concrete Containing Metakaolin. *Journal of Building Engineering* 7, 159–169.
- AMERICAN CONCRETE INSTITUTE (ACI) COMMITTEE 222 1975. Corrosion of metals in concrete. American Concrete Institute.
- ANDRADE, C., ALONSO, C. & MOLINA, F. J. 1993. Cover cracking as a function of bar corrosion: Part 1—Experimental test. *materials and Structures*, 26, 453–464.
- BADOGIANNIS, E. & TSIVILIS, S. 2009. Exploitation of poor Greek kaolins: Durability of metakaolin concrete. *Cement and Concrete Composites*, 31, 128–133.
- BALAFAS, I. & BURGOYNE, C. J. 2010. Modeling the structural effects of rust in concrete cover. *Journal of Engineering Mechanics*, 137, 175–185.
- BATIS, G., PANTAZOPOULOU, P., TSIVILIS, S. & BADOGIANNIS, E. 2004. The effect of metakaolin on the corrosion behavior of cement mortars. *Cement and Concrete Composites*, 27, 125–130.
- BAYRAMOV, F., TAŞDEMİR, C. & TAŞDEMİR, M. A. 2004. Optimisation of steel fibre reinforced concretes by means of statistical response surface method. *Cement and Concrete Composites*, 26, 665–675.
- BAZANT, Z. P. 1979. Physical model for steel corrosion in concrete sea structures--theory. *Journal of the Structural Division*, 105.
- BELYTSCHKO, T. & BLACK, T. 1999. Elastic crack growth in finite elements with minimal remeshing. *International journal for numerical methods in engineering*, 601–620.
- BELYTSCHKO, T., GRACIE, R. & VENTURA, G. 2009. A review of extended/generalized finite element methods for material modeling. *Modelling and Simulation in Materials Science and Engineering*, 14, 1–24.
- BONAKDAR, M., BAKHSHI, M. & GHALIBAFIAN, M. 2005. Properties of high-performance concrete containing high reactivity metakaolin. *ACI-SP*, 228, 287–296.
- BROWNE, R. D. 1982. Design Prediction of the Life for Reinforced Concrete in Marine and Other Chloride Environments. *Durability of Building Materials*, 1, 113–25.

- CASTOREÑA, J., ALMERAYA-CALDERON, F., VELÁSQUEZ, J., GAONA-TIBURCIO, C., CÁRDENAS, A., BARRIOS-DURSTEWITZ, C., LEÓN, L. L. & MARTINEZ-VILLAFANE, A. 2008. Modeling the time-to-corrosion cracking of reinforced concrete structures by finite element. *Corrosion*, 64, 600-606.
- CHEN, J., XU, Q., LI, J. & FAN, S. 2010. Improved response surface method for anti-slide reliability analysis of gravity dam based on weighted regression. *J. Zhejiang Univ.-Sc A.*, 11, 432-439.
- CHERNIN, L. & VAL, D. V. 2011. Prediction of corrosion-induced cover cracking in reinforced concrete structures. *Construction and Building Materials*, 25, 1854-1869.
- DU, Y. G., CHAN, A. H. C. & CLARK, L. A. 2006. Finite element analysis of the effects of radial expansion of corroded reinforcement. *computers & structures*, 84, 917-929.
- DUAN, P., SHUI, Z., CHEN, W. & SHEN, C. 2013. Enhancing microstructure and durability of concrete from ground granulated blast furnace slag and metakaolin as cement replacement materials. *Journal of Materials Research and Technology*, 2, 52-59.
- EL MAADDAWY, T. & SOUDKI, K. 2007. A model for prediction of time from corrosion initiation to corrosion cracking. *Cement and Concrete Composites*, 29, 168-175.
- GRUBER, K. A., RAMLOCHAN, T., BODDY, A., HOOTON, R. D. & THOMAS, M. D. A. 2001. Increasing concrete durability with high-reactivity metakaolin. *Cement and Concrete Composites*, 23, 479-484.
- HANSSON, C. M. & SØRENSEN, B. 1990. The threshold concentration of chloride in concrete for the initiation of reinforcement corrosion. *Corrosion rates of steel in concrete*. ASTM International.
- HASSAN, A. A. A., HOSSAIN, K. M. A. & LACHEMI, M. 2009. Corrosion Resistance of Self-Consolidating Concrete in Full-Scale Reinforced Beams. *Cement and Concrete Composites*, 31, 29-38.
- HASSAN, A. A. A., HOSSAIN, K. M. A. & LACHEMI, M. 2012. Effect of Metakaolin and Silica Fume on the Durability of Self-Consolidating Concrete. *Cement and Concrete Composites*, 34, 801-807.
- HOOTON, R. D. & MCGRATH, P. F. 1995. Issues Related to Recent Developments in Service Life Specifications for Concrete Structures. *Chloride Penetration into Concrete, International RILEM Workshop St. Remy - Les Chevreuse*, 10.
- JANG, B. S. & OH, B. H. 2010. Effects of non-uniform corrosion on the cracking and service life of reinforced concrete structures. *Cement and Concrete Research* 40, 1441-1450.
- JUSTICE, J. M., KENNSION, L. H., MOHR, B. J., BECKWITH, S. L., MCCORMICK, L. E., WIGGINS, B., ZHANG, K. Z. Z. & KURTIS, E. Comparison of two metakaolins and a silica fume used as supplementary cementitious materials. Proc. Seventh International Symposium on Utilization of High-Strength/High Performance Concrete, 2005 Washington D.C.

- KANG, S. C., KOH, H. M. & CHOO, J. F. 2010. An efficient response surface method using moving least squares approximation for structural reliability analysis. *Probab. Eng. Mech*, 25, 365-371.
- KHAYET, M., COJOCARU, C. & ESSALHI, M. 2011. Artificial neural network modeling and response surface methodology of desalination by reverse osmosis. *Journal of Membrane Science*, 368, 202–14.
- LIU, Y. & WEYERS, R. E. 1998. Modeling the Time-to-Corrosion Cracking in Chloride Contaminated Reinforced Concrete Structures. *ACI Materials Journal*, 95, 675-681.
- LU, C., JIN, W. & LIU, R. 2011. Reinforcement corrosion-induced cover cracking and its time prediction for reinforced concrete structures. *Corrosion Science*, 53, 1337-1347.
- MEHTA, P. K. & MONTEIRO, P. J. M. 1993. *Concrete: Structure, Properties and Materials*, New Jersey, U.S.A., Prentice Hall
- MÖES, N., GRAVOUIL, A. & BELYTSCHKO, T. 2002. Non-planar 3D crack growth by the extended finite element and level sets-part I: mechanical model. *International Journal for Numerical Methods in Engineering*, 55, 2549-2568.
- MONTGOMERY, A. D. 2012. *Design and analysis of experiments* New York, Wiley.
- NEHDI, M. L. & SUMMER, J. 2002. Optimization of ternary cementitious mortar blends using factorial experimental plans. *Materials and Structures*, 35, 495–503.
- PIETRUSZCZAK, S. & HAGHIGHAT, E. 2014. Modeling of fracture propagation in concrete structures using a constitutive relation with embedded discontinuity. *Studia Geotechnica et Mechanica*, 36.
- POON, C. S., KOU, S. C. & LAM, L. 2006. Compressive strength, chloride diffusivity and pore structure of high performance metakaolin and silica fume concrete. *Journal of Construction and Building Materials*, 20, 858–865.
- ROUGERON, P. & P.C. AITCIN 1994. Optimization of the Composition of a High-Performance Concrete. *Cement, Concrete and Aggregates*, 16, 115-124.
- SABIR, B. B., WILD, S. & BAI, J. 2001. Metakaolin and calcined clays as pozzolans for concrete: a review. *Cement and Concrete Composites*, 23, 441-454.
- SIMULIA 2013. Abaqus 6.13 Abaqus/CAE User's Guide.
- SONEBI, M. 2004. Medium strength self-compacting concrete containing fly ash: modelling using factorial experimental plans. *Cement and Concrete Research*, 34, 1199–1208.
- SOUDKI, K. A., EL-SALAKAWY, E. F. & ELKUM, N. B. 2001. Full factorial of optimization of concrete mix design for hot climates. *Journal of Materials in Civil Engineering*, 13, 427–433.
- STANDARD CSA 1994. A23. 3-94, 1994. *Design of Concrete Structures*.
- SUKUMAR, N., MÖES, N., MORAN, B. & BELYTSCHKO, T. 2000. Extended finite element method for three-dimensional crack modelling. *International Journal for Numerical Methods in Engineering*, 48, 1549–1570.
- TELFORD, T. 1993. CEB-FIP Modelcode 1990. *European Design Code, Lausanne, Switzerland*.

- TORRES-ACOSTA & MARTINEZ-MADRID 2003. Residual life of corroding reinforced concrete structures in marine environment. *Journal of Materials in Civil Engineering*, 15, 344-353.
- TUUTTI, K. 1982. Corrosion of steel in concrete. *Research Report, Swedish Cement and Concrete Research Institute, Stockholm, Sweden*.
- UNGER, J. F., ECKARDT, S. & KÖNKE, C. 2007 Modelling of cohesive crack growth in concrete structures with the extended finite element method. *Computer Methods in Applied Mechanics and Engineering*, 196, 4087-4100.
- WONG, S. M., HOBBS, R. E. & ONOF, C. 2005. An adaptive response surface method for reliability analysis of structures with multiple loading sequences. *Structure safety*, 27, 287-308.
- ZELJKOVIC, M. 2009. *Metakaolin Effects on Concrete Durability*. M.A.Sc. Thesis, University of Toronto.
- ZHANG, X. & BUI, T. Q. 2015. A fictitious crack XFEM with two new solution algorithms for cohesive crack growth modeling in concrete structures. *Engineering Computations*, 32, 473 - 497.

8. Conclusions and Recommendations

In this final chapter, we summarize the contributions presented in the dissertation and discuss several potential extensions to our work.

8.1 Conclusions

The following summarized conclusions can be drawn from the dissertation:

- The developed prediction models and design charts in this study can be used as fast and useful tools to design optimized MK concrete mixtures with target RCPT, chloride diffusion factor, chloride reduction diffusion factor, f_c , MOE, STS, FS, corrosion initiation probability, corrosion internal pressure and/or target cost. These charts depend on the total binder content, percentage of MK, W/B ratio, and/or concrete cover.
- The developed XFEM for concrete containing MK, with different mixture proportions and concrete covers, was found to be suitable for predicting the corrosion-induced cracking time and crack propagation pattern.
- Based on the analysis of variance (ANOVA), the most significant factors affecting the chloride diffusion at early ages (28 and 90 days) were the W/B ratio followed by the percentage of MK and binder content. On the other hand, the most significant factors affecting the chloride diffusion at late ages (360 and 720 days) were the percentage of MK followed by the W/B ratio and binder content.

- The diffusion reduction coefficient was more noticeable in mixtures with lower W/B ratios and/or higher binder content compared to mixtures with higher W/B ratios and/or lower binder content.
- The most significant effect on the strength of the tested mixtures, was the W/B ratio followed by MK and total binder content. Meanwhile, the binder content, followed by MK and W/B ratio were the most significant factors affecting the cost per cubic meter of the mixture.
- The increase in the MK replacement from 0 to 20% significantly extended both the initiation and propagation periods at all values of cover thickness.
- The increase of cover thickness significantly increased both the initiation period (T_i) and propagation period (T_p) regardless of curing condition or mixture composition.
- Higher concrete quality associated with better curing technique required higher levels of chloride at the bar surface to initiate corrosion in both impressed current and wet/dry cycles testing. Also, concrete with higher chloride permeability (represented by the RCPT) and/or higher chloride diffusion had lower chloride thresholds. Concrete with high pH values also required higher concentrations of chloride ions at the bar surface to destroy the passive film around the steel bar and initiate corrosion.
- The impressed current corrosion test showed similar trend of variation as that of the wet-dry test during the initiation and propagation periods, which can be considered

a reliable technique to compare the corrosion activates before the initiation of the cracks.

- The most significant factors affecting the chloride-induced corrosion time (time for 10% probability of corrosion initiation) and corrosion induced cracking in 30-mm, 40-mm, and/or 60-mm cover MK mixtures were found to be the percentage of MK, W/B ratio, and binder content, respectively, in order of significance.
- Decreasing the W/B ratio significantly affected the reactivity of MK and its ability to reduce the probability of corrosion. MK mixtures with a lower W/B ratio (0.3) had a reduced probability of corrosion compared to MK mixtures with a higher W/B ratio (0.5). Also, increasing the binder content from 350 kg/m³ to 600 kg/m³ had a positive effect on MK's ability to reduce the probability of corrosion.

8.2 Recommendations for Future Research

- The experimental program could be extended by varying more ambient parameters such as humidity and temperature and studying their effects on the properties of concrete containing MK.
- It would be valuable to enhance the corrosion prediction models by including the propagation phase (in addition to the initiation phase) of corrosion in order to better evaluate the total service life of the structure.
- The XFEM modeling in chapter 7 can be enhanced by developing 3D model to simulate full member corrosion cracking. Also the model can be enhanced by

applying different corrosion pressure shapes (uniform and non-uniform) to account for more complex corrosion product formation.

Bibliography

- 2012a. Design Expert. 9 ed. Minneapolis: Design-Ease® Software
- 2012b. Life-365 Service Life Prediction Model and Computer Program for Predicting the Service Life and Life-Cycle Cost of Reinforced Concrete Exposed to Chlorides Version 2.1.
- AKALIN, O., ULAS, A. K. & BAHAR, S. 2010. Self-consolidating high-strength concrete optimization by mixture design method. *ACI Materials Journal*, 107, 357–364.
- AL-ALAILY, H. S. & HASSAN, A. A. A. 2016a. Refined statistical modeling for chloride permeability and strength of concrete containing metakaolin. *Construction and Building Materials*, 114, 564–579.
- AL-ALAILY, H. S. & HASSAN, A. A. A. 2016b. Time-Dependence of Chloride Diffusion for Concrete Containing Metakaolin. *Journal of Building Engineering* 7, 159–169.
- AL-GAHTANI, A. S. 2010. Effect of curing methods on the properties of plain and blended cement concretes. *Cement and Concrete Composites*, 24, 308–314.
- ALIZADEH, R., GHODS, P., CHINI, M., HOSEINI, M., GHALIBAFIAN, M. & SHEKARCHI, M. 2008. Effect of Curing Conditions on the Service Life Design of RC Structures in the Persian Gulf Region. *Journal of Materials in Civil Engineering*, 20, 2-8.
- ALONSO, C., ANDRADE, C. & GONZÁLEZ, J. A. 1988. Relation Between Concrete Resistivity and Corrosion Rate of the Reinforcements in Carbonated Mortar Made with Several Cement Types. *Cement and Concrete Research*, 687-698.
- AMERICAN CONCRETE INSTITUTE (ACI) COMMITTEE 222 1975. Corrosion of metals in concrete. American Concrete Institute.
- AMLEH, L. B. 2000. Deterioration of reinforcing steel in concrete due to corrosion. A thesis submitted to the Faculty of Graduate Studies and Research in partial fulfillment of requirements for the degree of Doctor of Philosophy, McGill University, Montreal, Canada.
- ANDRADE, C. 1993. Calculation of chloride diffusion coefficients in concrete from ionic migration measurements. *Cem. Concr. Res.*, 23, 724-742.
- ANDRADE, C. 2015. Prediction of service life of reinforced concrete by considering the initiation and the propagation periods. *ACI*, SP 305-4, 1–10.
- ANDRADE, C., ALONSO, C. & MOLINA, F. J. 1993. Cover cracking as a function of bar corrosion: Part 1—Experimental test. *materials and Structures*, 26, 453–464.
- ANDRADE, C., CASTELLOTE, M. & D’ANDREA, R. 2011. Measurement of ageing effect on chloride diffusion coefficients in cementitious matrices. *Nuclear Materials* 412, 209–216.
- ANGST, U., BERNHARD ELSENER, CLAUDIUS K. LARSEN & ØYSTEIN VENNESLAND 2009. Critical chloride content in reinforced concrete — A review. *Cement and Concrete Research*, 39, 1122–1138.
- ANN, K. Y., PACK, S. W., HWANG, J.-P., SONG, H. W. & KIM, S. H. 2010. Service life prediction of a concrete bridge structure subjected to carbonation. *construction and building materials*, 24, 1494-1501.

- ASBRIDGE, A. H., CHADBOURN, G. A. & PAGE, C. L. 2001. Effects of metakaolin and the interfacial transition zone on the diffusion of chloride ions through cement mortars. *Cement and Concrete Research*, 31, 1567-1572.
- AUSTIN, S. A., LYONS, R. & ING, M. J. 2004. Electrochemical Behavior of Steel-Reinforced Concrete During Accelerated Corrosion Testing. *Corrosion - NACE*, 60, 203-212.
- BADOGIANNIS, E. & TSIVILIS, S. 2009. Exploitation of poor Greek kaolins: Durability of metakaolin concrete. *Cement and Concrete Composites*, 31, 128-133.
- BAI, J., WILD, S., SABIR, B. B. & KINUTHIA, J. M. 1999. Workability of concrete incorporating pulverized fuel ash and metakaolin. *Magazine of Concrete Research*, 51, 207-216.
- BALAFAS, I. & BURGOYNE, C. J. 2010. Modeling the structural effects of rust in concrete cover. *Journal of Engineering Mechanics*, 137, 175-185.
- BALLESTER, P., HIDALGO, A., MÁRMOL, I., MORALES, J. & SÁNCHEZ, L. 2009. Effect of Brief Heat-Curing on Microstructure and Mechanical Properties in Fresh Cement Based Mortars. *Cement and Concrete Research*, 39, 573-579.
- BARNES, P., BENSTED, J. & JONES, T. R. 2003. Metakaolin as pozzolanic addition to concrete. *Structure and performance of cements*. 2 ed. England: CRC press.
- BASTIDAS-ARTEAGA, E., CHATEAUNEUF, A., SÁNCHEZ-SILVA, M., BRESSOLETTE, P. & SCHOEFS, F. 2011. A comprehensive probabilistic model of chloride ingress in unsaturated concrete. *Engineering Structures*, 33, 720-730.
- BATIS, G., PANTAZOPOULOU, P., TSIVILIS, S. & BADOGIANNIS, E. 2004. The effect of metakaolin on the corrosion behavior of cement mortars. *Cement and Concrete Composites*, 27, 125-130.
- BAYRAMOV, F., TAŞDEMİR, C. & TAŞDEMİR, M. A. 2004a. Optimisation of steel fibre reinforced concretes by means of statistical response surface method. *Cement & Concrete Composites*, 26, 665-675.
- BAYRAMOV, F., TAŞDEMİR, C. & TAŞDEMİR, M. A. 2004b. Optimisation of steel fibre reinforced concretes by means of statistical response surface method. *Cement and Concrete Composites*, 26, 665-675.
- BAZANT, Z. P. 1979. Physical model for steel corrosion in concrete sea structures--theory. *Journal of the Structural Division*, 105.
- BEDIAKO, M., KEVERN, J. T. & AMANKWAH, E. O. 2015. Effect of Curing Environment on the Strength Properties of Cement and Cement Extenders. *Materials Sciences and Applications*, 6, 33-39.
- BELYTSCHKO, T. & BLACK, T. 1999. Elastic crack growth in finite elements with minimal remeshing. *International journal for numerical methods in engineering*, 60, 601-620.
- BELYTSCHKO, T., GRACIE, R. & VENTURA, G. 2009. A review of extended/generalized finite element methods for material modeling. *Modelling and Simulation in Materials Science and Engineering*, 14, 1-24.
- BENTZ, E. C. 2003. Probabilistic Modeling of Service Life for Structures Subjected to Chlorides. *ACI Materials Journal*, 100, 391-397.

- BODDY, A., HOOTON, R. D. & GRUBER, K. A. 2001. Long-term testing of the chloride penetration resistance of concrete containing high-reactivity metakaolin. *Cement and Concrete Research*, 31, 759-765.
- BONAKDAR, M., BAKHSHI, M. & GHALIBAFIAN, M. 2005a. Properties of high-performance concrete containing high reactivity metakaolin. *ACI-SP*, 228, 287-296.
- BONAKDAR, M., M. BAKHSHI & GHALIBAFIAN, M. 2005b. Properties of high-performance concrete containing high reactivity metakaolin. *ACI-SP*, 228, 287-296.
- BOULFIZA, M., SAKAI, K., BANTHIA, N. R. & YOSHIDA, H. 2003. Prediction of Chloride Ions Ingress in Uncracked and Cracked Concrete. *Materials journal*, 100, 38-48.
- BROOMFIELD, J. 2007. Corrosion of steel in concrete, understanding, investigating and repair. *Taylor & Francis, London, UK*.
- BROWNE, R. D. 1982. Design Prediction of the Life for Reinforced Concrete in Marine and Other Chloride Environments. *Durability of Building Materials*, 1, 113-25.
- CABRER, J. G. 1996. Deterioration of concrete due to reinforcement steel corrosion. *Cement and Concrete Composites Journal*, 18, 47-59.
- CABRERA, J. G., CLAISSE, P. A. & HUNT, D. N. 1995. A statistical analysis of the factors which contribute to the corrosion of steel in Portland cement and silica fume concrete. *construction and Building Materials*, 9, 105-113.
- CADY, P. D. & WEYERS, R. E. 1979. Deterioration rates of concrete bridge decks. *J. Transport. Eng*, 110, 34-44.
- CADY, P. D. & WEYERS, R. E. 1983. Chloride Penetration and the Deterioration of Concrete Bridge Decks, Cement, Concrete, and Aggregates. *CCAGDP*, 5, 81-87.
- CASSAGNABÈRE, F., ESCADEILLAS, G. & MOURET, M. 2009. Study of the reactivity of cement/metakaolin binders at early age for specific use in steam cured precast concrete. *Construction and Building Materials*, 23, 775-784.
- CASSAGNABÈRE, F., MOURET, M., ESCADEILLAS, G., BROILLIARD, P. & BERTRAND, A. 2010. Metakaolin, a solution for the precast industry to limit the clinker content in concrete: Mechanical aspects. *Construction and Building Materials*, 24, 1109-1118.
- CASTOREÑA, J., ALMERAYA-CALDERON, F., VELÁSQUEZ, J., GAONA-TIBURCIO, C., CÁRDENAS, A., BARRIOS-DURSTEWITZ, C., LEÓN, L. L. & MARTINEZ-VILLAFANE, A. 2008. Modeling the time-to-corrosion cracking of reinforced concrete structures by finite element. *Corrosion*, 64, 600-606.
- CEB 1985. Guide to Durable Concrete Structures. *Comité Euro-International du Béton, Lausanne, Switzerland*.
- CHEEWAKET, T., JATURAPITAKKUL, C. & CHALEE, W. 2012. Initial corrosion presented by chloride threshold penetration of concrete up to 10 year-results under marine site, *Constr. . Build. Mater*, 37, 693-698.
- CHEN, H.-J., HUANG, S.-S., TANG, C.-W., MALEK, M. A. & EAN, L.-W. 2012. Effect of curing environments on strength, porosity and chloride ingress resistance of blast furnace slag cement concretes: A construction site study. *Construction and Building Materials*, 35, 1063-1070.

- CHEN, J., XU, Q., LI, J. & FAN, S. 2010. Improved response surface method for anti-slide reliability analysis of gravity dam based on weighted regression. *J. Zhejiang Univ.-Sc A.*, 11, 432-439.
- CHERNIN, L. & VAL, D. V. 2011. Prediction of corrosion-induced cover cracking in reinforced concrete structures. *Construction and Building Materials*, 25, 1854-1869.
- COLEMAN, J. & PAGE, C. L. 1997. Aspects of the pore solution chemistry of hydrated cement pastes containing metakaolin. *Cement and concrete research*, 27, 147-154.
- CORNET, I., ISHIKAWA, T. & BRESLER, B. 1968. The mechanism of steel corrosion in concrete structure. *Materials Protection*, 7, 44-7.
- COURARD, L., DARIMONT, A., SCHOUTERDEN, M., FERAUCHE, F., WILLEM, X. & DEGEIMBRE, R. 2003. Durability of mortars modified with metakaolin. *Cement and Concrete Research*, 33, 1473-1479.
- CRANK, J. 1956. *Mathematics of diffusion*, bristol, clarendon press.
- CRUMPTON, C. F., SMITH, B. J. & JAYAPRAKASH, G. P. 1989. Salt Weathering of Limestone Aggregate and Concrete Without Freeze-Thaw. *Transportation Research Record 1250 Transportation Research Board*, 8-16.
- CUSSON, D. & ISGOR, B. 2004. Durability of concrete structures: prevention, evaluation, inspection, repair and prediction. *canadian civil engineer*, 21, 4-5.
- DETWILER, R. J., KJELLEN, K. O. & GJORV, O. E. 1991. Resistance to chloride intrusion of concrete cured at different temperatures. *Materials Journal*, 88, 19-24.
- DHINAKARAN, G., THILGAVATHI, S. & VENKATARAMANA, J. 2012. Compressive strength and chloride resistance of metakaolin concrete. *KSCE Journal of Civil Engineering*, 16, 1209-1217.
- DÍAZ, B., NOVOA, X. R. & PEREZ, M. C. 2006. Study of the chloride diffusion in mortar: A new method of determining diffusion coefficients based on impedance measurements. *Cement and Concrete Composites*, 28, 237-245.
- DU, Y. G., CHAN, A. H. C. & CLARK, L. A. 2006. Finite element analysis of the effects of radial expansion of corroded reinforcement. *computers & structures*, 84, 917-929.
- DUAN, P., SHUI, Z., CHEN, W. & SHEN, C. 2013. Enhancing microstructure and durability of concrete from ground granulated blast furnace slag and metakaolin as cement replacement materials. *Journal of Materials Research and Technology*, 2, 52-59.
- DUBEY, A. & BANTHIA, N. 1998. Influence of high-reactivity metakaolin and silica fume on the flexural toughness of high-performance steel fiber-reinforced concrete. *ACI Materials Journal*, 95, 284-292.
- EHLEN, M. A., THOMAS, M. D. A. & BENTZ, E. C. 2009. Life-365 Service Life Prediction Model™ Version 2.0. *Concrete International*, 31, 41-46.
- EL MAADDAWY, T. & SOUDKI, K. 2007. A model for prediction of time from corrosion initiation to corrosion cracking. *Cement and Concrete Composites*, 29, 168-175.
- ENRIGHT, M. P. & FRANGOPOL, D. M. 1998. Probabilistic analysis of resistance degradation of reinforced concrete bridge beams under corrosion. *Eng. Struct.*, 20, 960-971.

- ERDOGDU, S., KONDRATOVAL, I. L. & BREMNER, T. W. 2004. Determination of chloride diffusion coefficient of concrete using open-circuit potential measurements. *Cement and Concrete Research*, 34, 603-609.
- ERHAN GÜNEYİSİ, GESOĞLU, M., AKOI, A. O. M. & MERMERDAŞ, K. 2014. Combined effect of steel fiber and metakaolin incorporation on mechanical properties of concrete. *Composites Part B: Engineering*, 56, 8-91.
- ERLIN, B. & VERBECK, G. J. 1975. Corrosion of metals in concrete-needed research. *Special Publication*, 49, 39-46.
- FERREIRA, R. M. & JALALI, S. 2006. Probability-based durability design of concrete structures in marine environment. *Concrete Repair, Rehabilitation and Retrofitting*.
- FLUGE, F. 2001. Marine chlorides – A probabilistic approach to derive provisions for EN 206-1. *Third DuraNet Workshop on Service life design of concrete structures, from theory to standardisation*.
- GHALI, A., GAYED, R. B. & KROMAN, J. 2016. Sustainability of Concrete Infrastructures. *Journal of Bridge Engineering*, 21.
- GHEZAL, A. & KHAYAT, K. H. 2002. Optimizing Self-Consolidating Concrete with Limestone Filler by Using Statistical Factorial Design Methods. *ACI Materials Journal*, 99, 264-272.
- GJØRV, O. E., SORENSON, S. I. & ARNESEN, A. 1977. Notch Sensitivity and Fracture Toughness of Concrete *Cement and Concrete Research*, 7, 333-344.
- GJØRV., O. E. 2009. *Durability Design of Concrete Structures in Severe Environments*, New York, Taylor & Francis.
- GLASS, G., REDDY, B. & BUENFELD, N. 2000. The participation of bound chloride in passive film breakdown on steel in concrete. *Corrosion Science*, 42, 2013-2021.
- GONNERMAN, H. F. & SHUMAN, E. C. 1928. Flexure and Tension Tests of Plain Concrete., *Major Series 171, 209, and 210 Report of the Director of Research, Portland Cement Association*, 149-163.
- GRUBER, K., RAMLOCHAN, T., BODDY, A., HOOTON, R. D. & THOMAS, M. D. A. 2001a. Increasing concrete durability with high-reactivity metakaolin. *Cem Concr Compos*, 23, 479-484.
- GRUBER, K. A., RAMLOCHAN, T., BODDY, A., HOOTON, R. D. & THOMAS, M. D. A. 2001b. Increasing concrete durability with high-reactivity metakaolin. *Cement and Concrete Composites*, 23, 479-484.
- GÜNEYİSİ, E., GESOĞLU, M. & MERMERDAS, K. 2008. Improving strength, drying shrinkage, and pore structure of concrete using metakaolin. *Materials and Structures*, 41, 937-949.
- GÜNEYİSİ, E. & MERMERDAŞ, K. 2007. Comparative study on strength, sorptivity, and chloride ingress characteristics of air-cured and water-cured concretes modified with metakaolin. *Materials and Structures*, 40, 1161-1171.
- GÜNEYİSİ, E., OZTURAN, T. & GESOĞLU, M. 2007. Effect of initial curing on chloride ingress and corrosion resistance characteristics of concretes made with plain and blended cements. *Journal of Building and Environment*, 42, 2676-2685.
- HALAMICKOVA, P., DETWILER, R. J., BENTZ, D. P. & GARBOCZI, E. J. 1995. Water Permeability and Chloride Ion Diffusion in Portland Cement Mortars: Relationship to Sand Content and Critical Pore Diameter. *Cem. and Conc. Res.*, 25, 790-802

- HANSSON, C. M. & SØRENSEN, B. 1990. The threshold concentration of chloride in concrete for the initiation of reinforcement corrosion. *Corrosion rates of steel in concrete*. ASTM International.
- HASSAN, A. A. A., HOSSAIN, K. M. A. & LACHEMI, M. 2009a. Corrosion Resistance of Self-Consolidating Concrete in Full-Scale Reinforced Beams. *Cement & Concrete Composites*, 31, 29-38.
- HASSAN, A. A. A., HOSSAIN, K. M. A. & LACHEMI, M. 2009b. Corrosion Resistance of Self-Consolidating Concrete in Full-Scale Reinforced Beams. *Cement and Concrete Composites*, 31, 29-38.
- HASSAN, A. A. A., HOSSAIN, K. M. A. & LACHEMI, M. 2010. Structural assessment of corroded self-consolidating concrete beams. *Eng. Struct.*, 32, 874-885.
- HASSAN, A. A. A., HOSSAIN, K. M. A. & LACHEMI, M. 2012a. Effect of Metakaolin and Silica Fume on the Durability of Self-Consolidating Concrete. *Cement and Concrete Composites*, 34, 801-807.
- HASSAN, A. A. A., HOSSAIN, K. M. A. & LACHEMI, M. 2012b. Effect of Metakaolin and Silica Fume on the Durability of Self-Consolidating Concrete. *Cement & Concrete Composites*, 34, 801-807.
- HAUSMANN, D. 1967. Steel corrosion in concrete--How does it occur? *Materials protection*.
- HONG, K. 1998. *Cyclic wetting and drying and its effects on chloride ingress in concrete*. National Library of Canada= Bibliothèque nationale du Canada.
- HOOTON, R. D. 1999. *Advances in Cement and Concrete*. Engineering Foundation, New York.
- HOOTON, R. D., GEIKER, M. R. & BENTZ, E. C. 2002. Effects of Curing on Chloride Ingress and Implications on Service Life. *ACI Materials Journal* 99, 201-206.
- HOOTON, R. D. & MCGRATH, P. F. 1995. Issues Related to Recent Developments in Service Life Specifications for Concrete Structures. *Chloride Penetration into Concrete, International RILEM Workshop St. Remy - Les Chevreuse*, 10.
- HOOTON, R. D., THOMAS, M. D. A. & STANISH, K. 2001. Prediction of Chloride Penetration in Concrete. Federal Highway Administration.
- HOPE, B. I. A. 1987. Chloride corrosion threshold in concrete. *ACI Materials Journal* 84, 306-313.
- IBRAHIMA, M., SHAMEEMA, M., AL-MEHTHEL, M. & MASLEHUDDINAM. 2013. Effect of curing methods on strength and durability of concrete under hot weather conditions. *Cement and Concrete Composites*, 41, 60-69.
- JANG, B. S. & OH, B. H. 2010. Effects of non-uniform corrosion on the cracking and service life of reinforced concrete structures. *Cement and Concrete Research* 40, 1441-1450.
- JUSTICE, J., KENNISON, L., MOHR, B., BECKWITH, S., MCCORMICK, L., WIGGINS, B., ZHANG, Z. & KURTIS, K. 2005a. Comparison of two metakaolins and a silica fume used as supplementary cementitious materials. *SP-228, ACI, Farmington Hills, Mich*, 213-236.
- JUSTICE, J. M., KENNISON, L. H., MOHR, B. J., BECKWITH, S. L., MCCORMICK, L. E., WIGGINS, B., ZHANG, K. Z. & KURTIS, E. Comparison of two metakaolins and a silica fume used as supplementary cementitious materials. *Proc.*

- Seventh International Symposium on Utilization of High-Strength/High Performance Concrete, 2005b Washington D.C.
- JUSTNES, H. 1998. A review of chloride binding in cementitious systems. *Nordic Concrete Research, Publication No. 21. 1/98*, Nordic Concrete Federation, Norsk Betongforening, Oslo, 48–63.
- KAMARUDIN, H., LIEW, Y., MOHD MUSTAFA AL BAKRI, A., LUQMAN, M., KHAIRUL NIZAR, I. & HEAH, C. 2011. Investigating the possibility of utilization of kaolin and the potential of metakaolin to produce green cement for construction purposes-A review.
- KANG, S. C., KOH, H. M. & CHOO, J. F. 2010. An efficient response surface method using moving least squares approximation for structural reliability analysis. *Probab. Eng. Mech*, 25, 365-371.
- KATO, Y. & UOMOTO, T. 2005. Modeling of effective diffusion coefficient of substances in concrete considering spatial properties of composite materials. *Advanced Concrete Technology* 3, 241-251.
- KHANZADEH-MORADLLO, M., MESHKINI, M., ESLAMDOOST, E., SADATI, S. & SHEKARCHI, M. 2015. Effect of Wet Curing Duration on Long-Term Performance of Concrete in Tidal Zone of Marine Environment. *International Journal of Concrete Structures and Materials*, 9, 487-498.
- KHATIB, J. M. & CLAY, R. M. 2004. Absorption characteristics of metakaolin concrete. *Cement and Concrete Research*, 34, 19-29.
- KHATIB, J. M. & HIBBERT, J. J. 2005. Selected engineering properties of concrete incorporating slag and metakaolin. *Construction and Building Materials*, 19, 460-472.
- KHAYET, M., COJOCARU, C. & ESSALHI, M. 2011. Artificial neural network modeling and response surface methodology of desalination by reverse osmosis. *Journal of Membrane Science*, 368, 202–14.
- KIRKPATRICK, T. J., WEYERS, R. E., ANDERSON-COOK, C. M. & SPRINKEL, M. M. 2002. Probabilistic model for the chloride-induced corrosion service life of bridge decks. *Cem. Concr. Res.*, 32, 1943–1960.
- LIANG, M., LIN, L. & LIANG, C. 2002. Service life prediction of existing reinforced concrete bridges exposed to chloride environment. *Journal of Infrastructure Systems*, 8, 76-85.
- LIFE-365 2015. Life-365 Service Life Prediction Model and Computer Program for Predicting the Service Life and Life-Cycle Cost of Reinforced Concrete Exposed to Chlorides Version 2.2.2.
- LIU, Y. & SHI, X. 2012. Stochastic modeling of service life of concrete structures in chloride-laden environments. *J. Mater. Civ. Eng.*, 24, 381-390.
- LIU, Y. & WEYERS, R. E. 1998. Modeling the Time-to-Corrosion Cracking in Chloride Contaminated Reinforced Concrete Structures. *ACI Materials Journal*, 95, 675-681.
- LIZARAZO-MARRIAGA, J. & CLAISSE, P. 2009. Determination of the concrete chloride diffusion coefficient based on an electrochemical test and an optimization model. *Materials Chemistry and Physics*, 117, 536–543.

- LOTHENBACH, B., WINNEFELD, F., ALDER, C., WIELAND, E. & LUNK, P. 2007. Effect of Temperature on the Pore Solution, Microstructure and Hydration Products of Portland Cement Pastes. *Cement and Concrete Research*, 37, 483-491.
- LU, C., JIN, W. & LIU, R. 2011. Reinforcement corrosion-induced cover cracking and its time prediction for reinforced concrete structures. *Corrosion Science*, 53, 1337-1347.
- MAAGE, M., HELLAND, S., POULSEN, E., VENNESLAND, Ø. & CARLSEN, J. E. 1996. Service life prediction of existing concrete structures exposed to marine environment. *ACI Materials Journal*, 93, 602-8.
- MADANDOUST, R. & MOUSAVI, S. Y. 2012. Fresh and Hardened Properties of Self-Compacting Concrete Containing Metakaolin. *Construction and Building Materials*, 35, 752-760.
- MAHESWARAN, T. & SANJAYAN, J. G. 2004. A semi-closed-form solution for chloride diffusion in concrete with time-varying parameters. *Magazine of Concrete Research*, 56, 359-366.
- MALHOTRA, V. M. 2000. Role of supplementary cementing materials in reducing greenhouse gas emissions. In: O.E. GJORN & SAKAI, K. (eds.) *Concrete Technology for a Sustainable Development in the 21st Century*. London, UK: E & FN Spon.
- MANERA, M., VENNESLAND, O. & BERTOLINI, L. 2008. Chloride threshold for rebar corrosion in concrete with addition of silica fume. *CORROSION SCIENCE*, 50, 554-560.
- MANGAT, P. S. & LIMBACHIYA, M. C. 1999. Effect of initial curing on chloride diffusion in concrete repair materials. *cement and concrete research*, 29, 1475-1485.
- MANGAT, P. S. & MOLLOY, B. T. 1994. Prediction of long term chloride concentration in concrete. *Materials and Structures* 27, 338-346.
- MAREK, P. 2001. *Probabilistic assessment of structures using Monte Carlo Simulation : background, exercises and software*, Inst. of Theoretical and Applied Mechanics.
- MAREK, P. & BROZZETTI, J. 2001. Probabilistic Assessment of Structures using Monte Carlo simulation. *GUŠTAR, M. Basics, Exercises, Software, ITAM Academy of Sciences Czech Republic*.
- MAREK, P., GUŠTAR, M. & TIKALSKY, P. J. 1993. Monte Carlo Simulation - Tool for Better Understanding of LRFD. . *Journal of Structural Engineering*, 119, 1586-1599.
- MARIKUNTE, S., ALDEA, C. & SHAH, S. P. 1997. Durability of Glass Fiber Reinforced Cement Composites: Effect of Silica Fume and Metakaolin. *Advanced Cement Based Materials*, 5, 100-108.
- MARSH, P. S. & FRANGOPOL, D. M. 2008. Reinforced concrete bridge deck reliability model incorporating temporal and spatial variations of probabilistic corrosion rate sensor data. *Reliab. Eng. Syst. Saf.*, 93, 394-409.
- MCNALLY, C. & SHEILS, E. 2012. Probability-based assessment of the durability characteristics of concretes manufactured using CEM II and GGBS binders. *construction and Building Materials*, 30, 22-29.

- MCPOLIN, D. O., BASHEER, P. A. & LONG, A. E. 2009. Carbonation and pH in Mortars Manufactured with Supplementary Cementitious Materials. *Journal of Materials in Civil Engineering*, 21, 217-225.
- MEHDIPOUR, I., VAHDANI, M., AMINI, K. & SHEKARCHI, M. 2016. Linking stability characteristics to material performance of self-consolidating concrete-equivalent-mortar incorporating fly ash and metakaolin. 105, 206–217.
- MEHTA, P. K. & MONTEIRO, P. J. M. 1993. *Concrete: Structure, Properties and Materials*, New Jersey, U.S.A., Prentice Hall
- MINDESS, S., YOUNG, F. J. & DARWIN, D. 2003. *Concrete*, Upper Saddle River, Prentice Hall.
- MÖES, N., GRAVOUIL, A. & BELYTSCHKO, T. 2002. Non-planar 3D crack growth by the extended finite element and level sets-part I: mechanical model. *International Journal for Numerical Methods in Engineering*, 55, 2549-2568.
- MONFORE, G. E. 1968. Electrical Resistivity of Concrete. *JPCA Res Develop Lab*, 2, 35-48.
- MONTGOMERY, A. D. 2012. *Design and analysis of experiments* New York, Wiley.
- MORINAGA, S. 1990. Prediction of service lives of reinforced concrete buildings based on the corrosion rate of reinforcing steel. *Proc., Building Materials and Components*, 5-16.
- MORRIS, W., VICO, A., VAZQUEZ, M. & DE SANCHEZ, S. R. 2002. Corrosion of reinforcing steel evaluated by means of concrete resistivity measurements. *Corrosion Science*, 44, 81-99.
- MOUKWA, M. 1990. Characteristics of the attack of cement paste by MgSO₄ and MgCl₂ from the pore structure measurements. *Cem. Concr. Res.*, 20, 148–158.
- NEHDI, M. L. & SUMMER, J. 2002. Optimization of ternary cementitious mortar blends using factorial experimental plans. *Materials and Structures*, 35, 495–503.
- NEVILLE, A. M. 1996. *Properties of Concrete*, New York, NY USA.
- NEWMAN, J. B. & CHOO, B. S. 2003. *Advanced Concrete Technology: Concrete Properties*. Butterworth-Heinemann.
- NIEVES-MENDOZA, D., GAONA-TIBURCIO, C., HERVERT-ZAMORA, H. L., TOBIAS, R. J., CASTRO-BORGES, P., COLAS, O. R., ZAMBRANO, R. P., MARTÍNEZ-VILLAFANE, A. & ALMERAYA-CALDERÓN, F. 2012. Statistical Analysis of Factors Influencing Corrosion in Concrete Structures. *International journal of electrochemical science*, 7, 5495-5509.
- NOWAK, A. S. & COLLINS, K. R. 2000. *Reliability of structures*, Michigan, McGraw Hill.
- PAGE, C. L. 1975. Mechanism of corrosion protection in reinforced concrete marine structures. *Nature*, 258, 514–515.
- PAIVA, H., VELOSA, A., CACHIM, P. & FERREIRA, V. M. 2012. Effect of metakaolin dispersion on the fresh and hardened state properties of concrete. *Cement and Concrete Research*, 42, 607-612.
- PANESAR, D. K. & CHIDIAC, S. E. 2011. Effect of cold temperature on the chloride-binding capacity of cement. *J. Cold Reg. Eng.*, 25, 133-144.
- PETTERSSON, K. 1995. Chloride threshold value and the corrosion rate in reinforced concrete. *In Proc. of the Nordic Seminar. Lund.* , 257-266.

- PIETRUSZCZAK, S. & HAGHIGHAT, E. 2014. Modeling of fracture propagation in concrete structures using a constitutive relation with embedded discontinuity. *Studia Geotechnica et Mechanica*, 36.
- POON, C. S., KOU, S. C. & LAM, L. 2006. Compressive strength, chloride diffusivity and pore structure of high performance metakaolin and silica fume concrete. *Journal of Construction and Building Materials*, 20, 858–865.
- POON, C. S., LAM, L., KOU, S. C., WONG, Y. L. & WONG, R. 2001. Rate of pozzolanic reaction of metakaolin in high-performance cement pastes. *Cement and Concrete Research*, 31, 1301–1306.
- POUPARD, O., L'HOSTIS, V., CATINAUD, S. & PETRE-LAZAR, I. 2006. Corrosion damage diagnosis of a reinforced concrete beam after 40 years natural exposure in marine environment. *Cement and Concrete Research*, 36, 504–520.
- POURBAIX, M. 1974. Atlas of Electrochemical Equilibria in Aqueous Solutions. *National Association of Corrosion Engineers*.
- QIAN, X. Q. & LI, Z. J. 2001. The relationships between stress and strain for high performance concrete with metakaolin. *Cement and Concrete Research*, 31, 1607–1611.
- QUANWANG, L., KEFEI, L., XINGANG, Z., QINMING, Z. & ZHIHONG, F. 2015. Model-based durability design of concrete structures in Hong Kong–Zhuhai–Macau sea link project. *Structural Safety*, 53, 1–12.
- RAMEZANIANPOUR, A. A., KAZEMIAN, A., MOGHADDAM, M. A., MOODI, F. & RAMEZANIANPOUR, A. M. 2015. Studying effects of low-reactivity GGBFS on chloride resistance of conventional and high strength concretes. *Materials and Structures*, 1–13.
- RAMLOCHAN, T., THOMAS, M. & GRUBER, K. A. 2000. The effect of Metakaolin on alkali-silica reaction in concrete. *Cement and Concrete Research*, 30, 339–344.
- RASHEEDUZZAFAR, A. S. AL-GAHTANI & AL-SAADOUN, S. S. 1989. Influence of Construction Practices on Concrete Durability. *Materials Journal*, 86, 566–575.
- RAZAK, H. A. & WONG, H. S. 2005. Strength estimation model for high-strength concrete incorporating metakaolin and silica fume. *Cement and Concrete Research*, 35, 688–695.
- RODRIGUEZ, O. G. & HOOTON, R. D. 2003. Influence of cracks on chloride ingress into concrete. *ACI Materials Journal*, 100, 120–126.
- ROUGERON, P. & AÏTCIN, P.-C. 1994. Optimization of the composition of a high-performance concrete. *Cement, Concrete and Aggregates*, 16, 115–124.
- ROUGERON, P. & P.C. AITCIN 1994. Optimization of the Composition of a High-Performance Concrete. *Cement, Concrete and Aggregates*, 16, 115–124.
- SABIR, B. B., WILD, S. & BAI, J. 2001a. Metakaolin and calcined clays as pozzolans for concrete: a review. *Cement & Concrete Composites*, 23, 441–454.
- SABIR, B. B., WILD, S. & BAI, J. 2001b. Metakaolin and calcined clays as pozzolans for concrete: a review. *Cement and Concrete Composites*, 23, 441–454.
- SANGOJU, B., PILLAI, R. G., GETTU, R., BHARATKUMAR, B. H. & IYER, N. R. 2015. Use of portland pozzolana cement to enhance the service life of reinforced concrete exposed to chloride attack. *J. Mater. Civ. Eng*, 27.

- SCHMIDT, S. R. & LAUNSBY, R. G. 1994. *Understanding Industrial Designed Experiments*, Colorado Springs, Colorado, Air Academic Press.
- SHAIKH, F. U. A., MIHASHI, H. & KOBAYAKAWA, A. 2015. Corrosion durability of reinforcing steel in cracked high-performance fiber-reinforced cementitious composite beams. *J. Mater. Civ. Eng.*, 27.
- SHAMSAD, A. 2003. Reinforcement Corrosion in Concrete Structures, its Monitoring and Service Life Prediction – A Review. *Journal of Cement and Concrete Composites*, 25, 459-471.
- SHAMSAD, A., ABUL KALAM, A. & KEVIN, F. L. 2012. Effect of the Key Mixture Parameters on Tortuosity and Permeability of Concrete. *Journal of Advanced Concrete Technology*, 10 86-94.
- SIMULIA 2013. Abaqus 6.13 Abaqus/CAE User's Guide.
- SONEBI, M. 2004. Medium strength self-compacting concrete containing fly ash: modelling using factorial experimental plans. *Cement and Concrete Research*, 34, 1199–1208.
- SONG, H., LEE, C. & ANN, K. 2008. Factors influencing chloride transport in concrete structures exposed to marine environments *Cement & Concrete Composites*, 30, 113-121.
- SOUDKI, K. A., EL-SALAKAWY, E. F. & ELKUM, N. B. 2001. Full factorial of optimization of concrete mix design for hot climates. *Journal of Materials in Civil Engineering*, 13, 427–433.
- SPEED, T. P. 1987. What is an analysis of variance? (with discussion). *Annals of Statistics*, 15, 885–941.
- STANDARD CSA 1994. A23. 3-94, 1994. *Design of Concrete Structures*.
- STANISH, K. D., HOOTON, R. D. & THOMAS, M. D. A. 2000. Testing the Chloride Penetration Resistance of Concrete: A Literature Review. Federal Highway Administration.
- STEWART, M. G. & ROSOWSKY, D. 1998. Time-dependent reliability of deteriorating reinforced concrete bridge decks. *Structural Safety*, 20, 91–109.
- SUDRET, B. 2008. Probabilistic models for the extent of damage in degrading reinforced concrete structures. *Reliability Engineering and System Safety*, 93, 410-422.
- SUKUMAR, N., MÖES, N., MORAN, B. & BELYTSCSKO, T. 2000. Extended finite element method for three-dimensional crack modelling. *International Journal for Numerical Methods in Engineering*, 48, 1549–1570.
- TAKEWAKA, K. & MATSUMOTO, S. Quality and cover thickness of concrete based on the estimation of chloride penetration in marine environments. In: MALHOTRA, V. M., ed. 2nd International Conference of Concrete in Marine Environment, 1988. ACI, 381-400.
- TANG, L. & NILSSON, L. 1992. Chloride diffusivity in high strength concrete at different ages. *Nordic Concrete Research, Nordic Concrete Federation*, Nordic Concrete Research, Nordic Concrete Federation, 162-171.
- TELFORD, T. 1993. CEB-FIP Modelcode 1990. *European Design Code, Lausanne, Switzerland*.
- THOMAS MDA & PB., B. 1999. Modelling chloride diffusion in concrete: effect of fly ash and slag. *Cem Concr Res*, 29, 487–95.

- THOMAS, M. D. A. & BAMFORTH, P. B. 1999. Modelling chloride diffusion in concrete: effect of fly ash and slag. *Cem Concr Res*, 29, 487–95.
- TORRES-ACOSTA & MARTINEZ-MADRID 2003. Residual life of corroding reinforced concrete structures in marine environment. *Journal of Materials in Civil Engineering*, 15, 344-353.
- TOWNSEND, H. E., CLEARY, H. J. & ALLEGRA, L. 1981. Breakdown of Oxide films in Steel Exposure to Chloride Solutions. *Corrosion - NACE*, 37, 384-391.
- TREJO, D. & PILLAI, R. G. 2003. Accelerated chloride threshold testing: Part I - ASTM A 615 and A 706 reinforcement. *ACI Mater. J.*, 100, 519-527.
- TUUTTI, K. 1982. Corrosion of steel in concrete. *Research Report, Swedish Cement and Concrete Research Institute, Stockholm, Sweden.*
- UNGER, J. F., ECKARDT, S. & KÖNKE, C. 2007 Modelling of cohesive crack growth in concrete structures with the extended finite element method. *Computer Methods in Applied Mechanics and Engineering*, 196, 4087–4100.
- VAL, D. V. & TRAPPER, P. A. 2008. Probabilistic evaluation of initiation time of chloride-induced corrosion. *Reliab. Eng. Syst. Safe*, 93, 364–372.
- VEDALAKSHMI, R., DEVI, R., EMMANUEL, B. & PALANISWAMY, N. 2008. Determination of diffusion coefficient of chloride in concrete: an electrochemical impedance spectroscopic approach. *Materials and Structures* 41 1315–1326.
- VERBECK, G. J. 1975. Mechanism of Corrosion in Concrete. *In Corrosion of Metals in Concrete International ACI SP-49.*
- VIDAL, T., CASTEL, A. & FRANÇOIS, R. 2007. Corrosion process and structural performance of a 17 year old reinforced concrete beam stored in chloride environment. *Cement and Concrete Research*, 37, 1551-61.
- VU, D. D., STROEVEN, P. & BUI, V. B. 2001. Strength and durability aspects of calcined kaolin-blended Portland cement mortar and concrete. *Cement and Concrete Composites*, 23, 471-478.
- WANG, Y., LI, Q. & LIN, C. 2016. Chloride diffusion analysis of concrete members considering depth-dependent diffusion coefficients and effect of reinforcement presence. *J. Mater. Civ. Eng.*, 28.
- WILD, S., KHATIB, J. M. & JONES, A. 1996. Relative strength, pozzolanic activity and cement hydration in superplasticised metakaolin concrete. *Cement and Concrete Research*, 26, 1537–1544.
- WONG, S. M., HOBBS, R. E. & ONOF, C. 2005. An adaptive response surface method for reliability analysis of structures with multiple loading sequences. *Structure safety*, 27, 287-308.
- XUEMEI, L., HONGJIAN, D. & MIN-HONG, Z. 2015. A model to estimate the durability performance of both normal and light-weight concrete. *construction and Building Materials*, 80, 255-261.
- YOUNG, J. F. 1988. Review of the Pore Structure of Cement Paste and Concrete and its Influence on Permeability. *American Concrete Institute SP-108*, 1-18.
- YUAN, Y., JI, Y. & SHAH, S. P. 2007. Comparison of two accelerated corrosion techniques for concrete structures. *ACI Structural Journal*, 104, 344–347.
- ZELJKOVIC, M. 2009. *Metakaolin Effects on Concrete Durability*. M.A.Sc. Thesis, University of Toronto.

- ZHANG, X. & BUI, T. Q. 2015. A fictitious crack XFEM with two new solution algorithms for cohesive crack growth modeling in concrete structures. *Engineering Computations*, 32, 473 - 497.
- ZHAO, Q., HE, X., ZHANG, J. & JIANG, J. 2016. Long-age wet curing effect on performance of carbonation resistance of fly ash concrete. *Construction and Building Materials*, 127, 577-587.